2014

Characterization of a water soluble, non-ionic, helical poly(α-amino acid)

Wayne Huberty
Louisiana State University and Agricultural and Mechanical College, wayne.huberty1@gmail.com

CHARACTERIZATION OF A WATER SOLUBLE, NON-IONIC, HELICAL POLY(A-AMINO ACID)

A Dissertation

Submitted to the Graduate Faculty of the
Louisiana State University and
Agricultural and Mechanical College
in partial fulfillment of the
requirements for the degree of
Doctor of Philosophy

in

The Department of Chemistry

by
Wayne Huberty
B.S., UW-Stevens Point, 2009
M.S., Louisiana State University, 2012
December 2014

Acknowledgements

I would like to first thank and praise the one and only savior of the world, Jesus Christ, who sustains us by His word, grace and mercy.

I would like to thank my wonderful wife who patiently endured the process (sometimes agonizing) of earning a Ph.D. My son also receives an acknowledgement for never complaining that daddy spent too much time working on science (it helps he could not speak at the time!). Much thanks to my parents for not complaining that their son and daughter-in-law moved across the country to attend graduate school and the rest of my family gets an honorable mention for not helping me, but definitely not hindering this process.

I would profusely like to thank my adviser, Paul Russo, for all his guidance and help, not just relegated to science, but for life in general. I am very thankful that he accepted me as a student, despite me being "persistent". In addition, I would like to thank Donghui Zhang, my co-adviser, who helped with synthetic issues -- she knows there were many! In addition, I would like to thank Rafael Cueto for all the instruction, patience, and assistance over the years. Last, I would like to thank all my fellow students that have helped me, with special thanks for all the students in Russo and Zhang labs.

Table of Contents

Abstract

A water soluble, non-ionic, rodlike polymer, PEGL, was synthesized and characterized in efforts to synthesize a novel model polymer to study stiff polymers in solution. The rodlike system is likely stiff due to a high relative percent helicity in water up to 50 °C, measured by circular dichroism, the observation of liquid crystalline domains in water, and from the slope measured from conformation plots supplied by GPC/MALS; however, it also apparent the system is aggregating in both a 2 mM azide solution and a buffer (200 mM $NaNO_3$ + 20 mM NaH_2PO_4 + 2 mM NaN_3), in corroboration of negative second virial coefficient values. Bulk light scattering experiments, both dynamic and static, support aggregates with a high polydispersity. Therefore, although PEGL was synthesized, it appears not to be a model system but exists in an aggregated state, even in a range of solvents tested.

Chapter 1 - α-amino acids

1.1 Amino Acids

Polypeptides are interesting for scientific study because they are vital for every biological system, with more than 10,000 different peptides providing different functions: lowering activation energy, structural support, storage, transport, cellular communication, movement, and defense.[9] Proteins constitute 50% of the dry weight of a cell[9] and have a complicated folded structure, which dictates function. The Protein Data Bank has over 90,000 protein structures in atomic detail.[10]

The body synthesizes peptides by sections of DNA called genes. These genes contain the genetic information needed for protein synthesis. When ready, RNA copies the DNA, creating messenger RNA. This messenger RNA is brought outside of the cell nucleus into the cytoplasm and peptide assembly occurs in the ribosome (Figure 2).[9] While the previous few sentences are the working hypothesis of natural peptide synthesis, this "archaic" idea is being challenged.[11] Chemists, while not able to shrink down to the size of a cell like in the Magic School Bus children's books to create peptides, can create peptide analogs using synthetic techniques.

Peptides are degraded when boiled, leaving dry crystalline substances.[8] Figure 1 outlines the discovery of the twenty peptide forming amino acids, including when and who discovered them and the method of which they were discovered.[8]

TABLE

Amino acids that have been demonstrated to be

	AMINO ACID	EARLIEST OBSERVATION OF THE AMINO ACID	
1	Cystine	Wollaston	1810
2	Leucine	Proust	1819
3	Glycine	Braconnot	1820
4	Aspartic acid	Plisson	1827
5	Tyrosine	Liebig	1846
6	Alanine	Strecker (synthesis)	1850
7	Valine	von Gorup-Besanez	1856
8	Serine	Cramer	1865
9	Glutamic acid	Ritthausen	1866
10	Phenylalanine	Schulze	1879
11	Arginine	Schulze	1886
12	Lysine	Drechsel	1889
13	Iodogorgoic acid	Drechsel	1896
14	Histidine	Kossel, Hedin	1896
15	Proline	Willstätter (synthesis)	1900
16	Tryptophane	Hopkins and Cole	1901
17	Oxyproline	Fischer	1902
18	Isoleucine	Ehrlich	1903
19	Thyroxine	Kendall	1915
20	Oxyglutamic acid	Dakin	1918
21	Methionine	Mueller	1922

products of the hydrolysis of proteins

AMINO ACID	EARLIEST OBSERVATION OF THE AMINO ACID AS A PRODUCT OF HYDROLYSIS OF PROTEINS	
Glycine	Braconnot	1820
Leucine	Braconnot	1820
Tyrosine	Bopp	1849
Serine	Cramer	1865
Glutamic acid	Ritthausen	1866
Aspartic acid	Ritthausen	1868
Phenylalanine	Schulze and Barbieri	1881
Alanine	Weyl	1888
	(Schützenberger	1879?)
Lysine	Drechsel	1889
Arginine	Hedin	1895
Iodogorgoic acid	Drechsel	1896
Histidine	Kossel, Hedin	1896
Cystine	Mörner	1899
Valine	Fischer	1901
Proline	Fischer	1901
Tryptophane	Hopkins and Cole	1901
Oxyproline	Fischer	1902
Isoleucine	Ehrlich	1903
Thyroxine	Kendall	1915
Oxyglutamic acid	Dakin	1918
Methionine	Mueller	1922

Figure 1. The discovery of the amino acids. The top shows, in order, the discovery of the amino acids by synthesis of naturally found peptides. The bottom shows, in order, the amino acids discovered by hydrolysis of peptides. Reprinted with permission from Vickery, H. B.; Schmidt, C. L. A. *Chem. Rev.* **1931,** 9, (2), 169-318. Copyright 1931 American Cheimcal Society. From reference 8.

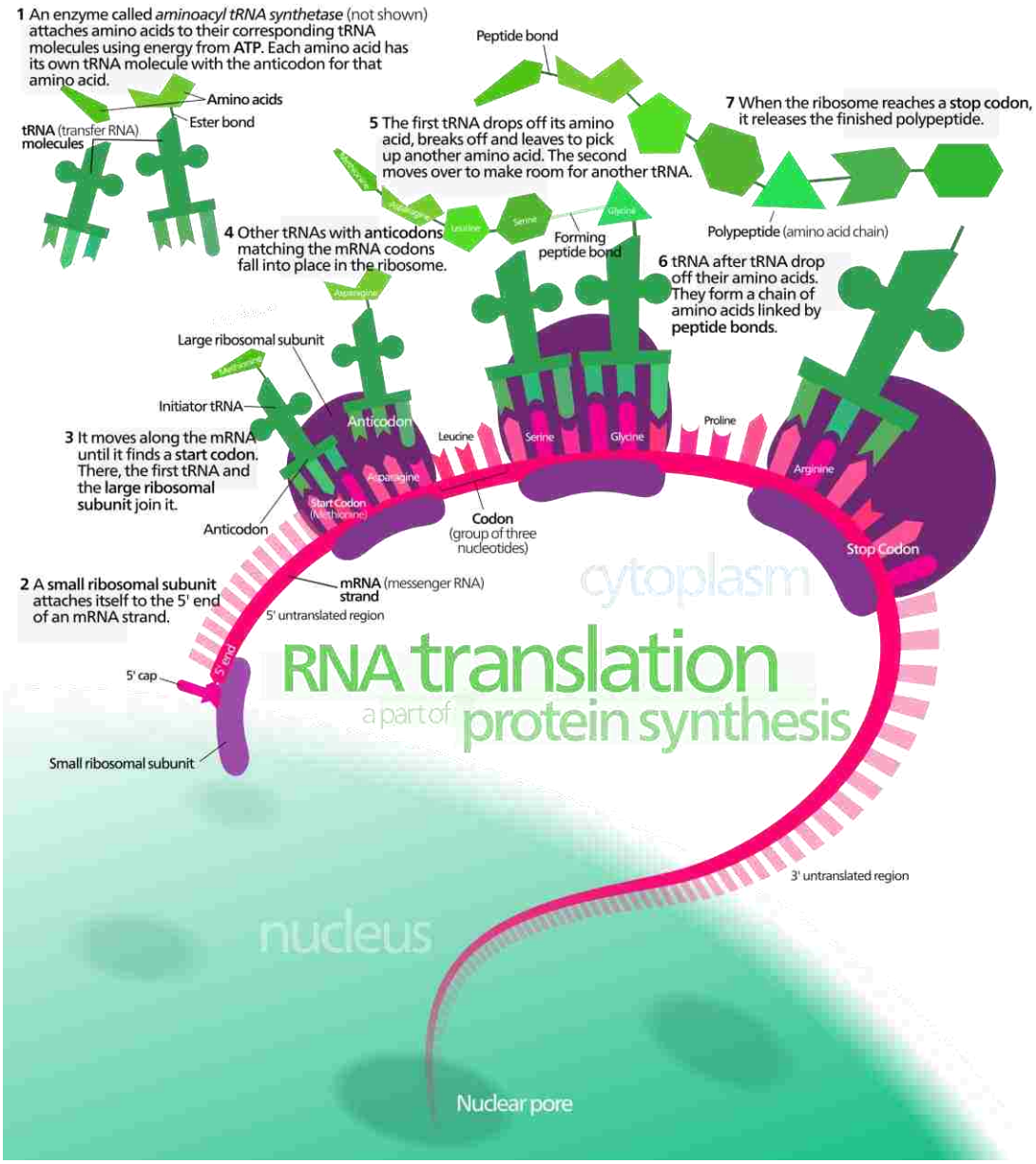

Figure 2. The process of natural peptide synthesis: the DNA is copied by messenger RNA inside the nucleus, it travels to the ribosome and the free amino acids in the cytoplasm are added in the correct sequence for the specific peptide. From reference 4.

While the discovery of some amino acids was intentional, the discovery of leucine, glycine, alanine, tyrosine, phenylalanine, glutamic acid, happened by fractional crystallization (some peptides would crystallize while the others would stay in solution). Cysteine, the first

amino acid discovered, found in a urinary calculus (kidney stone) proved the early chemists did not have a problem getting their hands dirty.

Amino acids have a general structure found in Figure 3. The twenty amino acids are characterized into four different groups dependent upon the functionality of the pendant R group: charged, uncharged, hydrophobic, and other (Figure 4).[9] The backbone carboxylic acid has a pKa ranging from 1.7 -2.4 and the backbone amine has a pKa of 8.8-10.5. An unusual amino acid, cysteine, has a sulfur group capable of making disulfide crosslinks.

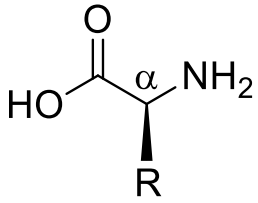

Figure 3. The general structure of an α-amino acid.

Because of the chirality of the amino acid unit and the complex intermolecular forces, sequences of amino acids can have very complex three-dimensional structures that determine peptide behavior. Proteins recognize and bind to target molecules, and the availability of these binding sites heavily depends on shape.[9] The first structure discussed is the least complex: the random coil, or globular shape.[12-14]

Prototypically, synthetic polymers do not have any defined long-range structure in solution and their properties are determined by these highly disordered states.[15] Peptides in the random coil conformation behave like other synthetic polymers. Conversely, in the right conditions (pH, temperature, salt, etc.) peptides can form different conformations, as found in Figure 5.

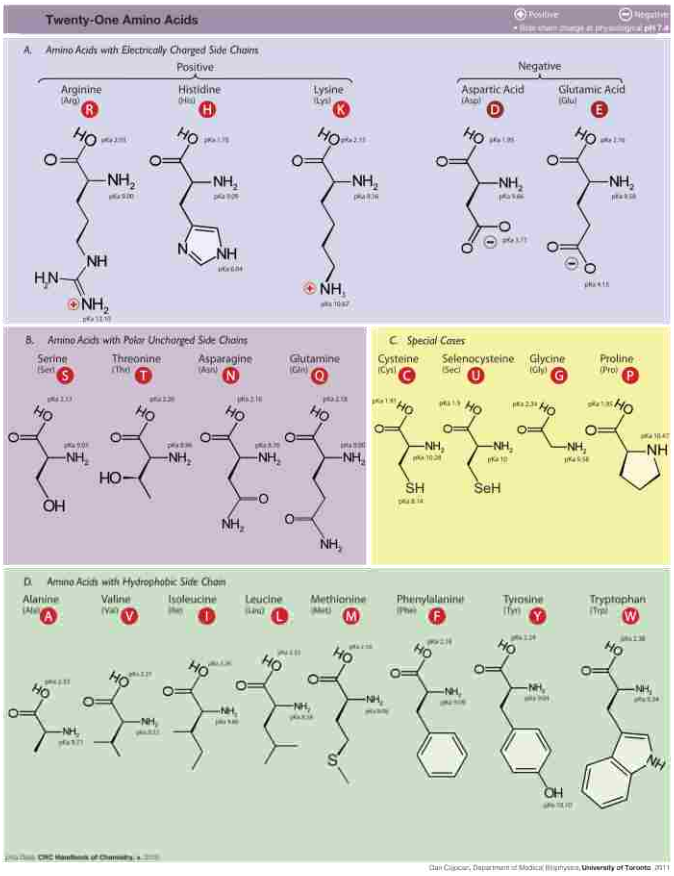

Figure 4. The structure and pKa of the twenty amino acids (selenocystine is considered rare and thus not normally included in the list of the amino acids). From reference 2.

Along with the random coil, peptides can fold into a beta sheets. These are prevalent in globular proteins, creating a synergy between the random coil and beta sheet.[9] Beta sheets form when two adjacent peptide chains align by intermolecular hydrogen-bonding and strength, and in the case of spider silk, provides a structure stronger than steel.[9]

A well-known structure for polypeptides is the α-helix. The helix occurs when extensive hydrogen bonding between amino acids along the peptide chain stabilizes the three dimensional structure, but this is different from the intermolecular hydrogen bonding of beta sheets.

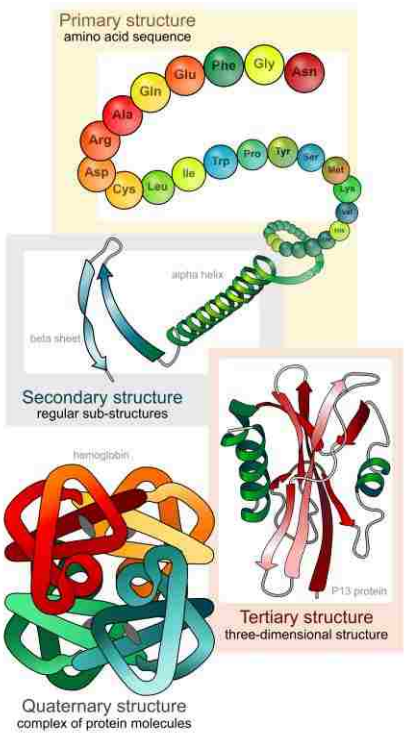

Figure 5. The possible conformations for peptides. From reference 1.

The inherent twist in the helix is due to both the intramolecular hydrogen bonding and the chirality of the amino acid. Pauling *et al.* was the first to discuss the dimensions and configuration of the helix.[16-18] In a video, Linus Pauling described how he discovered peptides contort into an α-helix. He said, "…and I thought, why don't I discover the α-helix?"[19] Pauling took a piece of paper, drew the correct bond angles and bond lengths and folded the paper along the alpha carbons. After several folds, he found a helix provided each N-H bond could be in place for hydrogen-bonding with the carbonyl group.[19] Thus, the discovery of the α-helix was through scientific study sprinkled with a little imagination. The stability of the helix partially comes from this hydrogen bonding but also comes from the optimization of packing.[15]

In a quantitative way, Pauling found two possible spirals. The first spiral, or helix, has about 3.7 residues per turn, with each residue hydrogen-bonded to the third residue in each direction on the chain.[16] Each residue would traverse 1.47 Å in one-directional space. The second spiral has about 5.1 residues per turn, hydrogen-bonded to the fifth residue in both directions, and traverse 0.96 Å per residue; however, Pauling pointed out the α-helix was very sensitive to the bond angle at the α-carbon and hydrogen-bond length. Consequently, the helix can have a wide range of dimensions.[15] Potential energy surfaces have shown the alpha helix is the most stable structure for poly(α-amino acids)[20, 21] but the helix can be disrupted.[22] The same investigators of the early potential energy surfaces are still working to illuminate the α-helix and other peptide conformations decades later.[23]

The α-helix owes its stability to hydrogen bonding and the optimization of packing but the latter only becomes possible because of the steroregularity of the amino acids.[15] External stimuli such as salt, pH, solvent, heat, hydrogen-bond disrupters, and reductive agents can change the conformation of a peptide, resulting in denaturation.[9] Solvents can also change the conformation of the polymer by changing the polarity of the solvated media.

1.2 Synthesis of N-carboxyanhydride

N-carboxyanhydrides (NCA) are an efficient method for polypeptide synthesis. Kricheldorf[24] and Hadjichristidis[25] have written extensive reviews about NCAs and their subsequent polymerization. N-carboxyanhydrides were first synthesized by Lecuhs in the early 1900s and were discovered while trying to purify N-ethoxycarbonyl or N-methoxycarbonyl amino acid chlorides by distillation (Scheme 1).[24, 26, 27] It is unfortunate Lecuhs did not pursue this reaction further, but it was in disrepute to believe in large molecules prior to Staudinger.

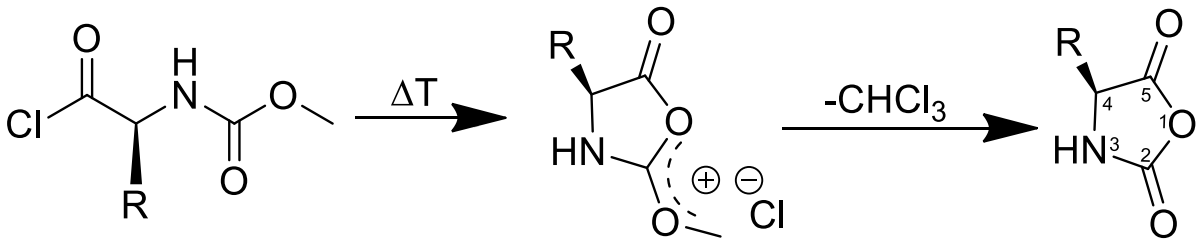

Scheme 1. Original Leuchs reaction.

Once Staudinger established the idea of large, covalently bonded molecules, Curtius[28-30] and Wessely[31-33] found the reaction of a NCA provided high-molar-mass polypeptides via initiation with water, primary amines, and alcohols. NCAs lend themselves to ring-opening polymerization because of the activated fifth carbon.[24] While advantageous when making polymers, it does limit the shelf life of the NCA, even while refrigerated. Some water can adhere to the NCA crystals and slowly initiate polymerization.[24]

A few highlighted ways to synthesize NCAs follow. Phosgene gas is a very effective cyclizing agent (Scheme 2)[34] and a typical method of producing NCAs until the early 1990's. Phosgene's advantage is its speed and low NCA racemization;[6] however, phosgene has some problems, such as difficulty keeping the correct stoichiometry throughout the reaction and side reaction from excess phosgene.[6] In a NCA-forming reaction, the α-amino acid precursor is suspended in a dry solvent, such as dioxane, at 50 °C until the amino acid is completely dissolved.[35] A continuous stream of phosgene gas flows through the solution until the reaction completes. The excess phosgene needs removal by nitrogen stream and neutralization before crystallization of the NCA product.

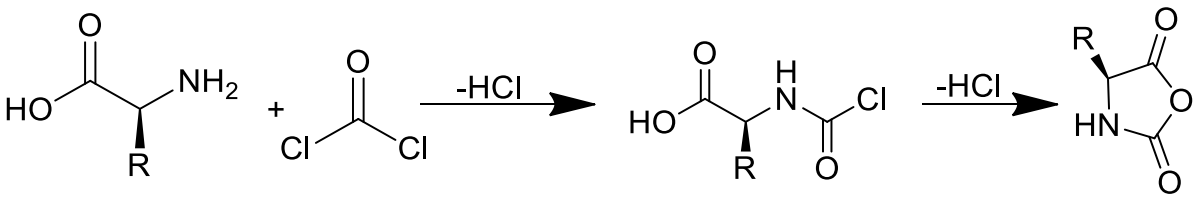

Scheme 2. Reaction of α-amino acid with phosgene.

To combat the large excess of phosgene, a benzene solution of phosgene gas was used to better control the amount of phosgene added.[35] Ideally, no more than three times excess phosgene is used. Bubbling phosgene gas into benzene creates a saturated benzene solution, stable for months.[35] This made synthesis easier by not needing to use the gaseous phosgene but cyclization required catalysis with carbon black.[36]

Table I. Reaction of *I* with Amino Acids in THF

Amino Acid (AA)	*I*/3 : AA	% yield [a]	mp °C [b]	Scale, g.	Dissolution time, hr	$[\alpha]_D$
γ-stearyl-L-glutamate	1.04	89.5	77-78	10.0	<1	-18.10 [e]
DL-2-aminostearic acid	1.07	81.8	98-99	0.3	1	---
γ-benzyl-L-glutamate	1.17	85.8	96-97	0.4	<3	-19.11
O-benzyl-L-tyrosine	1.20	89.4	142	0.4	3 [c]	-88.45
L-phenylalanine	1.13	83.0	91-92	5.0	3	-108.30
L-leucine	1.16	66.8	78-79	2.5	d	-37.40
L-alanine	1.26	58.5	91-92	5.0	d	---
DL-valine	1.11	82.7	80-81	5.0	d	---

a isolated yield
b uncorrected melting points, Fischer-Johns hot stage
c slight suspension remained
d insoluble material removed by filtration after about 4 h.
e filtered chloroform solution; approximate concentration 1.0 g/dl

Figure 6. Reaction results from cyclizing several different amino acids with triphosgene. From reference 6.

Solid triphosgene is the easiest method of supplying phosgene.[6, 37] Using triphosgene, the solid can be accurately weighed, safely delivered and stored, and does not require a catalyst.[6] Triphosgene decomposes into three equivalents of phosgene gas *in situ* to cyclize the amino acid.

The phosgene molecule liberated following nucleophilic attack of the carbonyl carbon on triphosgene reacts immediately, eliminating any excess phosgene.[37]

While phosgene and its derivatives are highly successful at cyclizing amino acids into NCAs, side products may affect polymerization. Some less influential side products are isocyanates,[38] acid chlorides, N-chloroformyl amino acids,[38] alkyl halides, excess cyclization agent, and recyclization of the NCA monomer.[39, 40] The main culprits affecting polymerization are HCl and HCl salts of the amino acids.[39,41] During the early stages of polymerization the amino acid reacts very quickly with phosgene. After about 1/3 of the amino acid has reacted, the reaction slows due to the HCl salt of the amino acid forming from the HCl byproduct of cyclization.[15] Removing the HCl byproduct, either with N_2 stream or some other means, is necessary for pure NCA. If the HCl is not removed the ring may open (Scheme 3).[15, 42]

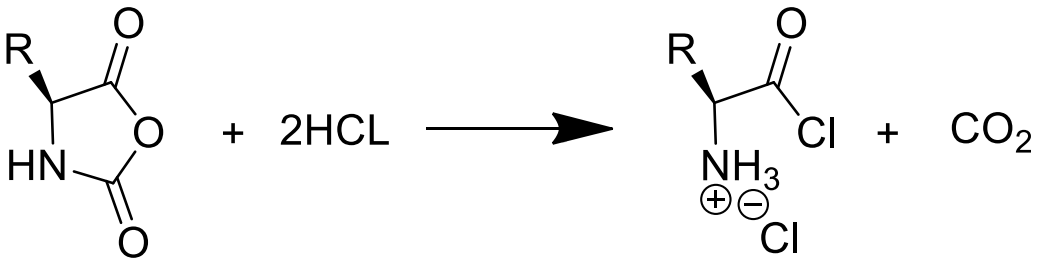

Scheme 3. Side reaction of NCA with excess HCl.

Purification of the NCA is very important, especially if the goal is high-molecular-weight polymer. To purify the NCA, a typical procedure includes precipitation in an alkane, followed by recrystallization.[15] To produce high molecular weight polymers the HCl w/w% needs to be less than 0.02%. Quantifying HCl content happens by boiling with nitric acid and titrating potentiometrically with silver nitrate. Block states adding silver nitrate and testing the turbidity is satisfactory for quick testing.[15] Several crystallizations decrease the HCl present, but if the

reaction is scaled up, the purity of the NCA dramatically decreases, the reaction time is much longer,[43] and recrystallizations are more difficult.[44] Figure 6 shows possible contaminants for a leucine NCA synthesis.

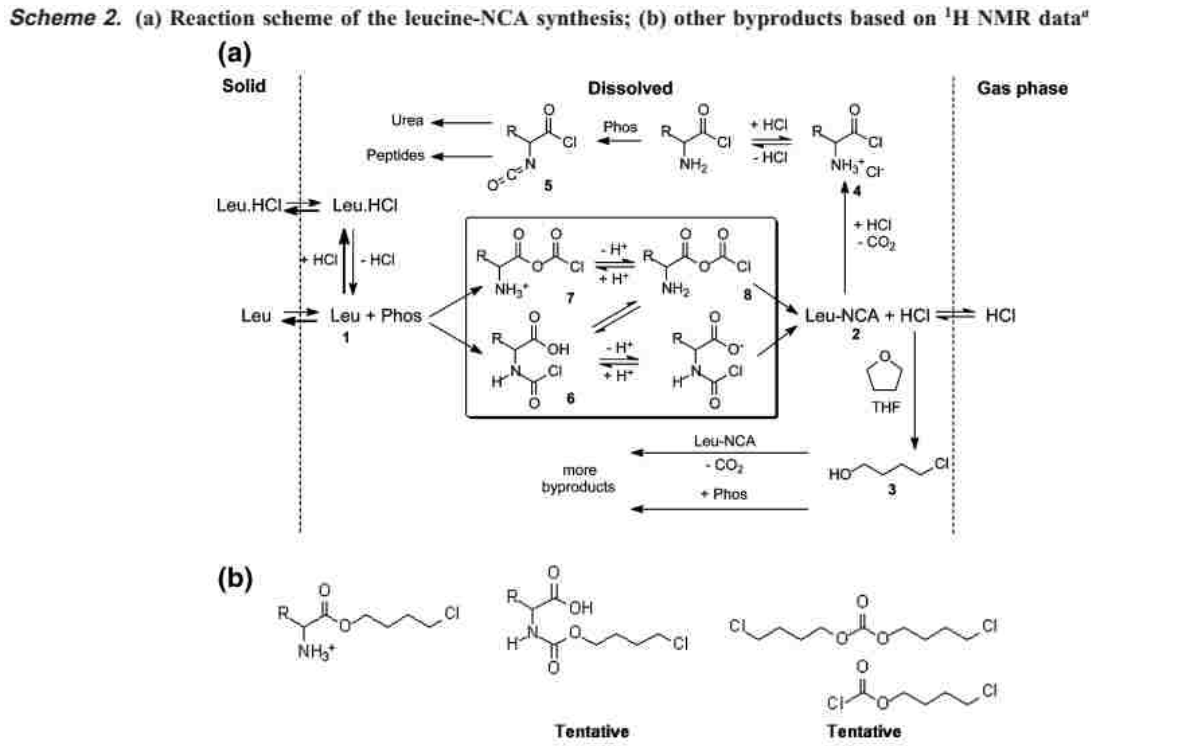

Figure 7. Leucine NCA synthesis with side products and their synthetic pathways. Reprinted with permission from Smeets, N. M. B.; van der Weide, P. L. J.; Meuldijk, J.; Vekemans, J.; Hulshof, L. A. *Organic Process Research & Development* 2005**,** 9, (6), 757-763. Copyright 2005 the American Chemical Society.

Other methods are capable of removing contaminants from the NCA. One option is sublimation, but some thermal initiation occurred.[45, 46] α-Pinene and limonene can consume HCl but can also create alkyl chlorides that can be laborious to remove.[47] Another NCA purification method is washing an ethyl acetate NCA solution with 0 °C aqueous bicarbonate to neutralize HCl and HCl salts.[48] This works well for some NCAs but can introduce water to initiate

polymerization. Rephosgenation, adding a second amount of phosgene, can be used to eliminate HCl but this can lead to isocyanates.[41]

Packing columns with multiple different materials such as activated charcoal, zeolites, or urea, with or without Ag_2O as a chloride scavenger decreased yield.[49] More recently, silica column chromatography separated pure NCA and side products for many different polypeptides.[49] This is most useful for NCAs that are not easily crystallized. With sufficient drying, the silica columns provided high yields of NCA and controllable polymer molecular weights.

1.3 NCA Polymerization

Purity of the NCA dictates polymerization characteristics: any impurities such as HCl and HCl salts can interfere with polymerization. NCAs lend themselves to two different possible ring-opening mechanisms, depending on the initiator and solvent conditions. The first discussed is the normal amine mechanism (NAM).

1.3.1 Normal Amine Mechanism

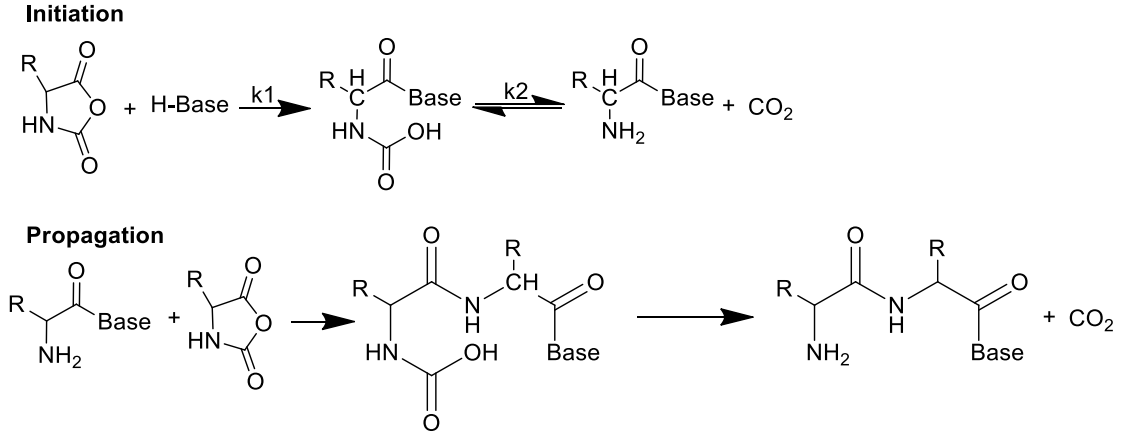

Scheme 4. Normal amine mechanism (NAM) for ring-opening polymerization of a NCA.

Nonionic initiators with more than one mobile hydrogen (basic hydrogen) initiate the normal amine mechanism of ring-opening polymerization of NCAs.[25] These initiators include primary amines, secondary amines, alcohols, and water. The initiator performs a nucleophilic attack on the #5 carbon in the NCA, opening the ring. The intermediate, carbamic acid, performs a decarboxylation, leaving a free amino group to propagate the polymerization (Scheme 4). Primary amines provide controllable molecular weights, with a low polydispersity index because they are more nucleophilic than the ω-amino group of the propagating species.[25] This makes initiation much faster than propagation, allowing control of the number average molecular weight (M_n) with the mole ratio of initiator to monomer.[50]

The NAM mechanism does not always provide controllable molecular weights. The equilibrium of the intermediate carbamic acid can affect the living nature of the polymerization. The carbamic acid can form a salt with the amino groups of the propagating chain, catalyzing the propagation step and inflating the kinetics,[46] but in dimethylformamide (DMF) the effect disappeared.[51] Following Le Chatelier's principle, performing the polymerization and removing the evolved CO_2 pushes the equilibrium away from the carbamic intermediate.[46] If CO_2 is not removed, the kinetics change.[52, 53] The kinetics can also change with the purity of the NCA. If highly pure NCA is used, the reaction has the typical two-stage kinetics, but are first order throughout the reaction if less pure NCA is used (Figure 8).[54] Data within the literature had conflicting reports; the best assumption is purity of the NCA has an effect on the polymerization.

Water can also initiate polymerization or hydrolyze the NCA into an amino acid.[55, 56] The rate of initiation or hydrolysis depends on temperature. Keeping the NCA in the freezer and using it quickly lowers the possibility of residual water initiating polymerization of the NCA, unless a large amount of water is present.[25] Initiation can even happen in the solid state.[57] A far

less studied issue with the NAM mechanism is the reaction of the initiator with the #2 carbon, forming an ureido acid.[25]

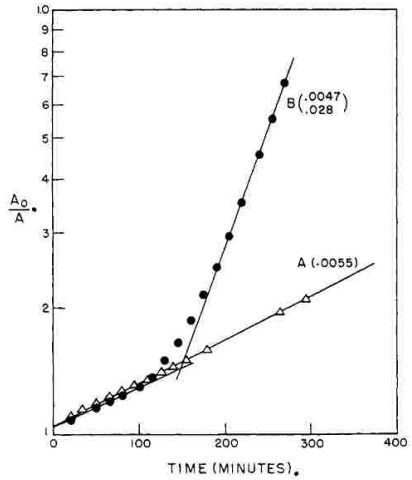

Fig. 1.—Polymerization of γ-benzyl-L-glutamate N-carboxy anhydride initiated with *n*-hexylamine ([A]/[I] = 20) in dioxane solution at concentration of 4 g./100 cc. at 25.0°. Case A corresponds to impure anhydride and case B to the same anhydride after one recrystallization.

Figure 8. Impure NCA follows first-order kinetics but if purified it shows a change in the kinetics after reaching a certain molecular weight. A_0 is the original anhydride concentration and A is the measured anhydride concentration. Reprinted with permission from Doty, P.; Lundberg, R. D. *Journal of the American Chemical Society* 1957**,** 79, (9), 2338-2339. Copyright 1957 the American Chemical Society.

1.3.2 Activated Monomer Mechanism

The other prevalent mechanism for NCA polymerization is the activated monomer mechanism (AMM). In contrast to the NAM mechanism, initiation for the AMM mechanism is by a secondary amine, tertiary amine, or an alkali halide. NAM has an additional step in the mechanism: pre-initiation. In pre-initiation, the initiator abstracts hydrogen from the #3N position in the NCA ring, creating an anion (Scheme 5). This is not a true initiation step, but rather the initiator acting as a catalyst.[25] This mechanism is limited to N-unsubstituted NCAs

because it requires hydrogen abstraction from the nitrogen. Once the anion forms and the dimer decarboxylates, the propagation proceeds with a stepwise addition of a NCA anion.

A few studies have confirmed the presence of the AMM mechanism. Radioactive labeling of the initiator allows identification of the different mechanisms for NCA polymerization.[50, 58] To confirm the AMM mechanism, diisopropylamine was used to initiate a sarcosine-NCA. Sarcosine-NCA, methylated at the #3N position, should not polymerize via AMM. Initiation did not happen, partly due to steric hindrance for the NAM mechanism and because the lack of a hydrogen to abstract.[59, 60] In the same study, γ-ethyl-L-glutamate NCA polymerized faster with diisopropylamine.

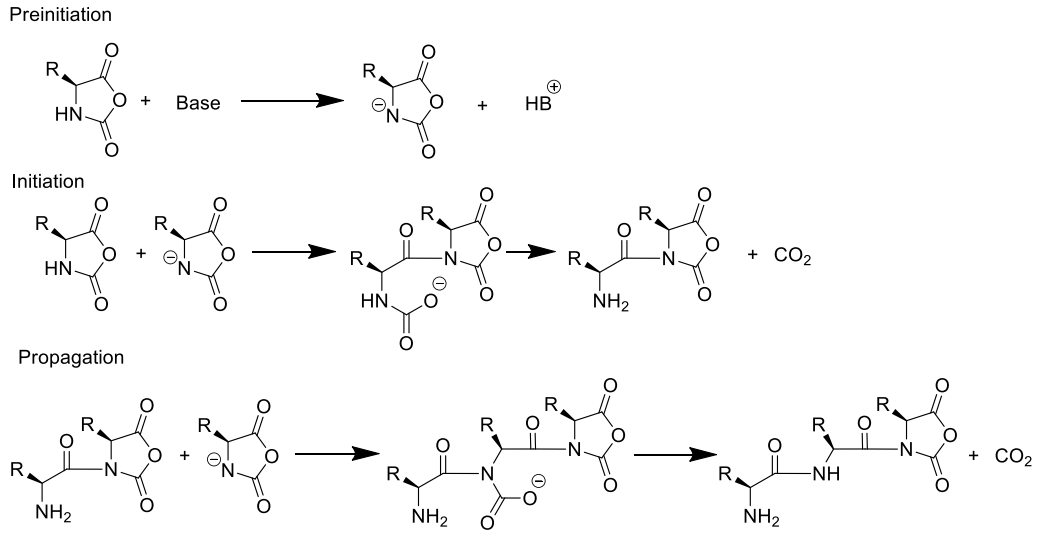

Scheme 5. Preinitiation, initiation, and propagation for activated monomer mechanism (AMM) ring-opening polymerization of a NCA.

Studies have also shown the AMM can happen even when the NCA is N-substituted; however, it is believed acidic impurities cause polymerization, either from the solution or from the NCA itself. In addition, #4C position is acidic and can protonate other NCAs, allowing the normal amine mechanism for polymerization of the sample.

A highly reactive NCA, proline was used to test the effect of impurities on the polymerization of NCAs. When highly purified proline-NCA was polymerized with a tertiary base, the reaction was slow; however, when not completely dry solvent was used, the reaction proceeded much faster.[61] This showed the pure proline-NCA was slowly proceeding via AMM in a dry solvent but via NAM in the presence of small amounts of water. If one desires the polymerization to proceed via AMM, the solvent and NCA must be free from impurities, even more so than for NAM. Water is not the only impurity; salts can affect the polymerization, LiCl was found to alter the AMM pathway.[59]

Overall, the AMM propagation is faster than NAM, thereby producing higher molecular weight polymers. This is due to the nature of AMM; the anionic NCA species is highly reactive. Conversely, the initiation step in AMM is slower than in NAM, increasing the PDI;[62] however, the polymerization still needs to "age" in order to have very high molecular weights.[51]

1.3.3 Metal-mediated Polymerization

Although ring-opening polymerization reactions of NCAs were the prototypical mechanism for peptide synthesis from the late 1940's to late 1990's, newer techniques have sometimes replaced them. Ring-opening polymerizations of NCAs provided high molecular weight polypeptides, but the polydispersity, PDI, was not well controlled or sometimes even known.[63-65] For self-assembly structures, the polypeptides need a well-defined molecular weight and PDI.[66] This can lead to efficient and controllable structure in solution, which, for example, is highly advantageous for controllable drug delivery.[66]

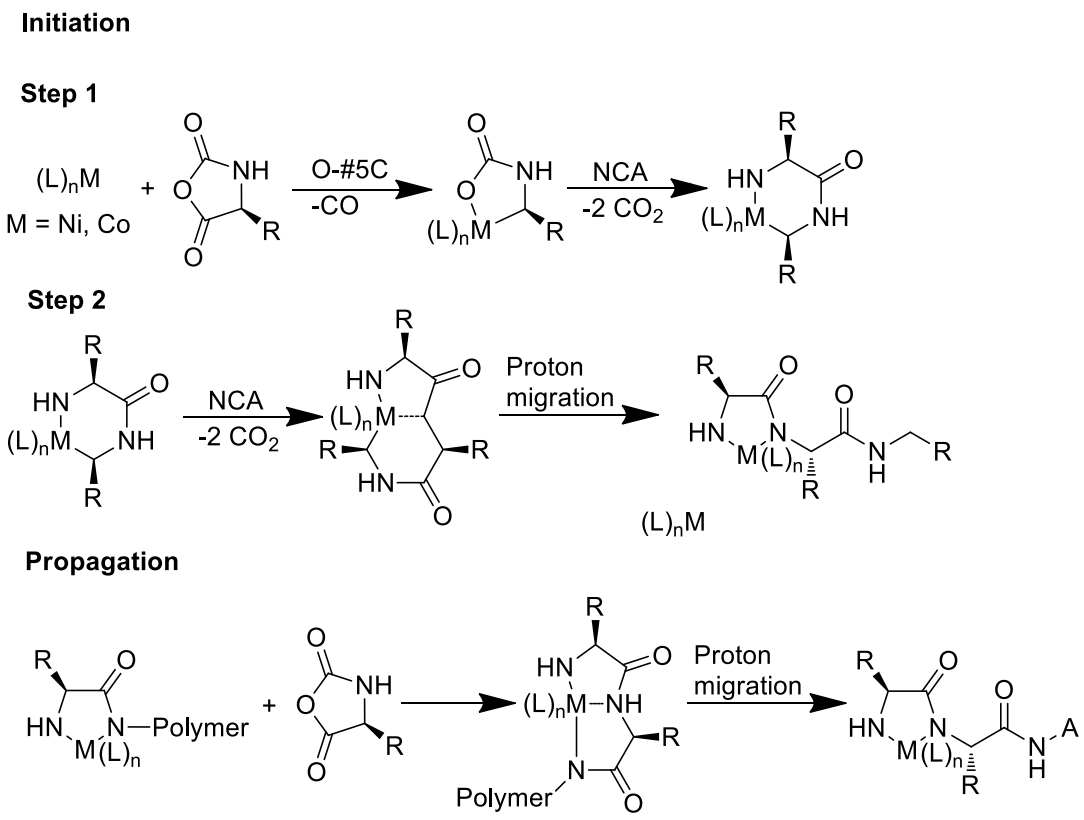

Scheme 6. Multistep initiation and propagation for metal-mediated NCA polymerization.

The reason NCAs do not have well-controlled polymerizations is the nature of the polymerization. Following initiation, the polymerization proceeds via the primary amine, carbamate, or NCA anion produced. This can lead to side reactions, such as chain termination or chain transfer.[67] Metal-mediated polymerizations have been used to better control molecular weight and PDI.

In a metal-mediated NCA polymerization, a metal end group replaces the primary amine, carbamate, or NCA anion (Scheme 6).[66] The early metal initiators synthesized were zerovalent nickel and cobalt, bpyNi(COD)[68, 69] and $(PMe_3)_4Co$.[70] During the multistep initiation, the zerovalent metal complexes perform an oxidative-addition reaction on the #5C position of the

NCA. Once this five-membered metallic ring forms, addition of another NCA gives a six-membered amido-alkyl metallacycle.[66]

Further reaction with NCA monomer contracts the five-membered amido-alkyl metallacycle by proton migration of the amide proton to the metal-bound carbon, completing the multistep initiation.[66] Once the amido-amidate complex forms, propagation follows by attack of the nucleophilic amido group on the #5C position of the NCA. This forms a new ring that undergoes proton transfer from the free amide to the amidate group, thus consolidating the ring to the amido-amidate propagating species. The polymerization proceeds in this fashion, keeping the reactive species "under control" to afford polymers with well-defined molecular weight and PDI.

Without fractionation, NAM or AMM exhibit less control than their metal-mediated polymerizations counterparts. After fractionation, NAM and AMM can produce polymers with very low PDI, and can best the PDI of metal-mediated polymerizations. Although fractionation is an added step to low PDI polymers, it may be easier than trying to remove a metal catalyst; however, with better control, metal-mediated polymerizations allow for more complicated architectures. This happens because the chain end is "living", or capable of adding more monomers to the polymer chain. Because of this, block copolymers,[71] stars, cycles, and other architectures have been synthesized.[25]

Metal-mediated NCA polymerization is not without drawbacks. First, adding a metal into the polymer solution requires its removal; dialysis against a chelating agent removes the metal.[72] Another issue is the C-terminus capping by the NCA that reacted with the metal (see initiation step 1 in Scheme 6). This limits polymerization and functionalization of other NCAs or

functional groups to the N-terminus. This problem was circumvented by having the first NCA that reacts with the metal have a latent functional group (Scheme 7).[73] Metal-mediated NCA polymerization opens the door to many functionalized peptides because it tolerates many different types of functionalities on the NCA.[74, 75]

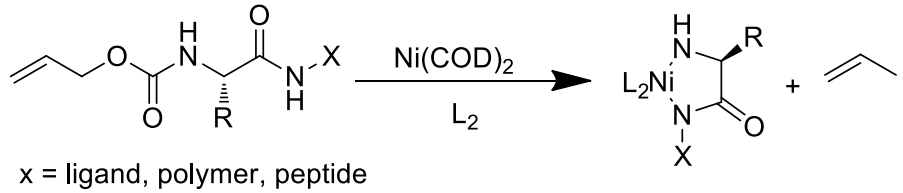

Scheme 7. Reaction of zerovalent metal with functionalized NCA precursor. This allows synthesis of block copolymers from the C-terminus of a polypeptide.

1.3.4 Other NCA Polymerization Techniques

Thus far, the discussion has included NCA polymerizations by primary amine, basic initiators, and metal-mediated NCA polymerization. While the metal-mediated polymerization does have some very distinct advantages over its predecessors, it is not perfect. This led others to investigate other methods for controllable polymerization of NCAs.

High-vacuum techniques (HVT) have been used to polymerize NCAs in a controllable manner (Figure 9).[76] The hypothesis was that impurities were making NCA polymerization difficult, whether in the solvent, NCA, initiator, or CO_2 released during the polymerization. Using HVT should minimize the possibility of trace impurities but not everyone agrees how HVT show controllable polymer characteristics. In addition, HVT can easily afford complex polymers from the C-terminus by choosing functionalized initiators, somewhat similar but easier to the metal-mediated polymerization.[76]

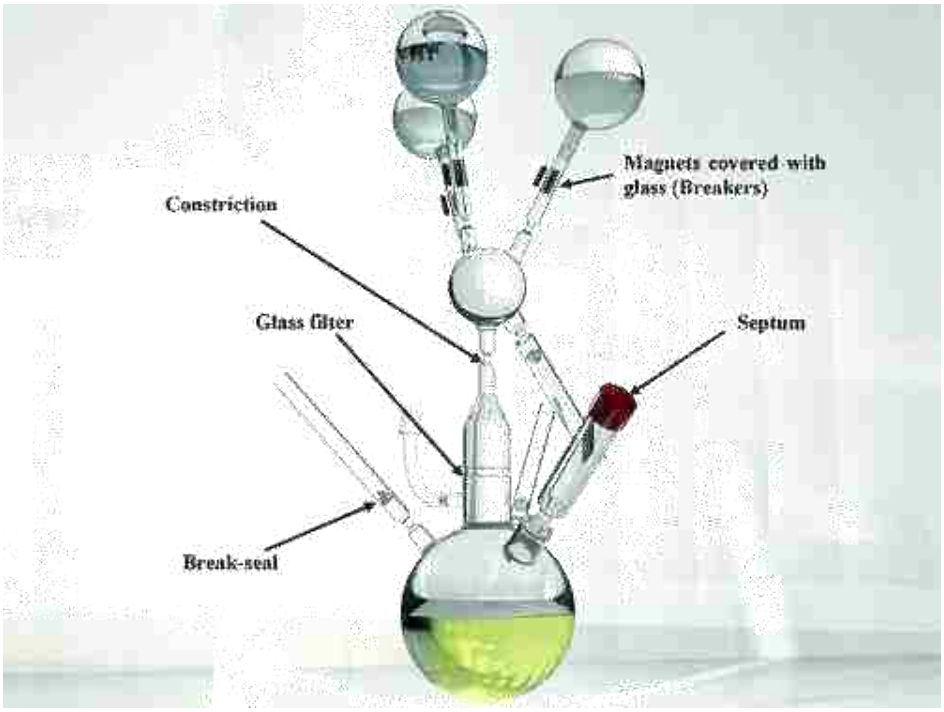

Figure 9. An illustration of the apparatus for the high-vacuum technique of NCA polymerization. See text for explanation. Reprinted with permission from Aliferis, T.; Iatrou, H.; Hadjichristidis, N. *Biomacromolecules* 2004**,** 5, (5), 1653-1656. Copyright 2004 the American Chemical Society.

In Hadjichristidis's apparatus, introduction of the sample happens through a septum. The solvent is vacuum distilled until the NCA is once again a solid. Freshly distilled DMF enters the flask following three recrystallizations of the NCA. Although the work-up of the completed polymer is easier for HVT, the difficulties lie in the glassware setup. HVTs were also used to study the details of primary amine-initiated NCA polymerization.[77] Performing end-group analysis of the oligopeptides elucidated the influence of impurities in the NCA polymerization. Impurities can come from solvent, the initiator, or the NCA itself. Normal glovebox practice led to many different types of chain ends. The observed products and possible termination products with DMF as a solvent are shown in Figure 9.[77] The end groups show the polymerization mechanism. Using a primary amine, NAM occurs for all three conditions in Figure 9; however,

AMM also occurs when glovebox techniques are used, showing unintended side reactions are occurring. Also, glovebox conditions lead to more types of "dead" chain ends — meaning the ends of the polymer are no longer reactive. This decreases molecular weight and increase PDI. Mass spectrometry cannot quantify the amount of dead chain ends, eliminating the possibility of understanding the exact influence on the molecular weight and PDI. This study shows the many possible side reactions possible for primary amines and why one might choose other NCA polymerization techniques, such as HVT.

If one does not have the technique of Blout and coworkers,[63, 64] does not want to remove metal initiators,[69] or does not have the specialized glassware required for high-vacuum techniques,[76] there are still more options for NCA polymerization. The problem with primary-initiated NCA polymerization are the possible products (see Figure 10); however, lowering the temperature of the reaction mixture these reactions can suppress side reactions.[78, 79] Unlike the previous study using mass spectrometry to detect dead chain ends, using non-aqueous capillary electrophoresis (NACE)[80] allows for a quantitative measurement of dead chain ends (formyl or carboxylate). Keeping the monomer/initiator ratio constant, decreasing the temperature from 50 °C to room temperature to 0 °C decreased the amount of dead chain ends from 80% to 78% to 1% respectively.[79]

Lowering the temperature allows primary amines to give controllable molecular weights and PDI, thus decreasing the amount of side reactions end capping the polymer chain. Also, block copolymers can be synthesized due to the living ends of the polymers.[78] Another simple option is to use urea as an initiator at 0 °C.[40] If one does not have a glove box or bag, a stream of nitrogen during the reaction allows well-controlled polymerizations.[81]

Sample	NAM	AMM	AMM_2	AMM_3	F_1	F_2	U_1	U_2	FU
HV	X					X			
GB1	X	X	X	X	X	X			
GB2	X	X	X	X	X	X		X	

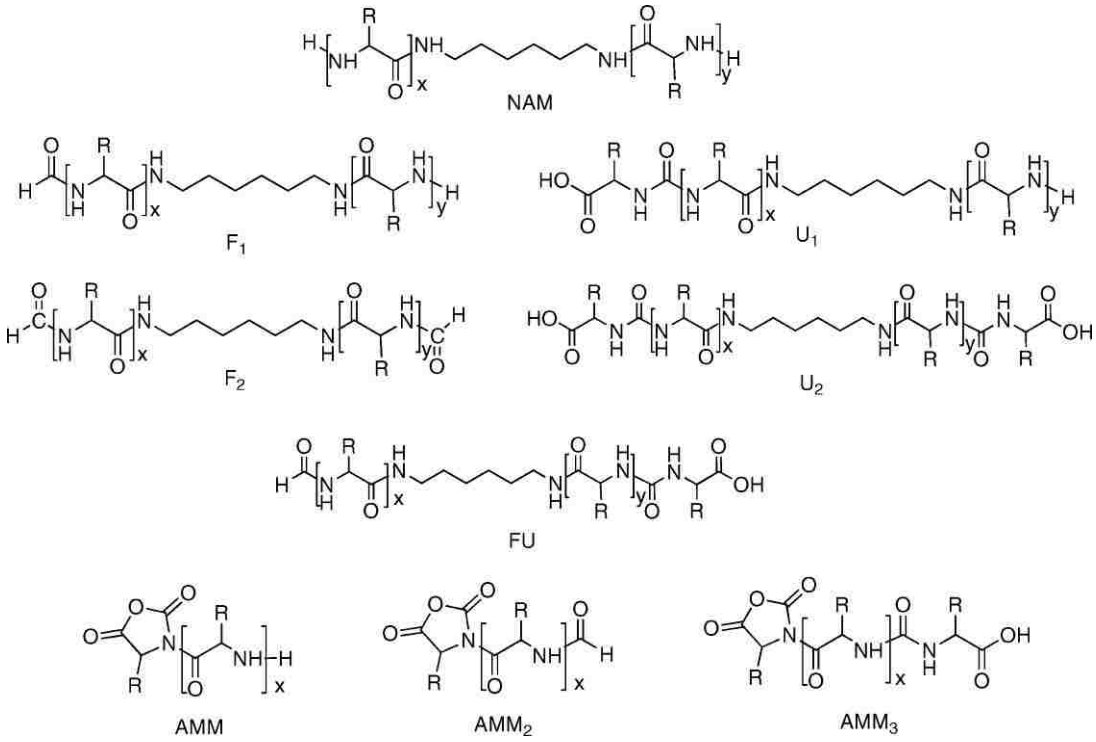

Figure 10. Possible byproducts in an NCA polymerization: HV = high-vacuum technique; GB = glovebox method; 1 = DMF was purified; 2 = DMF used as received; NAM = normal amine mechanism; AMM = activated monomer mechanism; F = formyl end-group; U = ureido acid end-group. Reprinted with permission from Pickel, D. L.; Politakos, N.; Avgeropoulos, A.; Messman, J. M. *Macromolecules* 2009**,** 42, (20), 7781-7788. Copyright 2009 the American Chemical Society.

A nitrogen stream allowed for higher conversions, closer to expected molecular weights and lowered the PDI. The rate of nitrogen flow could influence the kinetics of the reaction: a fast nitrogen flow increased the rate or reaction by 5×, still providing low PDI polymers.

Not discussed are several other pathways to polypeptides such as NCA polymerization via PCl_5, PCl_3, $SOCl_2$, sodium hydride, solid phase, etc.[6, 82, 83]

1.3.5 Choice Of NCA polymerization

The choice of NCA polymerization is dictated by the application needed for the polymer. If one wants to synthesize a less-controlled polymer, initiation by primary amine is adequate. Primary amine initiation is very useful because many initiators are commercially available. Also, some NCAs produce controllable molecular weights with low PDI, at least at low molecular weight. Using primary amine decreases the prep time needed to synthesize the polymer. Primary amine initiation provides polymers in high yields of low to mid molecular weights with a reasonable PDI (~1.2) after precipitation of the crude polymer. For some applications, a broad PDI is advantageous; a tertiary amine offers higher PDI and would work best. If the PDI is too broad for the desired application, separation techniques such as preparatory column separation can fractionate the polymer, providing many low PDI samples. If this decreases the yield of the desired molecular weight too drastically then other techniques are advantageous. If the reaction mixture can be cooled, the living nature of the polypeptide can be preserved and more complicated architectures can be synthesized (e.g. block copolymers).

If one's synthetic skills are more advanced, using metal mediated polymerization may provide polymers with lower PDI and higher molecular weights. If ease and time are more valuable, decreasing the temperature, using a nitrogen stream, or adding urea can help with polymerization. Ultimately, the method of polymerization distills to the type of polymer desired. High molecular-weight polymers require more care but lower molecular weight polymers are easier to synthesize. Scale-up can also be a factor when choosing a polymerization method. All of these methods have their place, but always search the current literature for other viable options.

1.4 Overview of Poly-γ-benzyl-L-glutamate

Poly-γ-benzyl-L-glutamate, is a very common polymer in the physical sciences. The layperson is more familiar with as its monomer, monosodium glutamate, or MSG. It was originally discovered by a Japanese biochemist who enjoyed his wife's soup.[84] Although this is not a commentary on the health effects of MSG, the food industry has made the monomer available in a grand scale.

Scientifically, PBLG is interesting because it is a helical polymer than behaves as a semi-rigid rod. The polymer was first synthesized by Doty *et al* and characterized in a series of papers.[54, 63, 64, 85-93] The chemical structure for PBLG is found in Figure 11 and PBLG has been studied in many different solvents (DCA[94], DMF[95-97], THF[98], m-cresol[86], pyridine[99]).

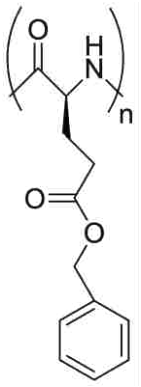

Figure 11. Structure of poly-γ-benzyl-L-glutamate, PBLG.

Being a stiff polymer, it is not highly soluble and depending on the solvent, PBLG can aggregate. When aggregated, PBLG can either aggregate in a head-to-tail or side-by-side fashion.[86, 100-102] A table of aggregation number, n, is found in Table 1. Aggregation is a problem for rod type polymers and limits the solvents studied.

Table 1. Aggregation number (n) of PBLG in various solvents

$M_w/10^{-3}$	n values			
	DMF	DCE	Dioxane	Chloroform
10	1	-	-	-
33	1	3	25	4
154	1	-	7	3
222	1	-	5	2

PBLG is helical only in a few solvents (DMF, cresols, pyridine) [99, 103, 104] and it is commonly used because the polymer is an un-aggregated helix. Parameters for the helix in DMF are well known[105] and phase diagrams have also been produced (Figure 13).[106, 107]

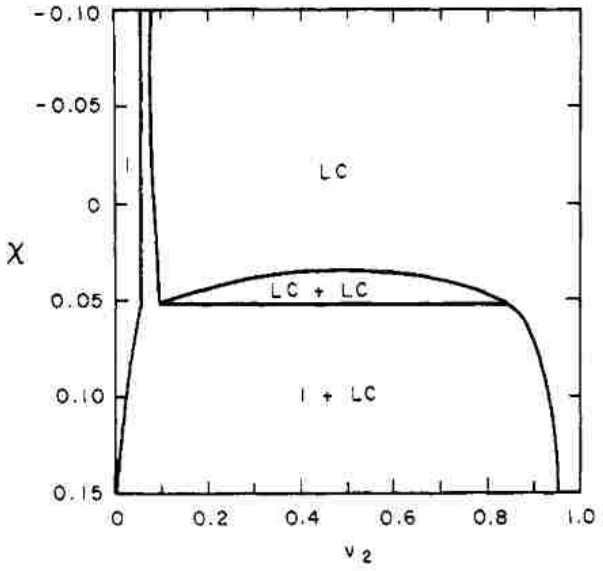

Figure 12. A binary phase diagram calculated for rigid, hard rods of axial ratio of 150 by Flory lattice model. (I) is isotropic phase and (LC) is a liquid crystalline phase. Reprinted with permission from Russo, P. S.; Miller, W. G. *Macromolecules* **1983,** 16, (11), 1690-1693. Copyright 1983 American Chemical Society.

The Flory lattice model predicts three regions for the phase diagram for rodlike polymers.[108] The first region is a biphasic region with isotropic and liquid crystalline regions, the second is a transition region, and the third has fully liquid crystalline regions with excluded solvent (see Figure 12).[109] There is some discrepancy between the Flory lattice model and the observed phase diagram for PBLG; this has been attributed to flexure of the polymer and flexible side chain-solvent mixing.[107] Liquid crystalline studies of PBLG have been performed in other solvents.[107, 109-112]

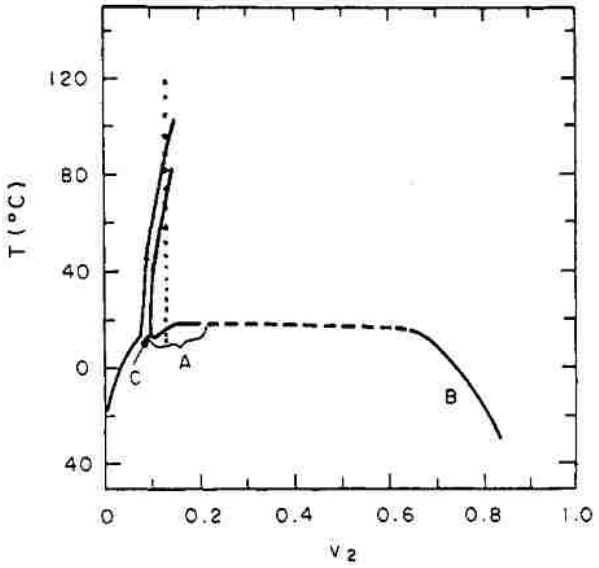

Figure 13. Temperature-composition phase diagram for PBLG in DMF. Reprinted with permission from Russo, P. S.; Miller, W. G. *Macromolecules* **1983,** 16, (11), 1690-1693. Copyright 1983 American Chemical Society.

PBLG has been shown to act as a stiff polymer in many experiments. The persistence length for PBLG is anywhere from 70 to ~300 nm.[97, 100, 101] A conformation plot (not in log scale) is found in Figure 14. Large molecluar weight PBLG shows a curvature, allowing the persistence length to be calcualted from Equation 1

$$R_g{}^2 = \frac{La_p}{3} - a_p{}^2 + \frac{2a_p{}^3}{L}\left[1 - \frac{a_p}{L}\left(1 - e^{-L/a_p}\right)\right] \qquad \text{Equation 1}$$

where L is the length of polymer and a_p is the persistence length. A single sample did not provide the entire gamut of molecluar weights but several samples were combined.

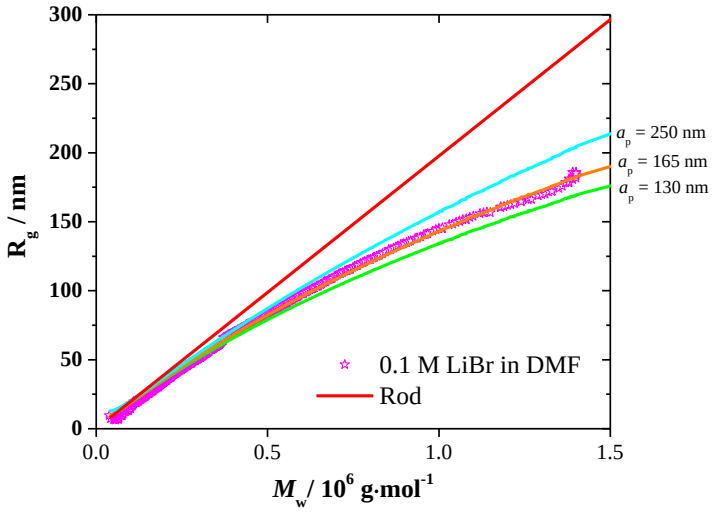

Figure 14. A plot of radius of gyration as a function of molar mass for PBLG in DMF. Reprinted with permission from Rafael Cueto.

Other experimental values show PBLG to be a rodlike polymer. The slope for a conformation plot in DMF was 0.78[96, 97] and for a Mark-Houwink plot the slope was 1.75 in DMF,[104] both consistent with a rodlike polymer. It was also shown stiff with viscosity,[85] analytical ultracentrifugation[104] flow birefringence,[15] and light scattering[95] and depolarized light scattering[113] Although many experiments have shown PBLG to behave as a rodlike polymer, it is not infinitely stiff; the best model for PBLG is of a flexible rodlike polymer.[15]

Although DMF is a helicogenic solvent for PBLG, it can be troublesome. It was found that an opaque gel could uncontrollably form;[114] water, even in low quantities, can cause aggregation.[115] At high concentrations, PBLG can form a gel in several solvents[114, 116, 117]

Although PBLG has been studied many times, it is not a perfect model polymer. PBLG shows some flexibility; it is only helical in a few solvents, and it is only soluble in a few solvents. DMF has been the usual solvent chosen but it is hydroscopic and PBLG has been shown to aggregate with low water content. This means the DMF used has to be dry and sample preparation need be more careful. Because of the difficulties associated with PBLG (and difficulty with other rods, for that matter), there lies an opportunity to synthesize a novel polymer that can combat these difficulties.

Chapter 2 - Synthesis and Characterization of PEGL in Dilute Solution

2.1 Introduction

As a quick review (see Chapter 1 for a more thorough explanation), NCA polymerization can be conducted in many ways. When NCA polymerization was first utilized, the two methods were normal amine mechanism (NAM) and activated monomer mechanism (AMM). Polymerization of NCAs with primary amines proceed via NAM because they are more nucleophilic than basic. Tertiary amines and strong bases proceed via AMM because they perform a base abstraction of the nitrogen in the NCA ring. These methods became highly developed over the years (over 60 years) and are still used today. Being the simplest NCA polymerizations to perform, they yield poly(amino acids) with fairly well controlled synthesis and acceptable PDI's for some applications. Both NAM and AMM can be used to synthesize a PEGylated (more properly, oligo-PEGylated) lysine, PEGL, which is the focus of this dissertation.

In addition to the two enduring NCA polymerization techniques, other methods to have been used such as metal-mediated NCA polymerization. This method of polymerization is more labor-intensive than either NAM or AMM, but it can afford polymers with better molecular weight control and lower PDI's.[27, 68, 72, 118, 119] The disadvantage is the metal initiator needs to be synthesized and removed. Despite these drawbacks, metal-mediated polymerization was used to synthesize high molecular weight PEGL with low PDI.

2.1.1 Justification of Project -- A New Stiff Model Polymer

PBLG is the semiflexible poly(α-amino acid) for rodlike polymer studies. It has been studied for over 50 years and in that time, many different experiments have determined its

properties. This does not eliminate novel experimentation with PBLG,[120] but PBLG does leave room for polymers that do not suffer the same drawbacks such as semiflexibility and difficult solvents. For example, DMF, a helicogenic, non-aggregating solvent for PBLG is hydroscopic. PBLG aggregates with low water content, making the use of the PBLG/DMF system difficult.

Designing a new stiff model polymer is a complicated problem. Conventional chemist thinking would lead to using a conjugated backbone but a conjugated backbone does not a stiff polymer make! Table 2 shows the persistence length (a measure of stiffness discussed shortly) of several different types of polymers. Poly(p-phenylene-benzobisthiazole) has a conjugated backbone but is not the stiffest polymer in the table. Another possible rodlike polymer is carbon nanotubes; while very stiff, they are not "polymer-like" enough. The same problem lies with other, less polymer-like stiff rods such as boehmite.[121]

Table 2. Persistence lengths for select polymers

Rod	**Persistence length, a_p (Å)**
Polystyrene (not a rod!)[122]	26
Bisphenol A polycarbonate[122]	20
Poly(*p*-phenylene-benzobisthiazole)[123]	640
DNA*[122]	1,100
Poly-γ-benzyl-L-glutamate†[122]	3,130
Single walled carbon nanotube[124]	>10,000
fd-virus[125]	22,000

* double helix in 0.2 M NaCl, † the persistence length varies with experiment type and investigator

The stiffest synthetic "polymer-like" polymer in the table is a poly(α-amino acid). The reason an α-helix is stiffer than a conjugated backbone polymer is demonstrated with an illustration: is a spring or a ribbon stiffer? It is clear the spring has a lower ability to bend axially. The ribbon, while stiff in a two-dimensional plane, can bend orthogonal to the plane of the ribbon. Try decorating a Christmas present with bow made of a spring! In the same fashion, the new model rodlike polymer should be a helix. It is unlikely that this new polymer is stiffer than PBLG but as long as it is nearly as stiff, it is still beneficial.

Using other stiff poly(α-amino acids) is not novel (i.e. DNA or PBLG analogs); peptide derivatives have been used for ages.[90, 126, 127] The difficulty with stiff polymers is the low solubility; single walled carbon nanotubes can take up to 40 hours of sonication to disperse.[128] A common practice has been to modify the stiff polymer to increase solubility. Frequently, poly(L-glutamic acid) is prepared by removing the benzoxy side chain, forming a water-soluble PBLG derivative. Typically, water solubility requires charge; while a charged polymer is not inherently unwanted, it adds unsolicited complication for some studies. In the late 1970's it was found the diffusion of charged polymers, polyelectrolytes, changed with salt concentration. If excess salt is present, the charges along the polymer are screened and the polymer diffuses in a well-defined manner; if the salt concentration is low, the apparent diffusion coefficient dramatically decreases to almost zero (Figure 15).[7]

The diffusion coefficients were measured by DLS. In that experiment, the two salt regimes are known as the fast-mode (high salt) and slow-mode (low salt). Literature is disharmonious concerning the cause of slow-mode diffusion. Due to confusion and adding complexity to our model system, charge should be excluded in these experiments designed to measure the fundamental solution properties of rodlike polymers.

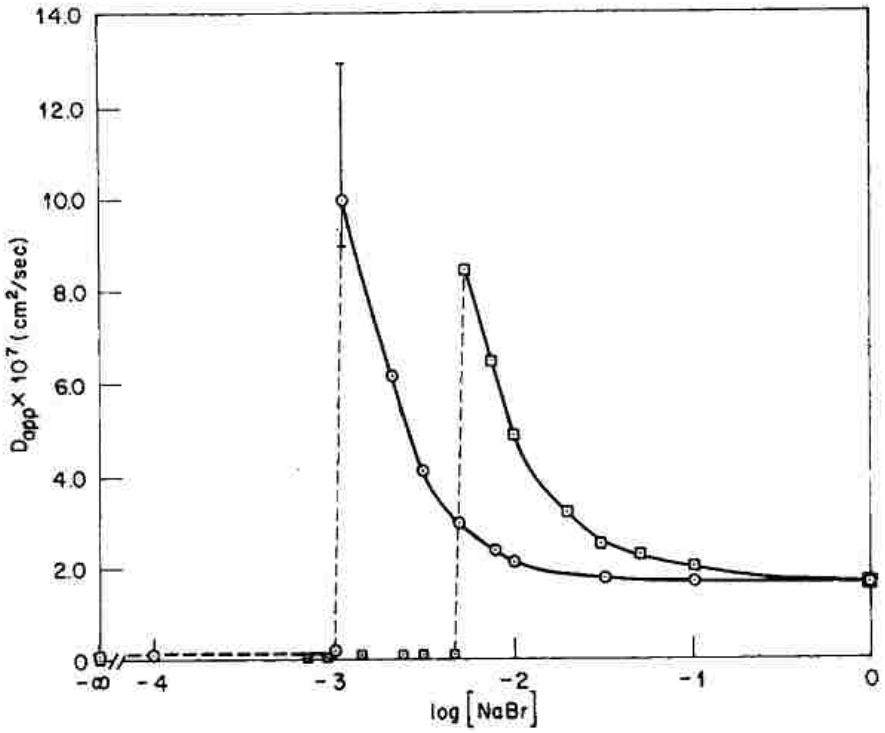

Figure 15. Apparent diffusion coefficient D_{app} vs log(NaBr) for poly(L-lysine)•HBr (D_p = 955) at 22-23 °C, and pH 7.8. Circles denote 1.0 mg/mL and squares denote 3.0 mg/mL. (Lys)n. From reference 7.

Following the arguments above, several criteria are required in designing a new model polymer and a water soluble, non-ionic, poly(α-amino acid) would fulfill all four requirements.

1) well-controlled synthesis
2) stiff polymer
3) no charge
4) solubility in "easy-to-use" solvents

2.1.2 Persistence Length

Persistence length, a_p, is a measure of stiffness for any flexing object (lightning has a persistence length). Stiff polymers have a large persistence length and random coil polymers

have a short persistence length (Table 2). Figure 16 shows a cartoon describing the persistence length. To calculate the persistence length, a vector is drawn along the first two backbone bonds of a hypothetically infinite length rod (Red arrow in Figure 1, along the x-axis). Repeat this procedure on the next set of two backbone bonds until reaching the last two repeat units (green lines on Figure 16). If the polymer is stiff, a large vector results in the direction of the x-axis because of the x-component of the vector projection for the many repeats units. If the polymer is a random coil, a large portion of the polymer does not add to the vector projection in the x direction, reducing the resultant vector length. The dotted orange lines show the representative persistence length for the stiff and random coil polymers.

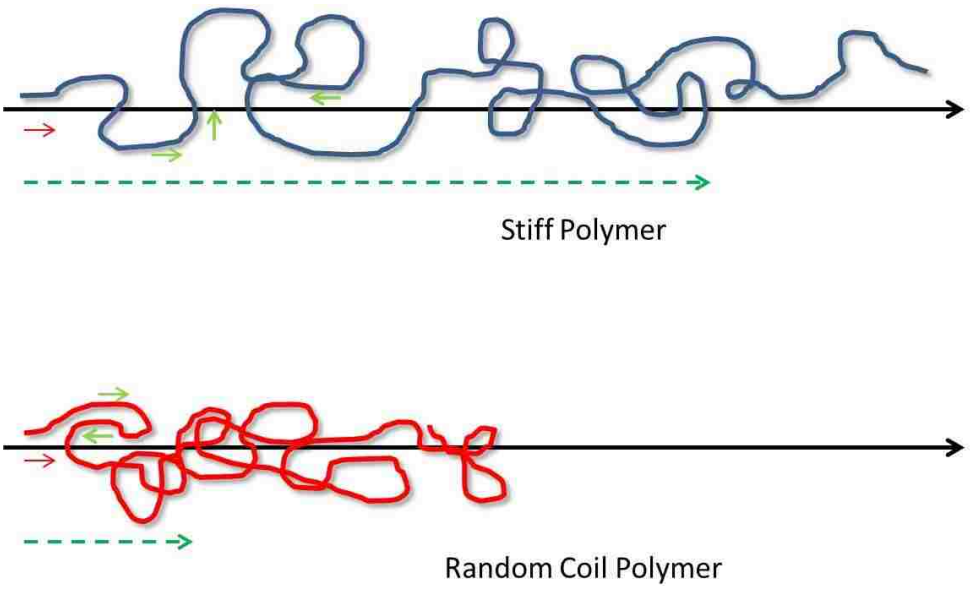

Figure 16. A cartoon of persistence length. The blue stiff polymer has a longer persistence length than the red random coil. The persistence length is denoted by the dotted orange line.

Many different experiments can measure persistence length: light scattering, flow dichroism, cyro-electron microscopy, scanning force microscopy, force-measuring laser tweezers, transient electric birefringence, transient electric dichroism and gel permeation

chromatography.[129] To measure the persistence length the polymer needs to be large enough to have appreciable flexure and investigation needs to include a large range of molecular weights.

Although persistence length is an inherent quality of the polymer, shorter chains do not show enough flexure to measure the persistence length. An analogy is a steel beam: if the beam is 1 inch long, beam flex cannot be perceived. Obvious flexure occurs if the beam is 1 mile long. Following this argument, low molecular weight polymers do not flex enough to measure the persistence length. To measure the persistence length, large molecular weight polymers need to be synthesized.

A requirement for accurate measurement of the persistence length by gel permeation chromatography is a wide breadth of molecular weights need to be measured that exhibit adequate flexure. Normally, a well-controlled polymerization provides low PDI. For a persistence length calculation, a broader molecular weight distribution provides the larger breadth of polymer molecular weights, eliminating the need for a low PDI, well-controlled polymerization. If only low PDI samples are available, a cocktail of several molecular weights can span the necessary molecular weight range. In this dissertation, gel permeation chromatography replaces a polymer cocktail. Column chromatography fractionates the polymer, giving many "slices" of highly monodisperse polymer molecular weights. This provides many different molecular weights with low PDI, allowing for an accurate determination of the radius of gyration and molecular weight. As long as the polymer is large enough, GPC eliminates the need to create a cocktail of several different molecular weights with low PDI.

2.2 Synthesis of PEGL

2.2.1 Materials

2-[2-(2-methoxyethoxy)ethoxy]acetic acid (> 90% technical grade), N-hydroxysuccinimde (98%), methylene chloride (> 99.8%), dicyclohexylcarbodiimide (98%), Bis(1,5-cyclooctadiene)nickel(0), and 2-2'-bipyridine (> 99%) were purchased from Sigma-Aldrich. THF (non-anhydrous, chromatography grade) was purchased from Macron chemicals. N_{α}-Z-L-Lysine (CAS number: 2212-75-1) was purchased from BACHEM. All dry solvents were dried by passing through an activated alumina column under argon and all purchased chemicals were used with no further purification.

2.2.2 General

Gel Permeation Chromatography

The molecular weight and polydispersity index were measured using a Wyatt DAWN DSP-F GPC/MALS detector equipped with a Helium-Neon laser, 632.8 nm. Two ISCO 500 mL pumps were used to prevent pulsing during pumping, the sample was injected manually, and the columns were PL Aquagel-OH Mixed 8 μm (2x) protected by a PL Aquagel 8 μm guard column. A Waters 410 differential refractive index detector was used and the samples were analyzed with ASTRA 6. The specific refractive index increment, d*n*/d*c*, was found to be 0.126 ± 0.001 mL/mg at 632.8 nm. Samples were dissolved in the mobile phase (denoted as *buffer* in the text), 200 mM $NaNO_3$ + 10 mM NaH_2PO_4 + 2 mM NaN_3 adjusted to pH 7.5 or 2 mM aqueous azide solution (denoted as *water* in the text). The injected volume was 100 μL and the flow rate was 0.5 mL/min. The weight average molecular weight and its standard deviation were calculated from three or more repeat measurements unless otherwise stated.

^{1}H NMR Spectra.

^{1}H NMR spectra were acquired on either a Bruker APX 250 MHz or Bruker DPX-400 400 MHz spectrometer at 25 °C. The product was dissolved in $CDCl_3$ for all reactants except for the formed polymer was dissolved in D_2O.

FT-IR

FT-IR spectra were collected on two different systems. The first was a Bruker Tensor 27 instrument with a Pike diamond/ZnSe ATR cell. The other was a Bruker Alpha FT-IR system with a diamond ATR accessory. The spectra were collected with OPUS 7.2 with an ATR cell. The background measurement was subtracted from the sample measurement.

Circular Dichroism

Circular dichroism spectra were taken on a Jasco J-815 spectrophotometer with a 0.1 cm path length cell and scanned from 180 to 250 nm. Sample concentrations were 0.5 mg/mL in water. CD spectra were not collected in the *buffer* solution because of absorbance in the scanned wavelengths. The background water absorption was subtracted using SpectraManager software and the data were saved as a text file. After importing the text file into Excel, the percent helicity was calculated based on a theoretical value of the mean molar ellipticity at 222 nm.[130]

Partial Specific Volume

Measurements were performed on a DMA 58 density meter with a DURAN 50 glass oscillator. The calibration was performed with boiled (30 min) Nanopure water. Following calibration, the polymer samples were injected from lowest to highest concentration. Between each sample, the density meter was cleaned profusely with water and then rinsed with ethanol to prevent dilution or contamination. Bubbles were prevented by slowly injecting the sample

because bubbles can cause erroneous measured values. The sample concentration region was 0.25 to 1 weight percent polymer.

Viscosity

Experiments were performed on an Anton Paar AMVn automated microviscometer. The steel ball used had a capillary diameter of 1.60 mm. Boiled Nanopure water was used as the calibrant. The polymer sample was pulled into the capillary by a pipet bulb, slowly to prevent bubble formation. Polymer samples were measured from least to most concentrated with copious amounts of water and then finally rinsed with ethanol. During each experiment the viscosity was calculated from 10 repeat runs and then averaged. This was repeated at least three times.

Mass Spectrometery

Mass spectrum experiments were performed on a MALDI-TOF system in linear mode. A Nd-YAG laser was used at 1 kHz, 500 shots, and an ion voltage of 25 kV. The matrix was α-cyano-4-hydroxycinnamic acid (CHCA), dithranol, or sinapinic acid. The mass range measured varied from 400 – 50,000 Da.

Optical Microscopy

Microscopy was performed on an Olympus BH2 polarizing optical microscope with a digital AmScope Camera (Model MD 1900-CK). Images were captured with software provided by AmScope. Samples were placed in Vitrocom flat capillary cells (of varying width and height).

Cell Viability

To test cell viability, PEGL was dissolved in Dulbecco's modified eagle medium (DMEM) with 10% fetal bovine serum (FBS) and placed in a plate well that housed 30,000 3T3

mouse fibroblast cells. Polymer and dead control were performed to ensure the measured fluorescence was not due to polymer.

Electron Microscopy

Cryo-transmission electron microscopy (cryo-TEM) was performed at Tulane University with a FEI G2F30 TECNAI TEM with a GATAN Cryo-System (-170 °C, 200 kV). The samples were dissolved in DI water and a single drop of the solution was placed on a Lacey carbon grid. The grid was placed in a FEI Vitrobot Mark III with 100% humidity at room temperature. The grid was blotted with filter paper and then plunged into liquid ethane.

Dynamic Light Scattering

DLS measurements were made on a custom-built apparatus[113] that is now equipped with an ALV5000 autocorrelator. The experimental setup is a two-pinhole-plus-lens with homodyne detection.[131] An Argon ion laser was (488 nm) focused in the sample using a lens with an 8 cm focal length and measurements were made at multiple angles by moving a detector arm. The correlation function was converted to electric field autocorrelations by the Siegert relation and the decay rates were found by taking the third-order cumulant fit (unless otherwise denoted in the text). Decay rates less than 0.5 μs were ignored due to detector afterpulsing and dead time. Polymer samples were allowed to dissolve overnight with solvent that had been filtered with a 0.1 μm PVDF filter. The polymer samples were placed in the DLS cells via a syringe fitted with a 0.22 μm PVDF filter. All polymer samples in water had a final concentration of 2 mM sodium azide to inhibit microbe growth.

2.2.3 Synthesis of N-Hydroxysuccinimidyl 2-[2-(2-methoxyethoxy)ethoxy]acetate (Figure 17, 4)

A mixture of 2-[2-(2-methoxyethoxy)ethoxy]acetic acid (30.01 g, 168 mmol) and N-hydroxysuccinimide (21.4 g, 185.0 mmol) was dissolved in dry THF (1000 mL) in a round-

bottom flask while in an ice bath. Dicyclohexylcarbodiimide (36.4 g, 176.7 mmol) was added while stirring. A white precipitate formed quickly and the reaction was stirred for 2 h before being placed in the freezer for 24 h. The white solid was filtered and the filtrate was concentrated with a rotoevaporator without heating until it was an oil. The oil was dissolved in a small amount of THF (~20 mL) and allowed to stir for another 2 h and then chilled in the freezer. This concentration and redissolution procedure was repeated until a clear oil was obtained with no precipitate. ^{1}H NMR (CDCl3): δ 4.52 (s, -OC(O)C$\underline{H}_2$O-, 2H), 3.7 (m, -C$\underline{H}_2$O(C$\underline{H}_2$C$\underline{H}_2$O)$_2$-, 8.9H), 3.38 (s, -CH$_2$OC$\underline{H}_3$, 2.84H), 2.85 (s, -C(O)C$\underline{H}_2$C$\underline{H}_2$C(O)-, 4.8H).

2.2.4 Synthesis of N_{ε}-2-[2-(2-methoxyethoxy)ethoxy]acetyl-N_{α}-Z-L-Lysine (Figure 17, 6)

To a mixture of N_{α}-Z-L-Lysine (40.1 g, 143.0 mmol) and $NaHCO_3$ (18.0 g, 220 mmol) in THF:H_20 (1,000 mL:1,000 mL) was added N-hydroxsuccinimidyl 2-[2-(2-methoxyethoxy)ethoxy]acetate (32.6 g, 118 mmol) predissolved in THF (60 mL). The reaction stirred overnight at room temperature and was brought to pH 2 by concentrated HCl. The THF was evaporated and a white precipitate formed after being in the freezer overnight. The solid was filtered and recrystallized in 80 mL hot isopropanol twice to yield white crystals. The yield was 60% (31.6 g) and had a melting point of 106.5-107.3 ºC, significantly less than previously reported (115-117 °C).[72] ^{1}H NMR ($CDCl_3$): δ 7.34 (m, -CH$_2$C$_6\underline{H}_5$, 5.33H), 5.18 (s, -C$\underline{H}_2$C$_6$H$_5$, 0.8H), 4.41 (-NHC$\underline{H}$(R)C(O)OH, 0.33H), 3.97 (m, -NHCH((CH$_2$)$_3$C$\underline{H}_2$NHC(O)R)C(O)-, 1.65H), 3.65 + 3.32 (m, -C$\underline{H}_2$O(C$\underline{H}_2$C$\underline{H}_2$O)$_2$C$\underline{H}_3$, 12.6H), 1.85 (m, NHCH((C$\underline{H}_2$)$_3$CH$_2$NHC(O)R)C(O)-, 6H).

2.2.5 Synthesis of Nε-2-[2-(2-methoxyethoxy)ethoxy]acetyl-Nα-Z-L-Lysine-N-Carboxyanhydride, EGL NCA (Figure 17, 8)

To a solution of N_{ε}-2-[2-(2-methoxyethoxy)ethoxy]acetyl-N_{α}-Z-L-Lysine (6) (3.0 g, 6.8 mmol) in anhydrous CH_2Cl_2 (150 mL) under argon was added 1,1,-dichlorodimethylether (2.40

mL, 27.5 mmol) via syringe. A room temperature condenser was attached and then purged with N_2 for 20 min. The solution was heated to 50 ºC for 15 h and the solvent was removed. A slight yellow oil resulted. The oil was recrystallized by bringing into a glove box, dissolving in THF as vigorously as possible, layering hexane on top of the THF. The flask sat for 24 h with a few slight "swishes" to stir the THF and hexane, but still keeping two layers. White crystals formed at the interface of the THF and hexane. The hexane was decanted by pipet and the THF was evaporated, giving white crystals and a yellow solid on the bottom of the flask. The white crystals were collected (1.89 g, 84%). ^{1}H NMR($CDCl_3$): δ 4.31 (m, NHC<u>H</u>(R)C(O)O-, 0.42H), 4.0 (m, -NHCH((CH_2)$_3$C<u>H$_2$</u>NHC(O)R)C(O)-, 5.42H), 3.65 + 3.32 (m, -C<u>H$_2$</u>O(C<u>H$_2$</u>C<u>H$_2$</u>O)$_2$C<u>H$_3$</u>, 8.7H), 1.85 (m, NHCH((C<u>H$_2$</u>)$_3$CH$_2$NHC(O)R)C(O)-, 6H).

2.2.6 Synthesis of Poly(N_ε-2-[2-(2-methoxyethoxy)ethoxy]acetyl-N_α-Z-L-Lysine), PEGL (Figure 17, 9)

In a glove box, EG_2-Lys NCA (750 mg, 2.25 mmol) was dissolved in THF (5 mL) and 78 μL aliquot of 63.7 mmol Ni(bpy)COD in THF was added. The reaction stirred for 48 h at RT. The conversion was monitored by FT-IR. Following full conversion, the THF was evaporated and the resultant clear polymer was dissolved in H_2O (10 mL). Dialysis was performed (10,000-12,000 molecular weight cutoff) for 2 days against 10 molar EDTA and 2 days against water. After removal of the H_2O, the polymer varied from a soft wax-like texture to very sticky (619.5 mg, yield 82.6%). ^{1}H NMR($CDCl_3$): δ 7.20 (br, -N<u>H</u>, 0.763) δ 5.25 (br, NHC<u>H</u>(R)C(O)O-, 0.7559H), 3.95 (m, -NHCH((CH_2)$_3$C<u>H$_2$</u>NHC(O)R)C(O)-, 2.77H), 3.65 + 3.35 (m, -C<u>H$_2$</u>O(C<u>H$_2$</u>C<u>H$_2$</u>O)$_2$C<u>H$_3$</u>, 14.6H), 1.55 + 1.917 (br, m, NHCH((C<u>H$_2$</u>)$_3$CH$_2$NHC(O)R)C(O)-, 6H).

2.2.7 Synthesis of Ni(bpy)COD

Bis(1,5-cyclooctadiene)nickel(0) (2.76 g, 10.0 mmol) and 2-2'-bipyridine (1.67 g, 10.7 mmol) were dissolved in 150 mL dry THF. The reaction stirred for 3 hours to give a deep blue

color. The solution was filtered and the filtrate was evaporated. The solid Ni(bpy)COD was washed with 80 mL diethyl ether and hexanes and filtered. The solid product was stored as a solid in the freezer under nitrogen atmosphere. Yield: 79%.

Another technique used involved making fresh Ni(bpy)COD prior to every reaction. Bis(1,5-cyclooctadiene)nickel(0) and 2-2'-bipyridine in 1:1 molar ratio were stirred overnight and used without purification.

2.2.8 Reaction Scheme for the Synthesis of PEGL

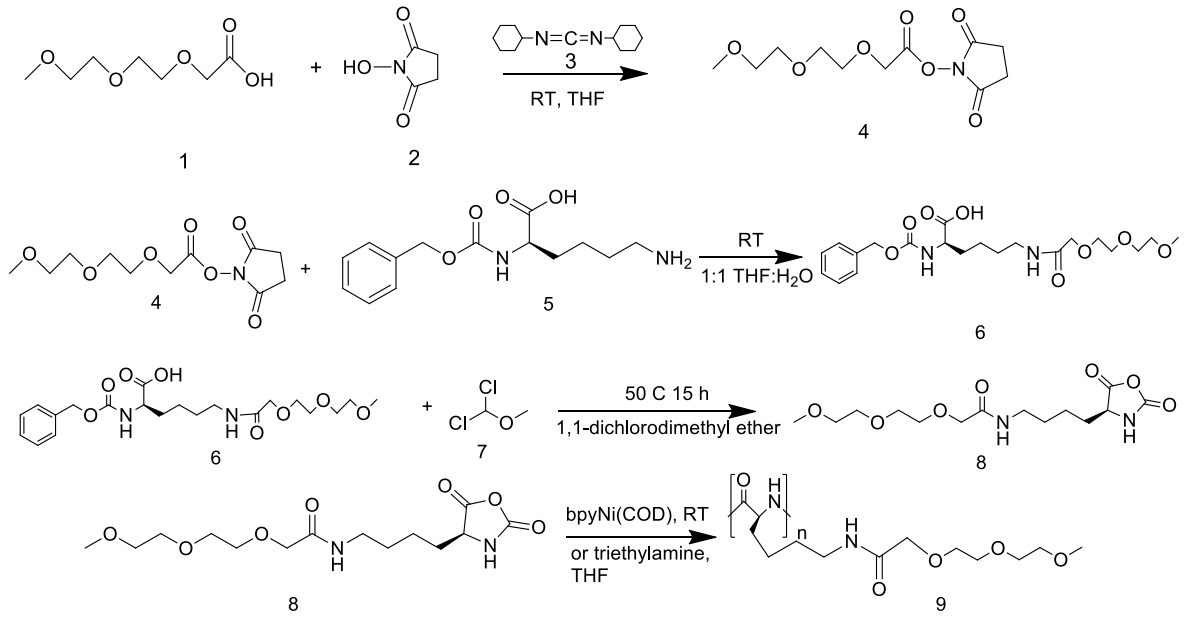

Figure 17. Reaction scheme for PEGL synthesis.

2.2.9 Crystal Structure of PEG-Lys NCA

The crystal structure for N_{ε}-2-[2-(2-methoxyethoxy)ethoxy]acetyl-N_{α}-Z-L-Lysine (6) is found in Figure 18. Not only does the crystal structure confirm the reaction was complete, it shows the PEG side chain bends backwards, towards the aliphatic chain of lysine. It is stabilized by hydrogen bonding to the nitrogen of the amide bond connecting the PEG to the lysine.

Logically, in an aqueous system the PEG chain should try to “cover up” the hydrophobic side chain. This same phenomenon is observed in the crystal structure for EGL NCA. The two conformations seen were in a 1:1 ratio and may indicate why recrystallization of the NCA can be difficult. It is likely this back-bending of the PEG chain would occur in the polymer as well but not certain due to steric hindrance.

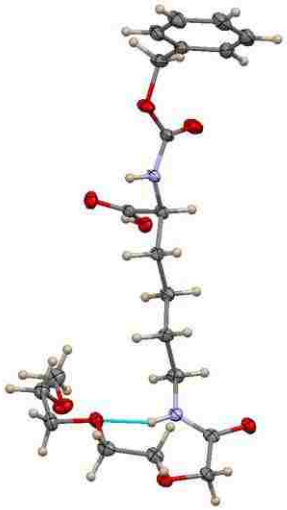

Figure 18. Experimental crystal structure for N_{ε}-2-[2-(2-methoxyethoxy)ethoxy]acetyl-N_{α}-Z-L-Lysine (6). Gray atoms are carbon, white are hydrogen, red are oxygen, and purple are nitrogen. The blue line is a hydrogen bond between the side chain nitrogen and an oxygen group of the short PEG chain.

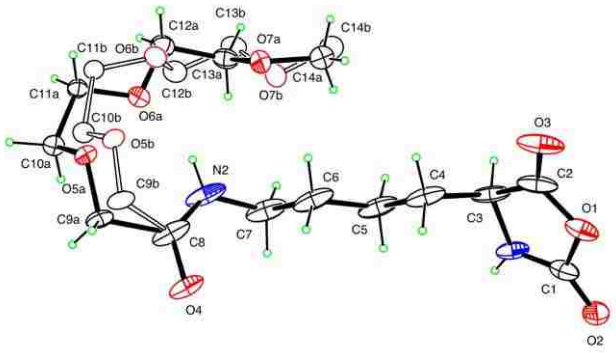

Figure 19. Experimental crystal structure for PEGL NCA. There are two different crystals in a 1:1 ratio. The unit cell if Orthorhombic, $P2_12_12_1$.

2.3 Tips For Synthesis

Although the synthesis is described above, a few tips may ensure success. To begin, confirm all the solvents are dry by Karl-Fisher titration or other highly sensitive measurement. Also, the glass needs to be flame-dried. Some water was noticed if the flask was only left in the oven, even overnight. During synthesis of N-Hydroxysuccinimidyl 2-[2-(2-methoxyethoxy)ethoxy]acetate (4), allowing the reaction to stir longer before filtration in the first step did not increase the yield of the reaction. Typically, stirring too long causes the product to become yellowed (slight yellow hue to very yellow). More as an anecdote, the yellow product never afforded N_ε-2-[2-(2-methoxyethoxy)ethoxy]acetyl-N_α-Z-L-Lysine (6). Other chemistries are available to produce N-Hydroxysuccinimidyl 2-[2-(2-methoxyethoxy)ethoxy]acetate (4), such as synthesis of an acid chloride. The acid chloride has been completed successfully with high yields and greatly decreases the time required for this first step (30 min vs. several days). The acid chloride was not attempted on a typical scale of the acetate; therefore the acetate was still the reaction of choice. It was recently found in our lab that the acid chloride can be successfully used in a 50 g scale. Further, the acetate oil should be used quickly (a few days if

stored in the refrigerator). If the oil was allowed to sit at room temperature and room light, the oil had a tendency to turn yellow. Once again, the yellowish oil barely reacts in the next step. Carbon-black successfully removes the color but the next step in the synthesis still does not work well.

The synthesis of N_{ε}-2-[2-(2-methoxyethoxy)ethoxy]acetyl-N_{α}-Z-L-Lysine (6) was more straightforward. The white solid product was easily crystallized if the procedure was followed. Sometimes, the reaction does not proceed when the N-Hydroxysuccinimidyl 2-[2-(2-methoxyethoxy)ethoxy]acetate (4) oil was yellow. Occasionally, when the solid product was crystallized, a yellow oil was observed. It was difficult to separate the crystal and oil, lowering the yield of product. Allowing the reaction to stir longer did not eliminate the yellow oil. Also, the white solid can have a slight pink hue. This can be rectified by stirring with carbon-black but the pink product did not provide easily crystallized NCA. During the recrystallization, several solvent-nonsolvent combinations were used, such as methanol and ether, but hot isopropanol was most successful at separating the products from unreacted lysine. The melting point was lower than published (expected 115-117 °C).

The ring-closure and purification of the lysine NCA was the most difficult step of the polymer synthesis. Alteration of the published synthesis provided the best results and others have noticed this as well.[132] Dichlorodimethyl ether was used because it is a gentle cyclization agent. Other cyclization agents, such as phosgene, create more side reactions. Initially, the amount of cyclization agent to lysine was 1:1 and the reaction was heated at 50 °C for 48 h; this provided the recurrent yellow oil. Reflux overnight with 3:1 ratio of cyclization agent to lysine provided the best results. Recrystallization of the NCA product was poor if the oil turned yellow during reflux. The NCA was recrystallized in THF and hexane; because they are miscible,

hexane was added very slowly to a semi-dilute NCA solution in THF. Crystals formed at the interface after sitting for ~24 hours at room temperature (this can be done in the freezer, but be careful to use a refrigerator rated for volatile solvent storage). Gentle stirring, causing visible crystallization of the NCA (the solution would become cloudy), increased the yield to a maximum of 84%. The hexane was decanted and the THF evaporated. White crystals formed on top of a yellow solid and were separated. Typically, the NCA crystals needed to be recrystallized multiple times in 3:1 hexane:THF to provide a highly pure NCA. If the NCA was not pure, the polymerization was hindered. An alternate procedure for NCA purification is column chromatography.[49] A primary crystallization by adding 3:1 hexane:THF and putting in the freezer overnight produced crude, yellowish crystals. These crystals are purified through column chromatography. The two-layer crystallization (providing white crystals on top of yellow solid) was not able to be scaled up but the column chromatography can be scaled as large as needed. This means that large quantities of NCA can be purified in a single sitting. The polymerization proceeds as long as the NCA was pure (white, needle like crystals).

2.4 ^{1}H NMR of PEGL

Although the ^{1}H NMR performed was consistent with the structures expected, the integration of the backbone proton, NHCH(R)C(O)O-, was frequently low. Varying delay times, up to 15 seconds, still produced a low integration value.

The reaction for N-Hydroxysuccinimidyl 2-[2-(2-methoxyethoxy)ethoxy]acetate (4) can be easily tracked by following the disappearance of the peak centered at 2.8 for N-hydroxysuccinimde (Figure 111). See Appendix 1 for all spectra and the synthesis section for NMR peak assignments.

2.5 FT-IR of PEGL

The NCA and polymerization conversions were followed by FT-IR. This is advantageous compared to NMR because the reaction solvent can be subtracted, no overlap of absorption wavelengths for anhydride absorption and other functional groups, and ^{1}H NMR of polymers have band broadening (depending on the average chain length). The NCA aliquots were immediately tested to prevent reaction with ambient moisture and characteristic peaks associated with the NCA are ~1850 cm^{-1} and ~1775 cm^{-1} due to anhydride stretching were compared. The anhydride peaks decreased as conversion to polymer increased, providing a reliable test for polymer conversion.

Figure 20 shows a FT-IR spectrum of EGL NCA with peaks centered from the anhydride stretching at 1847 cm^{-1} and 1778 cm^{-1}. The average frequencies measured for a right-hand α-helix amine I and II stretching are 1653 cm^{-1} and 1544 cm^{-1}.[133] Figure 21 shows almost 100% conversion from NCA to polymer. The characteristic peaks for the anhydride have all but disappeared and peaks at 1651 cm^{-1} and 1541 cm^{-1} are the amide I and II bands for a helical peptide, respectively. The FTIR spectra are known for poly(lysine) for a random coil, α-helix, and antiparallel chains.[134]

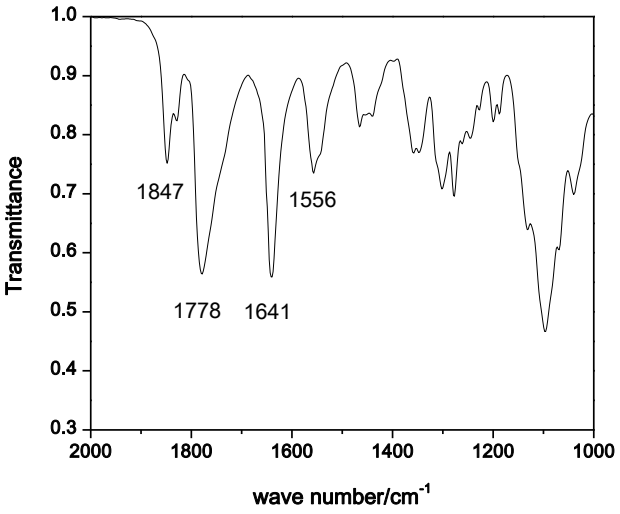

Figure 20. FT-IR spectrum of PEG-Lysine NCA.

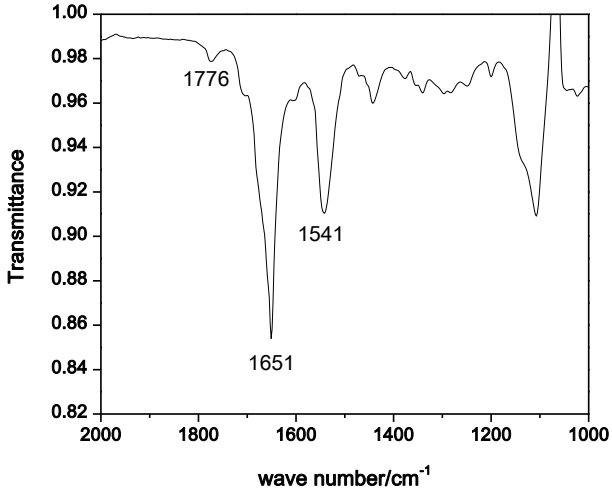

Figure 21. FT-IR of PEGL.

2.6 Circular Dichroism of PEGL

Circular dichroism,[135] a measure of the interaction of a sample and circularly polarized light, can elucidate the secondary structure of the sample in coordination with FT-IR. The

asymmetry of the samples, due to the α-helix, provides a sensitive measure of secondary structure.[135] Light can be polarized vertically by using a vertical polarizer or by having an equal amount of left and right circularly polarized light. If the sample interacts with a right or left circularly light greater than the other, the transmitted light rotates.

The word interaction has thus far been intentional because two interactions are possible: absorption and refraction. Because circular dichroism and optical rotary dispersion are similar in nature, their difference is highlighted. An optical rotary dispersion (ORD) experiment measures the angle at which the observed plane-polarized light rotates as a function of wavelength. The left and right circularly polarized light are equal in magnitude, creating vertically polarized light. The angle of rotation of the vertically polarized light depends on the difference of the refractive index in the sample of left and right circularly polarized light. Depending on the retardation of the light, the observed plane-polarized light is rotated left or right. Optical rotary dispersion is a measure of the difference in refractive index between left and right circularly polarized light. Circular dichroism is different from optical rotary dispersion in that it measures the absorbance difference between left and right circularly polarized light. In a circular dichroism experiment, the sample again interacts with left and right circularly polarized light, but the difference in absorption is measured.

Absorption and refractive index are not independent, both occur concurrently. Rather than having a vertically polarized plane of light after the sample, the polarization of the emergent light traces an ellipse. This happens because the sample absorbs left and right circularly light differently but also retards one preferentially due to difference in refractive index. A circular dichroism experiment measures this ellipticity. The mean molar ellipticity, [θ], is found in Equation 2

$$[\theta] = 3300 \cdot \Delta\varepsilon \qquad \text{Equation 2}$$

where $\Delta\varepsilon = \epsilon_{L-}\epsilon_R$, ϵ_L is the extinction coefficient for left circularly polarized light and $\epsilon_R$is the extinction coefficient for right. The mean molar ellipticity is normalized by concentration of monomer in solution to eliminate differences in absorbance minima due to different polymer concentrations.

Circular dichroism spectra can be found for poly(L-lysine) in Figure 22. The usefulness of circular dichroism becomes immediately apparent because the possible conformations of poly(L-lysine) have dramatically different absorbance traces. The α-helix shows two peaks centered at 208 nm and 222 nm. These peaks are due to a $n \rightarrow \pi^*$, when non-bonding electrons of the carbonyl oxygen go to an antibonding π orbital.[135]

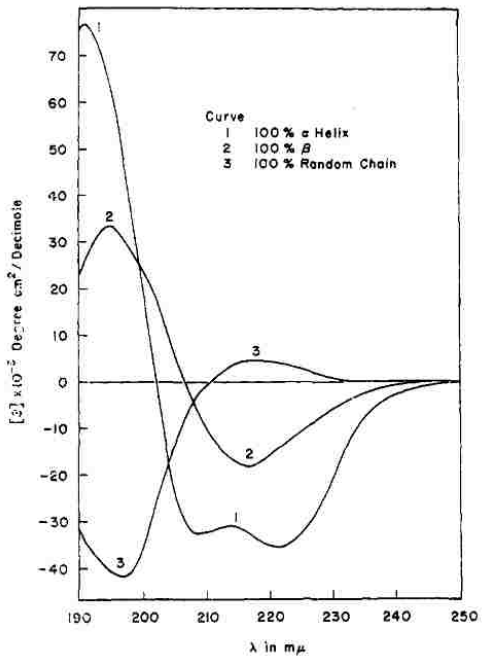

Figure 22. Circular dichroism of 1) α-helix, 2) β-sheet, and 3) random coil conformations of poly(L-lysine). Reprinted with permission from Greenfield, N. J.; Fasman, G. D. *Biochemistry* 1969, 8, (10), 4108-4116.

Figure 23 shows a circular dichroism spectrum of PEGL at room temperature and 50 °C. The sample is highly helical, as evidenced by the two peaks at 208 and 222 nm. The relative percent helicity can be calculated based on theoretical mean molar ellipticity value at 222 nm of poly(L-lysine).[130, 136]

The percentage helicity was based on a theoretical 100% lysine and found by using Equation 3

$$\%\ helicity = \left(\frac{[\theta]_{222\ nm}}{-35{,}700}\right) \cdot 100 \qquad \text{Equation 3}$$

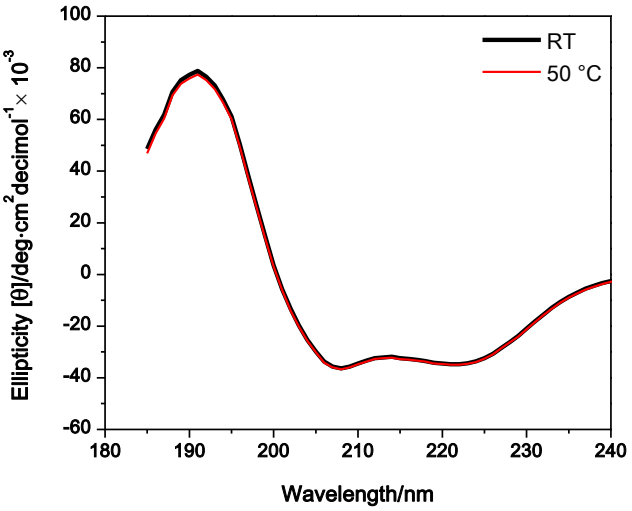

Figure 23. Mean molar ellipticity of sample #2 (M_w = 211 ± 1, PDI = 1.21 ± 0.01) in *water*, after 2 years in the refrigerator. Black line is room temperature and red line is 50 °C. The polymer concentration was 0.5 mg/mL.

The percent helicity for PEGL was 98% at room temperature and 50 °C. Both of these experiments were performed after the polymer had aged in the refrigerator for 2 years. This shows the polymer is highly helical in water but no polymer is 100% helical. PEGL does not change the percent helicity up to 50 °C (it retains 75% helicity at 85 °C)[72], it does not change

helicity over time (the percent helicity being 95% at RT after 1 month), and it does not change helicity over the concentration regime studied ($\leq$ 1 mg/mL). Higher polymer concentrations were attempted but the CD detector was overloaded with any PEGL concentration above 1 mg/mL. Other solvent conditions, pH of 2-12, 3 M NaCl, 1 M urea, 1 M guanidium-HCl, THF, methanol, and chloroform, showed the helix to be stable.[72]

Because of the circular dichroism studies, it was believed some polymer samples were highly helical and consequently should behave as a rodlike polymer. This shows PEGL may satisfy the criteria for forming a novel, water-soluble, non-ionic, rodlike polymer; it will become apparent although PEGL met the set-forth criteria, a *model* polymer requires more. Table 3 shows relative percent helicity for multiple PEGL samples.

Table 3. Circular dichroism and molecluar weight data from GPC/MALS for multiple PEGL samples (0.5 mg/mL in water for CD and 10.0 mg/mL for GPC/MALS)

Sample #	M_w	% helicity
1	53 ± 6	75
2	211 ± 1	95
3	225 ± 1	98
6, 19	210 ± 4, 9.2 ± 0.5	33
12	18.0 ± 0.1	50
13	18.0 ± 0.2	25
18	190 ± 1	51

It is well known that helix formation happens once the polymer reaches a critical length.[15] Based on the measured molecular weights these polymers should vastly outreach that short length requirement. This may indicate some branching, other unintended reactions, or aggregation that is giving an inflated molecular weight from the GPC. Based on other experiments (see GPC section) aggregation is a real problem for PEGL in *water* or *buffer*. Also, branching is a possibility, especially if free amino groups are present from incomplete reaction of lysine and PEG. Figure 24 shows a plot of the percent helicity calculated from Equation 3 as a function of PEGL molecular weight.

A

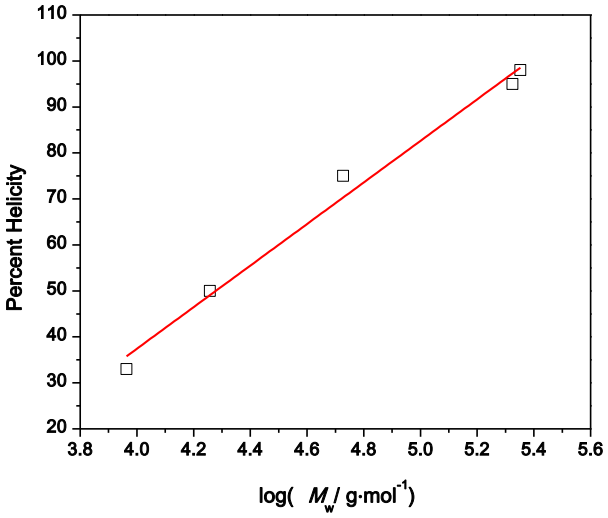

B

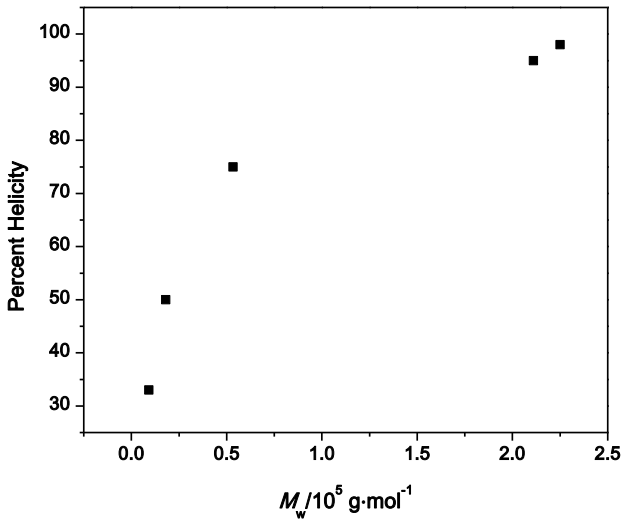

Figure 24. Percent helicity calculated from Equation 3 as a function of the measured molecular weight of different PEGL samples. The abscissa is in log scale in plot A and a linear scale in plot B. The red line is a linear fit.

There appears to be a linear dependence, indicating high helicity only happens with large molecular weight. It is strange that the measured molecular weights, coming from aggregates,

show such a linear dependence but this may explain the change in helicity from sample to sample. It well known that short peptide chains have difficulty in forming complete helices[135, 136] because the transition from coil to helix is enthalpically driven. Therefore, helix formation depends on chain length.[137]

The difference in percent helicity between PEGL samples can be explained by the purity of the NCA. The presence of trace impurities in high monomer:initiator ratios deactivate the metal catalyst, stopping polymerization. For samples 1-3 in Table 10, a small-scale NCA reaction (< 1 g) was performed and purified. For the rest of the samples in Table 10 the NCA reaction was performed on a much larger scale (~10 g). Scale up of the NCA reaction is may produce a larger amount of impurities and make purification more difficult.[15] Several recrystallizations and column chromatography were performed to further purify the NCA crystals in attempt to combat the impurities but from the lower-than-expected molecular weights, it appears the NCA was not pure enough to make long-chain polymers. PEGL polymers with a lower percent helicity are likely short chains that are not long enough to form a stable helix due to the inactivation of the metal catalyst. All the measured molecular weights by GPC are of an aggregated state (see section 2.11 below); thus, the measured molecular weights are higher than the actual molecular weight (see Figure 57 for one plot showing PEGL aggregation) For example, sample #13 in Table 3 shows a percent helicity of 25% but only has a measured molecular weight of 18.2 kg/mol. Because it is aggregated, the actual polymer chains are shorter than this and they should not exhibit a high percent helicity. For sample #2, although it is also aggregated, the measured molecular weight is much larger, indicating the polymer chains are longer than sample #13 and are long enough to form a helix.

2.7 Partial Specific Volume of PEGL

Partial specific volume, $\bar{v}$, is a measure of the correlation of volume to sample concentration. It is necessary to find true concentrations for polymer solutions if calculating concentration by weight only (Equation 4)

$$Concentration = \frac{mass_{solute}}{(mass_{solute} \cdot \bar{v}_{solute}) + (mass_{solvent} \cdot \bar{v}_{solvent})} \qquad \text{Equation 4}$$

where $\bar{v}$ is partial specific volume.

Partial specific volume is measured using a density meter. In this case, a U-shaped glass piece filled with sample is excited to oscillation and the density is measured by timing the period of the undamped oscillation of the glass tube.[138] The sample weight percent was limited to less than one percent, meaning a large extrapolation is needed to find the partial specific volume of the polymer at one-hundred weight percent (right intercept in Figure 25). This was done to allow for a linear approximation to the inverse density as a function of polymer concentration because over a too large polymer concentration range the plot may show curvature. A plot of inverse density as a function of weight percent PEGL is found in Figure 25. The partial specific volume for PEGL was 0.75 ± 0.06 mL/g, found from the right intercept at one-hundred weight percent PEGL. The red line is the fit line for the data and the green lines are the 95% confidence interval lines (how the uncertainty was calculated). This partial specific volume value is consistent with a common value of 0.75 mL/g for proteins.[139]

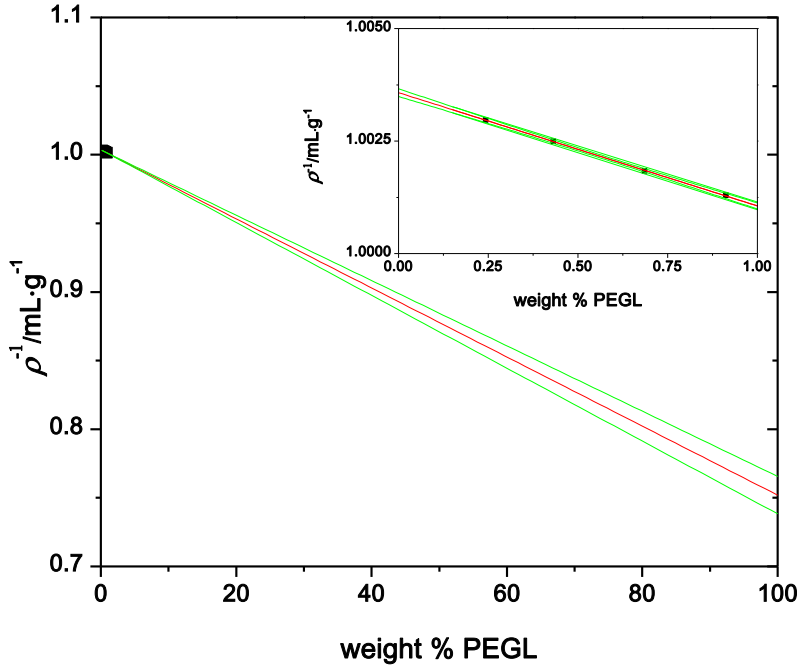

Figure 25. Inverse density as a function of PEGL weight percent in *water* at 20 °C. The partial specific volume of PEGL was 0.75 ± 0.01 mL/g. The red line is the fit to the data and the green lines are the 95% confidence interval lines.

2.8 d*n*/d*c* of PEGL

2.8.1 d*n*/d*c* of PEGL by Brice-Phoenix Differential Refractometer

In a differential refractometer, a split cell holds the pure solvent in one side and solution in the other.[140] This setup increases sensitivity because the absolute refractive index is not measured, but the deflection caused by the solute in solution. In addition, each cell is going to be at an equivalent temperature (assuming ample equilibration time),[141] which lessens the need for tight temperature control compared to direct refractive index measurement tools. The differential refractometer is accurate to the sixth decimal place.[121]

The split cell is illuminated and the light passing through a slit before it enters the cell. The light bends at an angle proportionate to the difference in refractive index of the solution and the solvent, and a minimum deflection of ~0.01 can be measured. An image of the slit is focused on a microscope with a filar micrometer eyepiece with a drum that has a 10 mm fixed scale.

Lining up a crosshair in the microscope eyepiece with the deflection of the image of the slit allows highly accurate measurement of the differential refractive index. This is repeated for several concentrations and a plot of the scale read on the microscope as a function of solute concentration affords the differential index of refraction. The calibration plot should be close to the most linear plot made in graduate school! If there is an offset on the y-axis, it is inconsequential and due to misalignment of the instrument.

Using a sample with a known d*n*/d*c*, KCl in this instance, a calibration plot for 632.8 nm wavelength was done as shown in Figure 26 where the S and Δn are defined in Equation 5 and Equation 6. From the calibration plot, d*S*/d*n* = 587.1 ± 2.4 with $r^2 = 0.99995$.

$$\Delta n = c \cdot \frac{dn}{dc} \qquad \text{Equation 5}$$

$$S = O + \frac{dS}{dn} \cdot \Delta n \qquad \text{Equation 6}$$

S is the signal read from the differential refractometer (the measurement was made at half deflection) and *O* is the offset (the y-intercept).

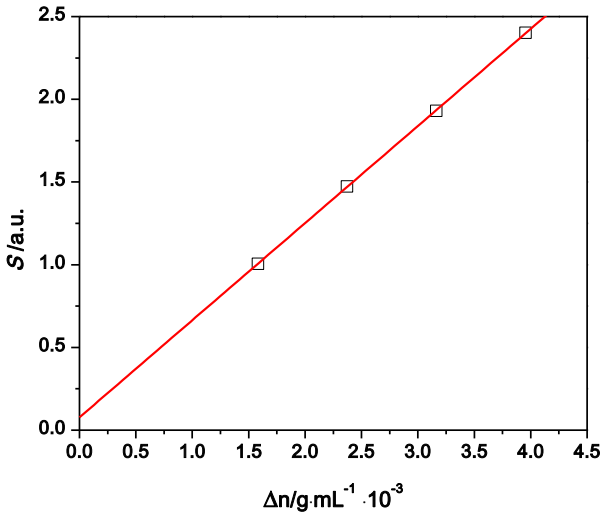

Figure 26. Differential refractometer calibration plot of KCl at room temperature. S is the measured signal. d*S*/d*n* = 587 ± 2. d*n*/d*c* of KCl used was 0.13182 mL/g at 632.8 nm. r^2 = 0.999.

From the slope, d*S*/d*n*, the d*n*/d*c* can be measured for an unknown sample by using Equation 7

$$\frac{dn}{dc} = \frac{dS/dc}{dS/dn} = \frac{measured\ slope}{calibration\ slope} \qquad \text{Equation 7}$$

Figure 27 shows a plot of the measured signal as a function of PEGL concentration. Inserting the measured values for d*S*/d*n* and d*S*/d*c* into Equation 7, the d*n*/d*c* of PEGL was 72.81/587.1 = 0.124 ± 0.001 mL/g.

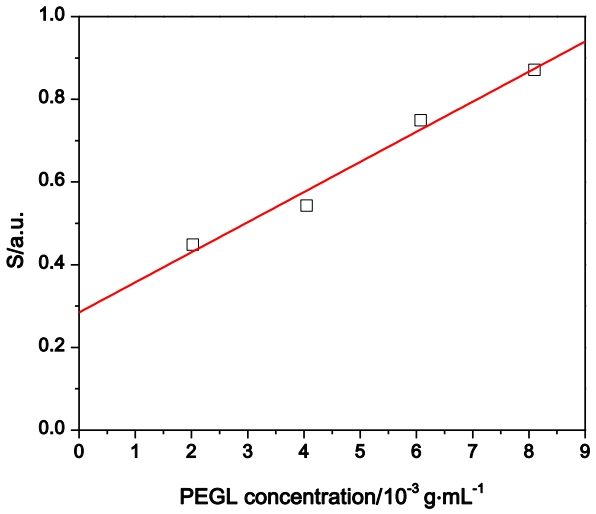

Figure 27. Plot of *S* as a function of PEGL concentration at room temperature and 632.8 nm. Red line is the fit. d*S*/d*c* = 72.8 ± 7.2. d*n*/d*c* of PEGL is 0.124 ± 0.001 mL/g. Sample #8 (M_w = 7.60 ± 0.26, PDI = 1.04 ± 0.05). r^2 = 0.971.

2.8.2 d*n*/d*c* of PEGL by Wyatt Light Scattering Detector

The experiment for finding the d*n*/d*c* of a sample using a Wyatt Dawn DSP Light Scattering Detector is very similar to finding the d*n*/d*c* with the differential refractometer. A calibration plot is built for signal as a function of sample concentration, and the slope is multiplied by the calibration constant (see Equation 7: the calibration constant is d*n*/d*S*). Figure 28 shows the signal of PEGL as a function of polymer concentration and the calibration constant for the Wyatt (d*n*/d*S*) was 0.000184. The d*n*/d*c* calculated from the Wyatt Light Scattering Detector is $687.4 \cdot 1.84 \times 10^{-3}$ = 0.1265 ± 0.001 mL/g.

Table 4 shows the final calculated values for the d*n*/d*c* of PEGL for different conditions, wavelengths, and molecular weights. Poly(ethylene glycol) is known to have a d*n*/d*c* that changes with molecular weight for low molecular weight polymers.[142] With different molecular

weights of PEGL, it can be thought of as changing the amount of oligo(ethylene glycol) in solution.

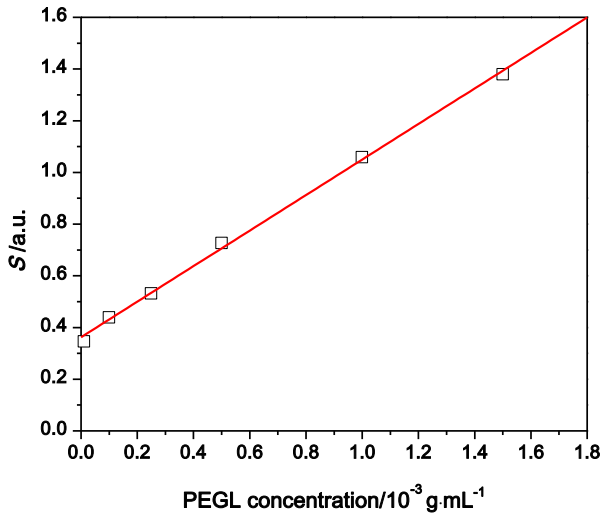

Figure 28. Signal of PEGL measured by the Wyatt Dawn DSP Light Scattering Detector at room temperature and 632 nm in *buffer* (200 mM $NaNO_3$ + 20 mM NaH_2PO_4 + 2 mM NaN_3). Sample #2 (M_w = 211 ± 1, PDI = 1.21 ± 0.01). r^2 = 0.998.

Table 4. d*n*/d*c* of PEGL measured and from literature

Method	Wavelength (nm)	M_w (kDa)	Solvent	Temp (°C)	d*n*/d*c*	Reference	Sample #
-	-	43-95*	DMF	60	0.123 ± 0.001	72,49	-
DR	632.8	7.6	*Water*	RT	0.124 ± 0.001	-	8
DR	488.0	7.6	*Water*	RT	0.123 ± 0.001	-	8
W	632.8	211	*Buffer*	RT	0.126 ± 0.001	-	2

A dash means no data. * means the paper did not state which polymer was tested. DR means the d*n*/d*c* was found with the Brice-Phoenix differential refractometer. W means the d*n*/d*c* was found via Wyatt DSP Light Scattering Detector. *Buffer* consists of 200 mM $NaNO_3$ + 10 mM NaH_2PO_4 + 2 mM NaN_3 adjusted to pH 7.5. The d*n*/d*c* used to calculate all molecular weights was 0.126. Error is discussed in the text.

It may be possible to change the dn/dc based upon the molecular weight of PEGL, based solely on the oligo(ethylene glycol) affecting it. The dn/dc shows little change with different solvent, wavelength, and PEGL molecular weight. The uncertainty for the dn/dc is taken as the

average of the measurements of the dn/dc and the difference of the maximal value (0.1265) and the average (0.125). The dn/dc used to calculate all molecular weights was 0.126 ± 0.001 mL/g

2.9 Viscosity of PEGL

In a falling ball viscosity measurement, a ball of known density and diameter is placed into a glass cell, and inverted to initiate ball movement. Assuming the ball reaches its terminal velocity and is following laminar flow, Stokes' law can be applied (Equation 8) to obtain the friction, *F*.[143]

$$F = 6\pi \cdot \eta \cdot r \cdot \omega \qquad \text{Equation 8}$$

where η is the dynamic viscosity, r is the radius of the ball, and ω is the terminal velocity. When the ball falls as a constant rate the gravitational force equals the buoyant and friction force. When this happens, the viscosity can be described by Equation 9

$$\eta = K \cdot (\rho_2 - \rho_1) \cdot t \qquad \text{Equation 9}$$

where $K = \frac{2}{9} \cdot r^2 \cdot \frac{g}{s}$ (g is the acceleration due to gravity, *s* is the distance traveled by the ball), ρ_2 is the density of the sphere, and ρ_1 is the density of the fluid, and t is the time needed to travel the distance *s*. Figure 29 shows a cartoon of the falling ball viscometer. The red lines denote inductive sensors measuring the time needed to travel a distance, *s*. This microviscometer was used because it requires very small sample (< 0.5 mL).

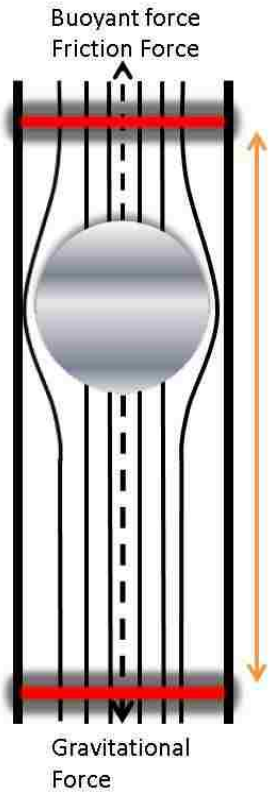

Figure 29. Cartoon of falling ball viscometer. Red lines are sensors that read when the ball passes to calculate the relative viscosity. Orange line shows the distance the ball travels.

Polymeric systems have multiple viscosities. The first discussed is relative viscosity (Equation 10). The variable t denotes the time needed to traverse the two sensors in Figure 29. The subscripts explain either the polymer solution or the pure solvent.[144]

$$\eta_{rel} = \frac{t_{solution}}{t_{solvent}} \qquad \text{Equation 10}$$

Another common viscosity used for polymer solutions is specific viscosity (Equation 11). Instead of measuring the time needed to travel a standard distance, the specific viscosity is a solvent normalized increase in viscosity when adding polymer to a pure solvent.

$$\eta_{sp} = \frac{\eta_{solution} - \eta_{solvent}}{\eta_{solvent}} \qquad \text{Equation 11}$$

To find intrinsic properties of the polymer, it is necessary to extrapolate to zero polymer concentration. In the limit of zero concentration, the specific viscosity affords the intrinsic viscosity of the polymer, [η].

$$[\eta] = \lim_{c \to 0} \frac{\eta_{sp}}{c} = \lim_{c \to 0} \frac{\ln(\eta_{rel})}{c} \qquad \text{Equation 12}$$

A plot of the specific viscosity normalized with concentration is found in Figure 30. It should show a linear dependence with concentration but it shows significant curvature for sample #6 at higher concentrations.

At lower concentrations (less than 3 mg/mL) the polymers appeared to follow a linear dependence, and at higher concentrations the viscosity dependence no longer is linear for sample #6. Sample #2 is highly helical and tested only at the lower polymer concentrations. The intrinsic viscosity for sample #2 from a linear fit to the data for η_{sp}/c is 20.7 ± 0.8 mL/g, which is much larger than sample #6. This is expected because by GPC sample #2 has a much larger average molecular weight. Also, being highly helical reduces the possibility for branching. Sample #6 is only 33% helical, meaning branching is much more plausible and may be the cause of the lower intrinsic viscosity. Branching can be tested by comparing Mark-Houwink and conformation plots of a linear and branched polymer. A good solvent system is needed prior to quantification of branching.

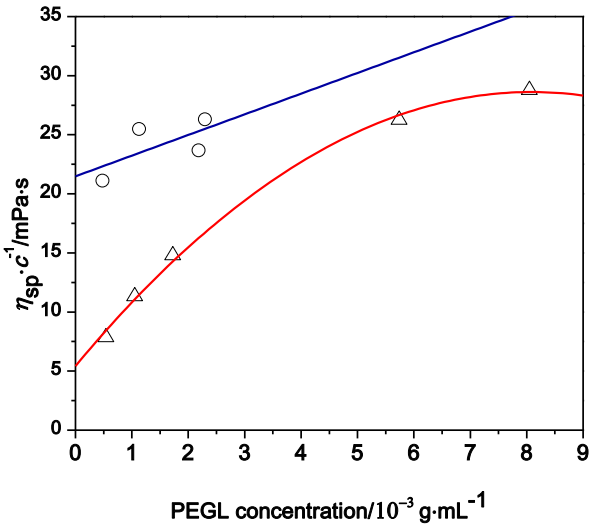

Figure 30. Specific viscosity as a function of PEGL concentration in *water*. Open triangles are sample #6 and the open circles are sample #2 (M_w = 211 ± 1, PDI = 1.21 ± 0.01).The red line is a polynomial fit to the data and the intercept for is 5.42 ± 0.69 mL/g. The blue line is a linear fit and the intercept is 21.48 ± 2.37. Uncertainty from fit is found by 95% confidence interval.

Sample #6 is more complicated than sample #2: two different slopes that can be fit to the data (one at low and one at higher polymer concentration). GPC data for sample #6 showed large aggregates and circular dichroism of sample #6 showed a 33% relative helicity, increasing the complexity. It is hypothesized the higher polymer concentration viscosities are due to large aggregates. Data in this dissertation show an increased size dependence on concentration for PEGL samples with low percent helicity (Figure 73). The intrinsic viscosity for sample #6 from fitting a second order polynomial to the data for η_{sp}/c is 5.52 ± 0.10 mL/g. If only the lower concentration range is fit, the intrinsic viscosity is 4.91 ± 0.10 mL/g. The calculated intrinsic viscosities are averages from repeat runs and the uncertainty is the difference between the largest value from the fit and the average.

Figure 31 shows a plot comparing $\lim_{c\to 0}\frac{\eta_{sp}}{c}$ and $\lim_{c\to 0}\frac{\ln(\eta_{rel})}{c}$ with the expected result[145] that they have the same intercept, as mathematically required when the solutions are sufficiently dilute and the data sufficiently quiet. Figure 32 shows the result for PEGL. Figure 31 shows both plots in Figure 32 should have identical y-intercepts, this is not the case. Aggregation is likely causing the two intercepts to not match. If the aggregates are not tightly bound, the ball dropped in the cell may be shearing the aggregates.

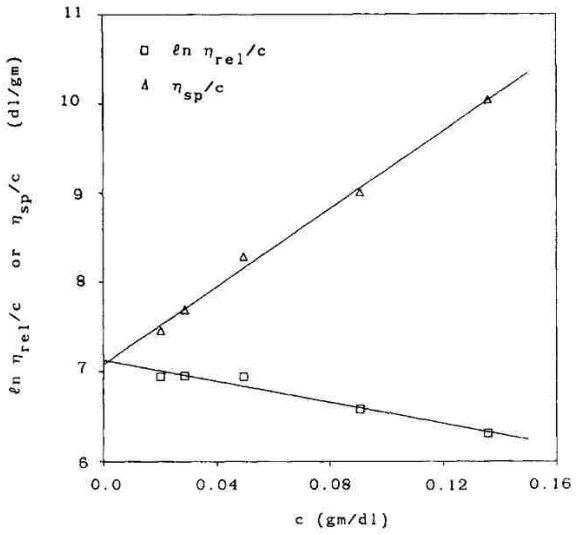

Figure 31. Double plot of viscosity data to obtain intrinsic viscosity, [η]: squares, $c^{-1}\ln(\eta_{rel})$; triangles, η_{sp}/c; solid lines, unweighted least-squares fits. PBT-7.3 in 97% H_2SO_4 at 100 °C. Reprinted with permission from Russo, P. S.; Siripanyo, S.; Saunders, M. J.; Karasz, F. E. *Macromolecules* 1986, 19, (11), 2856-2859. Copyright 1986 American Chemical Society.

The inverse of intrinsic viscosity approximates the overlap concentration needed for the polymer to interpenetrate.[146] From the intrinsic viscosities measured (sample #6: η_{sp}/c is 5.53 ± 0.10 mL/g and $\ln(\eta_{rel})/c$ is 6.77 ± 0.10 mL/g; sample #2: η_{sp}/c is 20.7 ± 0.8 mL/g and $\ln(\eta_{rel})/c$ is 28.3 ± 0.3 mL/g) the approximate overlap concentrations are much higher (the lowest overlap concentration was sample #2 at 35 mg/mL) than the concentrations regimes studied. The

polymers should behave independently in these concentrations and follow linear trends. It appears for both sample #2 and sample #6 they do follow a linear trend at lower polymer concentrations. Sample #6 exhibits considerable curvature at higher concentrations (discussed in the previous paragraph).

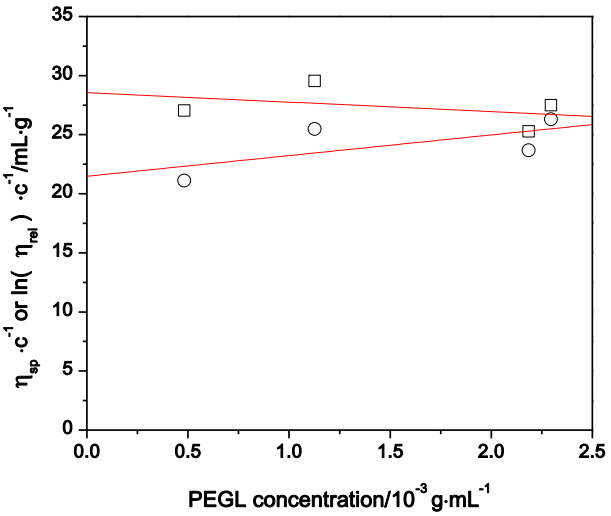

Figure 32. Double plot of viscosity data to obtain intrinsic viscosity, η_{sp}/c: circles, $c^{-1}\ln(\eta_{rel})$: squares; red lines are polynomial fits. η_{sp}/c is 20.7 ± 0.8 mL/g and $\ln(\eta_{rel})/c$ is 28.3 ± 0.3 mL/g. Sample #2 (M_w = 211 ± 1, PDI = 1.21 ± 0.01) in *water*.

Another issue is the slope for η_{sp}/c (Figure 32) is positive when it should be negative. This may be due to the type of viscometer used. An Ubbelohde type viscometer was used for the experiment in Figure 31.[145] With large polymer concentrations, the η_{rel} is very large, increasing the accuracy of the measurement. For this experiment, a falling ball viscometer was used. The relative viscosity for the lowest concentrations were very close to the pure solvent (η_{rel} = 1.005) and for the highest concentration η_{rel} = 1.15. Ideally, the relative viscosity would be much larger but the concentrations regimes tested had viscosities similar to the solvent. The advantage to the

microviscometer used was the low sample concentrations needed. Higher concentrations of PEGL were not tested because other techniques used (DLS, GPC, etc.) used lower polymer concentrations (less than 10 mg/mL) and a comparison was desired between them.

2.10 Mass Spectrometry of PEGL

Figure 33 shows a MALDI spectrum of sample #8 in water with a CHCA (α-cyano-4-hydroxycinnamic acid) matrix. Although the National Institute of Standards and Technology have published MADLI recipes for quantitatively characterizing polymers, it can be a challenging endeavor. However, true molecular weight determination is impossible if intensity is not correctly calibrated for quantifying the intensity peak.[147] For PEGL, the goals were to observe the molecular weight distribution and to find different chain lengths based on the measured mass-to-charge ratio (2-mer, 3-mer, etc.). Figure 33 shows, and it is more clearly seen in the inset, at least two major distributions. The masses and calculated chain length are found in Table 5. There appears to be more than two distributions present but only the main two distributions were characterized. The average mass/charge between each peak in the main distribution was 288.46 and was 288.49 for the secondary distribution. Each was consistent with the mass of the PEGL repeat unit, 288.34 g/mol.

Figure 34 shows a MALDI spectrum of sample #2 in water. Again, there appears to be multiple distributions. Only the main distribution (the set of peaks with the highest intensity) was characterized and is found in Table 6. The average difference between peaks was 282.72 *m/z* for sample #2, only nominally close to the expected *m/z* of 288.34 g/mol for PEGL. There was no cation (K^+ or Na^+), solvent (H_2O, methanol), or combination of both that would afford integer values for the number of repeat units. There are small peaks above *m/z* of 6,000, maybe indicating longer polymer chains or branching.

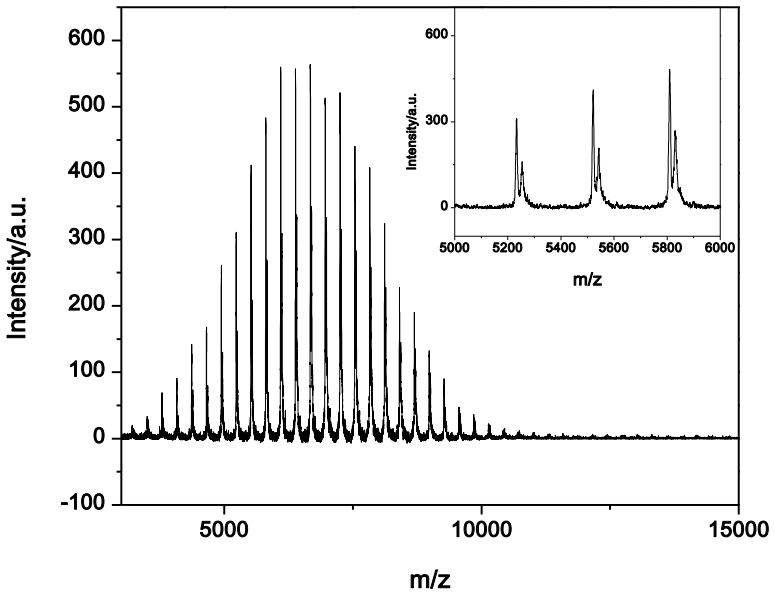

Figure 33. MALDI spectrum of sample #8 (M_w = 7.60 ± 0.26 kDa, PDI = 1.04 ± 0.05) in *water*. The matrix was CHCA and the measurement was in linear mode.

Table 5. Peak data from the MADLI spectrum for sample #8 in water from Figure 33

Main distribution		Second distribution	
m/z (end group and Na subtracted)	#of repeat units	*m/z* (end group and K^+ subtracted)	#of repeat units
3767.199	13.08	4042.948	14.02
4038.491	14.02	4330.89	15.02
4326.135	15.02	4619.76	16.02
4612.972	16.02	4909.029	17.03
4902.807	17.02	5196.595	18.02
5191.364	18.03	5485.275	19.02
5480.133	19.03	5772.785	20.02
5767.784	20.03	6063.038	21.03
6056.458	21.03	6351.002	22.03
6344.614	22.03	6638.618	23.02

Table 5 continued

Main Distribution		Second Distribution	
m/z (end group and Na subtracted)	#of repeat units	*m/z* (end group and K^+ subtracted)	#of repeat units
6633.573	23.03	6926.933	24.02
6922.944	24.04	7216.748	25.03
7210.421	25.04	7505.028	26.03
7499.045	26.04	7792.141	27.02
7788.14	27.04	8083.413	28.03
8076.192	28.04	8369.647	29.03
8365.747	29.05	8660.429	30.04
8654.08	30.05	8947.159	31.03
8943.013	31.05		
9231.9	32.06		
9518.303	33.05		

Table 6. Peak data from the MALDI spectrum for sample #2 in water for Figure 34

Main distribution	
m/z (end group and Na subtracted)	#of repeat units
1288.355	4.47
1564.767	5.43
1885.675	6.54
2167.299	7.52
2447.865	8.49
2731.939	9.47
3013.43	10.45
3322.458	11.52
3577.148	12.41
3860.646	13.39
4146.057	14.38
4428.537	15.36
4714.313	16.35
4996.104	17.33
5287.985	18.34
5560.649	19.29

MALDI was used to investigate aggregation of sample #6 in *buffer* solution. Figure 35 shows the chromatogram of sample #6 in *buffer*. Clearly, the sample is bimodal. The peaks in the

light scattering data to the left (fraction 1) and right (fraction 2) of the blue line in Figure 35 were collected and characterized by MALDI (Figure 36).

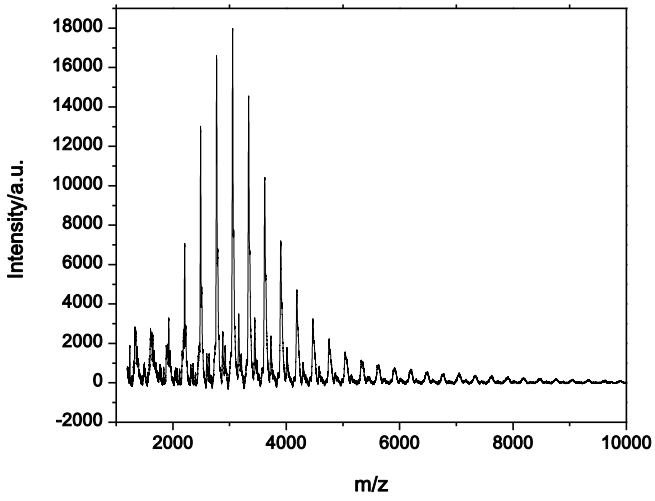

Figure 34. MALDI spectrum of sample #2 (M_w = 211 ± 1 kDa, PDI = 1.21 ± 0.01) in *water*. The matrix was dithranol and the measurement was performed in linear mode.

From the MALDI spectrum, the average difference in *m/z* value between the main distribution peaks for fraction 1 was 290.3 and for fraction 2 was 287.7. In a gel permeation experiment, larger molecular weight polymers elute prior to smaller polymers. Fraction 1 should have larger molecular weight and *m/z* values than fraction 2. In the contrary, fraction 2 has a larger *m/z* and this may be due to several reasons.

First, larger polymers do not charge as well smaller ones. This may eliminate any signal for larger polymers, giving decreased *m/z* values compared to the polymers actual *m/z* ratio. Also, the polymer may become charged in multiple places along the same chain, decreasing the *m/z* ratio measured.

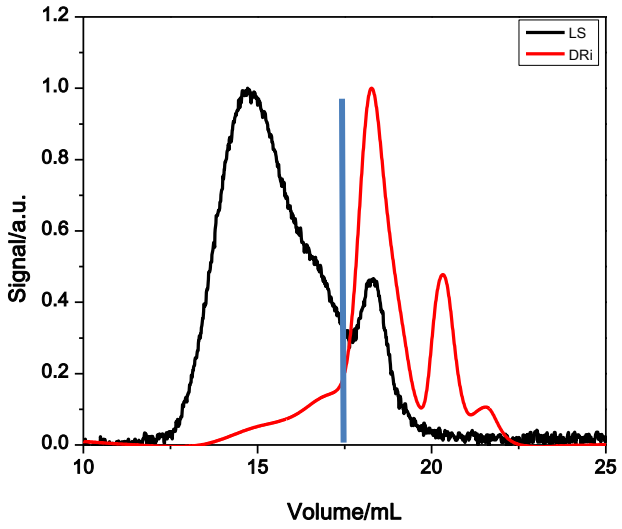

Figure 35. Gel permeation chromatogram of sample #6 in *buffer* (200 mM $NaNO_3$ + 20 mM NaH_2PO_4 + 2 mM NaN_3). The black line is the light scattering signal and the red line is the DRI signal. Left peak M_w = 189 ± 1 kDa, PDI = 2.60 ± 0.03; right peak M_w = 9.2 ± 3.2 kDa, PDI = 1.10 ± 0.09. The blue denotes the separation in collection for fraction 1 and fraction 2.

Table 7. Peak data from the MALDI data for sample #6 in water from Figure 36

Fraction 1		Fraction 2	
m/z (end group and Na subtracted)	#of repeat units	*m/z* (end group and K^+ subtracted)	#of repeat units
953.256	3.31	1451.868	5.04
975.134	3.38	1741.392	6.04
997.575	3.46	2030.199	7.04
1019.629	3.54	2319.102	8.04
1087.847	3.77	2607.22	9.04
1110.475	3.85	2896.379	10.05
1133.129	3.93	3183.937	11.04
1155.139	4.01	3472.799	12.04
1177.984	4.09	3759.856	13.04
1199.924	4.16	4048.459	14.04
1222.269	4.24	4336.228	15.04
1244.545	4.32	4625.264	16.04
1267.189	4.39	2911.991	10.10
1289.16	4.47	5199.726	18.03

Table 7 continued

Fraction 1		Fraction 2	
m/z (end group and Na subtracted)	#of repeat units	*m/z* (end group and K^+ subtracted)	#of repeat units
1379.237	4.78	5487.506	19.03
1401.9	4.86	5775.556	20.03
1425.174	4.94	6062.795	21.03
1447.803	5.02	6350.085	22.02
1470.118	5.10	6638.251	23.02
1491.578	5.17	6924.85	24.02
1601.815	5.56	7211.694	25.01
1626.996	5.64	7500.005	26.01
1648.132	5.72	7787.14	27.01
1670.43	5.79	8074.551	28.00
1693.721	5.87	8359.694	28.99
1715.224	5.95	8647.649	29.99
1738.098	6.03	8932.972	30.98

The sensitivity of the detector also decreases with increased molecular weight. These reasons seem unlikely because of the dramatic difference in the peak shapes for fraction 1 and 2. In addition, the average *m/z* ratio between peaks is much different. MALDI was chosen to elucidate the difference between fraction 1 and 2 because if aggregation were occurring of a monodisperse system, the MALDI spectra should be similar. In this case, they are very different, possibly meaning the large aggregates are composed of much smaller and polydisperse polymers. The shorter chain polymers have less percent helicity, indicating they are random coils. They may aggregate more being random coils as opposed to helical polymers. Another option consistent with the data is the larger polymers were heavily fragmented and caused the multiple distributions (> 4 are visible). Therefore, each distribution is the same polymer but with more or less charge. This may also be seen in fraction 2 because of the several overlapping distributions.

A

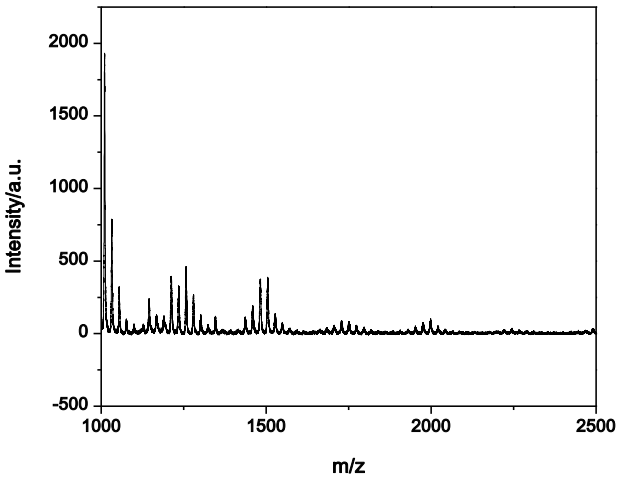

B

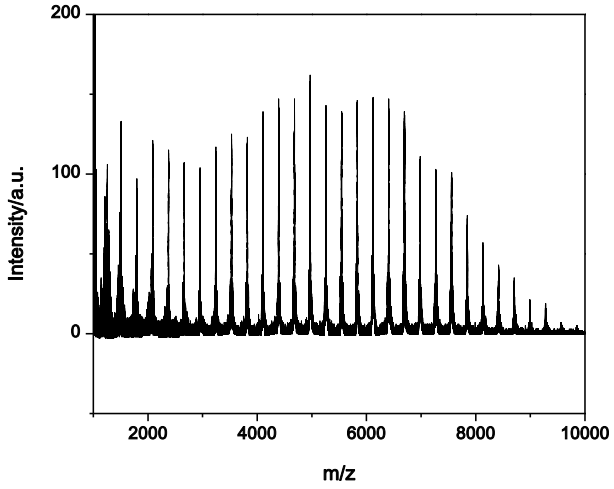

Figure 36. MALDI spectra of sample #6 (M_w = 210 ± 4 kDa, PDI = 2.23 ± 0.07) in *buffer* (200 mM $NaNO_3$ + 20 mM NaH_2PO_4 + 2 mM NaN_3). A is fraction 1 and B is fraction 2. The matrix was sinapinic acid and the experiment was performed in linear mode.

Additionally, the polymers may be interacting with the column and reversing the elution order. If true, this would cause problems with persistence length calculations and conformation

plots; because the conformation plots are molecular weight measured as function of elution volume linear (Figure 60), it appears this reversal in elution did not occur.

2.10 Microscopy of PEGL

2.10.1.1 Optical Microscopy

Optical microscopy is highly valuable for characterizing stiff polymers because they have unmistakable visual cues. The main one is in the form of liquid crystals because random coil polymers do not form liquid crystals. Liquid crystals may form in several ways: increasing polymer concentration, known as lyotropic liquid crystals, or with temperature change, known as thermotropic liquid crystals. Liquid crystals form a mesogenic state, somewhere between a solid and liquid, and form when rigid rodlike structures align in a liquid phase. The alignment of liquid crystals is quantified by the order parameter, *S*, found in Equation 13.

$$S = \frac{1}{2} < 3\cos^2\theta - 1 > \qquad \text{Equation 13}$$

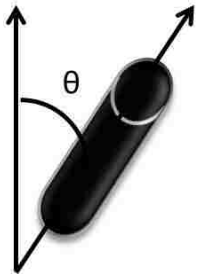

Figure 37. Cartoon of the alignment of a rodlike mesogen.

Liquid crystals can order several ways (Figure 38) and can be identified by the structures observed in a polarizing optical microscope.[148] Nematic liquid crystals have orientational order in one direction while smectic and cholesteric have orientation in multiple directions. Another

name for cholesteric liquid crystals is twisted nematic because each plane is oriented like a nematic liquid crystal.

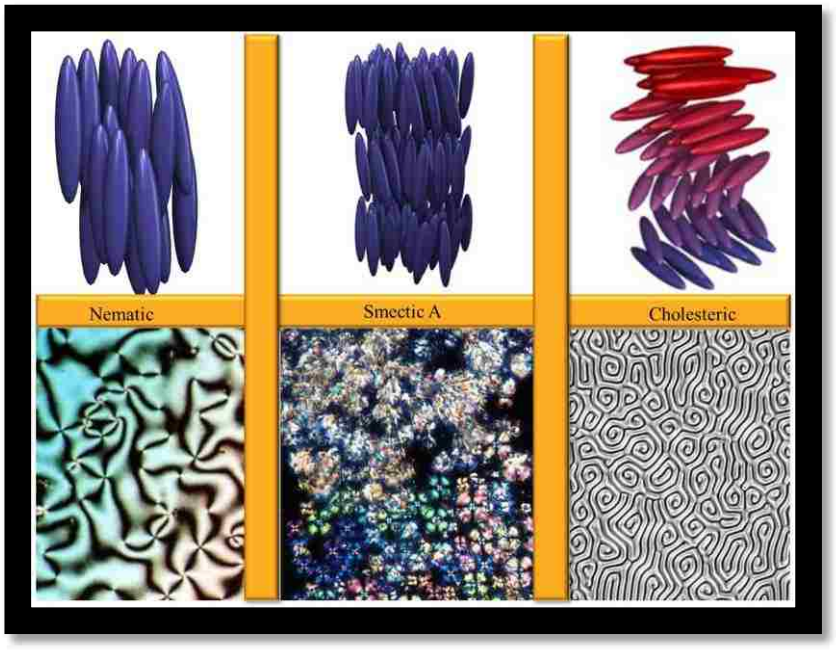

Figure 38. A sampling of common liquid crystals orientations. From reference 3.

For a cholesteric liquid crystal, the director twists as we travel from one plane to another. The pitch is defined as the distance required for the director to rotate by a full 360 degrees. Theory can predict the liquid crystal concentration onset based upon the axial ratio of the rodlike polymer. Onsager and Flory predict the onset of nematic liquid crystals forms at the number density, v^*

$$v^* = \frac{4}{A_2} = \frac{16}{\pi d L^2} \qquad \text{Equation 14}$$

$$\emptyset^* = 4/x \qquad \text{Equation 15}$$

$$\emptyset_A \cong (8/x)/(1 - 2/x) \qquad \text{Equation 16}$$

where d is the diameter of the rod, and L is the length of the rod, x is the axial ratio (L/d), $\emptyset^*$ is the Onsager volume fraction and $\emptyset_A$ is the Flory volume fraction.[149]

Amazingly, liquid crystals form an ordered phase "even in the absence of any specific energetic interaction between the rods or between rods and solvent".[149] The formation of a liquid crystal forms spontaneously and is highly stable for rods because of little entropic penalty compared to random coils due to their decreased flexibility.

Rodlike polymers possess this unique feature due to a parameter the Flory interaction parameter, χ, a measure of the solvent-polymer interaction. Random coil polymers possess a χ also, but it depends on the axial ratio (x), a small value for random coils. For rodlike polymers, phase separation occurs at much lower values than for random coils due to the increased axial ratio; this means phase separation is easily attainable in experimental conditions.

2.10.1.2 PEGL Liquid Crystals in *Water*

Several different samples of PEGL were tested for liquid crystal formation in water. Figure 39 shows images taken on an Olympus BH2 polarizing optical microscope with a digital AmScope Camera.

Cholesteric liquid crystals show fingerprint patterns due to the rotating order parameter with each plane (from dark stipe to dark stipe is half the pitch). Figure 39 shows PEGL forms a cholesteric liquid crystal, evidenced by the fingerprint pattern, consistent with previous observations.[119] Experimentally measured, the pitch was 8 ± 2 microns, larger than previously reported data reported at a lower concentration.[119]

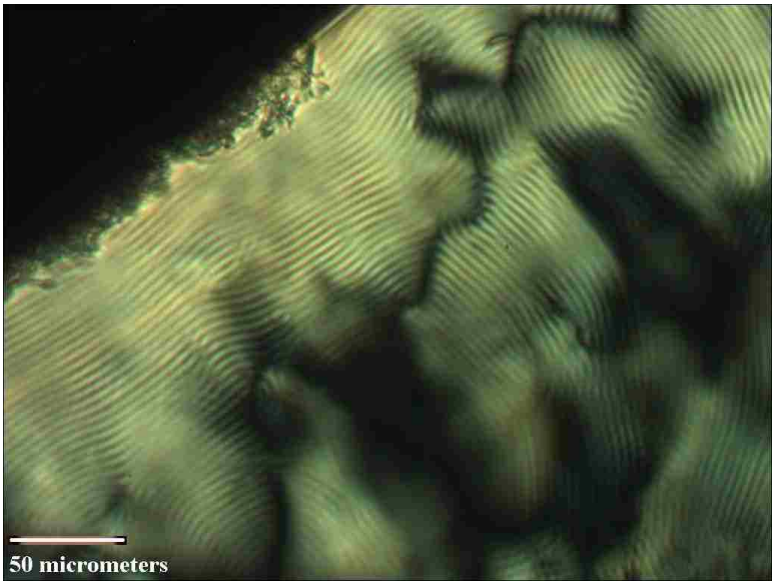

Figure 39. Optical image of sample #1 (M_w = 53.4 ± 5.9 kDa, PDI = 1.32 ± 0.23) at room temperature and 60 weight percent in *water*. Pitch is 7.5 ± 1.7 microns. Cross polarization was 90°.

There were no error bars in the previously measured[119] sample pitch so a direct comparison cannot be made, but at 55 weight percent the pitch was approximately 8 microns (very close to the 60 weight percent PEGL from Figure 25). Figure 40 shows many different orientations for the fingerprint banding, indicative of multiple domains. The dark regions (i.e. in the middle of the image) in Figure 39 are expected to be due to impurities or the orientation of the liquid crystal. The impurities may be low molecular weight PEGL that are present in the GPC trace or aggregates that do not form liquid crystals.

An interesting observation was the viewing of aggregates both with and without cross polarization (Figure 40). Table 8 follows the growth of the aggregates under cross polarization after loading into the Vitrocom cell. As time progressed, aggregation increased in the solution. A curious observation can be seen in images C-E: the aggregates resemble an empty tube, like a

drinking straw. This may indicate a rod like morphology for aggregates observed in solution, a not uncommon occurrence.[150]

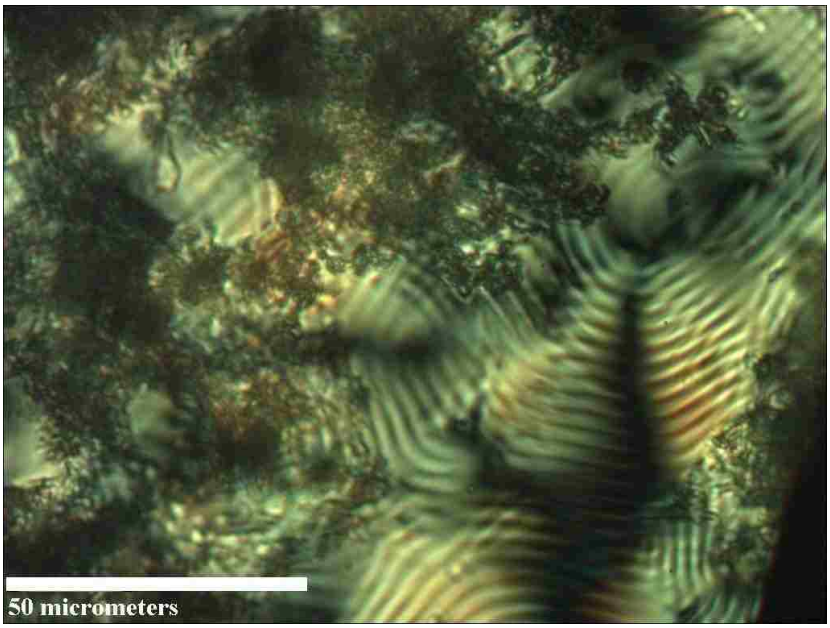

Figure 40. Optical image of sample #1 (M_w = 53.4 ± 5.9 kDa, PDI = 1.32 ± 0.23) at room temperature and 60 weight percent in *water*. Pitch is 6.5 ± 2.0 microns. Cross polarization was 90°.

The aggregates are also birefringent, suggesting they are either crystals or liquid crystals. The cholesteric banding was lost upon heating but returned when cooled. The aggregates did not reform possibly due to several reasons: the impurities were excluded from the liquid crystal domains (the dark line separating cholesteric liquid crystal domains) or they became soluble upon heating. Also, the cholesteric banding and pitch was more uniform following heating (22.3 ± 2.8 μm).

Table 8. Sample #3 (M_w = 225 ± 2 kDa, PDI = 1.16 ± 0.01, 66 wt% in *water*). The scale bar on each image is 100 μm.

A 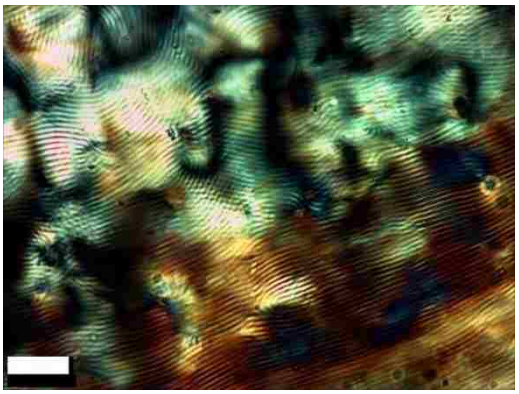 1 day	B 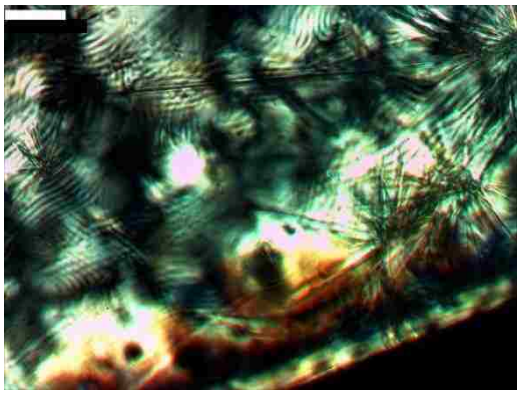 1day
C 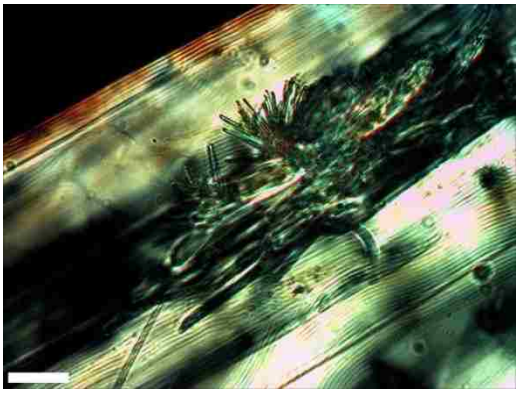 4 days	D  4 days
E 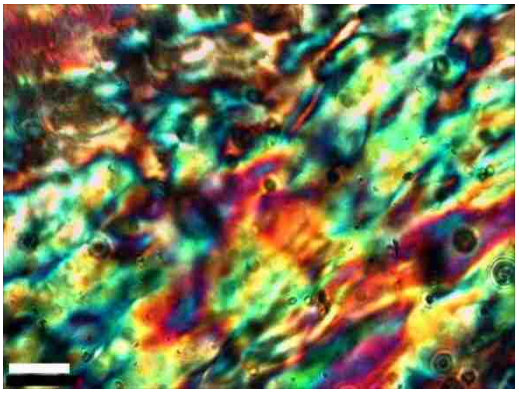 Heated until no cholesteric banding	F 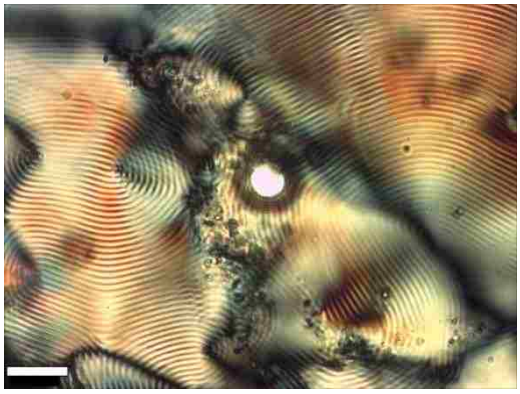 After heating, sat several days

Sample #12 was also tested to see if it would form liquid crystals. Following the Onsager and Flory predictions, (M_n = 15.5 kDa, PDI = 1.2, diameter = 2.2 nm) $\emptyset^* = 109\%$ and $\emptyset_A = 99\%$. Theoretically, this polymer should not form a liquid crystal at this low of a concentration because its axial ratio is too small. This shows that even at the low measured molecular weight, PEGL can form liquid crystals. Figure 41 shows liquid crystals forming at 50 weight percent. Cholesteric banding is present (Figure 41 B) but also is an apparent crystal. Either the molecular weight found from GPC is too low or the polymer is behaving like a larger polymer, possibly from aggregation that forms a semi-rigid rod. Also, if it is aggregating in a segmental fashion (see conclusions for chapter 3) the diameter may be larger, further increasing the concentration needed, further suggesting the polymer is aggregating into an extended structure. This suggests the polymer is aggregating and it must be in an extended conformation in order to form a liquid crystal. This would explain why the polymer appears to be rodlike, even if the polymer is aggregating.

A)

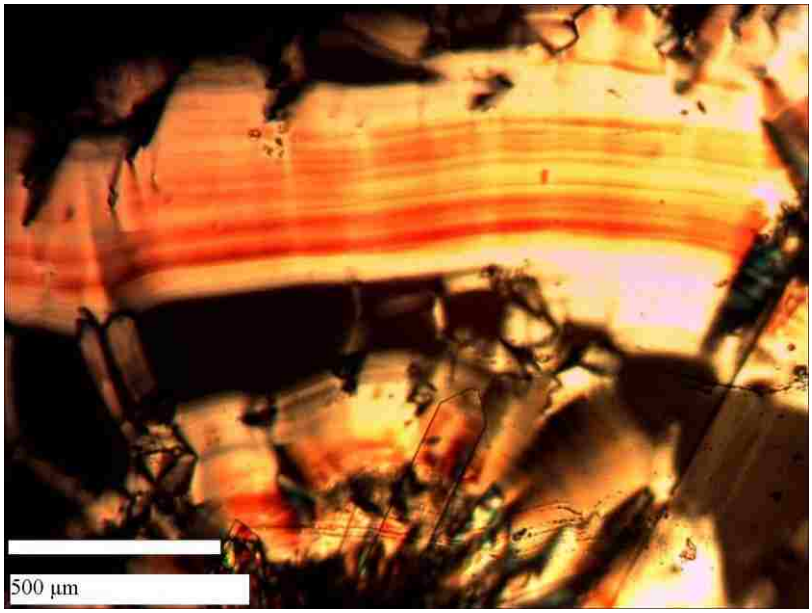

B)

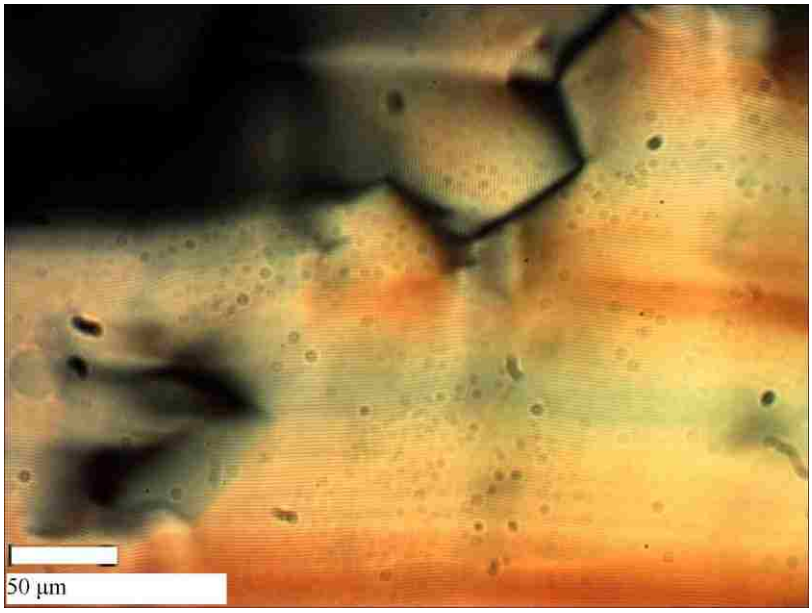

Figure 41. 50 weight percent sample #12 (M_w = 18 ± 1 kDa, PDI = 1.16 ± 0.01) in *water*. Cross polarization at 90°. The pitch is 3.3 ± 0.3 µm.

2.10.1.3 PEGL Liquid Crystals in B*uffer*

This same polymer (sample #12) behaves differently in the *buffer* solution than water. At 50 weight percent the polymer did not form a liquid crystalline phase. It appears at this high concentration, the polymer precipitates and forms many crystals (Figure 42). These crystals are visible with and without cross polarization (Figure 43) and were also visible as small white crystals by eye. This shows the polymer is less soluble in the *buffer* than pure water. This is fully plausible because from the Hofmeister salt series, sodium is a cation known to salt-out polymers and explains why in further data PEGL behaves differently in water and *buffer*.

Figure 42. 50 weight percent sample #12 (M_w = 18 ± 1 kDa, PDI = 1.16 ± 0.01) in *buffer* (200 mM $NaNO_3$ + 20 mM NaH_2PO_4 + 2 mM NaN_3). Cross polarization at 90° with colored filter to exaggerate colors.

Figure 43. 50 weight percent sample #12 (M_w = 18 ± 1 kDa, PDI = 1.16 ± 0.01) in *buffer* (200 mM $NaNO_3$ + 20 mM NaH_2PO_4 + 2 mM NaN_3).

2.10.1.4 PEGL Liquid Crystals in Dimethylformamide

PEGL shows possible liquid crystalline phases in dimethylformamide, DMF (Figure 44).

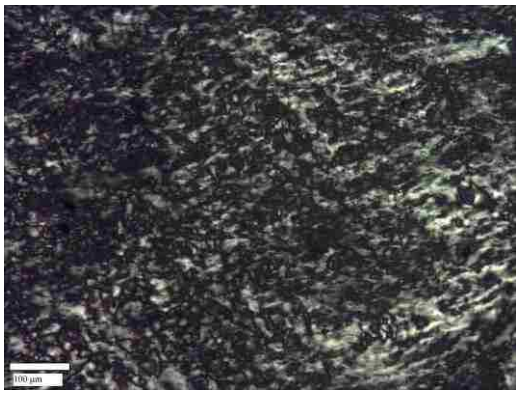

Figure 44. Sample #17 (M_w = 190 ± 1 kDa, PDI = 1.37 ± 0.01) in DMF, room temperature, concentration not known. Cross polarization at 90°.

The exact concentration of the polymer is not known because the sample was an aliquot from the polymerization solvent. Although a possible liquid crystal formed, it was not a cholesteric liquid crystal like in water. According to circular dichroism, sample #17 is 51% helical and the conformation plot from GPC in DMF + 0.1 M LiCl shows the polymer to be a

random coil (slope = 0.57). Despite the low helicity and the conformation plot data showing the polymer to be a random coil, the polymer may have formed a liquid crystal. This shows PEGL behaving differently than expected again. The polymer has to be in some type of extended structure, contrary to the GPC data. Once again, this may be happening due to an aggregate in an extended structure. Table 9 shows optical micrographs of sample #12 in DMF when heated. It appears the type of liquid crystal structure may be stable when heated. Another possibility is the polymer has made a gel, not a liquid crystal, and the images above are due to multiple scattering.

Table 9. Sample #12 (M_w = 18 ± 1 kDa, PDI = 1.16 ± 0.01) in DMF when heated. The scale bar on each image is 100 μm.

A  30 °C	B 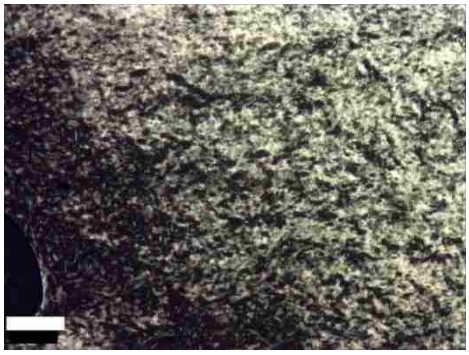 60 °C
C 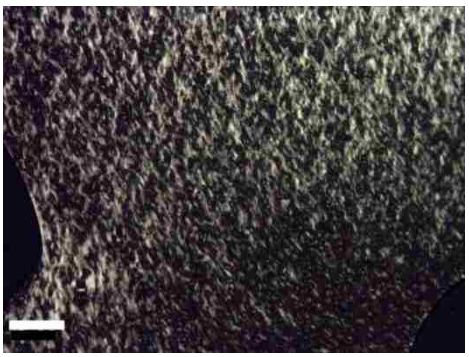 95 °C	D 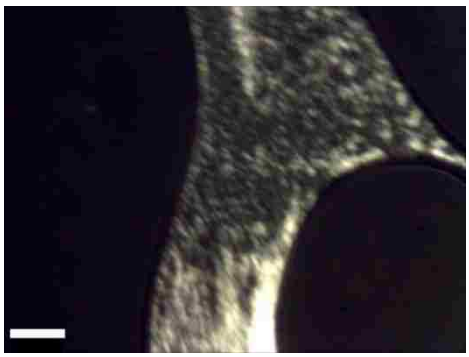 120 °C

2.10.2 Cryo-TEM of PEGL

Cyro-TEM was performed to try to directly image the shape of the polymer. If the measured molecular weights are to be believed, sample #2 and sample #18 should have lengths of 110 nm and 274 nm respectively, assuming a rigid rod (sample #18 only is 51% helical by CD so a more accurate length is much less). The contrast and brightness of the image have been changed to accentuate the dark lines seen in Figure 45, presumed to be rodlike polymer.

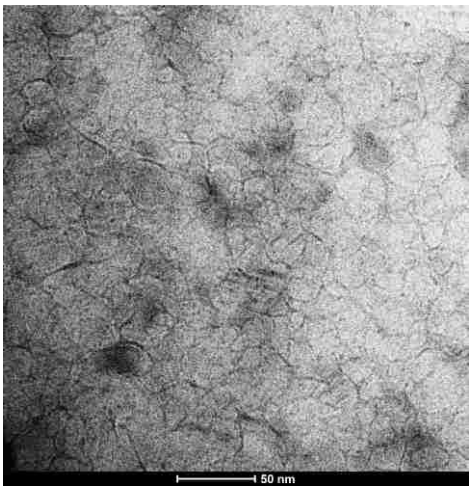

Figure 45. Cryo-TEM micrograph of sample #2 in *water* (M_w = 211 ± 1 kDa, PDI = 1.21 ± 0.01).

Measuring the length of six dark lines on the image give an average length and molecular weight of the presumed PEGL rods in the image to be 23 ± 7 nm for length and 44.6 ± 13.3 kg/mol for the molecular weight (from Equation 24). The sampling from measuring dark lines in the Cryo-TEM image is much smaller than from GPC. Comparing the molecular weights measured by GPC, this is half of the molecular weight measured in water and almost five times smaller than the molecular weight measured in GPC solvent. Also, tracing some of the dark lines that are expected to be rodlike polymer, it appears there may be branching. This may be a consequence of multiple focal planes in focus or actual branches.

A)

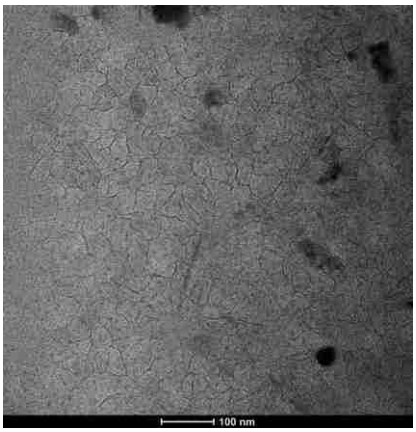

B)

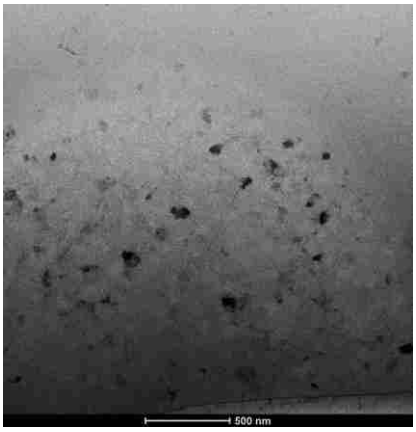

C)

Figure 46. Cryo-TEM images of sample #11 in A (*buffer*, 200 mM $NaNO_3$ + 20 mM NaH_2PO_4 + 2 mM NaN_3) B (*buffer*), and C (ethanol).

Cryo-TEM was also performed on a larger polymer, sample #18 (Figure 47). Although the measured molecular weight is larger for sample #18 than sample #2, the micrograph possess no notable features. If the GPC measured molecular weight is accurate, the cryo-TEM would easily show the polymer, suggesting the measured molecular weight from GPC is much higher than the true molecular weight. It might also be possible that PEGL samples with lower percent helicity aggregate in a more aggressive fashion.

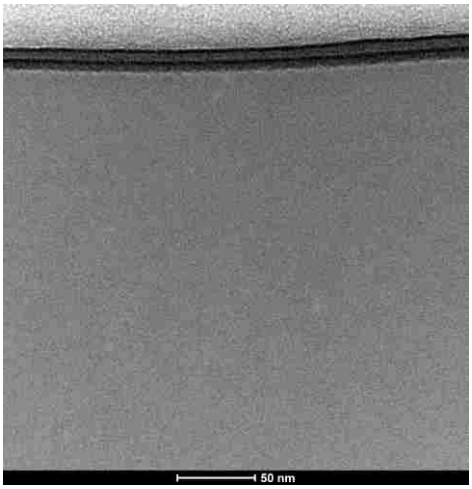

Figure 47. Cryo-TEM micrograph of sample #18 (M_w = 530 ± 4 kDa, PDI = 1.27 ± 0.02) in *water*.

2.11 Gel Permeation Chromatography of PEGL

2.11.1 GPC Theory

Gel permeation chromatography, GPC, is one of the most important polymer characterization techniques. GPC is an analog to HPLC, a column separation technique, flowing an analyte solution through a solid phase separation media. HPLC requires interaction between the analyte and the separation medium but GPC works differently. The separation occurs due to the difference in size of the molecules: small molecules stick in the pores of column while the

larger polymers are not as hindered. Because the separation is based on size and not molecular weight, different columns are needed to separate different sized polymers (unless the column is meant for large range in molecular weight).

If a GPC is set-up for a general polymer query, multiple mixed columns are required for a thorough separation. This allows polymers of different molecular weights to elute from the column at different volumes, creating many narrowly dispersed molecular weight fractions. This eliminates the need to perform experiments with samples that have a narrow PDI, unlike other characterization techniques.

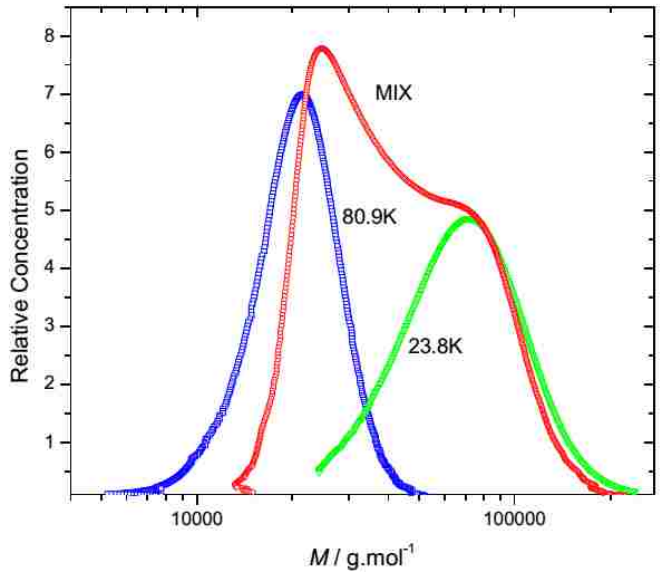

Figure 48. GPC-MALS separation of two mixed dextrans, red line, (M = 80.9K and 23.8K from Polymer Standard Services, Mainz, Germany). Individual runs for each polymer (blue line 80.9K and green line 23.8K) are also present.

These fractions of molecular weights are flowed into different types of detectors: light scattering, differential refractive index (DRI), viscosity, UV, etc. If the GPC is calibrated or if multiple detectors are used, quantitative information can be found about many aspects of the polymer: PDI, molecular weight, conformation, branching, etc.[151] The different molecular

weights are too close to successfully separate due to an inherent separation limitation in a GPC experiment. The resultant peaks (typically measured by light scattering and differential refractive index) are broad and not the typical narrow peaks associated with chromatographic separations.

Many different types of columns are available, and if the molecular weight of the analyte is previously known, a corresponding column can be used to increase the separation. It has been shown GPC struggles to separate polymers with a molecular weight that differs by three (Figure 48).[152] Multiple distributions can be seen but not quantitatively separated. If the polymer has a unimodal distribution and a reasonably small PDI, GPC works well. If the polymer has several distributions or if the PDI is too large, it should be separated on a preparative column prior to the GPC experiment.

Along with molecular weight and PDI, GPC can give other parameters. A conformation plot, log(molecular weight) along the abscissa axis and log(radius of gyration) along the ordinate axis, shows the morphology of the polymer. If the slope = 1, the polymer is an infinitely long stiff rod, if the slope = 0.5 the polymer is a random coil, and if the slope is below 0.5 the molecule is globular in shape.[5] A typical value for PBLG, a semiflexible rod, is 0.83-0.78.[96]

2.11.2 GPC Molecular Weight Calculation of PEGL

A GPC chromatogram of a PEGL sample with 100:1 [M]:[I] in *buffer* solution (200 mM $NaNO_3$ + 20 mM NaH_2PO_4 + 2 mM NaN_3) can be found in Figure 49. The signal shows the polymer was not of unimodal distribution, a shoulder appears. The peak of the DRI signal shows the shoulder at lower elution volume was the less abundant species. This means the sample was not highly dispersed but had high molecular weight impurities. This is expected because dialysis was performed, eliminating small molecular weights. The DRI signal shows two other peaks at

high elution volumes. The DRI is more sensitive to small molecules than the light scattering detector; the small peaks in the DRI were due to very low molecular weight impurities (possibly salt that was separated by the column).

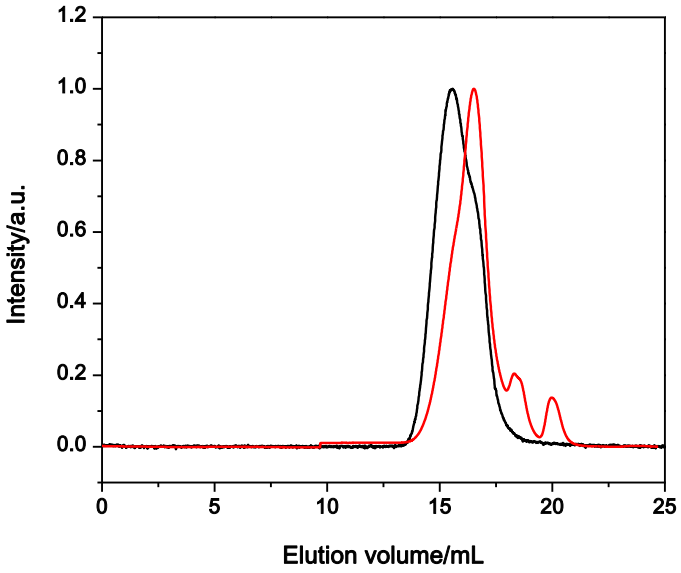

Figure 49. GPC of PEGL in *buffer* (200 mM $NaNO_3$ + 20 mM NaH_2PO_4 + 2 mM NaN_3, sample #2, M_w = 211 ± 1 kDa, PDI = 1.21 ± 0.01). The black line is the light scattering signal and the red line is the DRI signal.

Table 10 is a comprehensive list of the different PEGL polymers synthesized. The molecular weights were all calculated with aqueous GPC (except sample #18) with a d*n*/d*c* = 0.126 mL/g. The uncertainty is estimated by either of two ways: the preferable method is averaging three repeat runs but if three repeat runs were not performed, the uncertainty is estimated from different fits of the same data. Repeat runs give more insight for the results, i.e. if the polymer is aggregated, each run should provide quite different results because the aggregate may be broken in a non-repeatable fashion; this cannot be checked if only one injection is used.

Three different initiators were used, Nibpy(COD) (the nickel initiator discussed in section 3.2.3), sodium methoxide ($NaOCH_3$), and triethylamine (TEA). The nickel catalyst was predominately used because it has been proven capable to produce controllable molecular weights and low PDI.[72] Sodium methoxide was used because Blout synthesized poly(lysine) in dioxane with a molecular weight in the millions using it. Triethylamine was used because it is an AMM initiator, theoretically providing higher molecular weight polymers (at the cost of higher polydispersity).

Although the secondary goal of the synthesis was to have many different molecular weight polymers, the primary goal was a high molecular weight polymer. Table 9 shows that sample 18 has the highest molecular weight, but much shorter than the goal of one million. Table 9 also shows a large discrepancy between each sample with equal monomer:initiator loading. The polymerization did not proceed in a well-controlled fashion for several possible reasons. First, the purity of the NCA is of utmost importance for a well-controlled polymerization. The method used for purifying the NCA was crude at best (see synthesis of N_ε-2-[2-(2-methoxyethoxy)ethoxy]acetyl-N_α-Z-L-Lysine-N-Carboxyanhydride (8)). Although the NCA appeared to be fluffy, needle-like crystals, some impurities such as HCl may still be present because the pH was not tested on every sample. Also, NCA reactions were run on a ten gram scale. This means that multiple polymerization attempts can be ruined if the crop of NCA is impure. A larger NCA reaction may have more impurities, making purification more difficult.[15] This would pose a large problem, especially if the NCA is not used immediately after purification. The method used to purify the latest NCA reaction products was column chromatography.[49] This method, although tedious and ruinous to the NCA crop if the column is not dry, provided acceptable yields (> 50%) of highly pure NCA. A second problem with the

polymerization may be the nickel catalyst -- in a prototypical procedure, the Nibpy(COD) was synthesized, dried, and re-suspended in THF.

Table 10. PEGL molecular weights calculated from GPC/MALS for multiple samples in *buffer* solution

#	[M]:[I]	Theoretical Mn (kDa)	Book #	M_n (kDa)	M_w (kDa)	PDI	% helicity	Initiator
1	100	28.83	2.160	40.5 ± 5.3	53.4 ± 5.9	1.32 ± 0.23	75	Nibpy(COD)
2	100	28.83	2.166	174 ± 1	211 ± 1	1.21 ± 0.01	95	Nibpy(COD)
3	150	43.25	2.167	194 ± 1	225 ± 1	1.16 ± 0.01	98	Nibpy(COD)
4	200	57.67	3.28	52.8 ± 0.7	157 ± 1	2.94 ± 0.39	-	TEA
5	250	72.09	3.29	43.9 ± 0.6	50.3 ± 0.9	1.15 ± 0.03	-	TEA
6	300	86.50	3.44	94.4 ± 2.4	210 ± 4	2.23 ± 0.07	33	TEA
7	250	72.09	3.45	6.5 ± 0.5	6.8 ± 0.4	1.04 ± 0.11	-	TEA
8	350	100.90	3.59	7.3 ± 0.3	7.6 ± 0.3	1.04 ± 0.05	-	TEA
9	300	86.50	3.60	6.9 ± 0.4	7.1 ± 0.4	1.02 ± 0.07	-	TEA
10	250	72.09	3.61	8.1 ± 0.1	8.3 ± 0.1	1.03 ± 0.01	-	TEA
11	500	144.20	3.75	12.2 ± 0.1	14.9 ± 0.1	1.22 ± 0.01	-	Nibpy(COD)
12	200	57.67	3.76	15.5 ± 0.1	18.1 ± 0.1	1.16 ± 0.01	50	Nibpy(COD)
13	300	86.50	3.77	15.6 ± 0.2	18.2 ± 0.2	1.17 ± 0.02	25	Nibpy(COD)
14	400	115.30	3.78	17.4 ± 0.2	20.9 ± 0.2	1.20 ± 0.02	-	Nibpy(COD)
15	400	115.30	3.111	18.4 ± 0.6	22.8 ± 0.5	1.24 ± 0.05	-	$NaOCH_3$
16	400	115.30	3.117	394 ± 3	423 ± 1	1.07 ± 0.01	-	Nibpy(COD)
17*	500	144.20	3.128	138 ± 1	190 ± 1	1.37 ± 0.01	-	Nibpy(COD)
18	500	144.20	3.128	414 ± 4	526 ± 4	1.27 ± 0.02	51	Nibpy(COD)
19	300	86.50	3.44	8.7 ± 0.6	9.2 ± 0.5	1.06 ± 0.09	33	TEA
20	200	57.67	3.28	46.3 ± 4.6	84 ± 8	1.80 ± 0.18	-	TEA
21	200	57.67	3.28	230 ± 2	700 ± 70	3.05 ± 0.31	-	TEA
22†	100	28.83	2.166	85 ± 6	90 ± 7	1.07 ± 0.11	-	Nibpy(COD)

* Molecular weight data was found in DMF, † molecular weight data was found in water

As long as the THF solution was a dark purple, the catalyst was considered active. This was bad practice as the catalyst may decompose over time although enough time had passed

between polymerization attempts that new catalyst was almost always synthesized; a different method was adopted for the last few polymers (#16-18), using freshly synthesized catalyst for each polymerization that was not dried and stored. The catalyst was easily synthesized by stirring the requisite reactants overnight, provided polymers with lower PDI and more controllable molecular weight.

In accordance with the NCA and catalyst purity, if large molecular weight polymers are desired, it requires a very small loading of catalyst. This means the NCA and catalyst needs to be ultra-pure because any trace impurity can deactivate the catalyst. This was likely the cause for polymer samples #7-15 having small loadings of catalyst but only low molecular weights.

Another problem may be the purity of the solvent used. It was discussed in the first chapter that side reactions with the growing poly(α-amino acid) chains can terminate the chain ends. THF was almost exclusively used to lower likelihood the chains were end-capped by reaction with solvent. DMF was used only once as the polymerization solvent and the resultant polymer had the highest molecular weight to date. It is plausible DMF made a difference but a greater likelihood was the NCA was very pure because it was purified by column chromatography.

2.11.3 GPC/MALS Conformation Plots of PEGL

GPC/MALS can measure the molecular weight distribution to find average molecular weight and PDI of polymeric samples. It is not limited to molecular weight, but can illuminate the morphology of the polymer by building a conformation plot of size as a function of molecular weight. This gives information on the shape or conformation of the scattering object. In a prototypical GPC, a light scattering detector is used. The light scattering detector has many

different detectors (18 if are all working) at different angles to measure the scattered intensity. This can be plotted in a non-Zimm fashion (what it is called in our lab, meaning a Zimm plot without the concentration scaling term on the *x*-axis) to find the radius of gyration, R_g, and molecular weight. This is performed for each "slice" separated by the column, providing the molecular weight distribution. Then log(R_g) and log(M) can be plotted. A line is fit to the data and the slope changes depending upon the morphology of the polymer. If the polymer is a globule the slope = 0.3, a random-coil the slope = 0.5, and an infinitely long stiff rod the slope = 1. Because PEGL is supposed to be a helical poly(α-amino acid), it should be a semiflexible rod with a slope ~0.8. [96, 97]

A conformation plot for sample #2 is shown in Figure 50. The polymer was synthesized and dried (residual water content ~2%). The polymer was a soft, sticky, clear candle wax type substance. The molecular weight was analyzed one year and two years after synthesis and a conformation plot was calculated. Figure 50 shows the polymer to be stiff one year after storage in the refrigerator. It was noted that the polymer may oxidize so the polymer was kept under nitrogen atmosphere by filling the vial and capping quickly prior to storage.[153] After one year the slope was 0.84 ± 0.01, indicating the polymer was equally as stiff as the commonly used PBLG (slope = ~0.8). After two years, the slope was 0.65 ± 0.01 indicating the polymer has changed conformation from a rodlike morphology to a more random coil like morphology. This is contrary to the circular dichroism studies that show the polymer to persist as an α-helix after two years (Figure 23).

Unexpectedly, a specific molecular weight provided different radii for the same polymer at different times. This should not occur because they are both sample #2, showing after two years the polymer is likely aggregated worse over time. Although sample #2 is old, newly

synthesized polymers show the same problems. Other polymers, such as PBLG, do not show this phenomena (see Figure 14).

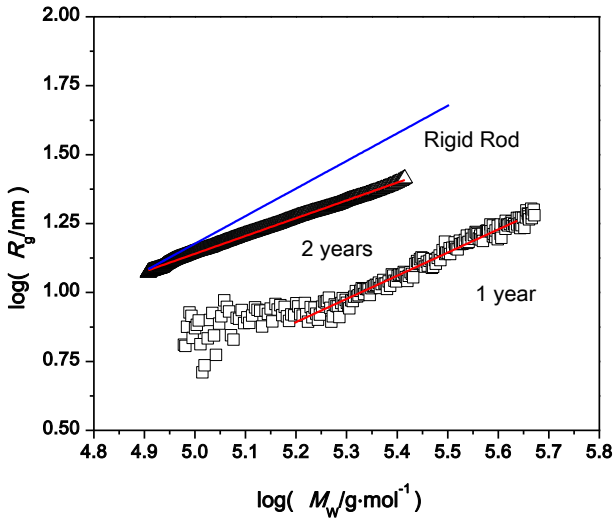

Figure 50. Conformation plots of PEGL (sample #2, M_w = 211 ± 1 kDa, PDI = 1.21 ± 0.01) in *buffer* (200 mM $NaNO_3$ + 20 mM NaH_2PO_4 + 2 mM NaN_3) after one or two years aging in the refrigerator as a solid. The slope of the fitted line after one year was 0.84 ± 0.01 and after two years was 0.65 ± 0.01. The blue line is the calculated radius of gyration for a perfectly stiff rigid rod based on the measured molecular weights.

Although the slope in Figure 50 was 0.84 ± 0.01 after one year, the fit was not very trustworthy. The goal of the project is to make a stiff rigid rod that behaves as a model system. To characterize the polymer reliably, we need to have several decades of molecular weight. Figure 50 does not meet the prerequisite. The molecular weight was not large, M_w = 211 kDa and the PDI was not broad, PDI = 1.21. Because of the size of the polymer, only a fraction of the peak that can be analyzed. Due to the limitations of the sensitivity of the light scattering detector, it cannot reliably calculate R_g that are below 10 nm. This shows as noise below 1 on the ordinate

axis in Figure 50. The maximum measured R_g was only ~20 nm. It is now apparent why high molecular weights are desired; they provide larger R_g, leading to more reliable data.

Figure 51 shows several conformation plots of sample #2 in azide and *buffer*. It shows that the conformation does not dramatically change between azide and *buffer* but also shows inconsistency between runs in the *buffer*. Regardless, the slopes show the polymer is more random coil than rodlike polymer after 2 years in the refrigerator. Once again, the change may have been due to the polymer degrading over time. This may not be happening because the circular dichroism still shows the same helicity at 2 years as the fresh polymer (Figure 23).

Figure 52 shows a conformation plot sample #18 (M_w = 526 kDa and a much younger polymer) in *buffer* solution. The slope was 0.41 ± 0.01. This shows a larger molecular weight polymer, in this instance, was no longer a stiff polymer, but something between a random coil and a globule. This may be more telling than the other conformation plots because the sizes are larger. If the sample is too small, the polymer does not appreciably bend and the persistence length cannot be measured.

For larger molecular weights, ample bending allows a true persistence length to be calculated. An analogy is trying to measure the persistence length of a steel rod one inch long or one mile long. The short steel rod does not bend as significantly as the long rod. This conformation plot has the same untrustworthiness as previous figures because the fit data does not span a large enough breadth of molecular weight. For this larger molecular weight polymer, the narrow molecular weight range was not due to its small size but rather to the narrow window of linearity in the log-log scale. Another issue with this polymer is its limited helicity (51%).

Attempting to synthesize a rodlike polymer, the highest helicity is desired. Lowering the helicity can cause problems, branching.

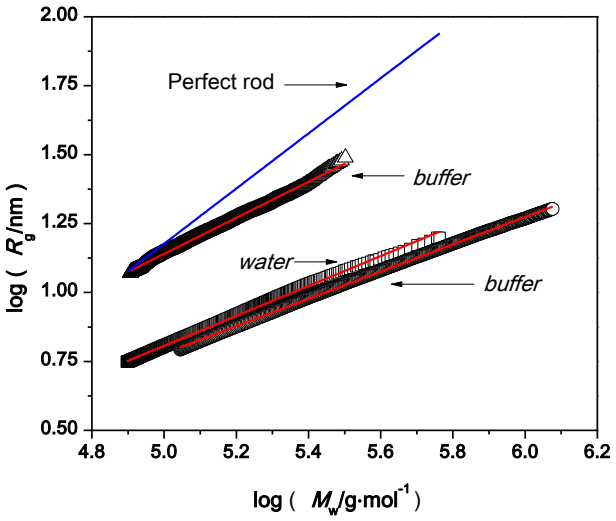

Figure 51. Conformation plot of sample #2 (M_w = 211 ± 1 kDa, PDI = 1.21 ± 0.01) in *water* and *buffer* (200 mM $NaNO_3$ + 20 mM NaH_2PO_4 + 2 mM NaN_3) after 2 years. The slope for *water* is 0.54 ± 0.01 (squares) and for *buffer* 0.49 ± 0.01 (circles) and 0.65 ± 0.01 (triangles). The two buffer lines are two different experiments after 2 years aging. The blue line is the calculated radius of gyration for a perfectly stiff rigid rod based on the measured molecular weights.

Figure 53 shows a conformation plot of sample #18 in DMF + 0.1 M LiBr. The slope is larger than when the polymer was in buffer solution (Figure 52) and is consistent with a random coil polymer. This is the only conformation plot available in DMF because the polymer was not able to be redissolved in DMF if previously dried after dialysis, even with time at elevated temperature (several weeks at 50 °C).

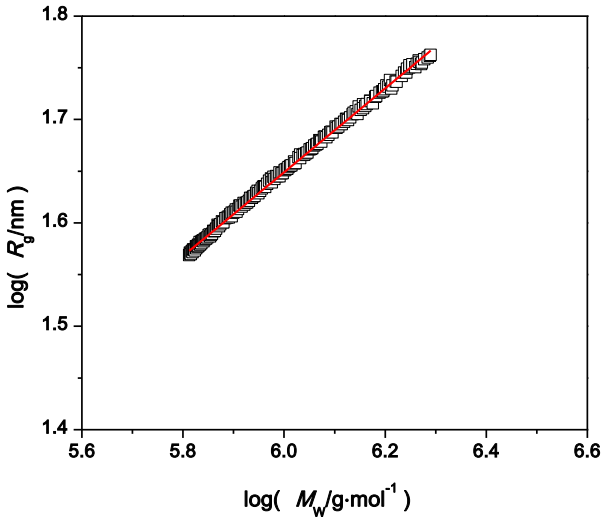

Figure 52. Conformation plot of sample #18 (M_w = 526 kDa ± 4 and PDI = 1.27 ± 0.02) in *buffer* solution (200 mM $NaNO_3$ + 20 mM NaH_2PO_4 + 2 mM NaN_3,). Black squares are data and the red line is a linear fit with slope = 0.41 ± 0.01.

When the polymerization was conducted in THF and dried, the polymer aggregates when attempting to redissovle in DMF. As an example, sample #2 was dried and analyzed in the buffer solution and DMF and the molecular weights were M_w = 211,000 and M_w = > 1,000,000 g/mol, respectively, showing an inability to redissovle in DMF following drying of the polymer. Because of this, DMF was not used as a GPC solvent, although it has been used at elevated temperatures by others.[72, 132] For polymer #18, the polymerization was performed in DMF and the crude product was directly injected into the GPC using DMF + 0.1 M LiBr as eluent. In this instance, the polymer did not aggregate as if it were previously removed from the reaction solvent.

The molecular weight changed dramatically between the buffer and DMF; this is not likely due to a calculation error because the d*n*/d*c* found for DMF + 0.1 M LiBr at 50 °C and

buffer at room temperature are very close in value (0.123 vs. 0.126). While it is true that small changes in d*n*/d*c* can change the apparent molecular weight, it should not increase the molecular weight > 2.75 fold. Also, in DMF the polymer had a larger PDI than when in the buffer. This agrees with previous statements made in this dissertation that the polymer tends to aggregate in DMF. This might also suggest the aggregates in water are less stable than in DMF, explaining why the PDI is larger in DMF than in water.

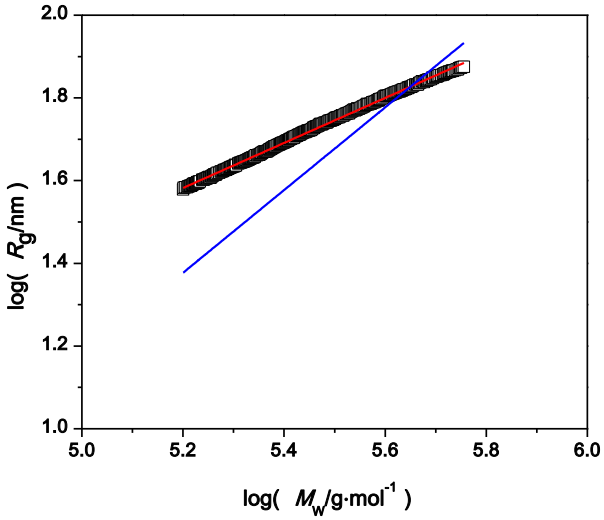

Figure 53. Conformation plot of sample #17 (M_w = 190 kDa ± 1 and PDI = 1.37 ± 0.01) in DMF + 0.1 M LiBr. The slope = 0.54 ± 0.01. The blue line is the calculated radius of gyration for a perfectly stiff rigid rod based on the measured molecular weights.

Figure 54 shows a GPC chromatogram of sample #2 in 2 mM aqueous azide. Both light scattering and DRI signals show significant tailing, but not multiple peaks. Because the light scattering trace shows the same tailing as the DRI, this indicates possible column adhesion. This was also unexpected because the PEG side chains should impart water solubility.

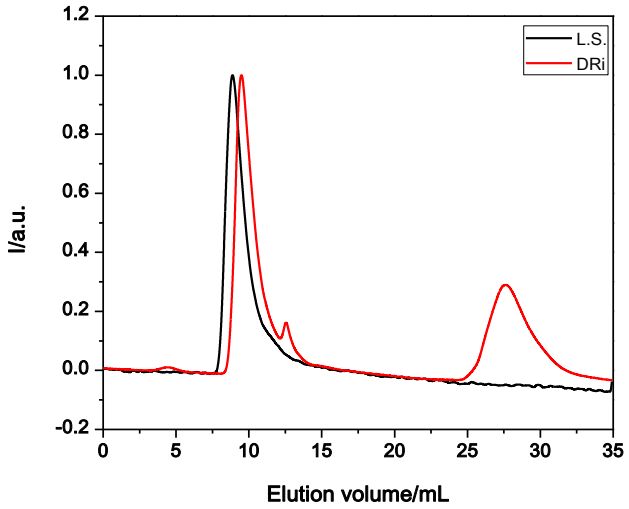

Figure 54. GPC chromatogram of sample #2 (M_w = 211 ± 1 kDa, PDI = 1.21 ± 0.01) in 2 mM aqueous NaN_3. The black line is the light scattering signal and the red line is the DRI signal.

The PDI was smaller in the aqueous azide solution (1.07 ± 0.10) compared to the buffer solution (1.21 ± 0.01) and the molecular weight was much lower in the aqueous azide solution (M_n = 84.7 ± 6.3 and M_w = 90.4 ± 7.0). This is less than half of the molecular weight calculated in the buffer solution. This may suggest worse aggregation in the buffer solution and these aggregates are more stable than those formed in the azide solution (see chapter 4 about controlling aggregation with salt). Once again, this would be consistent with sodium, the Hofmeister salt, making the polymer salt-out while in the buffer solution.

Figure 55 shows the worst example of aggregation seen for the PEGL samples and corresponding molecular weights. The order-of-magnitude difference between the two peaks molecular weights shows extreme aggregation. Aggregation does occur in DMF + 0.1 M LiBr, even though it has provided the lowest measured molecular weight of sample #18 (Figure 56).

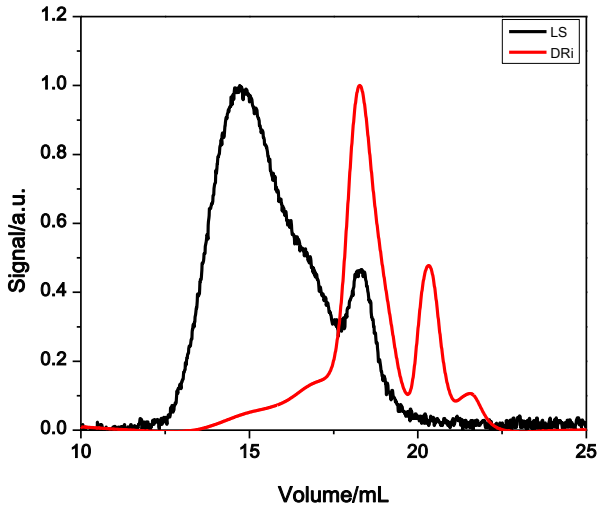

Figure 55. GPC chromatogram of sample #6 (M_w = 210 ± 4 kDa and PDI = 2.23 ± 0.07) in *buffer* solution (200 mM $NaNO_3$ + 20 mM NaH_2PO_4 + 2 mM NaN_3). The black line is the light scattering signal and the red line is the DRI signal. Left peak M_w = 190 ± 1 kDa, PDI = 2.60 ± 0.03; right peak M_w = 9.2 ± 3.2 kDa, PDI = 1.06 ± 0.09.

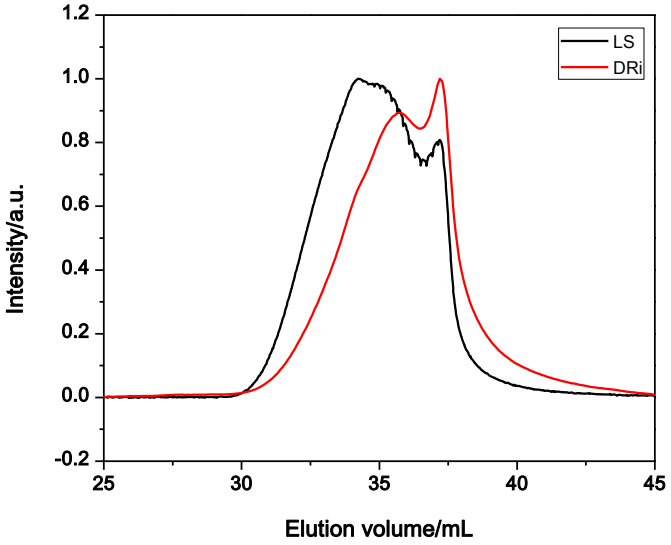

Figure 56. GPC chromatogram of sample #18 (M_w = 526 ± 4 kDa, PDI = 1.27 ± 0.02) in DMF + 0.1 M LiBr.

Figure 57 shows an overlay of a conformation plot for several samples (sample #2, sample #3, and sample #6). For PBLG, overlaying a conformation plot for several different molecular weights provides a single curve (Figure 14). PEGL showed for a particular molecular weight, each sample had a different measured radius, consistent with aggregation.

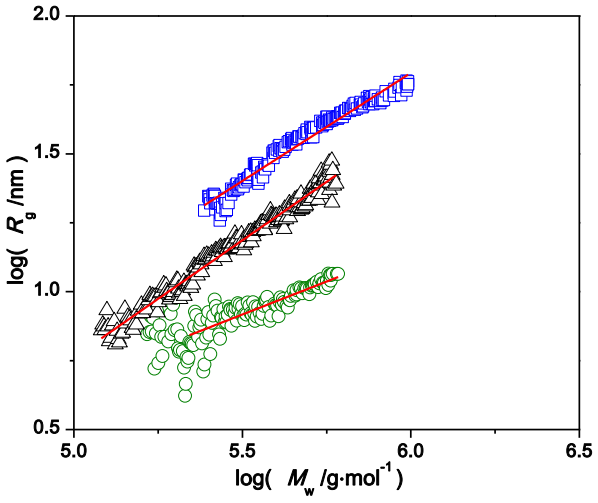

Figure 57. Conformation plots for sample #6 (blue squares, M_w = 210 ± 4 kDa, PDI = 2.23 ± 0.07), sample #3 (black triangles, M_w = 225 ± 2 kDa, PDI = 1.16 ± 0.01) and sample #2 (green circles, M_w = 211 ± 1 kDa, PDI = 1.21 ± 0.01) in *buffer* (200 mM $NaNO_3$ + 20 mM NaH_2PO_4 + 2 mM NaN_3).

2.11.4 GPC Shearing tests

Because aggregation has been established, it is useful to perform GPC experiments with different number of columns. This will change the shearing forces and should change the molecular weight of the polymer. The shearing tests results for sample #2 in buffer are found in Table 11 .When adding columns the molecular weight decreases and does so in a reproducible way (Figure 58). The decrease in molecular weight with increased shearing forces is consistent with aggregation but the reproducibility of the experiment is contrary to this idea. This may

suggest the polymers do not aggregate very quickly -- the time needed to travel from the column to the light scattering detector is about 0.5 seconds (Equation 17). If the polymer can aggregate semi-quickly, it is difficult to perform a study of the size over time (see Figure 77). Also, the PDI is much lower for the two-column runs compared to the single-column runs; again, with increased shearing forces, the PDI should decrease when adding columns.

Table 11. Molecluar weights from GPC for sample #2 (M_w = 211 ± 1 kDa, PDI = 1.21 ± 0.01) in buffer (200 mM $NaNO_3$ + 20 mM NaH_2PO_4 + 2 mM NaN_3). Uncertainty is calculated from repeat runs. All runs were performed ~2 years after the polymer was first synthesized, during which time it was dispersed in water and held at 0 ^oC.

Solvent	Condition	M_w (kDa)	PDI
Buffer	1 column	212 ± 20	1.54 ± 0.20
Buffer	1 column	154 ± 20	1.65 ± 0.20
Buffer	2 columns	103 ± 13	1.07 ± 0.11
Buffer	2 columns	107 ± 17	1.07 ± 0.11

It is not likely that the two-column experiment is breaking apart polymer chains and not aggregates because in bulk light scattering, the apparent radius measured at low angles is much larger than at high angles, suggesting aggregation. If the polymer chains were broken during translation through the columns, bulk light scattering measurements would show only large radii. Further, if the two columns were breaking the individual polymer chains, there should be a decrease in the molecular weight with no larger sizes measured by GPC/MALS.

$$Time\ between\ column\ and\ detector = \frac{volume}{flow\ rate} = \frac{\pi r^2 h \cdot 0.001}{0.5\ mL \cdot min^{-1}} \quad \text{Equation 17}$$

where 0.001 is the conversion from mm^3 to mL and the radius of the tubing was 0.0875 mm. Another observation is the decreased molecular weight measured with two columns for sample

#2 (Table 10). This may be due to the experiment being performed ~2 years following the synthesis of the polymer, although care was taken to prevent degradation by storing under nitrogen in a refrigerator.

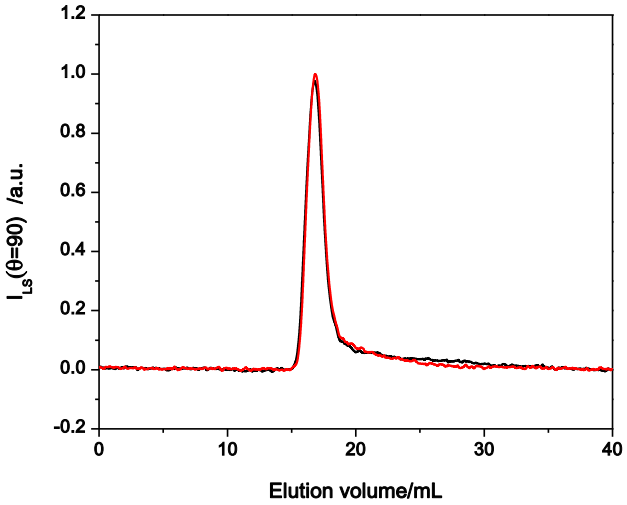

Figure 58. GPC chromatogram for sample #2 (M_w = 211 ± 1 kDa, PDI = 1.21 ± 0.01) in *buffer* (200 mM $NaNO_3$ + 20 mM NaH_2PO_4 + 2 mM NaN_3) with two columns attached. The red and black are repeat runs and the light scattering signal at 90 degrees.

2.11.5 Mark-Houwink Plots of PEGL

Intrinsic viscosity, [η], is a unique polymer attribute. This feature cemented the belief in macromolecules! Intrinsic viscosity is the lower limit of viscosity increment for a polymer solution above to the solvent viscosity, relative to concentration. Typically, with small molecules, diluting the solution decreases the viscosity until the solvent viscosity is reached. For polymers, intrinsic viscosity is some lower limit of viscosity, exceeding the pure solvent viscosity and is defined as

$$[\eta] \equiv \lim_{c \to 0} \left(\frac{\eta - \eta_s}{c \cdot \eta_s} \right)$$ Equation 18

where η is the measured viscosity, η_s is the viscosity of the solvent, and c is the concentration. Intrinsic viscosity is directly related to the size and mass of the polymer in solution; because of this, prior to size exclusion chromatography, intrinsic viscosity was used to find polymer molecular weights in solution. The units for intrinsic viscosity are mL/g making it a coefficient describing the rate of increase in viscosity of added solute.[151]

Scaling relations are found throughout polymer chemistry and one of the oldest—the $R_g \sim M^{\nu}$ relation between radius and mass–was already discussed in the background for conformation plots (ν is well known for different shapes: ν = 1/3 for a solid sphere, ½ for a random coil in a theta solvent or melt, 3/5 for a random coil in a good solvent, and 1 for a rigid rod).[151, 154] From the units of intrinsic viscosity, we can find how intrinsic viscosity relates to shape.

$$[\eta] \sim \frac{Polymer\ volume}{Molar\ Mass} \sim \frac{{R_g}^3}{M} \sim \frac{M^{3\nu}}{M} \sim M^{3\nu-1}$$ Equation 19

Depending upon shape, different scaling relations exist: $[\eta]$ is independent of M for a rigid sphere, increases as $M^{1/2}$ for random coil in a theta solvent or melt, $M^{4/5}$ for random coil in good solvent, and M^2 for a stiff rod.[151] This gives us the Mark-Houwink equation

$$[\eta] = kM^a$$ Equation 20

where k and a are the Mark-Houwink parameters.

These parameters are tabulated for many polymers in different conditions.[155] A log-log scale plot of intrinsic viscosity and molecular weight provides *k* and *a* from a linear fit. A Mark-Houwink plot can be found in Figure 59 for sample #2 in water (squares). The *a* parameter from the slope was 0.66 ± 0.01, the *k* value from the y-intercept was (6.28 ± 0.01) × 10^{-3} mL/g, and the average intrinsic viscosity was 15.2 ± 0.6 mL/g. The intrinsic viscosity for sample #2 in the *buffer* (circles in Figure 59) had a similar value to the value from water. The Mark-Houwink parameters for sample #2 in the *buffer* were *a* = 0.65 ± 0.01, *k* = (7.45 ± 0.05) × 10^{-3} mL/g and the average intrinsic viscosity of was 14.81 ± 0.04 mL/g.

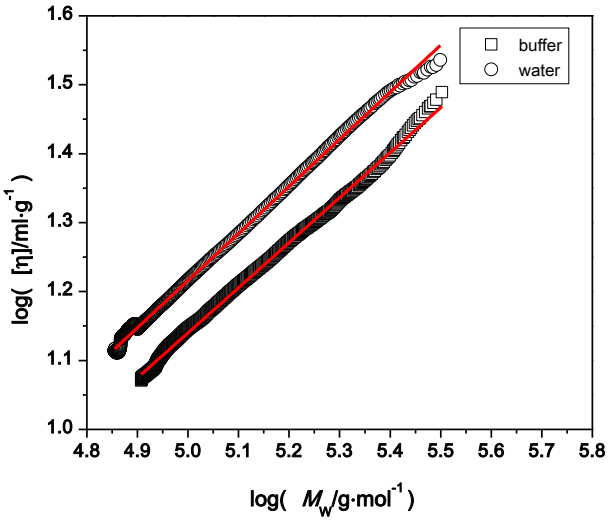

Figure 59. Mark-Houwink plot of sample #2 (M_w = 211 ± 1 kDa, PDI = 1.21 ± 0.01) in *water* (squares) and *buffer* (circles). For *water* the slope = 0.66 ± 0.01 (*a* value) and the y-intercept = (6.28 ± 0.01) × 10^{-3} mL/g (*k* value). For the *buffer* solution, *a* = 0.65 ± 0.01 and *k* = (7.45 ± 0.05) × 10^{-3} mL/g. The red lines are linear fits to the data.

The Mark-Houwink *a* parameter for sample #2 is close to the value for a random coil polymer in a good solvent, 0.6, for both *water* and *buffer* solution, indicating sample #2 is not rigid, but rather some other shape, e.g. a random coil. This suggested the polymer had changed

morphology over time and the conformation plot should be tested again (Figure 51). The conformation plot showed the polymer is no longer helical but circular dichroism (Figure 23) showed the polymer to be helical, contradicting the GPC data. This effect can be explained by interaction of the polymer and the column.

If the polymer bound to the column, the chromatography would suffer with each experiment; typical chromatograms did not show severe tailing or loops in the molecular weight trace (Figure 60), consistent with column adhesion. These data suggest the polymer is behaving differently in the bulk then when separated and may have changed over time. It is believable the polymer had aggregated worse over time, but it likely has always been aggregated. A caveat to the Mark-Houwink data is the same as for the conformation plot data, a narrow molecular weight range was tested. Therefore, more experiments need be done on a larger molecular weight range.

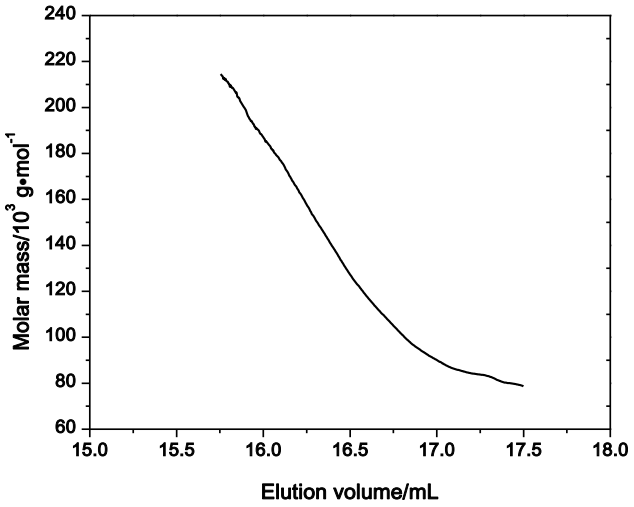

Figure 60. Plot of the molar mass as a function of the elution volume for sample #2 (M_w = 211 ± 1 kDa, PDI = 1.21 ± 0.01) in *buffer* (200 mM $NaNO_3$ + 20 mM NaH_2PO_4 + 2 mM NaN_3).

2.12 Bulk Light Scattering of PEGL

2.12.1 Why Use Bulk Light Scattering?

Light scattering used during a GPC experiment has some limitations: weak laser, only one wavelength of light can be used, but the most important difference is that the polymer solution had to go through a column prior to measurement. While not necessarily a hindrance, this may cause complications as discussed in this dissertation. Bulk light scattering on the other hand can show long-term stability, the quality of solvent, many different solvents at different temperatures (do-able with a column but harder), and it does not rely on column separation. For an analyte that may interact with a column, bulk scattering is necessary and may be more illuminating.

2.12.2 Dynamic Light Scattering Background

Dynamic light scattering (DLS) is one of several ways to determine diffusion coefficients. Depending upon the characteristics of your system, DLS may or may not be a wise decision. Other techniques to find diffusion coefficients, such as fluorescence photobleaching recovery (FPR), fluorescence correlation spectroscopy (FCS), analytical ultracentrifugation (AUC), NMR, and particle tracking all offer advantages and disadvantages. The best polymer characterization compares the results from multiple techniques.

Dynamic light scattering measures the diffusion coefficient by building a correlation function (Equation 21).

$$g^{(2)}(t) = \lim_{T\to\infty} \frac{1}{2T} \int_{-T}^{T} I(t')\, I(t'+t) dt' \qquad \text{Equation 21}$$

where $g^{(2)}(t)$ is the normalized second order correlation function, T is the time of the experiment, I is the intensity of the scattered light, and t is the lag time. A representative correlation function is found in Figure 61. At short lag times the polymers exhibit high correlation and it decays until at large enough lag times, the particles are no longer correlated. The inflection point of the sigmoidal curve in Figure 61 is known as the decay time, τ. Smaller particles have a short decay time because they are moving quickly and can become uncorrelated faster while large particles have a long decay time because they are moving slowly.

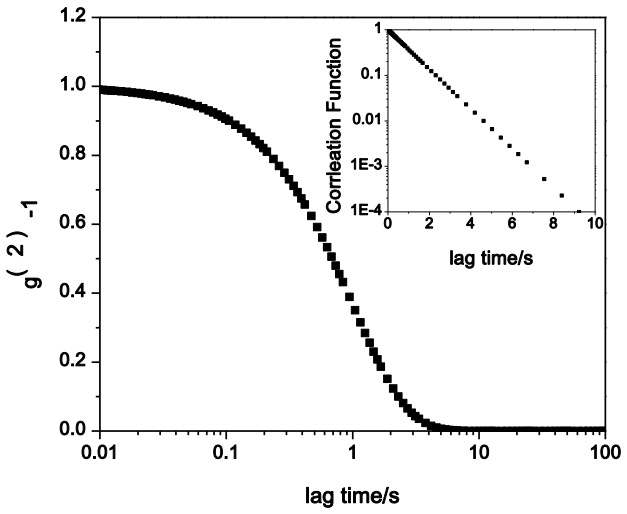

Figure 61. Ideal correlation function. The inset is the same correlation function in semi-log form.

The diffusion coefficient of a simple, monodisperse system can be found by fitting the correlation function with an exponential equation (Equation 22).

$$g^{(1)}(t) = A_1 e^{-\Gamma_1 t} + A_2 e^{-\Gamma_2 t} + \cdots A_n e^{-\Gamma_n t} \qquad \text{Equation 22}$$

$$\Gamma_{Vv} = \tau^{-1} = q^2 D_t \qquad \text{Equation 23}$$

$$q = \frac{4\pi n}{\lambda_o} \sin\left(\frac{\theta}{2}\right) \quad \text{Equation 24}$$

$$\Gamma_{\mathrm{Hv}} = q^2 D_t + 6D_r \quad \text{Equation 25}$$

$$D_t = \frac{k_B T}{6\pi\eta_o R_h} \quad \text{Equation 26}$$

where A_n is the amplitude, Γ_{Vv} is the decay rate of vertically polarized incident and measured light, Γ_{Hv} is the decay rate of vertically polarized incident and horizontally polarized measured light, t is time, τ is decay time, q is the scattering vector, D_t is the translational diffusion coefficient, D_r is the rotational diffusion coefficient, n is the refractive index of the solvent, λ_o is the wavelength of the laser light in vacuum, and θ is the angle when measuring in radians, T is temperature, k_B is Boltzmann's constant, η_o is the viscosity of the solvent, and R_h is the hydrodynamic radius. Equation 22 shows a correlation function can be fit with multiple exponentials in an attempt to separate multiple sized scatters in the same solution. Equation 23 shows the decay rate (Γ_{Vv}) is directly proportional to the diffusion coefficient and inversely related to the decay time in a typical DLS experiment.

Many different diffusion coefficients are measureable: apparent diffusion coefficient, mutual diffusion coefficient, and self-diffusion coefficient. The apparent and mutual diffusion coefficients are directly measured by DLS but the self-diffusion coefficient is found from DLS only by extrapolating to zero polymer concentration.[151] Other methods can measure self-diffusion at finite concentrations.

The prototypical path to the diffusion coefficient is measuring the decay rate, Γ, at multiple q and building a plot of Γ as a function of q^2 (Figure 62). The apparent diffusion coefficient is found from the slope. The intercept is also telling: a non-zero intercept shows

measurement of non-translational diffusive motions (or multiple scattering, which is not a factor in any of the DLS work reported in this dissertation).

A Γ vs. q^2 plot for a rod is found in Figure 63.[156] It has two concentrations but the upturn is only observed in the lower one; for this discussion, the higher concentration is ignored. Rodlike polymers have a characteristic feature of an increase in the decay rate at higher angles when the decay rate is plotted against q^2. At low concentrations and low q, the characteristic distance measured by DLS is large; this means DLS can only measure translational diffusion of the rodlike polymer.

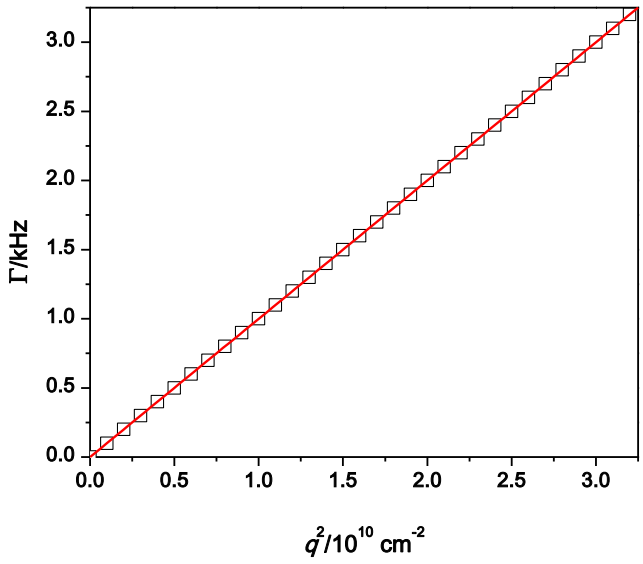

Figure 62. How the decay rate scales with the magnitude of the squared scattering vector (schematic).

At higher q, a smaller characteristic distance, rotation of the rod becomes prevalent as an increase in the decay rate. PEGL, showing characteristics of a rodlike polymer should exhibit

this feature. The high-q, high-concentration behavior is beyond the scope of this discussion; it suffices to say that it cannot be interpreted as motion from single, isolated rods.

Another possible reason for the increase in the decay rate against q^2 is polydispersity. At low q values, large particles contribute more to the scattered signal but this preference decreases with angle. For very large particles, the intensity decreases dramatically at high angles. If the sample is highly polydisperse, the average decay rate is slow at low q (large particles) but faster at higher q (smaller particles). This resembles the appearance of a monodisperse rigid-rod type polymer; in either case, the measured average decay rate increases at higher angles.

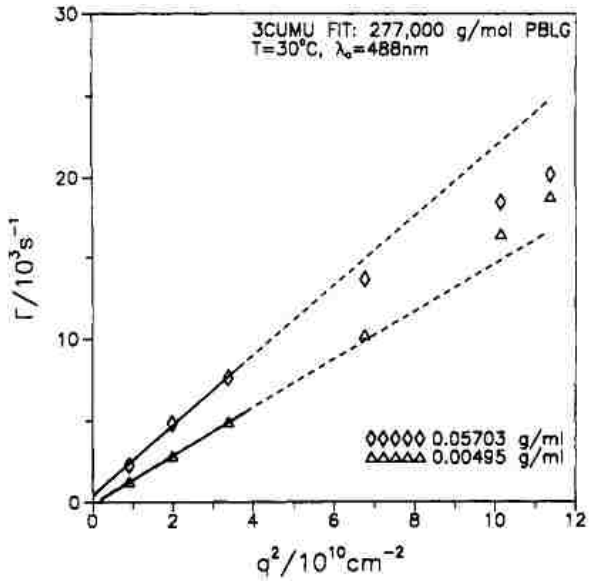

Figure 63. 3rd cumulant decay rates plotted against q^2 for PBLG-277000. Reprinted with permission from DeLong, L. M.; Russo, P. S. *Macromolecules* **1991,** 24, (23), 6139-6155. Copyright 1991 American Chemical Society.

Depolarized light scattering can determine if the increase in the decay rate as a function of q^2 is due to polydispersity or rotation of the rod. In a typical DLS experiment, the initial laser light is vertically polarized and the measured scattered light can be vertically polarized or

unpolarized (indicated by Vv or Uv). Vv indicates having two vertical polarizers in place, one between the laser and sample and the other between the sample and detector. Uv is when only one polarizer is used and placed between the sample and laser to help eliminate any stray non-vertical light.

In an Hv experiment, a vertical polarizer is placed between the laser and the sample and a horizontal polarizer is placed between the sample and detector. The reason the Hv signal can be measured for a rodlike polymer is due the anisotropy along the two axes of the rod. Rods can have two different polarizabilities depending on which axis is measured, either the long or short axis, and light scattering directly relies upon the polarizability of the sample. Most random coils on the other hand, provide a much weaker Hv signal than polymers with large anisotropy.

Equation 25 shows why rodlike polymers have an increase in the decay rate during a Hv experiment: rotation of the rod. The added term, $6D_r$, is only measurable in an Hv experiment when the polymer has sufficient anisotropy of the polarizability. Consequently, measuring the decay rate as a function of q^2 from the Hv signal of a polymer provides a positive y-intercept directly due to rotation. If the measured sample has an increase in the decay rate for Vv, has no rotational diffusion coefficient measured from the depolarized signal, and no value of qL provides a measure of the rotation in a Vv experiment, the increase is due to polydispersity. This provides an easy way to check if the increase in the decay rate from a Vv experiment is from polydispersity or the morphology of the polymer.

Not all rods show the increase in the decay rate as a function of q^2 in a Vv experiment. A value $qL > 4$ has to be reached in order to see the rod rotating, meaning short rods do not show the increase in the decay rate, unless measured in an Hv experiment. This is another reason why

higher molecular weights were desired for this project. This poses a problem for sample #2: calculating the expected length for a M_w = 211,000 g/mol and the length is 110 nm. With a blue laser, the largest qL value at θ = 120 degrees is 2.5, and this value is even lower if the length of the rod is found from the the translational diffusion coefficient using the Kirkwood-Riseman Equation. This suggests the increase in the decay rate should be due to polydispersity for sample #2 because end-over-end rotation should not be measureable in a Vv experiment. While the qL is too small based on the meaured molecular weight from GPC and the zero PEGL concentration diffusion coefficient, many PEGL samples show the increase in the decay rate, even sample #6 where the majority of the polymer is < 10 kDa. This further agrees with the postulation of polydispersity.

2.12.3 Static Light Scattering Background

Static light scattering needs very little introduction after introducing dynamic light scattering. Scattering from large molecules shows an angular intensity dependence, and can be quantified by the form factor, $P(\theta)$. The form factors for many shapes are well known and can be fit to the measured data, elucidating the shape of the polymer in solution. If the shape of the polymer is not known beforehand, measuring the scattering of a sample in the Guinier regime, $qR_g < 1$, allows for calculation of the radius of gyration independent of shape. The radius of gyration, R_g, is the mass-weighted radius from the object's center of mass. In a Guinier plot, the radius of gyration is found from the slope of the natural log of intensity as a function of scattering vector magnitude (Figure 64).

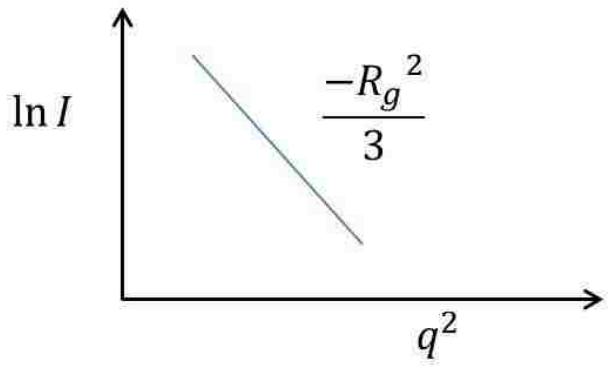

Figure 64. Guinier plot. Slope = $-R_g^2/3$.

2.12.4 Dynamic Light Scattering of PEGL

A waterfall and semi-log plot of the correlation functions for multiple angles of sample #2 in *buffer* are found in Figure 65. As the angle is increased, the decay time shifted to shorter times. The semi-log plot had significant curvature, showing significant polydispersity is measureable, even at higher angles. Monitoring each run prevented this polydispersity being due to dusting events.

As stated in the previous section, rodlike polymers show in increase in the decay rate at high q due to rotation of the rod. The decay rate as a function of q^2 for sample #2 is found in Figure 66, showing the expected increase in the decay rate at high q for a rod; alternatively, the increase in the decay rate may be due to polydispersity. Figure 67 shows the measured diffusion coefficient and polydispersity as a function of q^2. These plots show the diffusion coefficient (increased by 38%) and the PDI (decreased by 27%) vary when changing the scattering vector magnitude, suggesting the sample exists as a mixture of smaller and larger polymers; this would be consistent with aggregation or polydispersity. If rod tumbling was observed, the PDI (which represents non- exponentiality of any kind) should increase at high q, not decrease, making the

A

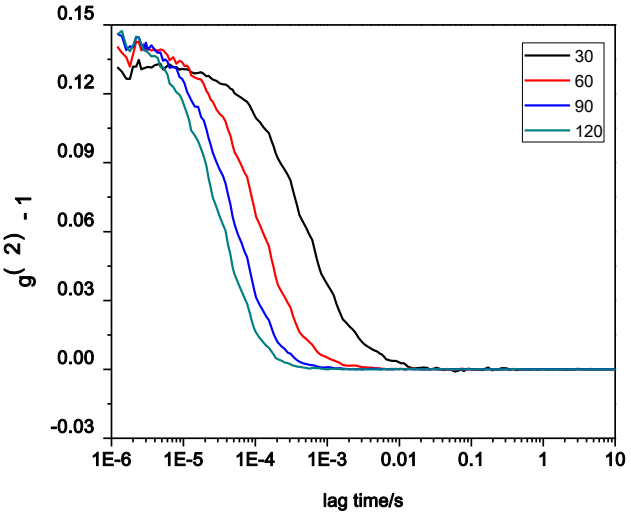

B

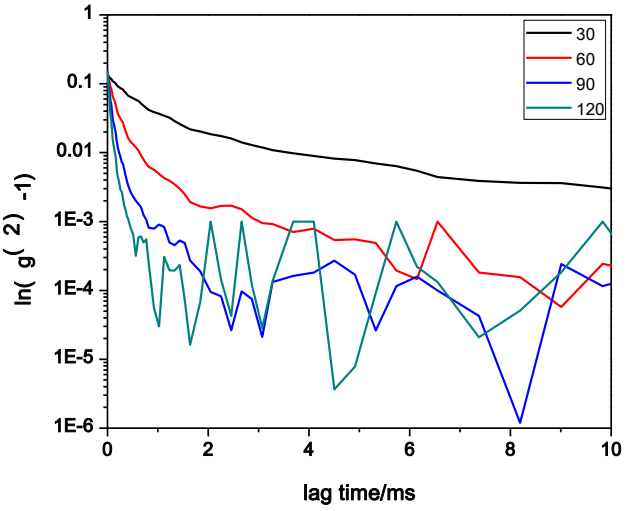

Figure 65. A) Waterfall plot of the correlation function B) Semi-log plot of the correlation function. Sample #2 (M_w = 211 ± 1 kDa, PDI = 1.21 ± 0.01) in *buffer* solution (200 mM $NaNO_3$ + 20 mM NaH_2PO_4 + 2 mM NaN_3), 4.6 mg/mL PEGL at room temperature.

hypothesis of PEGL behaving as a rod less valid. PEGL has a measureable Hv signal, possibly providing a rotational diffusion coefficient in the future. Cumulant fits were applied to the

correlation functions to find the decay rates. Because PEGL showed an increase in the decay rate as a function of *q* only the first three linear points were used to find the diffusion coefficient. The sizes from the diffusion coefficient extrapolated to zero concentration are going to be skewed to lower values because the sample is polydisperse and only low angles were fit (Figure 70). Figure 70 shows no appreciable change in the measured diffusion coefficient of sample #2 in *buffer* when changing the polymer concentration. If aggregation was a problem, the diffusion coefficient normally decreases with polymer concentrations to reflect the increased size. It may be masked by the limited *q* values used for the 3CUMU fits.

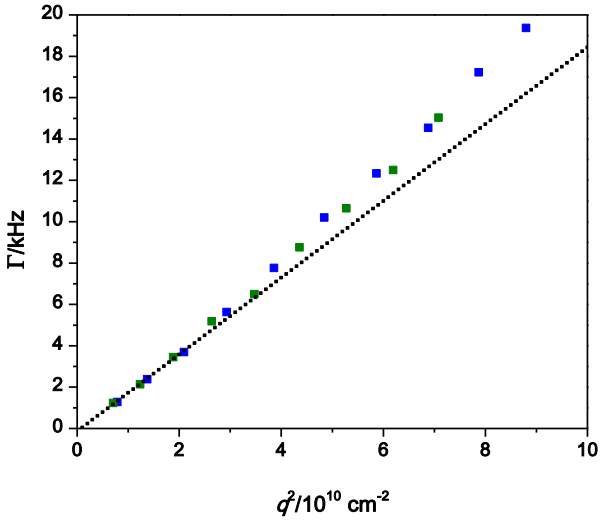

Figure 66. A plot of the decay rates as a function of squared scattering vector magnitude for sample #2 (M_w = 211 ± 1 kDa, PDI = 1.21 ± 0.01) in *buffer* (200 mM $NaNO_3$ + 20 mM NaH_2PO_4 + 2 mM NaN_3), 4.6 mg/mL PEGL at room temperature. Blue points are measured with a blue argon ion laser (488 nm) and the green points are measured with a green argon laser (514.5 nm). The black points are linear fit to the first 6 points.

The effect of aggregation may be minimized in this case because of the fitting used, but the diffusion coefficient should still change with concentration The diffusion coefficient was

calculated by taking the average of the diffusion coefficient found from the slope of the decay rate as a function of q^2 (at low angles) and the measured diffusion coefficient as a function of q^2 (Figure 67 A). The uncertainty is the greatest difference between the average diffusion coefficient found and either diffusion coefficient measured.

Fitting the zero PEGL concentration diffusion coefficient to the Kirkwood-Riseman equation (Equation 27) [157] gives the length of the polymer, assuming it is a rigid rod

$$D_0 = \frac{k_B T \ln(L/d)}{(3\pi\eta_0 L)} \qquad \text{Equation 27}$$

where k_B is Boltzmann constant, T is temperature in Kelvin, L is the length of the polymer, d is the diameter of the polymer (taken as 2.2 nm), and η_0 is the solvent viscosity. Equation 27 is not a solvable equation, but it can be numerically approximated to a high accuracy with Excel Solver. From the fit D_0 = (1.85 ± 0.04) × 10^{-7} $cm^2 \cdot s^{-1}$, R_h = 13 ± 1 nm, and L = 101 nm. Assuming each repeat unit of the polymer traverses 0.15 nm along the chain axis, Equation 28 allows for the molecular weight of the polymer to be calculated.

$$L = \left(\frac{MW}{MW_0}\right) \times 0.15\ nm \qquad \text{Equation 28}$$

where L is the polymer length calculated from the Kirkwood-Riseman equation (Equation 27), MW is the molecular weight of the polymer (either M_w or M_n, but M_w was used in this case), MW_0 is the repeat unit molecular weight (taken as 288 g/mol), and 0.15 nm is the length of each repeat unit projected along the helix axis.

A

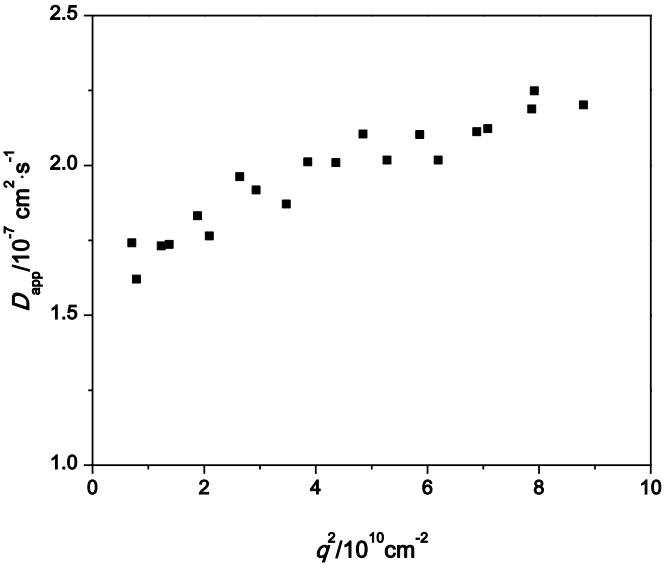

B

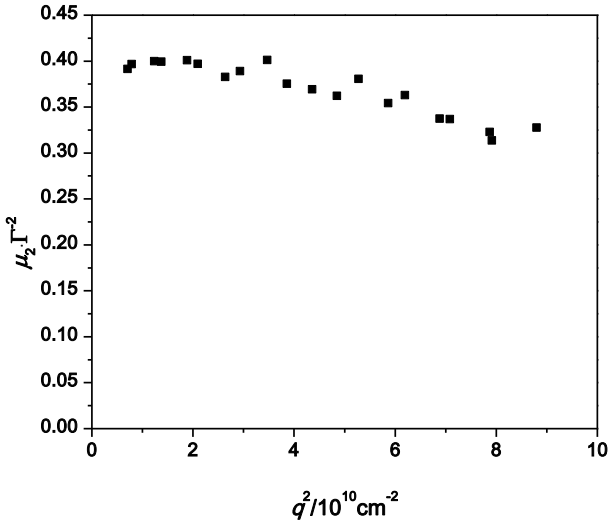

Figure 67. Sample #2 (M_w = 211 ± 1 kDa, PDI = 1.21 ± 0.01) A). Measured diffusion coefficient as a function of scattering vector magnitude. B) μ_2/Γ^2 (PDI) as a function of scattering vector magnitude from third cumulant fits. Both A and B are in *buffer* (200 mM $NaNO_3$ + 20 mM NaH_2PO_4 + 2 mM NaN_3) and at room temperature.

The molecular weight calculated in Equation 28 is somewhat ambiguous in this case; the Kirkwood-Riseman equation is only valid for samples with a PDI equal to unity. The calculated *MW* was 215 kDa, L = 101 nm. Comparing this to GPC (M_n = 174 kDa, M_w = 211 kDa; sample #2 in Table 10) sample #2 shows agreement between bulk and GPC light scattering data for weight average molecular weights but fair agreement between number average molecular weights.

When the PDI exceeds about 0.3, other fits, such as CONTIN, are profitable. Figure 68 and Figure 69 show 3CUMU, 2-EXP, and CONITN fits for sample #2 in *buffer* at 30 and 90 degrees. For 30 degrees, the 2-EXP fit bracketed the 3CUMU fit; they do not fully agree but both show a fast and slow decay rate. The 3CUMU fit landing between the 2-EXP fit is typical (Reference 156, Figure 12), showing the 3CUMU fits at low angles to find the apparent diffusion coefficient was an appropriate technique.

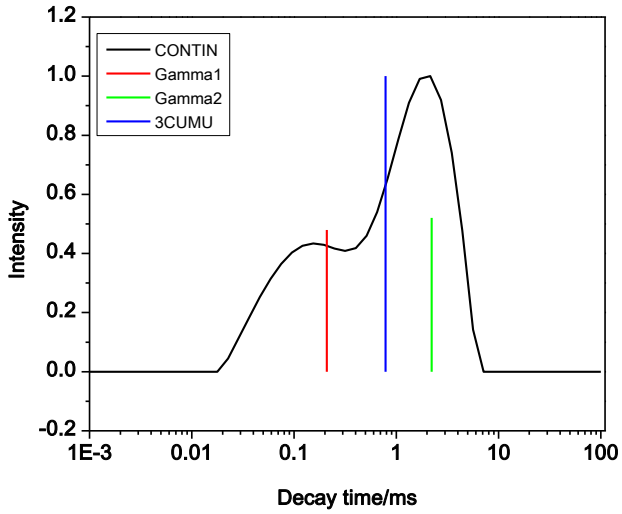

Figure 68. CONTIN, 2-EXP, and 3rd cumulant fits for sample #2 (M_w = 211 ± 1 kDa, PDI = 1.21 ± 0.01), 4.6 mg/mL in *buffer* (200 mM $NaNO_3$ + 20 mM NaH_2PO_4 + 2 mM NaN_3), θ = 30 degrees at room temperature.

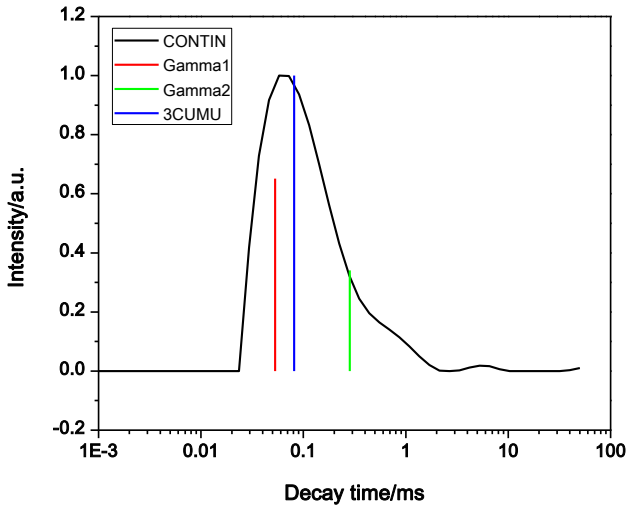

Figure 69. CONTIN, 2-EXP, and 3rd cumulant fits for sample #2 (M_w = 211 ± 1 kDa, PDI = 1.21 ± 0.01), 4.6 mg/mL in *buffer* (200 mM $NaNO_3$ + 20 mM NaH_2PO_4 + 2 mM NaN_3), θ = 90 degrees and room temperature.

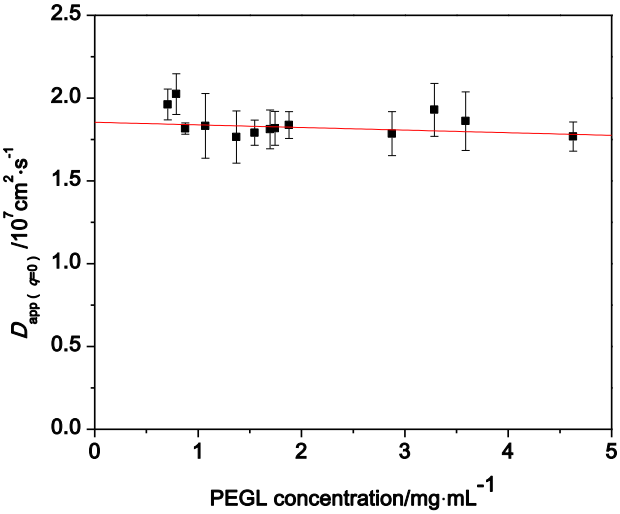

Figure 70. Plot of the measured diffusion coefficient found from 3rd cumulant fits for multiple PEGL concentrations (sample #2 in *buffer*, M_w = 211 ± 1 kDa, PDI = 1.21 ± 0.01, 200 mM $NaNO_3$ + 20 mM NaH_2PO_4 + 2 mM NaN_3) at room temperature. See text for the diffusion coefficient and uncertainty calculations. D_0 = (1.85 ± 0.04) × 10^{-7} $cm^2 \cdot s^{-1}$, the length from Kirkwood-Riseman equation was 101 nm.

Although the 3CUMU approach is able to fit the data, CONTIN and 2-EXP fits were used. In a typical preparation, the amplitude of the 2-EXP fits are tracked with angle because translational diffusion should dominate at low angles (large amplitude of A_1 in Equation 22) but as the angle is increased, rotational diffusion should become more prevalent (increasing amplitude of A_2 in Equation 22).

Figure 71 shows the CONTIN fits for eight angles of sample #2 in *buffer* at 4.6 mg/mL. The fit decay rate heavily depends upon angle, once again, this would be consistent with aggregation. The main peak at every angle provides a calculated R_h = 9.8 ± 0.9 nm, MW = 141 ± 14 kDa, L = 66 ± 7 nm. If these fits are believable, the polymer is severely aggregating. The GPC data show the polymer aggregates but it did not show to what extent. This DLS data does give an indication of the severity of the aggregation.

Figure 72 A shows the decay rate measured with 2-EXP fits as a function of q^2 and B shows the amplitude of the fits. The amplitude of the slower decay ($A1$) decreases and the amplitude of the faster decay ($A2$) increases at higher angles, as expected for rodlike polymers. Although the amplitude change follows expectation, the amplitude ($A2$) from rod tumbling should be small, not equal to the amplitude of the translation ($A1$). This is not consistent with the expected rodlike behavior. As stated before, the qL value for the measured molecular weight for sample #2 is too small to observe rod-tumbling. This means the polymer must be aggregating if rod tumbling is observed or the polymer system is highly bimodal; Figure 71 suggests the latter argument. Figure 74 and Figure 75 show decay rates and amplitudes as a function of squared scattering vector magnitude for multiple samples to show PEGL in general, exhibits the increase in the decay rate at higher q values.

A

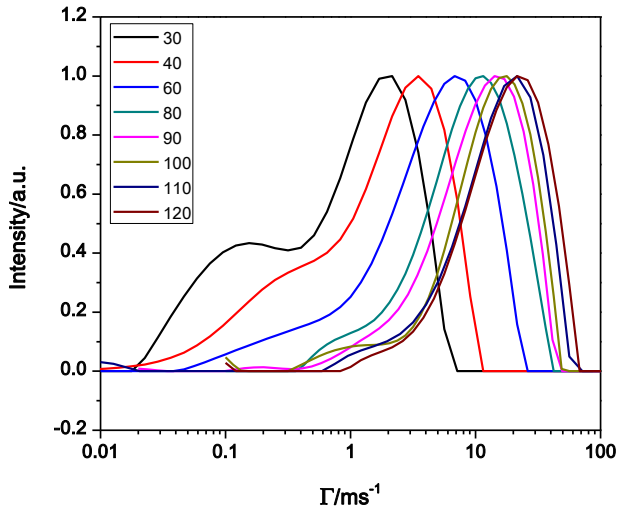

B

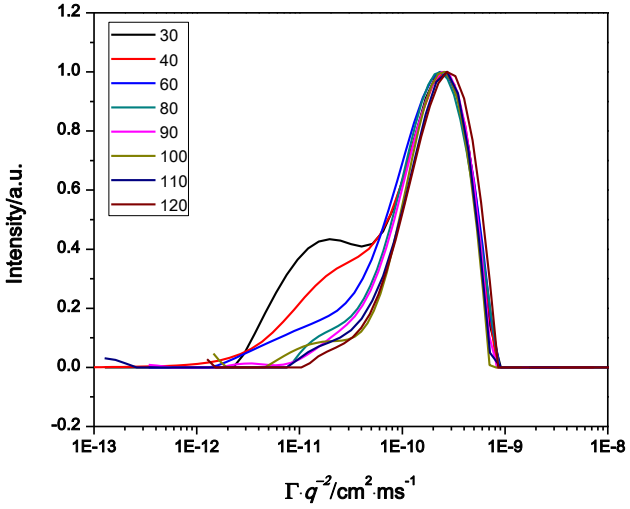

Figure 71. CONTIN fits for multiple angles. Sample #2 (M_w = 211 ± 1 kDa, PDI = 1.21 ± 0.01), *buffer* solution (200 mM $NaNO_3$ + 20 mM NaH_2PO_4 + 2 mM NaN_3), 4.6 mg/mL, room temperature.

A)

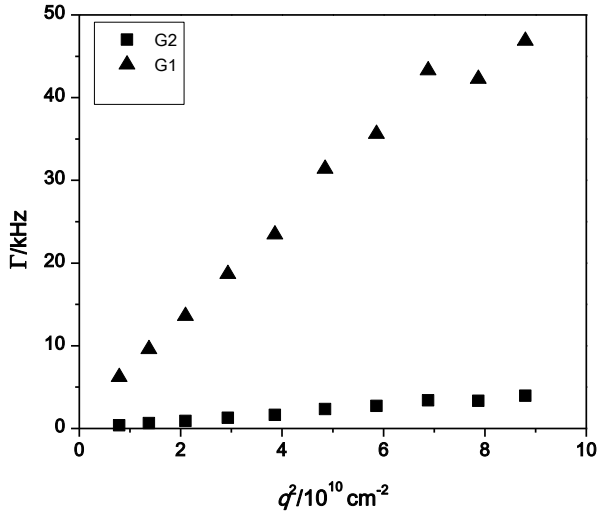

B)

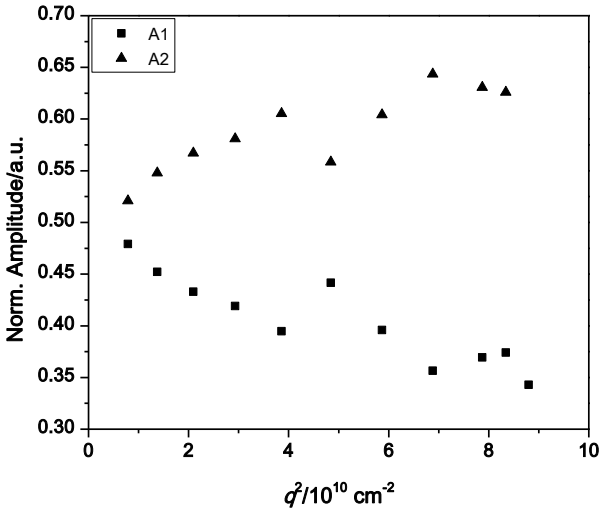

Figure 72. A) Decay rates found form 2-EXP fits. B) Normalized amplitude for 2-EXP fits. Sample #2 (M_w = 211 ± 1 kDa, PDI = 1.21 ± 0.01) in *buffer* (200 mM $NaNO_3$ + 20 mM NaH_2PO_4 + 2 mM NaN_3), 4.6 mg/mL, room temperature.

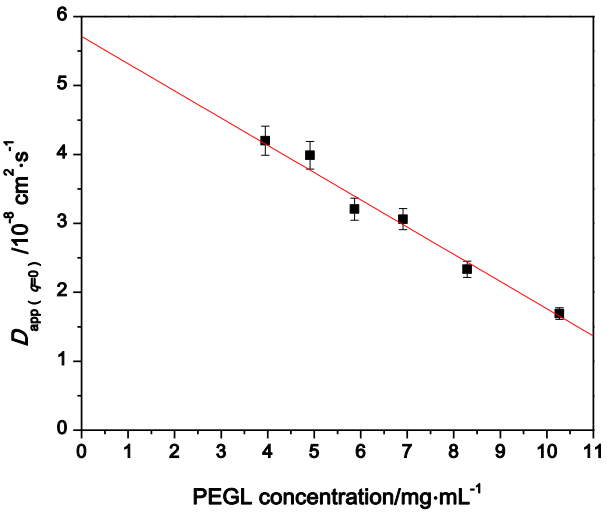

Figure 73. A plot of the apparent diffusion coefficient found from 3rd cumulant fits extrapolated to zero angle as a function of PEGL concentration in *water* for sample #18 (M_w = 526 ± 4 kDa, PDI = 1.27 ± 0.02) at room temperature. Error bars are set at 5%.

In Figure 74, sample #6 shows the increase in the decay rate but this may be due to the high polydispersity. Figure 75 shows an in increase in the decay rate as a function of *q*. Figure 73 shows a plot of the measured diffusion coefficient found from third cumulant fits for multiple PEGL concentrations of sample #18 in water. This behaves differently than sample #2 in *buffer* (Figure 70). The decrease in the measured diffusion coefficient when the concentration was increased is indicative of aggregation. This aggregation mechanism may differ from the aggregation hypothesized for samples with ~100% helicity.

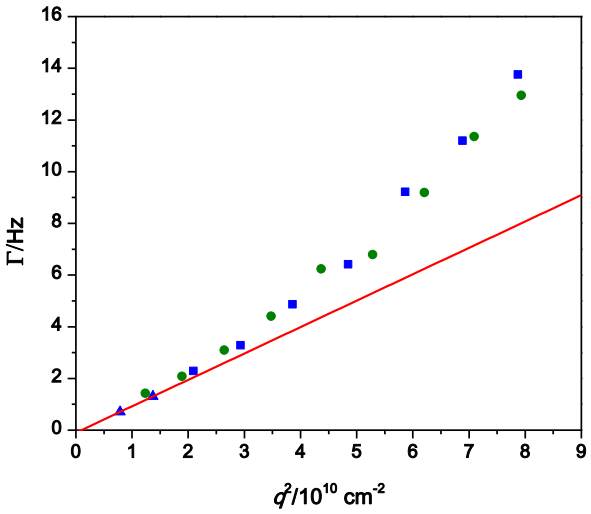

B)

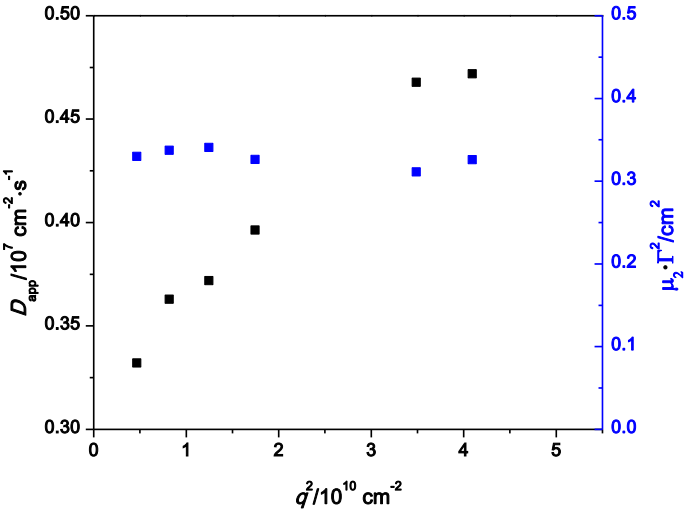

Figure 74. A) Plot of the decay rates found from 3rd cumulant fits as a function of squared scattering vector magnitude for sample #6 (M_w = 210 ± 4 kDa, PDI = 2.23 ± 0.07) in *buffer* (200 mM $NaNO_3$ + 20 mM NaH_2PO_4 + 2 mM NaN_3), Blue points are measured with a blue argon laser (488 nm) and the green points are measured with a green argon laser (514.5 nm). The red line is linear fit to the first two blue points. B) Plot of the apparent diffusion coefficient and a measure of polydispersity as a function of scattering vector magnitude. All experiments were measured at PEGL concentration of 11.07 mg/mL at room temperature.

A)

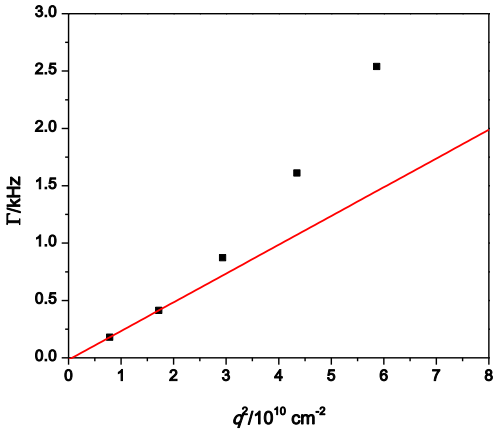

B)

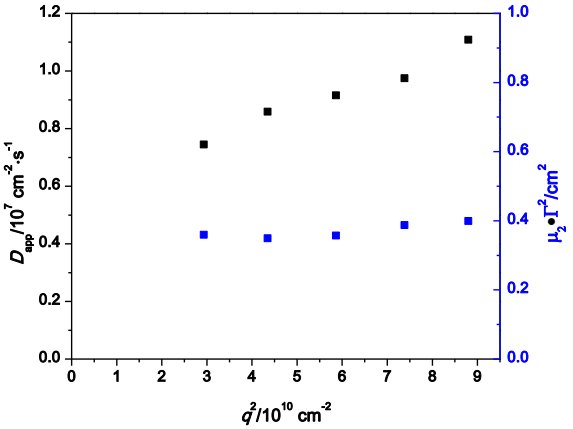

Figure 75. A) A plot of the decay rates found from 3rd cumulant fits as a function of squared scattering vector magnitude for sample #18 (M_w = 526 ± 4 kDa, PDI = 1.27 ± 0.02) B) Plot of the apparent diffusion coefficient and a measure of polydispersity as a function of scattering vector magnitude. All experiments were 10 mg/mL PEGL in *buffer* (200 mM $NaNO_3$ + 20 mM NaH_2PO_4 + 2 mM NaN_3) at room temperature. The red line is linear fit to the first two blue points.

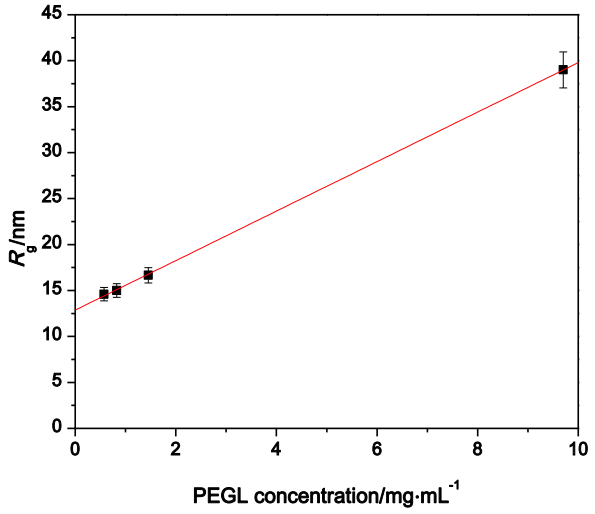

Figure 76. A plot of the radius of gyration found from 3rd cumulant fits extrapolated to zero angle as a function of PEGL concentration in *water* for sample #18 (M_w = 526 ± 4 kDa, PDI = 1.27 ± 0.02) at room temperature. Error bars are set at 5%.

To quantify the time scale needed for aggregate formation, a PEGL sample was freshly filtered and the size was monitored as a function of time by double exponential fits. Figure 77 shows the apparent sizes from double exponential fits as a function of the scattering vector magnitude after sitting 6 days.

The size is the average from multiple runs and the uncertainty is taken as the difference between the average and the maximal value. At low angles, the size is large and the uncertainty is small but at higher angles the reverse is true. This would be consistent for a polydisperse system. At low angles there are large, semi-uniform polymers but as the angle increases the contribution to the scattering decreases, allowing for measurement of the smaller aggregates. The two sizes at zero q are 134 ± 5 nm and 16 ± 1 nm and may suggest an aggregation number of 9 ± 1. The uncertainty for the size at zero q was calculated from a 95% confidence interval and the

error for the aggregation number was calculated from the maximal deviation of the average aggregation number and the most extreme value.

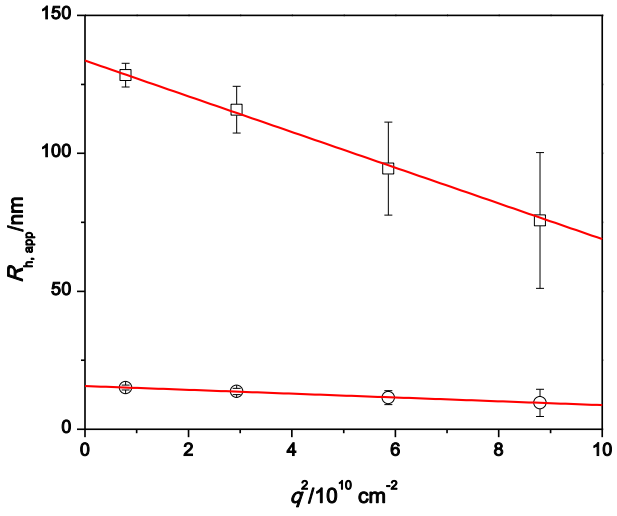

Figure 77. A plot of the apparent radius found from 2-EXP fits as a function of the scattering vector magnitude after aging for 6 days. Sample #18 (M_w = 526 ± 4 kDa, PDI = 1.27 ± 0.02), 3.96 mg/mL in *water* at room temperature. The two radii at zero q are 134 ± 5 nm and 16 ± 1 nm.

Comparing the sizes at each angle at different times is illuminating: the aggregates form quickly. The sample was measured immediately after freshly filtering the sample and the apparent diffusion coefficient barely changed after 6 days (Figure 78). This suggests the aggregates form very quickly (less than 30 seconds, See Figure 85) and are persistent. This poses a problem for GPC experiments because the columns should break any weakly associated aggregates (see Table 11); this would prevent GPC from showing a more representative PDI because light scattering is dominated by larger aggregates.

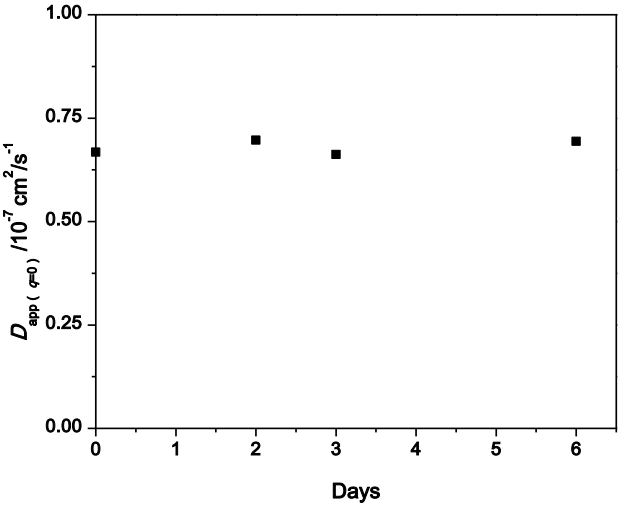

Figure 78. A plot of the apparent diffusion coefficient measured after aging for up to 6 days. Sample #18 (M_w = 526 ± 4 kDa, PDI = 1.27 ± 0.02), 3.96 mg/mL in *water* at room temperature.

The type of aggregation can be deduced by a simple plot as long as the polymer is in a theta solvent based on Equation 29.

$$(\overline{M_w})_{app,\theta} = (\overline{M_I})_w + Kc(\overline{M_I})_w \qquad \text{Equation 29}$$

where $(\overline{M_w})_{app,\theta}$ is the measured molecular weight at some angle, $(\overline{M_I})_w$ is the weight average of the unaggregated polymer, K is the aggregation equilibrium constant, and c is the weight percent of polymer. [102]

Figure 79. Possible segmental aggregation of rodlike polymers.

Even though the theory is only valid under theta conditions, it proves illustrative. Two types of aggregation can exist: end-to-end or segmental. In end-to-end aggregation, the aggregation occurs at the chain ends, eliminating chain length dependence. For segmental

aggregation, or side-by-side aggregation, the chain length alters the ability of the polymer to aggregate. Plotting the apparent molecular weight in a theta solvent as a function of concentration indicates the type of aggregation. If the plot is linear, segmental aggregation occurs but if it is non-linear, end-to-end aggregation is occurring. Figure 80 shows the plot of $(M_w)_{app,\theta}$ as a function of polymer concentration is linear, suggesting segmental aggregation for PEGL in *buffer*.

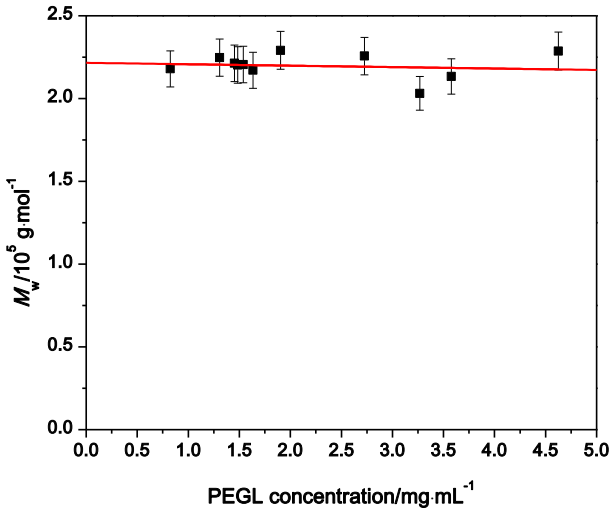

Figure 80. Plot of the apparent molecular weight found via DLS from the Kirkwood-Riseman equation for sample #2 (M_w = 211 ± 1 kDa, PDI = 1.21 ± 0.01) in *buffer* (200 mM $NaNO_3$ + 20 mM NaH_2PO_4 + 2 mM NaN_3) at room temperature. The diffusion coefficient was calculated using 3rd cumulant fits. The uncertainty is set at 5%.

Some invalid assumptions were made. First, the *buffer* is a bad solvent for PEGL, not a theta solvent. Second, the Kirkwood-Riseman equation is only valid when extrapolated to zero concentration of polymer. To find each molecular weight, the Kirkwood-Riseman equation was applied at each concentration. Third, 3CUMU fits are not best applied to these data because the

PDI is too large, 2EXP or CONTIN fits are required (see above). An analogous plot of D_{app} as a function of concentration can also be performed (Figure 70 and Figure 73). This doesn't require using the Kirkwood-Riseman equation to find molecular weight, but it was also linear, suggesting segmental aggregation for PEGL in water and GPC and with ~100% or ~50% helicity. This suggests the solvent and percent helicity do not change the type of aggregation.

2.12.5 Depolarized Dynamic Light Scattering of PEGL in *Water*

Depolarized light scattering experiments (denoted by Hv) can elucidate whether the increase in the decay rate as a function of the scattering vector magnitude is due to polydispersity or due to the rotation of the polymer. Equation 25 shows for rodlike polymers that depolarize (not all do) the decay rate is due to both translation and rotation of the polymer in a depolarized experiment. This is true, no matter the size of the rod. In contrast, a rotational term appears in Vv scattering only for long rods. Plotting the depolarized decay rate as a function of the scattering vector magnitude squared (Figure 66) provides the translational diffusion coefficient from the slope and the y-intercept gives the rotational diffusion coefficient. Although depolarized light scattering can provide the rotational diffusion coefficient, the experiment can be difficult due to low signal. As an example, PTFE, a strong scatterer in the horizontal plane, only shows a depolarization ratio (I_{Hv}/I_{Vv}) of 5%.[158] Because of the low signal, acquisition times are long and baseline choice can largely influence the analysis. One might think that the long-time signal (e.g., lag times > ~0.1 s) could serve as baseline. While this is sometimes done, the results are suspect because signals that are steady compared to the decaying part mix in heterodyne fashion. The resulting mixed homodyne-heterodyne signal is not easily analyzed; even a single decay term splits into two weighted exponentials.

Two different samples were tested because they had different relative percent helicity (sample #2: ~100% and 18: 51%). Based on the GPC data, sample #18 was expected to behave as a random coil, not providing a measureable rotational diffusion coefficient. On the other hand, sample #2 may have a measurable rotational diffusion coefficient due to the rodlike shape of the polymer if the depolarized signal is sufficiently larger than the solvent. Figure 81 shows the correlation function for sample #2 in water. A plot of the decay rate as a function of the scattering vector is required to find the rotational diffusion coefficient, but at lower angles there were enormous structures that could not be adequately characterized.

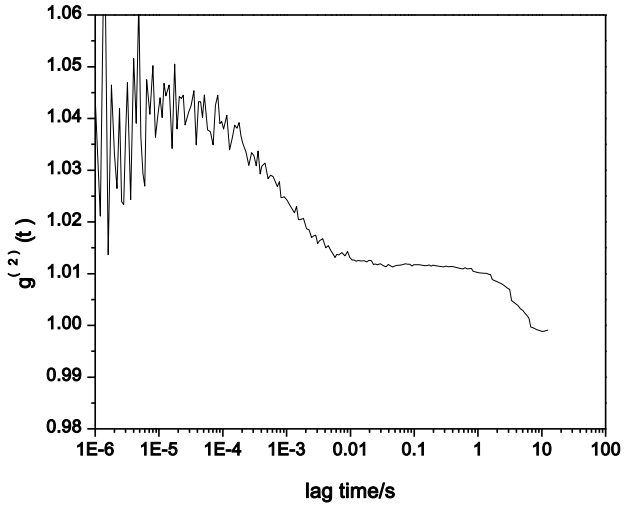

Figure 81. Depolarized light scattering correlation function of sample #2 (M_w = 211 ± 1 kDa, PDI = 1.21 ± 0.01) in *water*, 3.75 mg/mL and 90 degrees and room temperature. The two decay times are 102 ms and 4.19 s.

Although a risky business and done as a consolation, data from a single angle, 90 degrees, were used. In Figure 81, the slower decay found was 4.19 seconds, corresponding to a

hydrodynamic radius of 490 nm. The faster decay should be from the rotation of the rod was 1.02 ms. Using Equation 30, the hydrodynamic radius was 5.7 nm.

$$R_h = \left(\frac{k_B T}{8\pi\eta_0 D_r}\right)^{1/3} \quad \text{Equation 30}$$

As previously stated, depolarized light scattering has very little signal and may be the cause for the slow decay seen at 4.19 s.

2.12.6 Static Light Scattering of PEGL

A Guinier plot for sample #2 in *buffer* is found in Figure 82 and a summary of the data is found in Table 12. The length of the polymer was calculated from Equation 31 to find the corresponding molecular weight, assuming a rodlike morphology where R_g is the radius of gyration and L is the length of the polymer.

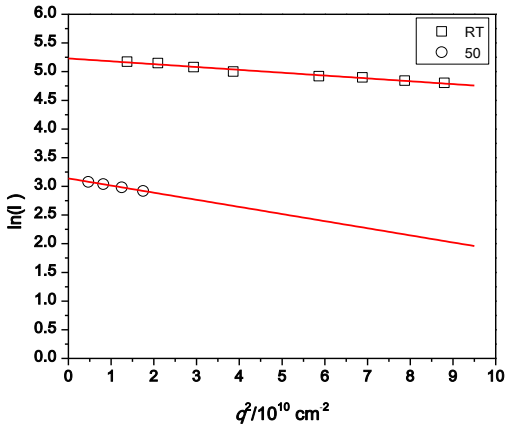

Figure 82.Guinier plot of sample #2 (M_w = 211 ± 1 kDa, PDI = 1.21 ± 0.01) in *buffer* (200 mM $NaNO_3$ + 20 mM NaH_2PO_4 + 2 mM NaN_3), 9.7 mg/mL PEGL at room temperature (R_g = 39 ± 1 nm) and 50 °C (R_g = 61 ± 1 nm).

$$R_g = L/\sqrt{12} \quad \text{Equation 31}$$

Once L is obtained in this way, M follows from Equation 28. Uncertainty was calculated from 95% confidence interval fits. Table 12 shows the radius of gyration, length, and molecular weights change as the temperature is increased. The circular dichroism (Figure 23) shows the polymer does not change helicity up to 50 °C indicating the change in size is not due to the helix unwinding.

Because PEG is most stable around 35 °C,[159] it appears the polymer has aggregated at both room temperature and 50 °C, consistent with the previously discussed DLS data having a large PDI. The DLS experiment was performed for sample #2 in *buffer* at 9.7 mg/mL. Table 12 shows at a higher concentration the polymer had a larger R_h than expected based on Figure 70 (R_h = 13.2 nm), consistent with aggregation.

Table 12. Light scattering data for sample #2 (M_w = 211 ± 1 kDa, PDI = 1.21 ± 0.01) in *buffer* (200 mM $NaNO_3$ + 20 mM NaH_2PO_4 + 2 mM NaN_3) at room temperature and 50 °C

	Room Temperature	50 °C
R_g/nm (Equation 31)	27 ± 1	61 ± 1
R_h/nm (Equation 26)	13 ± 1	11 ± 1
Length/nm (Equation 31)	94 ± 5	211 ± 5
M_n/kDa (Equation 28)	199 ± 10	160 ± 10
R_g/R_h	2.2 ± 0.1	5.5 ± 0.4

The value of $R_g/(R_h)_{app}$ is also telling of the structure of the polymer. A sphere has a $R_g/(R_h)_{app}$ of $0.78 = \sqrt{3/5}$, a polydisperse random coil in a good solvent equals 2.05, a polydisperse random coil in a theta solvent equals 1.73, and a rod is > 2.[160] The $R_g/(R_h)_{app}$ value shows the polymer to behave as a rod at room temperature, but it becomes more aggregated and

in an extended structure at elevated temperatures. PEG is known to aggregate at elevated temperatures and this aggregation (and LCST) are molecular weight dependent.[161, 162]

Figure 83 shows a 2-D Guinier plot of sample #2 in *buffer* at 9.7 mg/mL. At room temperature PEGL shows significant curvature but is linear for 50 °C; because rodlike polymers show a linear dependence the polymer is aggregating into rodlike structures in the *buffer* solution and this is consistent with the R_g/R_h values in Table 12.

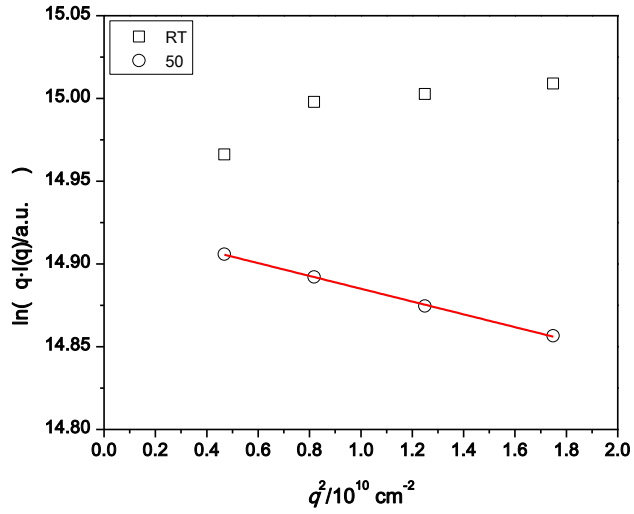

Figure 83. 2-D Guinier plot of sample #2 (M_w = 211 ± 1 kDa, PDI = 1.21 ± 0.01) in *buffer* (200 mM $NaNO_3$ + 20 mM H_2PO_4 + 2 mM NaN_3) at 9.7 mg/mL. The empty black squares are measured at room temperature and the circles are measured at 50 °C.

It appears then the polymer is aggregated at room temperature, helical from the circular dichroism, but still behaves like a random coil during bulk light scattering experiments at room temperature. This phenomenon may happen if the polymer, although highly helical, does not have continuous helical sections, but rather helical sections broken up by random coil segments. Other lysine derivatives have shown these broken helical structures.[163]

At elevated temperatures, the circular dichroism shows no change (up to 50 °C). This indicated as the polymer solution is heated larger radii are measured (Table 12), suggesting the polymer is less soluble and forms larger extended aggregates. Decreased solubility is consistent with the behavior of PEG; PEG, exhibiting a LCST, becomes less soluble upon heating and ultimately phase separates. In this instance, the LCST is not reached but heating the sample decreases its solubility (see Figure 97 for A_2 values) and makes the polymer aggregate further.

Figure 84 shows a plot of the apparent $R_g/(R_h)_{app}$ as a function of PEGL concentration for sample #2 and sample #18 at room temperature. The polymer behaves differently with varying concentration and varying percent helicity. A highly helical polymer, sample #2 (squares), behaves as a rodlike polymer at the lower concentrations but at the highest concentration studied started to behave as a random coil.

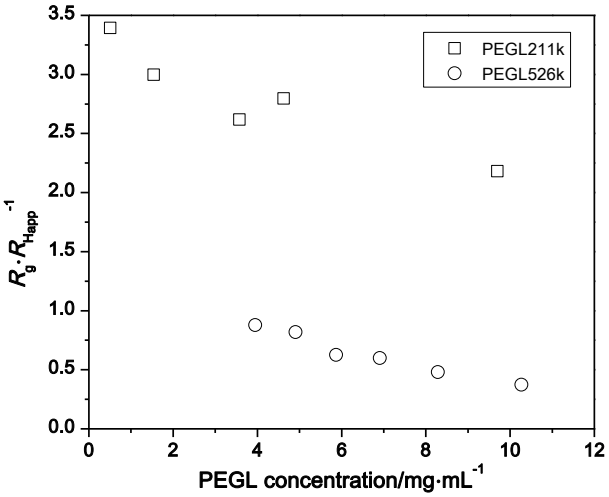

Figure 84. Plot of $R_g/(R_h)_{app}$ as a function of PEGL concentration in *buffer* (200 mM $NaNO_3$ + 20 mM H_2PO_4 + 2 mM NaN_3) for sample #2 (M_w = 211 ± 1 kDa, PDI = 1.21 ± 0.01, squares, 97% helical) and #18 (M_w = 526 ± 4 kDa, PDI = 1.27 ± 0.02, circles, 51% helical) at room temperature.

This seems to be counterintuitive because at higher concentrations the polymer forms liquid crystals. The circular dichroism was not performed above 1 mg/mL in water because it overloaded the detector, even when using 0.1 mL volume cells. Other investigations have observed that liquid crystal forming polymers can behave strangely when comparing GPC and light scattering.[164]

They found in a light scattering experiment a liquid crystal former can behave as a random coil polymer in a certain concentration regime. For sample #18, it is only 51% helical and behaves much differently. At low concentrations, it behaves as a homogenous sphere and then at higher concentrations gives a perplexing value. This may be due to different aggregates forming for sample #18. Figure 70 shows the diffusion coefficient for sample #2 is independent of PEGL concentration in the measured concentration regime in *buffer*. Sample #18 shows a large deviation in the diffusion coefficient with PEGL concentration (Figure 73) in water, a telltale sign of aggregation. Although *water* and *buffer* are two different solvents, quantitatively, they should behave similar because the A_2 is very close between the two although the *buffer* solution has a substantial concentration of a Hofmeister salt. In practice, although the A_2 values are close, they behave differently.

2.12.7 Temperature Jump Light Scattering Experiments

Because *water* and *buffer* were bad solvents, a temperature jump study was performed to monitor the scattered light intensity over time when rapidly changing the temperature. Light scattering depends on the concentration and radius of the analyte. When heated both in water and *buffer*, A_2 became more negative; this should increase the measured intensity. To perform the experiment, sample #2 in water was equilibrated in an ice bath for 10 min. It was then quickly placed in the Wyatt Light Scattering detector set to 70 °C. The intensity of the scattered light was

measured as a function of time (Figure 85). There is an initial delay in measured scattered light because the experiment was started prior to placing the sample in the Wyatt detector. Once the cold sample was placed in the hot Wyatt detector, it equilibrated very quickly (less than 30 seconds, see Figure 85).

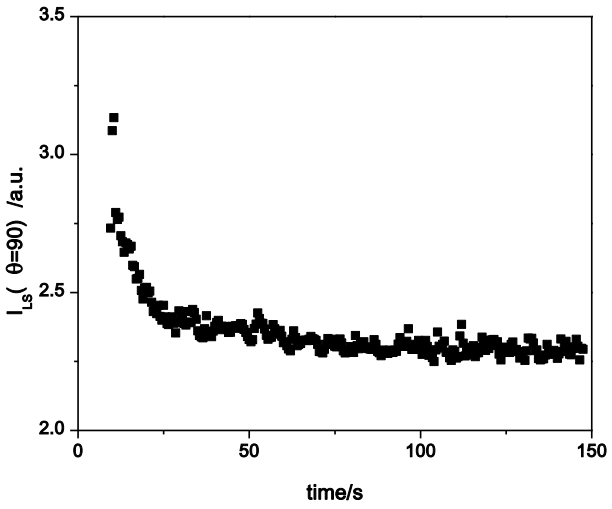

Figure 85. Static light scattering intensity of sample #2 (M_w = 211 ± 1 kDa, PDI = 1.21 ± 0.01) in *water* as a function of time. The sample was cooled in an ice bath and then plunged into the Wyatt detector set to 70 °C.

Following the first 30 seconds of equilibration, the intensity did not change for the entire length of the experiment (30 minutes). Because water is a bad solvent, as the sample increased in temperature, the scattered light intensity was expected to increase. The data show the scattered intensity decreases upon heating.

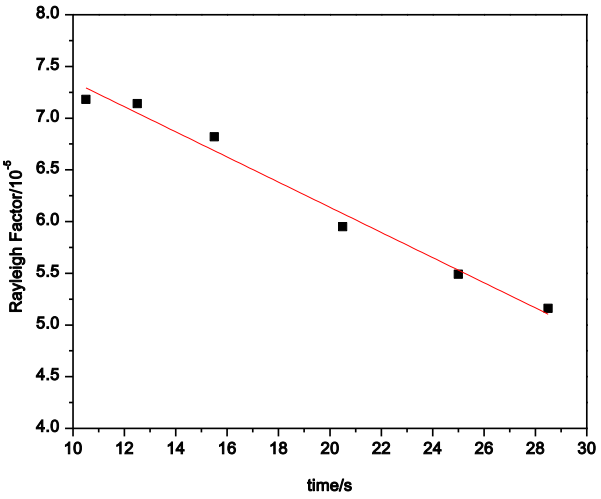

Figure 86. Rayleigh factor of sample #2 (M_w = 211 ± 1 kDa, PDI = 1.21 ± 0.01) in *water* as a function of time. The sample was cooled in an ice bath and then plunged into the Wyatt detector set to 70 °C.

2.12.8 PEGL Zimm Plots

The Zimm plot is a valuable tool for polymer chemists. In one plot, the radius of gyration, second virial coefficient, and absolute molecular weight are found. The Zimm equation is found in Equation 32 and Figure 87 shows a Zimm plot for polystyrene in THF. The inverse of the y-intercept of both dark extrapolated lines give M_w, the slope from the zero angle line gives the R_g, and the slope of the zero concentration line gives A_2. Although a Zimm plot is presented in this dissertation, making two plots of concentration and angle dependence is more instructional for the PEGL samples. The typical Zimm equation is found below

$$Kc/R_\theta = M^1(1 + q^2R_g^2/3) + 2A_2c \qquad \text{Equation 32}$$

where $K = 4\pi^2n^2(dn/dc)^2/\lambda_o^4N_a$, n is the refractive index, λ_o is the wavelength of the laser light in vacuum, N_a is Avogadro's number, R_θ is the Rayleigh factor, q is the scattering vector, R_g is the radius of gyration, c is the concentration, and A_2 is the second virial coefficient. Other

formalisms to find these parameters such as a Debye or Berry give slightly different values. The Zimm format was used because the data can be well linearly for large particles.[5]

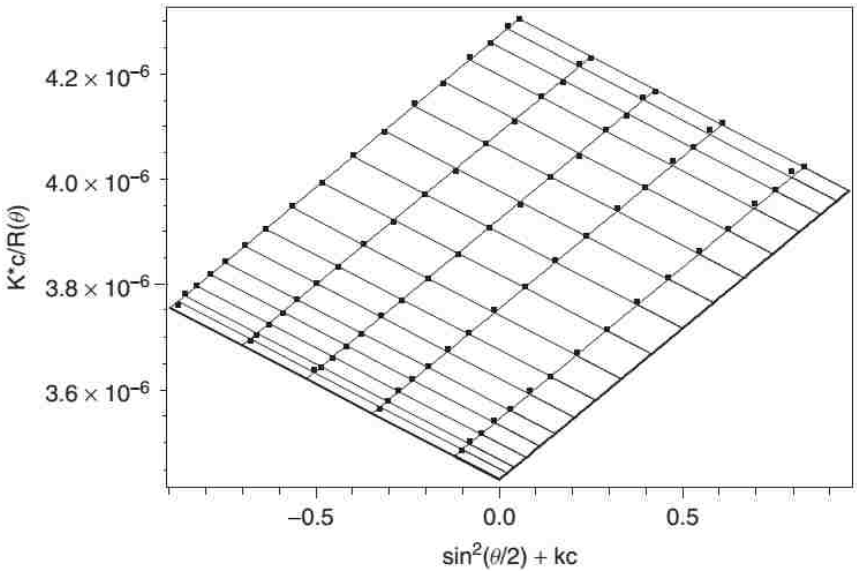

Figure 87. Zimm plot for NIST SRM 706 polystyrene in THF. Each of the five lines consist of 17 data points showing the angular variation of the scattered light. The dark lines are extrapolated data to zero angle and zero concentration. From reference 5.

The batch experiment was preferred because the GPC showed strange behavior. The examination of PEGL with Zimm formulation was performed in a Wyatt multi-angle light scattering detector in water and *buffer* with an adapter (Figure 88). A DLS cell was placed in the adapter for the Wyatt and the holder was filled with toluene to match the refractive index of glass. Because of this adapter, a batch mode Zimm plot can be performed. The Wyatt typically is set up to run flow experiments to build Zimm plots. Also, the exact same sample can be measured on the Wyatt to find the radius of gyration, second virial coefficient, hydrodynamic radius and molecular weight. A plot of Kc/R_θ as a function of the squared scattering vector magnitude is found in Figure 90. The difference between PEGL and the polystyrene sample above are apparent: PEGL shows significant curvature to the intensity of the scattered light at

Figure 88. Adapter to use DLS cells in the Wyatt GPC detector.

different *q*; because of this, a polynomial fit was used, even though it can lead to dangerous extrapolations. An attempt to linearize the data was used prior to using the polynomial fit. The y-intercept was plotted for each concentration, giving the inverse of the molecular weight.

Figure 89 shows a test of the normalization for the adapter using the isoscatter bovine serum albumin. The normalization is flat and linear, showing good normalization of the adapter. Figure 90 shows a plot of Kc/R_θ as a function of the squared scattering vector for sample #2 (M_w = 211 ± 1 kDa, PDI = 1.21 ± 0.01) in water at 27 °C. The inverse of the y-intercept provides a measure of the molecular weight. Each concentration was fit using a polynomial. The results are found in Figure 91 with the calculated M_w = 40 ± 6 kDa. The uncertainty was calculated by fitting different number of concentrations, taking the average, and the uncertainty is the difference between the average and the largest deviation. The calculated molecular weight from the Zimm plot is much lower than the molecular weights calculated form GPC at the same temperature. If the molecular weight calculated from each y-intercept is plotted with the highest

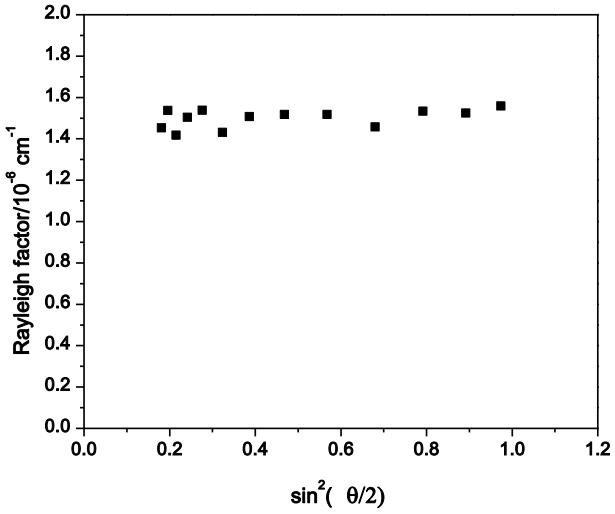

Figure 89. Normalization test of the adapter in Figure 88 with bovine serum albumin in *water*.

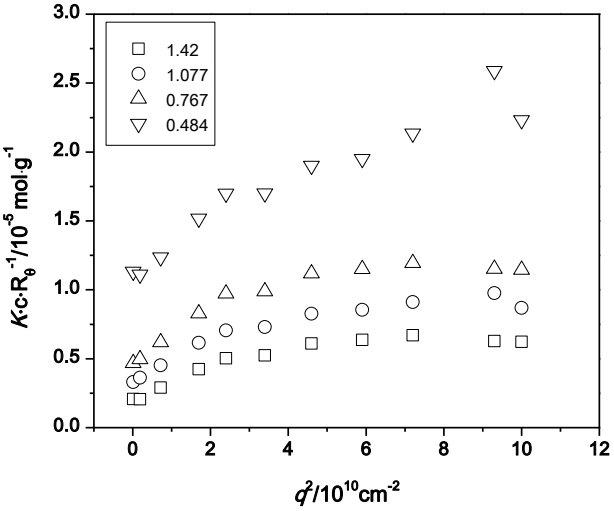

Figure 90. Plot of Kc/R_θ as a function of the squared scattering vector. Sample #2 (M_w = 211 ± 1 kDa, PDI = 1.21 ± 0.01) in *water* at 27 °C. The legend shows PEGL concentration in mg/mL.

concentration of PEGL not included in the fit, a polynomial fit gives a very low molecular weight of 9.2 ± 0.9 kDa (Figure 92). The uncertainty was taken at 10%. This value is much lower

than when fitting all the concentrations and may suggest that above 1.08 mg/mL aggregation is occurring, artificially inflating the molecular weight.

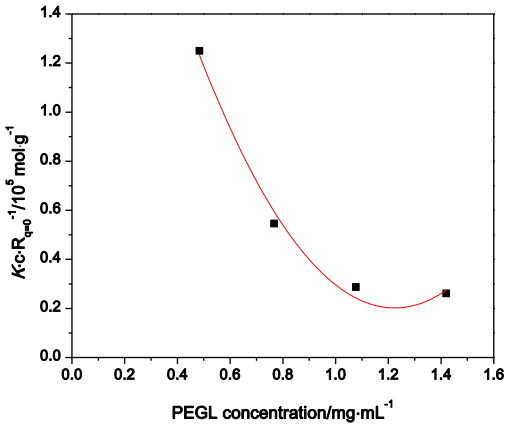

Figure 91. Plot of the y-intercept of Kc/R_θ as a function of PEGL concentration, fit with a 3rd order polynomial. Sample #2 (M_w = 211 ± 1 kDa, PDI = 1.21 ± 0.01) in *water* at 27 °C. The calculated of M_w = 40 ± 6 kDa was found by taking the inverse of the extrapolation to zero polymer concentration.

There was also curvature when plotting $\log_{10}(R_\theta)$ as a function of q^2 (Figure 93) at 27 °C. Therefore, a second-order polynomial fit was again applied to all the angles and radii of gyration found from the slopes are plotted in Figure 94. When fitting all four concentrations a negative radius was calculated (Figure 94). Therefore, the highest concentration was not included in the fit to find the radius of gyration at zero PEGL concentration (just like in Figure 92).

The uncertainty was found by fitting the three concentrations with a second-order polynomial fit and a linear fit, taking the average, and the uncertainty was the difference between the average and the maximal value. The calculated radius of gyration was 26 ± 14 nm. All calculated values from the Zimm plots for each solvent are found in Table 13. Other types of fits,

such as log(M_w) as a function of PEGL concentration did not greatly alter the fitted molecular weights (~2-3k difference).

Table 13 shows the molecular weight decreased at elevated temperatures in water. This is anomalous because PEGL exhibits a LCST, the A_2 becomes more negative when increasing the temperature, and DLS showed the size to increase with temperature. It is hypothesized the molecular weight is not consistent because of the aggregation observed. Many of the molecular weights could not be calculated because the curvature of the fit gave negative intercepts. Ideally, more concentrations would have been measured to determine if the highest concentration was an outlier or the system really shows curvature at the higher concentrations.

Table 13. Sample #2 in various solvents and temperatures

Temp/°C	M_w/kDa	R_g/nm	$A_2/mol \cdot mL \cdot g^{-2}$	*Solvent*
14	-	19 ± 8	-3.73E-2 ± 3.7E-3	*Water*
27	-	26 ± 14	-4.53E-2 ± 4.5E-3	*Water*
35	-	32 ± 7	-2.77E-2 ± 2.8E-3	*Water*
40	-	56 ± 3	-3.26E-2 ± 3.3E-3	*Water*
50	-	21 ± 1	-7.07E-2 ± 7.1E-3	*Water*
27	-	15 ± 2	-6.84E-3 ± 0.7E-4	*Buffer*
50	-	18 ± 2	-7.20E-2 ± 2.3E-3	*Buffer*

- means the y-intercept gave a negative molecular weight from the polynomial fit

The second virial coefficient should be more reliable than the molecular weight calculation because it depends on the slope and not on the intercept. As the temperature increased the second virial coefficient decreased. It did not do so in a linear fashion but decreased the most around 50 °C (Figure 97). The decrease in the second virial coefficient was expected due to the observed

LCST. The unexpected observation was that water and *buffer* were bad solvents, even at lower temperatures, evidenced by the negative A_2.

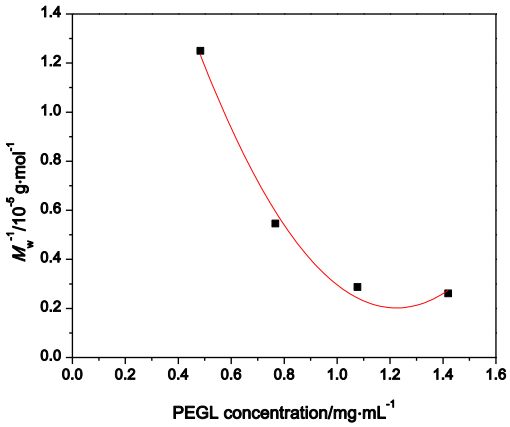

Figure 92. Plot of the M_w (calculated from the inverse of the y-intercept from the plot of Kc/R_θ as a function of the squared scattering vector) as a function of PEGL concentration, fit with a 3rd order polynomial. Sample #2 (M_w = 211 ± 1 kDa, PDI = 1.21 ± 0.01) in *water* at 27 °C. The fit M_w = 33 ± 3 kDa.

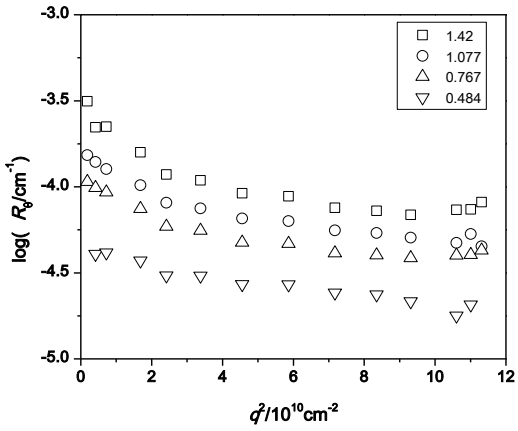

Figure 93. Plot of log(R_θ) as a function of the squared scattering vector magnitude. Sample #2 (M_w = 211 ± 1 kDa, PDI = 1.21 ± 0.01) in *water* at 27 °C. The legend shows PEGL concentration in mg/mL.

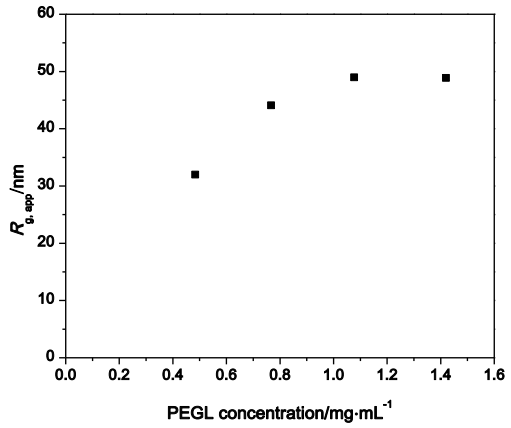

Figure 94. Plot of the apparent radius of gyration (found from the slope found from the log(R_θ) as a function of squared scattering vector magnitude) at different PELG concentrations. Sample #2 (M_w = 211 ± 1 kDa, PDI = 1.21 ± 0.01) in *water* at 27 °C. The radius of gyration was 26 ± 14 nm.

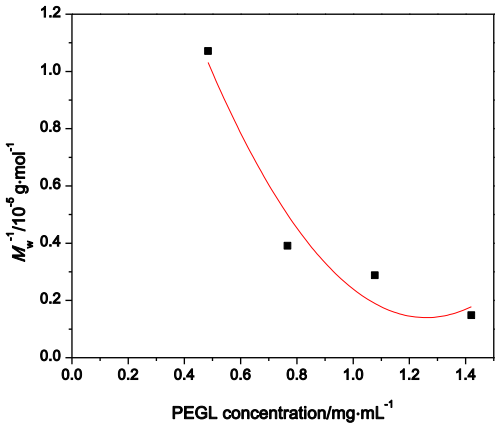

Figure 95. Plot of the M_w (calculated from the y-intercept from the plot of Kc/R_θ as a function of the squared scattering vector) as a function of PEGL concentration, fit with a 3rd order polynomial. Sample #2 (M_w = 211 ± 1 kDa, PDI = 1.21 ± 0.01) in *water* at 14 °C. The fit M_w = 42 ± 3 kDa.

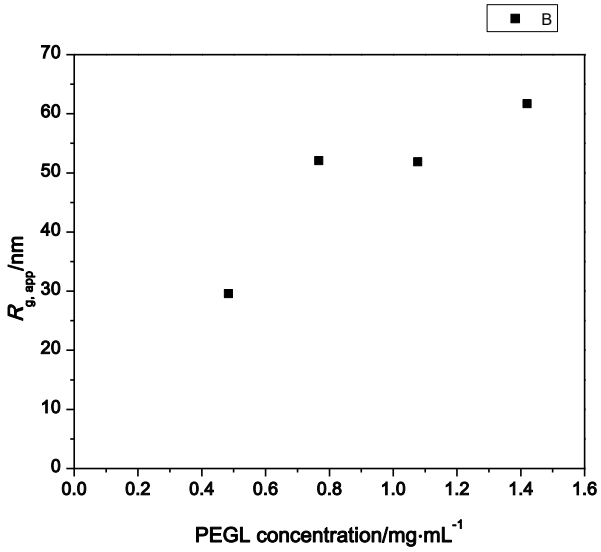

Figure 96. Plot of the apparent radius of gyration (calculated from the slope of $\log(R_\theta)$ as a function of scattering vector magnitude) at different PELG concentrations. Sample #2 (M_w = 211 ± 1 kDa, PDI = 1.21 ± 0.01) in *water* at 14 °C. The radius of gyration was 18.5 ± 7.5 nm.

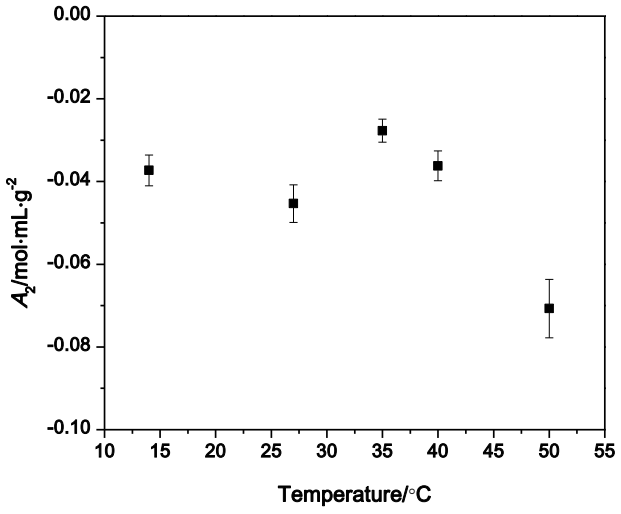

Figure 97. Plot of A_2 as a function of temperature for PEGL sample #2 (M_w = 211 ± 1 kDa, PDI = 1.21 ± 0.01) in *water*.

The Zimm plots for both *water* and *buffer* show either one is a bad solvent. This explains the previous experiments sometimes showing inconsistent data, indicative of aggregation. Although the polymer has a short PEG chain on each repeat unit, it is not enough to make it fully water-soluble. The crystal structure of EGL-NCA (Figure 101) shows the PEG chain bending backward toward the aliphatic chain. If the PEG chain were longer, it could bend backward into the solvent, too. Because PEGL isn't readily water soluble, a new solvent must be found; see the next section.

2.12.9 Dialysis DLS of PEGL

2.12.9.1 Dialysis Cell Explanation

Dialysis DLS was performed to test different solvents for the same exact PEGL sample. If the polymer is aggregating, different samples of the same batch of PEGL can behave differently. Using the dialysis cell eliminates variability due to sample dissolution or other aspects of preparation. A picture of the dialysis cell is found in Figure 98. For the dialysis cell, a Spectra/Por dialysis membrane with a molecular weight cut-off of 12-14,000 g/mol was glued to a cylindrical quartz cell. Superglue® was used because it is acetone soluble, permitting later removal of the membrane. A dialysis vat of ~500 mL of exchange solvent was circulated into the dialysis cell by two FMI lab pumps (one for input, one for output). The vat was cleaned with Nanopure water and then coated with SigmaCote® purchased from Sigma Aldrich to minimize dust in the dialysis cell. Before measurements, the solvent in the dialysis cell was circulated through a 0.1 μm PVDF filter until the vat was free from dust.

Figure 98. A picture of the dialysis DLS cell.

2.12.9.2 Dialysis DLS of PEGL

Figure 99 contains a plot of the intensity of scattered light at $\theta = 90$ degrees, for a NaPSS solution (exact concentration unknown) as a function of time and solvent. Two dialysis solutions were used, pure water and 1 M NaCl, because NaPSS is known to form temporary aggregates at low salt concentration.

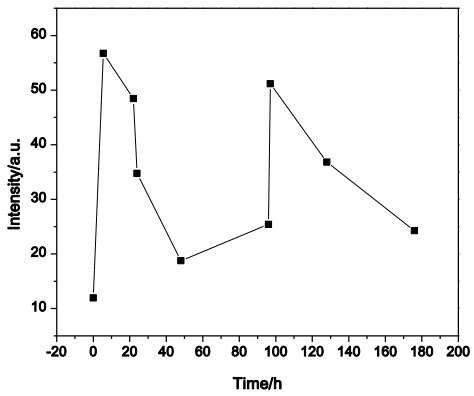

Figure 99. Intensity of NaPSS (exact concentration unknown) as a function of time and solvent condition. The valleys are after dialysis against pure water and the peak intensities are after dialysis against 1 M NaCl. The line is to aid the eye.

These two solutions were cycled twice to quantify dialysis equilibrium time. Upon visual observation with pure water as the exchange medium, the NaPSS solution would go cloudy in a few hours, why in Figure 100 the experimental time is short. The downturn in intensity after a few hours is due to the increasing turbidity of the solution decreasing the amount of light measured.

After the solution was cloudy, a 1 M NaCl solution was cycled through the cell. The solution would become clear with 1 M NaCl dialysis solution ~48 hours later and exhibited little difference in scattering from 48 to 96 hours. It was determined this clearing time, 48 hours, is sufficient for dialysis equilibrium. This was repeated to reaffirm 48 hours for the dialysis equilibrium.

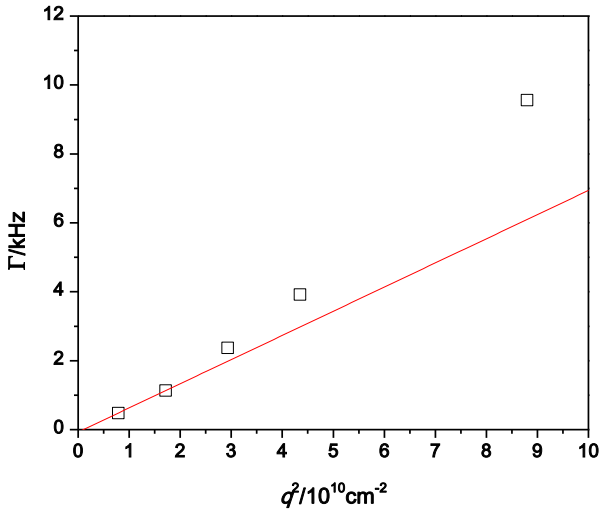

Figure 100. A plot of decay rate found by 3rd cumulant fits as a function of the squared scattering vector for sample #18 (M_w = 526 ± 4 and PDI = 1.27 ± 0.02) in the dialysis DLS cell in *water*. Original PEGL concentration was 2.71 mg/mL.

Figure 100 shows a plot of the decay rate as a function of q^2 for sample #18 in the dialysis cell with water. This shows the upturn seen prior in the PEGL DLS studies (Figure 66). The measured sizes from 3CUMU fits are found in Table 14 and the uncertainty is taken as 10%.

Table 14. Size of sample #18 (M_w = 526 ± 4 and PDI = 1.27 ± 0.02) in various solvents

Solvent	R_h/nm
Water	40 ± 4
23% Ethanol	44 ± 4

The experiment was repeated with 23% ethanol, showing minimal change in the size of the polymer. 50% ethanol was also attempted but it made the Superglue tacky, releasing the polymer into the dialysis cell. The entire solution became cloudy, suggesting higher concentrations of ethanol precipitate the polymer.

The real power of the dialysis cell lies in the variety of solvents that can be tried on the same exact sample. We have observed PEGL samples behaving differently, even from the same batch. If we can negate this with the dialysis DLS, a better solvent than water may be found. The size of PEGL will be compared for many solvents and the smallest size is considered the "best" solvent. Zimm plots can be performed to see if the solvent truly is a good solvent.

2.13 Data For Sample #18 in Different Solvents

In attempt to discover a good solvent for PEGL, DLS was performed in various solvent conditions. Sample #18 was studied and the results are found in Table 15. The D_{app} value is calculated as the average of the slope of the decay rate as a function of scattering magnitude and of the extrapolated to zero angle diffusion coefficient. The uncertainty is the difference between the largest value and the average value.

Table 15. DLS and GPC data for sample #18 (M_w = 526 ± 4 and PDI = 1.27 ± 0.02) in various solvents

Solvent	Experiment type	$D_{app}/10^8 cm^2 \cdot s^{-1}$	R_h/nm	M_w/kDa GPC data	Viscosity/ cP
Water	DLS	5.94 ± 0.11	41 ± 1	-	0.8904
Buffer	DLS	6.48 ± 0.67	38 ± 4	526 ± 4*	0.8983[165]
10% w/w urea	DLS	9.18 ± 0.09	27 ± 3	-	0.9612[166]
ethylene glycol	DLS	0.36 ± 0.13	37 ± 10	-	16.45
23% w/w ethanol	Dialysis DLS	2.95 ± 0.07	44 ± 10	-	2.161[167]
50% w/w ethanol	Dialysis DLS	-	Cloudy solution	-	-
DMF	DLS	31 ± 1	8.0 ± 0.2	190 ± 1*	0.8640[168]

* From GPC experiments performed in DMF + 0.1 M LiBr

2.14 Gaussian Calculations on EGL-NCA

A) B)

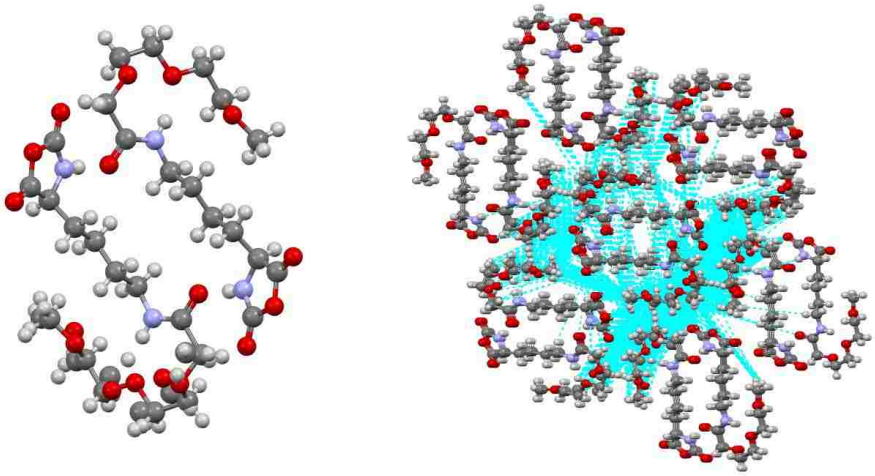

Figure 101. A) Packing of two PEGL NCA molecules from the experimental crystal structure. B) Packing of many PEGL NCA molecules from the experimental crystal structure. The blue lines denote hydrogen bonding.

In an attempt to understand what type of aggregation could be happening, calculations were performed using the software Gaussian 09. The .cif file from the crystal structure of EGL NCA (Figure 18) was used as the basis for each repeat unit. This is because calculations on the free-drawn NCA do not match the experimental results of the crystal structure. Figure 101 A shows the experimental conformation for two EGL NCA molecules found in the crystal structure, shown in the program Mercury. From the packing, the PEG chains are on the exterior, shielding the aliphatic lysine side chain. This can be seen better in Figure 101 B where a flower-like morphology is observed with the aliphatic chains in the interior and the PEG chains on the exterior. The blue lines are showing hydrogen bonding, but it seems some of the bonds are much too long to be real. Although this result is for a crystal, it is believable the polymer behaves in a

similar fashion when in a polar solvent due to the hydrogen bonding keeping a similar structure when solvated.

Gaussian calculations were performed by joining multiple EGL NCA units from the .cif file from the experimental crystal structure data. Then, increasingly complex calculations were performed (Mechanics → Semi-empirical AM1 → Hartree-Fock 3-21G → Hartree-Fock 3-21G*) and the results can be seen in Figure 102. Figure 102 A shows a view along the backbone of four PEGL repeat units. They appear to begin forming a helical type structure with the PEG groups on the exterior. Figure 102 B corroborates this idea. The helix is not perfect; hydrogen bonding along the backbone is not apparent because the carbonyl and nitrogen groups align with themselves, not in the expected hydrogen bonding formation. This may happen due to the limited ability of the program. It does appear to suggest a helix is starting to form, even with such a short chain. With longer chains, the hydrogen bonding begins to form appropriate bond distances (~3 Å) but the helix is less pronounced. This is likely to do many more local minima available.

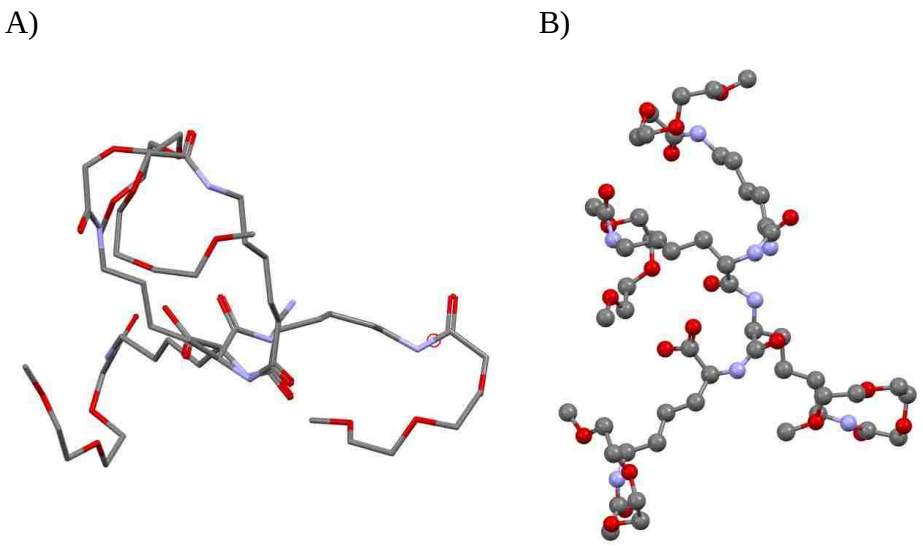

Figure 102. Results from Hartree-Fock 3-21G calculation in Gaussian on 4-repeat unit of PEGL. A and B are the same structure.

Based on observation in the NCA crystal structure, the PEG chains are too short to fully cover the aliphatic lysine side chain. This may leave hydrophobic patches, allowing aggregation of the polymer in an aqueous environment, although, diaminobutane is water soluble. Also, having a helical backbone would allow this aggregation to become some sort of extended aggregate. Due to the extended structure, individual chains do not need to aggregate exactly side-by-side, but can aggregate in a staggered segmental fashion.

2.15 Cell Viability

To test cell viability, 90 μL of 13 mg/mL of sample #9 was dissolved in Dulbecco's modified eagle medium (DMEM) with 10% fetal bovine serum (FBS) and placed in a plate well that housed 30,000 3T3 mouse fibroblast cells. Polymer and dead control were performed to ensure the measured fluorescence was not due to polymer. Figure 103 shows the results of the test. PEGL shows little to no cell death at 13.14 mg/mL in DMEM with 10% FBS.

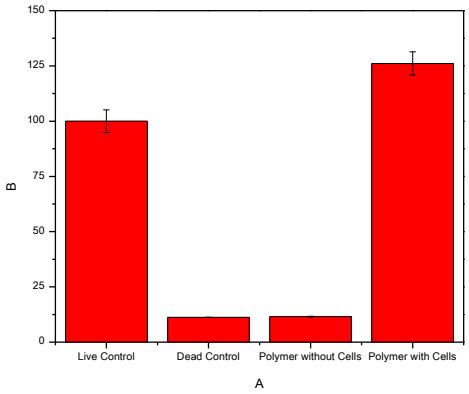

Figure 103. Cell viability of sample #9 (M_w = 7.1 ± 0.4 kDa and PDI = 1.02 ± 0.01) at 13.14 mg/mL in DMEM with 10% FBS.

2.16 Conclusions

A list of conclusions follows:

1. PEGL showed no change in amount of helicity as a function of temperature up to 1 mg/mL of polymer in water.
2. Different PEGL samples had different relative percent helicity, with only a few samples nearly reaching 100%.
3. Mass spectrometery showed peaks with a *m/z* difference consistent with the *m/z* of the repeat unit.
4. PEGL formed liquid crystals in water and DMF that were not completely stable when heated.
5. Cryo-TEM showed a mixture of apparent rodlike structures and large aggregates in *water* and *buffer*.
6. GPC showed variability in both repeat runs of a sample over time and between different samples.
7. The measured molecular weight range in GPC is not large enough for a reliable. measurement of the scaling factor found from the conformation plot.
8. Multi-angle dynamic light scattering showed an increase in the decay rate with an increase of the scattering vector magnitude, likely consistent with a polydisperse sample.
9. PEGL showed a measureable amount of depolarized light.
10. The Zimm plots show a negative second virial coefficient in both *water* and *buffer* but require polynomial fitting that may increase error.
11. With assumptions, it is possible the polymer is aggregating in a segmental fashion.

12. Based on the cumulative data, the system likely has a mixture of both free rods and globular aggregates.

Chapter 3 - Specific Ion Effects

3.1 Introduction to Specific Ion Effects

Specific ion effects, more commonly known as Hofmeister effects, occur in many different types of media, not just in aqueous environments where they affect viscosity, density, refractive index, heat capacity, and colligative properties in a way that is currently unexplained by polyelectrolyte theory.[169] The variation associated with different salts in different applications complicates the ability to synthesize a unified theory. An example is sodium chloride and lithium thiocyanate; although both are monovalent ion pairs, they behave very differently.

Hofmeister originally discovered the salt series by precipitation of proteins. The original list of Hofmeister salts is found below with increasing ability to precipitate proteins as one moves from right to left in the list.[169] The list was later updated to include cations as well.[170]

Anions:

(most able to precipitate) (least able to precipitate)

$OH^- > CO_3^{-2}, SO_4^{-2} > ClO_4^- > BrO_3^- > S_2O_3^{-2} > Cl^- > CH_3COO^- > IO_3^- > Br^-, I^- > NO_3^-$

Cations:

(most able to precipitate) (least able to precipitate)

$Na^+ > K^+ > Li^+ > Ba^{+2} > Rb^+ > Ca^{+2} > Ni^{+2} > Co^{+2} > Mg^{+2} > Fe^{+2} > Zn^{+2} > Cs^+ > Mn^{+2} > Al^{+3} > Fe^{+3} > Cr^{+3} > NH_4^+ > H^+$

Quantification of a salt's ability to "salt-in" or "salt-out" a polymer is found in Equation 33 where s_0 is the solubility of a nonelectrolyte in pure water, s is the solubility of a

nonelectrolyte in solution, c_s is the salt concentration, and k is the salting constant.[171] If the k value is positive, the salt decreases the solubility of the solute (salting-out) and if negative, the salt increases the solubility (salting-in).

$$\log\left(\frac{s_0}{s}\right) = kc_s \qquad \text{Equation 33}$$

These specific ion effects act by disrupting the hydrogen bonding of proteins in solution. They also help to salt-out hydrophobic groups but salt-in the peptide bonds in proteins.[172] For lysine, this can cause an issue because an increase in the number of carbon atoms in the side chain decreases solubility with added salt (reference 172, Figure 3).

Not all of the Hofmeister salts decrease solubility; sodium thiocyanate shows a slight increase in protein solubility.[173] Thiocyanate increases the solubility of the peptide bonds on the protein but denatures it in the process.[172] Other salts can salt-in proteins.[173] A cloud point temperature, T_{cp}, experiment can show how different salts affect polymer aggregation and salting-out. The cloud point temperature can be calculated several ways: 50% transmittance or fitting lines to the baseline and the point at which the slope is the greatest. Figure 104 shows the latter approach where the red lines are the fit data and the T_{cp} is taken as their intersection.

Experimentally, the cloud point graphs are be generated from one of two ways. First, a sample is placed in a UV/VIS spectrophotometer and the absorbance is measured at a wavelength the native solution does not absorb. Second, a cloud point graph is made by measuring the hydrodynamic radius from dynamic light scattering and plotting radius on the ordinate in Figure 104.

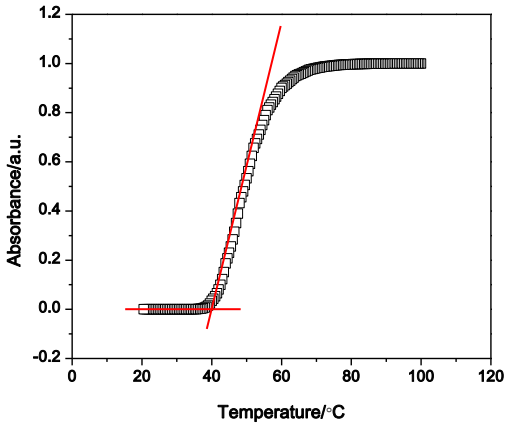

Figure 104. Hypothetical trace of absorbance as a function of temperature. Black squares are data and the red lines are the fits used to find the cloud point temperature, T_{cp}.

The cloud point transition is related to the lower critical solution temperature. A polymer that becomes insoluble when cooled shows an upper critical solution temperature (UCST) but when it becomes insoluble at elevated temperatures, it shows a lower critical solution temperature (LCST). The solution can phase separate to a point of gelation.[174]

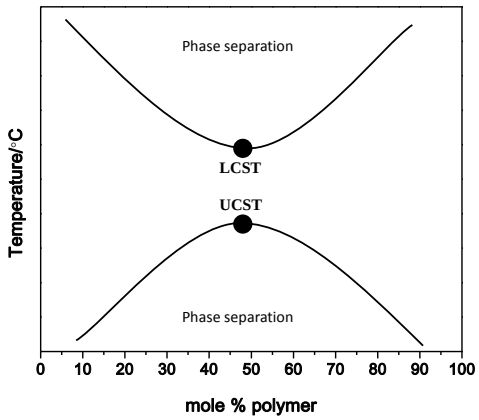

Figure 105. A plot of the phase behavior of a typical system as a function of mole percent of polymer.

3.2 LCST Studies of PEGL

The LCST of PEGL has already been observed in pure water at 103 °C (probably an extrapolated value).[136] Because PEGL was aggregating (see Chapter 2), the hypothesis was to control the aggregation by using salts from the Hofmeister salt series. Figure 106 A shows a plot of the absorbance as a function of temperature for sample #18 in water with varying NaCl concentrations. The plot was made by placing the dissolved sample into a quartz cuvette located in a UV/VIS spectrophotometer. An initial scan for absorbance was performed and a non-absorbing wavelength was chosen for the study (450 nm in this instance). 1.173 M NaCl is the lowest salt concentration measured because at lower salt concentrations the LCST was unattainable with our set-up. The maximum temperature of the UV/VIS was ~75 °C; below 1.173 M NaCl the LCST transition was higher than 75 °C and could not be recorded. Solid NaCl was added to the polymer solution and allowed to dissolve for ~1 h prior to measurement; this allowed measurement of the same sample for each salt concentration. A salty solution could have been added but this would have diluted the sample, changing two parameters at one time. Adding solid salt may "shock" the polymer and have local concentration variations, but it was deemed a better alternative than dilution. The salt solution was added to a room temperature cell and heated. Figure 106 shows as the NaCl concentration increased the cloud point temperature shifts to a lower value. This was expected because both Na^+ and Cl^- are salts that make the polymer salt out. A summary of all the LCST data for PEGL is found in Table 16.

Another way to measure the cloud point temperature is by light scattering. Typically, intensity of scattered light is monitored; in this case, dynamic light scattering was used because more information can be gleaned. Separate plots of the decay rate as a function of scattering vector magnitude were performed to take full advantage of our multi-angle DLS setup to find

hydrodynamic radii. A 6 M NaCl solution was made and filtered into the DLS vial because addition of solid NaCl also added dust. This complicated the light scattering studies because the polymer was being diluted while adding salt. Sample #2 shows no change for the 3CUMU fit as a function of polymer concentration, so the dilution effect, though undesirable, is not significant. For the hydrodynamic radius data, an analogous plot to Figure 106 A, was built but had hydrodynamic radius on the ordinate instead of absorbance.

Table 16. LCST of PEGL samples by different methods

Sample #	Method	T_{cp}/°C
4	UV/VIS	76 ± 4
18	UV/VIS	67 ± 2
18	DLS	95 ± 5

Figure 106 also shows the UV/VIS and DLS cloud point temperatures disagree, likely due to several reasons. First, the DLS instrument chosen cannot be heated at hot as the UV/VIS, severely limiting the amount of data points available. Second, although they are the same PEGL bath, dissolution and aggregation may cause variability. The UV/VIS do not match the cloud point temperature extrapolated to zero salt previously reported (103 °C, but this changes with molecular weight) but the DLS data appear to be much closer (Figure 106, B).

This set of experiments show the polymer aggregates can be altered with salt but the control does not last. The highest salt concentration in for the UV/VIS experiment was 2.685 M NaCl. If the salt solution was allowed to sit for 1 hour the T_{cp} was 34 °C but if allowed to sit overnight, the T_{cp} was 48 °C. This shows that although salt does affect the cloud point

A)

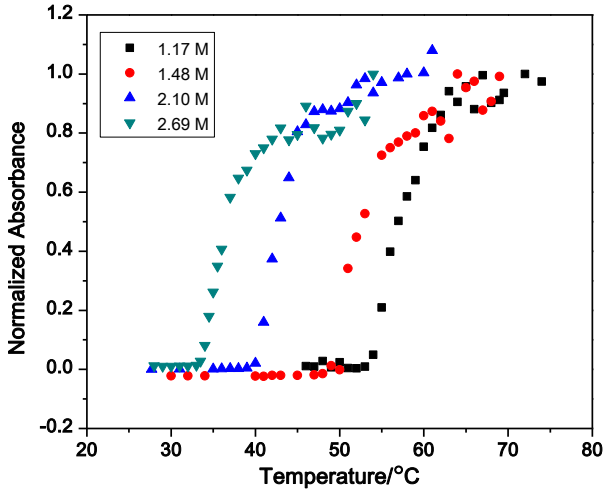

B)

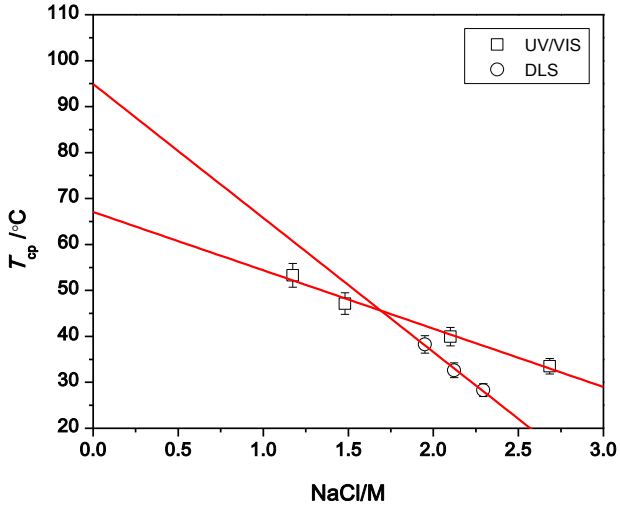

Figure 106. A) Plot of absorbance (at 450 nm) as a function of temperature for sample #18 (M_w = 526 ± 4 and PDI = 1.27 ± 0.02) in *water* with varying NaCl molarity. B) Plot of T_{cp} as a function of NaCl concentration for UV/VIS (squares, T_{cp} = 61 ± 2) and DLS (circles, T_{cp} = 95 ± 5). The red lines are fits to the data. Uncertainty is set at 10 percent.

temperature, equilibrium is not immediately reached, even with agitation following salt addition, and it may end up being a reversible process.

The effect of molecular weight was also tested and Table 16 shows the result. It appears the measured molecular weights may have influence on the cloud point temperature but uncertainty arises because all the measured molecular weights are due to an aggregating system. The two cloud point temperatures are close within uncertainty, suggesting measured molecular weight plays little role in the cloud point transition for PEGL in water.

Upon reaching a T_{cp} close to room temperature, a Hofmeister salt that salts-in proteins, thiocyanate, was added. In this instance, the NaCl concentration was increased until the sample was cloudy at room temperature. The sample was allowed to sit for several days and the solution became clear. More salt was added until the solution once again became cloudy (4.72 M NaCl) and immediately sodium thiocyanate was added until the solution became clear again (2.08 M thiocyanate). The cloud point experiment in the UV/VIS spectrophotometer was again performed but no cloud point was observed.

Chapter 4 - Future Work

4.1 Characterization in a Good Solvent

PBLG has a long career of experiments showing everything from phase diagrams, gelation, aggregation, comparison to theory, etc. in many solvents. The primary next step for PEGL is finding its solubility in many different solvents. It was hypothesized that PEGL would be water-soluble and well-behaved, meaning that the good-solvent, excluded volume limit could be attained. The Zimm plots suggest otherwise. Dialysis DLS allows for testing the solubility of one specific PEGL sample in different solvents. Although the sample is not charged, the pH will also be tested. Proteins have a narrow solvent window in which they behave, and PEGL should too. That window can be found with dialysis DLS. A good solvent to begin with is trifluroethanol because it is known to induce a helical conformation, even when the polymer nominally is a random coil.[175]

Once in a perceived "good" solvent, the helicity should be tested by circular dichroism. A way to direct the solvents chosen for dialysis DLS is to test the helicity of PELG in these solvents first. If the polymer is not helical, that solvent is not a top priority for dialysis DLS. Dialysis DLS is not the only experiment needed to find a better solvent. Once the lowest measured apparent radius is found, suggesting the polymer is fully dissolved and in "good" solvent, the d*n*/d*c* will be measured in order to perform static light scattering experiments (Zimm plots). SLS will measure radius of gyration, molecular weight, and second virial coefficient by building Zimm plots. Because this can be performed on the Wyatt GPC detector, Zimm plots can be easily made for many different temperatures and solvents. If the d*n*/d*c* is too low to provide ample scattering signal, the Zimm plots can be performed on our multi-angle light scattering setup.

Once the solvent is confirmed as thermodynamically good, as indicated by a positive second virial coefficient that reaches a constant value as a function of temperature, salt or pH, then Vv and Hv DLS experiments should be performed. PEGL has shown in increase in the decay rate as a function of the squared scattering vector magnitude in Vv experiments but it may partially be due to polydispersity. In a good solvent, the individual polymer chains should act independently at sufficiently low concentrations. This allows for a reliable measure of their rotational diffusion, a needed experiment for a rodlike polymer.

If PEGL is helical and shows rotational diffusion in this new solvent, other experiments can be performed to characterize it. The apparent diffusion coefficient can be measured for multiple polymer concentrations and the length can be found from the Kirkwood-Riseman equation. Also, GPC can be performed with the good solvent with intrinsic viscosity, concentration, and DLS detectors. A conformation plot can be performed as a measure of the polymers morphology and the resultant radius and molecular weight data can be used to calculate the persistence length.

4.2 Phase Diagrams

The phase diagrams for PBLG are well known. This has allowed for complicated study of its phase transitions. The first step is to build the phase diagram for PEGL. This can be done using the polarized optical microscope and visually observing the phases. Once the transitions are known, many light scattering experiments can be performed, i.e. measuring the diffusion coefficient of isotropic-LC phase transition.[176] The polymer can also be in a liquid crystalline phase and tested for change by external stimuli, such as magnetic fields.[119] The phase diagrams can also be made for many solvent systems, even using the Hofmeister salt series to control the phase boundaries.

4.3 Probe Diffusion

Model rodlike polymers have been used in probe diffusion experiments and PEGL should be no exception. Using a polymerization technique that retains the living chain ends allows for facile end labeling with a fluorescent dye. This would allow for probe diffusion experiments with a fluorescent-PEGL using FPR. This eliminates the need for index matching of the matrix polymer.

4.4 Gelation

Once the phase diagram is known for PEGL, possible gelation studies can be performed, assuming it gels. These studies would not be limited only to the good solvents, they might actually be aided by using solvents in which the polymer is not fully soluble. If the polymer gels at a reasonable temperature and concentration, the polymer could be used for drug delivery, etc. Thus far, water seems like a perfect solvent for gelation studies due to the aggregation present. A 10% w/w solution of a PEGL with low measured molecular weight was made and was visually cloudy at room temperature. Upon heating, the system did not gel but salts and non-solvent were not added to aid in aggregation and possible gelation.

4.5 Fluorescent Labeling

As being one of the few labs with a versatile, fringe-pattern FPR, florescent labeling will provide another way to test the diffusion of the polymer (probe diffusion, self-diffusion, etc). In addition, a fluorescent polymer can be directly visualized (assuming it is large enough, likely only after aggregating) by microscopy. If the polymer is aggregating, these aggregates can be visualized, maybe to the point of gelation. It is possible the fluorescent tag will change the morphology of the polymer and this will be tested.

4.6 Synthesis of a New Polymer

PEGL was chosen because experiments elsewhere suggested it was water-soluble but also because it had already been partially characterized and the synthesis understood. If PEGL proves not to be as fully soluble as expected, an analogous polymer with a shorter hydrocarbon portion of the side chain can be synthesized. The crystal structure and calculations from Gaussian suggest the aliphatic side chains may aggregate or cause some sort of instability. If this is the case, a lysine analogue can be used to shorten the side chain. The entire gamut of tests would need to be performed, but this is true of PEGL in a new solvent, too.

Another option is to make the PEG side chains longer, to help "cover up" the hydrophobic side chain of lysine. Adding PEG side chains has been performed with PBLG and the length of the side chain has been tested.[177, 178] This is probably the easiest analog to try because it should have a similar synthesis as the current PEGL. PEG has been used as an agent to prevent aggregation by using a large random coil type polymer. The random coil flexibility prevents aggregation due to the loss in entropy of an aggregated system. The PEG side chains in this work are too short to provide this function.

References

1. Wikipedia Protein Structure. http://en.wikipedia.org/wiki/Protein_structure
2. Wikipedia Amino Acid. http://en.wikipedia.org/wiki/Amino_acid
3. Senyuk, B., Liquid Crystals: a Simple View on a Complex Matter.
4. Wikipedia Translation (biology). http://en.wikipedia.org/wiki/Translation_(biology)
5. Podzimek, S., Light Scattering, Size Exclusion Chromatography and Asymmetric Flow Field Flow Fractionation: Powerful Tools for the Characterization of Polymers, Proteins and Nanoparticles. John Wiley and Sons, Inc: 2011.
6. Daly, W. H.; Poche, D. *Tetrahedron Lett.* 1988, 29, (46), 5859-5862.
7. Lin, S. C.; Lee, W. I.; Schurr, J. M. *Biopolymers* 1978, 17, (4), 1041-1064.
8. Vickery, H. B.; Schmidt, C. L. A. *Chem. Rev.* 1931, 9, (2), 169-318.
9. Campbell, N. A. R., Jane B., Biology. Pearson Education: 2005; Vol. 7, p 1231.
10. Berman, H. M.; Westbrook, J.; Feng, Z.; Gilliland, G.; Bhat, T. N.; Weissig, H.; Shindyalov, I. N.; Bourne, P. E. *Nucleic Acids Research* 2000, 28, (1), 235-242.
11. Pearson, H. *Nature* 2006, 441, (7092), 398-401.
12. Kendrew, J. C.; Bodo, G.; Dintzis, H. M.; Parrish, R. G.; Wyckoff, H.; Phillips, D. C. *Nature* 1958, 181, (4610), 662-666.
13. Kendrew, J. C.; Dickerson, R. E.; Strandberg, B. E.; Hart, R. G.; Davies, D. R.; Phillips, D. C.; Shore, V. C. *Nature* 1960, 185, (4711), 422-427.
14. Perutz, M. F.; Rossmann, M. G.; Cullis, A. F.; Muirhead, H.; Will, G.; North, A. C. T. *Nature* 1960, 185, (4711), 416-422.
15. Block, H., *Poly(γ-benzyl-L-glutamate) and Other Glutamic Acid Containing Polymers*. Gordon and Breach Science Publishers: New York, 1983; p 215.
16. Pauling, L.; Corey, R. B. *Journal of the American Chemical Society* 1950, 72, (11), 5349-5349.
17. Pauling, L.; Corey, R. B. *Proc. Natl. Acad. Sci. U. S. A.* 1951, 37, (5), 241-250.
18. Pauling, L.; Corey, R. B.; Branson, H. R. *Proc. Natl. Acad. Sci. U. S. A.* 1951, 37, (4), 205-211.
19. prokoption, Linus Pauling--How He Discovered the Alpha Helix. YouTube: 2008.
20. Némethy, G.; Scheraga, H. A. *Biopolymers* 1965, 3, (2), 155-184.

21. Nemethy, G.; Phillips, D. C.; Leach, S. J.; Scheraga, H. A. *Nature* 1967, 214, (5086), 363-365.

22. Zimm, B. H.; Bragg, J. K. *Journal of Chemical Physics* 1959, 31, (2), 526-535.

23. Scheraga, H. A. *Biopolymers* 2008, 89, (5), 479-485.

24. Kricheldorf, H. R. *Angewandte Chemie-International Edition* 2006, 45, (35), 5752-5784.

25. Hadjichristidis, N.; Iatrou, H.; Pitsikalis, M.; Sakellariou, G. *Chem. Rev.* 2009, 109, (11), 5528-5578.

26. Leuchs, H. *Berichte Der Deutschen Chemischen Gesellschaft* 1906, 39, 857-861.

27. Leuchs, H.; Geiger, W. *Berichte Der Deutschen Chemischen Gesellschaft* 1908, 41, 1721-1726.

28. Curtius, T.; Sieber, W. *Berichte Der Deutschen Chemischen Gesellschaft* 1921, 54, 1430-1437.

29. Curtius, T.; Sieber, W. *Berichte Der Deutschen Chemischen Gesellschaft* 1922, 55, 1543-1558.

30. Curtius, T. *Journal Fur Praktische Chemie-Leipzig* 1930, 125, (1/12), 211-218.

31. Schlogl, K.; Wessely, F.; Korger, G. *Monatshefte Fur Chemie* 1952, 83, (4), 845-864.

32. Wessely, F.; Swoboda, W. *Monatshefte Fur Chemie* 1951, 82, (4), 621-627.

33. Wessely, F.; Riedl, K.; Tuppy, H. *Monatshefte Fur Chemie* 1950, 81, (6), 861-872.

34. Babad, H.; Zeiler, A. G. *Chem. Rev.* 1973, 73, (1), 75-91.

35. Fuller, W. D.; Verlander, M. S.; Goodman, M. *Biopolymers* 1976, 15, (9), 1869-1871.

36. Katakai, R.; Iizuka, Y. *Journal of Organic Chemistry* 1985, 50, (5), 715-716.

37. Eckert, H.; Forster, B. *Angewandte Chemie-International Edition in English* 1987, 26, (9), 894-895.

38. Iwakura, Y.; Uno, K.; Kang, S. *Journal of Organic Chemistry* 1965, 30, (4), 1158-1161.

39. Katchalski, E.; Sela, M. *Adv.Protein Chem.* 1958, 13, 243-492.

40. Habraken, G. J. M.; Peeters, M.; Dietz, C. H. J. T.; Koning, C. E.; Heise, A. *Polym. Chem.* 2010, 1, (4), 514-524.

41. Dorman, L. C.; Shiang, W. R.; Meyers, P. A. *Synth. Commun.* 1992, 22, (22), 3257-3262.

42. Brenner, M.; Photaki, I. *Helvetica Chimica Acta* 1956, 39, (6), 1525-1528.

43. Geller, T.; Gerlach, A.; Krüger, C. M.; Militzer, H. C. *Tetrahedron Lett.* 2004, 45, (26), 5065-5067.

44. Baars, S.; Drauz, K. H.; Krimmer, H. P.; Roberts, S. M.; Sander, J.; Skidmore, J.; Zanardi, G. *Organic Process Research & Development* 2003, 7, (4), 509-513.

45. Waley, S. G.; Watson, J. *Proceedings of the Royal Society of London Series a-Mathematical and Physical Sciences* 1949, 199, (1059), 499-517.

46. Ballard, D. G. H.; Bamford, C. H. *Proceedings of the Royal Society of London Series a-Mathematical and Physical Sciences* 1954, 223, (1155), 495-520.

47. Smeets, N. M. B.; van der Weide, P. L. J.; Meuldijk, J.; Vekemans, J.; Hulshof, L. A. *Organic Process Research & Development* 2005, 9, (6), 757-763.

48. Poche, D. S.; Moore, M. J.; Bowles, J. L. *Synth. Commun.* 1999, 29, (5), 843-854.

49. Kramer, J. R.; Deming, T. J. *Biomacromolecules* 2010, 11, (12), 3668-3672.

50. Peggion, E.; Terbojevich, M.; Cosani, A.; Colombini, C. *Journal of the American Chemical Society* 1966, 88, (15), 3630-3632.

51. Cosani, A.; Deste, G.; Peggion, E.; Scoffone, E. *Biopolymers* 1966, 4, (5), 595-599.

52. Thunig, D.; Semen, J.; Elias, H.-G. *Die Makromolekulare Chemie* 1977, 178, (2), 603-607.

53. Rinaudo, M.; Domard, A. *Biopolymers* 1976, 15, (11), 2185-2199.

54. Doty, P.; Lundberg, R. D. *Journal of the American Chemical Society* 1957, 79, (9), 2338-2339.

55. Bartlett, P. D.; Jones, R. H. *Journal of the American Chemical Society* 1957, 79, (9), 2153-2159.

56. Bartlett, P. D.; Dittmer, D. C. *Journal of the American Chemical Society* 1957, 79, (9), 2159-2160.

57. Miller, E.; Fankuchen, I.; Mark, H. *Journal of Applied Physics* 1949, 20, (6), 531-533.

58. Goodman, M.; Hutchison, J. *Journal of the American Chemical Society* 1966, 88, (15), 3627-3630.

59. Bamford, C. H.; Block, H. *Journal of the Chemical Society (Resumed)* 1961, (0), 4989-4991.

60. Bamford, C. H.; Block, H. *Journal of the Chemical Society (Resumed)* 1961, (0), 4992-4995.

61. Bamford, C. H.; Block, H.; Pugh, A. C. P. *Journal of the Chemical Society (Resumed)* 1961, (0), 2057-2063.

62. Peggion, E.; Cosani, A.; Mattucci, A. M.; Scoffone, E. *Biopolymers* 1964, 2, (1), 69-78.

63. Blout, E. R.; Karlson, R. H.; Doty, P.; Hargitay, B. *Journal of the American Chemical Society* 1954, 76, (17), 4492-4493.

64. Doty, P.; Holtzer, A. M.; Bradbury, J. H.; Blout, E. R. *Journal of the American Chemical Society* 1954, 76, (17), 4493-4494.

65. Blout, E. R.; Karlson, R. H. *Journal of the American Chemical Society* 1956, 78, (5), 941-946.

66. Deming, T. J. *Adv. Drug Deliv. Rev.* 2002, 54, (8), 1145-1155.

67. Sekiguchi, H. *Pure and Applied Chemistry* 1981, 53, (9), 1689-1714.

68. Deming, T. J. *Journal of the American Chemical Society* 1998, 120, (17), 4240-4241.

69. Deming, T. J. *Nature* 1997, 390, (6658), 386-389.

70. Deming, T. J. *Macromolecules* 1999, 32, (13), 4500-4502.

71. Habraken, G. J. M.; Heise, A.; Thornton, P. D. *Macromol. Rapid Commun.* 2012, 33, (4), 272-286.

72. Deming, T. J.; Yu, M.; Nowak, A. P.; Pochan, D. J. *Journal of the American Chemical Society* 1999, 121, (51), 12210-12211.

73. Curtin, S. A.; Deming, T. J. *Journal of the American Chemical Society* 1999, 121, (32), 7427-7428.

74. Witte, P.; Menzel, H. *Macromol. Chem. Phys.* 2004, 205, (13), 1735-1743.

75. Sparks, B. J.; Ray, J. G.; Savin, D. A.; Stafford, C. M.; Patton, D. L. *Chem. Commun.* 2011, 47, (22), 6245-6247.

76. Aliferis, T.; Iatrou, H.; Hadjichristidis, N. *Biomacromolecules* 2004, 5, (5), 1653-1656.

77. Pickel, D. L.; Politakos, N.; Avgeropoulos, A.; Messman, J. M. *Macromolecules* 2009, 42, (20), 7781-7788.

78. Vayaboury, W.; Giani, O.; Cottet, H.; Bonaric, S.; Schué, F. *Macromol. Chem. Phys.* 2008, 209, (15), 1628-1637.

79. Vayaboury, W.; Giani, O.; Cottet, H.; Deratani, A.; Schue, F. *Macromol. Rapid Commun.* 2004, 25, (13), 1221-1224.

80. Cottet, H.; Vayaboury, W.; Kirby, D.; Giani, O.; Taillades, J.; Schue, F. *Anal. Chem.* 2003, 75, (20), 5554-5560.

81. Zou, J.; Fan, J. W.; He, X.; Zhang, S. Y.; Wang, H.; Wooley, K. L. *Macromolecules* 2013, 46, (10), 4223-4226.

82. Goodman, M.; Peggion, E.; Szwarc, M.; Bamford, C. H. *Macromolecules* 1977, 10, (6), 1299-1301.

83. Kent, S. B. H. *Annual Review of Biochemistry* 1988, 57, 957-989.

84. Renton, A., If MSG is so bad for you, why doesn't everyone in Asia have a headache? In *The Observer*, The Guardian: 2005.

85. Doty, P.; Bradbury, J. H.; Holtzer, A. M. *Journal of the American Chemical Society* 1956, 78, (5), 947-954.

86. Doty, P.; Bradbury, J. H.; Holtzer, A. M. *Journal of the American Chemical Society* 1956, 78, (5), 947-954.

87. Doty, P.; Lundberg, R. D. *Journal of the American Chemical Society* 1956, 78, (18), 4810-4812.

88. Doty, P.; Yang, J. T. *Journal of the American Chemical Society* 1956, 78, (2), 498-500.

89. Blout, E. R.; Doty, P.; Yang, J. T. *Journal of the American Chemical Society* 1957, 79, (3), 749-750.

90. Doty, P.; Wada, A.; Yang, J. T.; Blout, E. R. *Journal of Polymer Science* 1957, 23, (104), 851-861.

91. Lundberg, R. D.; Doty, P. *Journal of the American Chemical Society* 1957, 79, (15), 3961-3972.

92. Mitchell, J. C.; Woodward, A. E.; Doty, P. *Journal of the American Chemical Society* 1957, 79, (15), 3955-3960.

93. Yang, J. T.; Doty, P. *Journal of the American Chemical Society* 1957, 79, (4), 761-775.

94. Zero, K. M.; Pecora, R. *Macromolecules* 1982, 15, (1), 87-93.

95. Kubota, K.; Chu, B. *Biopolymers* 1983, 22, (6), 1461-1487.

96. Kubota, K.; Tominaga, Y.; Fujime, S. *Macromolecules* 1986, 19, (6), 1604-1612.

97. Jamil, T.; Russo, P. S. *Journal of Chemical Physics* 1992, 97, (4), 2777-2782.

98. Temyanko, E.; Russo, P. S.; Ricks, H. *Macromolecules* 2001, 34, (3), 582-586.

99. Bu, Z. M.; Russo, P. S.; Tipton, D. L.; Negulescu, II. *Macromolecules* 1994, 27, (23), 6871-6882.

100. Wada, A. *Journal of Polymer Science* 1960, 45, (145), 145-153.

101. Goebel, K. D.; Miller, W. G. *Macromolecules* 1970, 3, (1), 64-69.

102. Gerber, J.; Elias, H. G. *Makromolekulare Chemie-Macromolecular Chemistry and Physics* 1968, 112, (MAR), 142-159.

103. Spach, G.; Bendit, H.; Freund, L.; Daune, M. *J. Mol. Biol.* 1963, 7, (5), 468-482.

104. Fujita, H.; Teramoto, A.; Yamashita, T.; Okita, K.; Ikeda, S. *Biopolymers* 1966, 4, (7), 781-791.

105. Schmidt, M. *Macromolecules* 1984, 17, (4), 553-560.

106. Wee, E. L.; Miller, W. G. *Journal of Physical Chemistry* 1971, 75, (10), 1446-1452.

107. Miller, W. G.; Wu, C. C.; Wee, E. L.; Santee, G. L.; Rai, J. H.; Goebel, K. G. *Pure and Applied Chemistry* 1974, 38, (1-2), 37-58.

108. Flory, P. J. *Proceedings of the Royal Society of London Series a-Mathematical and Physical Sciences* 1956, 234, (1196), 73-89.

109. Russo, P. S.; Miller, W. G. *Macromolecules* 1983, 16, (11), 1690-1693.

110. Yen, C. C.; Edo, S.; Oka, H.; Tokita, M.; Watanabe, J. *Macromolecules* 2008, 41, (10), 3727-3733.

111. Jahanshahi, K.; Botiz, I.; Reiter, R.; Scherer, H.; Reiter, G. *Crystal Growth & Design* 2013, 13, (10), 4490-4494.

112. Vroege, G. J.; Lekkerkerker, H. N. W. *Reports on Progress in Physics* 1992, 55, (8), 1241-1309.

113. Russo, P. S.; Saunders, M. J.; DeLong, L. M.; Kuehl, S.; Langley, K. H.; Detenbeck, R. W. *Analytica Chimica Acta* 1986, 189, (0), 69-87.

114. Chowdhury, A. H.; Russo, P. S. *Journal of Chemical Physics* 1990, 92, (9), 5744-5750.

115. Russo, P. S.; Miller, W. G. *Macromolecules* 1984, 17, (7), 1324-1331.

116. Murthy, A. K.; Muthukumar, M. *Macromolecules* 1987, 20, (3), 564-569.

117. Horton, J. C.; Donald, A. M. *Polymer* 1991, 32, (13), 2418-2427.

118. Deming, T. J.; Curtin, S. A. *Journal of the American Chemical Society* 2000, 122, (24), 5710-5717.

119. Deming, T. *Journal of the American Chemical Society* 2004, 126, 9101-9105.

120. Wu, L.; Muller, E. A.; Jackson, G. *Macromolecules* 2014, 47, (4), 1482-1493.

121. Buining, P. A.; Veldhuizen, Y. S. J.; Pathmamanoharan, C.; Lekkerkerker, H. N. W. *Colloids and Surfaces* 1992, 64, (1), 47-55.

122. Yamakawa, H. *Annu. Rev. Phys. Chem.* 1984, 35, 23-47.

123. Zhang, R. S.; Mattice, W. L. *Macromolecules* 1993, 26, (16), 4384-4385.

124. Duggal, R.; Pasquali, M. *Phys. Rev. Lett.* 2006, 96, (24).

125. Fraden, S., Phase Transitions in Collodial Suspensions of Virus Particles. In *Observation, Prediction, and Simulation of Phase Transitions in Complex Fluids*, (M. Baus, L. F. R., and J. P. Ryckaert, Eds, Ed. Kluwer Academic Publishers: Dorcrecht, 1995; Vol. 460.

126. Poche, D. S.; Daly, W. H.; Russo, P. S. *Macromolecules* 1995, 28, (20), 6745-6753.

127. Fasman, G. D.; Idelson, M.; Blout, E. R. *Journal of the American Chemical Society* 1961, 83, (3), 709-712.

128. Xiao, Z.; Gupta, M.; Baltas, G.; Liu, T.; Chae, H. G.; Kumar, S. *Polymer* 2012, 53, (22), 5069-5077.

129. Lu, Y. J.; Weers, B.; Stellwagen, N. C. *Biopolymers* 2001, 61, (4), 261-275.

130. Greenfield, N. J.; Fasman, G. D. *Biochemistry* 1969, 8, (10), 4108-4116.

131. Chu, B., *Laser Light Scattering*. Academic Press: New York.

132. Atmaja, B.; Cha, J. N.; Marshall, A.; Frank, C. W. *Langmuir* 2009, 25, (2), 707-715.

133. Chirgadze, Y. N.; Nevskaya, N. A. *Biopolymers* 1976, 15, (4), 627-636.

134. Susi, H.; Timashef.Sn; Stevens, L. *Journal of Biological Chemistry* 1967, 242, (23), 5460-5466.

135. Van Holde, K. E., *Physical Biochemistry*. Second ed.; Prentice-Hall, Inc.: Englewood Cliffs, NJ, 1985.

136. Nowak, A. P. Resilient Self-Assembling Hydrogels from Block Copolypeptide Amphiphiles. UC-Santa Barbara, 2003.

137. Scholtz, J. M.; Baldwin, R. L. *Annual Review of Biophysics and Biomolecular Structure* 1992, 21, 95-118.

138. Paar, A., DMA 58 User Manual.

139. Ralston, G., *Introduction to Analytical Ultracentrifugation*. Beckman: p 87.

140. Phoenix, B., *Brice-Phoenix Differential Refractometer Model BP-2000-V*.

141. Thormählen, I.; Straub, J.; Grigull, U. *Journal of Physical and Chemical Reference Data* 1985, 14, (4), 933-945.

142. Huglin, M. B., *Light Scattering From Polymer Solutions*. Academic Press: London and New York, 1972.

143. Paar, A., AVMn Automated Microviscometer Manual.

144. Russo, P. S., Instrinsic Viscosity. macro.lsu.edu/howtoguides, 201.

145. Russo, P. S.; Siripanyo, S.; Saunders, M. J.; Karasz, F. E. *Macromolecules* 1986, 19, (11), 2856-2859.

146. Russo, P., Intrinsic Viscosity. 2008.

147. Hanton, S. D. *Chem. Rev.* 2001, 101, (2), 527-569.

148. University, C. W., Polymers and Liquid Crystals. 2003.

149. Brown, W., Dynamic Light Scattering From Rigid and Nearly Rigid Rods. In *Dynamic Light Scattering the Method and Some Applications*, Clarendon Press Oxford: 1993.

150. Hollingsworth, J. V.; Richard, A. J.; Vicente, M. G. H.; Russo, P. S. *Biomacromolecules* 2012, 13, (1), 60-72.

151. Lodge, T.; Hiemenz, P., *Polymer Chemistry*. Second ed.; CRC Press: Boca Raton, 2007.

152. Russo, P. S.; Doucet, G.; Neau, D. B.; DeKee, D. *Abstr. Pap. Am. Chem. Soc.* 2003, 225, U149-U149.

153. Bellomo, E. G.; Deming, T. J. *Journal of the American Chemical Society* 2006, 128, (7), 2276-2279.

154. Yamakawa, H., Modern Theory of Polymer Solutions. Harper and Row: New York, 1971.

155. Mark, J., *Physical Properties of Polymers Handbook*. Second Edition ed.; Springer Science: 2007.

156. DeLong, L. M.; Russo, P. S. *Macromolecules* 1991, 24, (23), 6139-6155.

157. Kirkwood, J. G.; Riseman, J. *Journal of Chemical Physics* 1948, 16, (6), 565-573.

158. Collins, M. E.; Soto-Cantu, E.; Cueto, R.; Russo, P. S. *Langmuir* 2014, 30, (12), 3373-3380.

159. Azri, A.; Giamarchi, P.; Grohens, Y.; Olier, R.; Privat, M. *J. Colloid Interface Sci.* 2012, 379, (1), 14-19.

160. Burchard, W., Combined Static and Dynamic Light Scattering. In *Light Scattering Principles and Development*, Clarendon Press: Oxford, 1996; pp 439-476.

161. Gokran, Y. Hydrodynamic Behavior and Thermal Stability of a Pegylated Protein: Studies with Hen Egg Lysozyme. New Hampshire, 2003.

162. Lodge, T. P.; Rotstein, N. A.; Prager, S. *Adv. Chem. Phys.* 1990, 79, 1-132.

163. Doty, P. A., J., alpha-Helix Formation in poly-epsilon-carbobenzoxy-L-lysine and poly-L-lysine. In *Polyamino Acids, Polypeptides, and Proteins*, Stahmann, M. A., Ed. University of Wisconsin Press, 1962; pp 161-176.

164. Richtering, W. H.; Schatzle, J.; Adams, J.; Burchard, W. *Colloid Polym. Sci.* 1989, 267, (7), 568-576.

165. Janz, G. J.; Oliver, B. G.; Lakshmin.Gr; Mayer, G. E. *Journal of Physical Chemistry* 1970, 74, (6), 1285-1289.

166. Kawahara, K.; Tanford, C. *Journal of Biological Chemistry* 1966, 241, (13), 3228-3232.

167. Khattab, I. S.; Bandarkar, F.; Fakhree, M. A. A.; Jouyban, A. *Korean Journal of Chemical Engineering* 2012, 29, (6), 812-817.

168. Bernal-Garcia, J. M.; Guzman-Lopez, A.; Cabrales-Torres, A.; Estrada-Baltazar, A.; Iglesias-Silva, G. A. *Journal of Chemical and Engineering Data* 2008, 53, (4), 1024-1027.

169. Lo Nostro, P.; Ninham, B. W. *Chem. Rev.* 2012, 112, (4), 2286-2322.

170. Randall, M.; Failey, C. F. *Chem. Rev.* 1927, 4, (3), 285-290.

171. Long, F. A.; McDevit, W. F. *Chem. Rev.* 1952, 51, (1), 119-169.

172. Baldwin, R. L. *Biophys. J.* 1996, 71, (4), 2056-2063.

173. Nandi, P. K.; Robinson, D. R. *Journal of the American Chemical Society* 1972, 94, (4), 1299-1308.

174. Tohyama, K.; Miller, W. G. *Nature* 1981, 289, (5800), 813-814.

175. Arunkumar, A. I.; Kumar, T. K. S.; Yu, C. *International Journal of Biological Macromolecules* 1997, 21, (3), 223-230.

176. Doucet, G. J.; Qiu, J.; Russo, P. S. *The Journal of Physical Chemistry B* 2010, 114, (14), 4777-4782.

177. Inomata, K.; Shimizu, H.; Nose, T. *J. Polym. Sci. Pt. B-Polym. Phys.* 2000, 38, (10), 1331-1340.

178. Inomata, K.; Ohara, N.; Shimizu, H.; Nose, T. *Polymer* 1998, 39, (15), 3379-3386.

Appendix 1 - NMR spectra

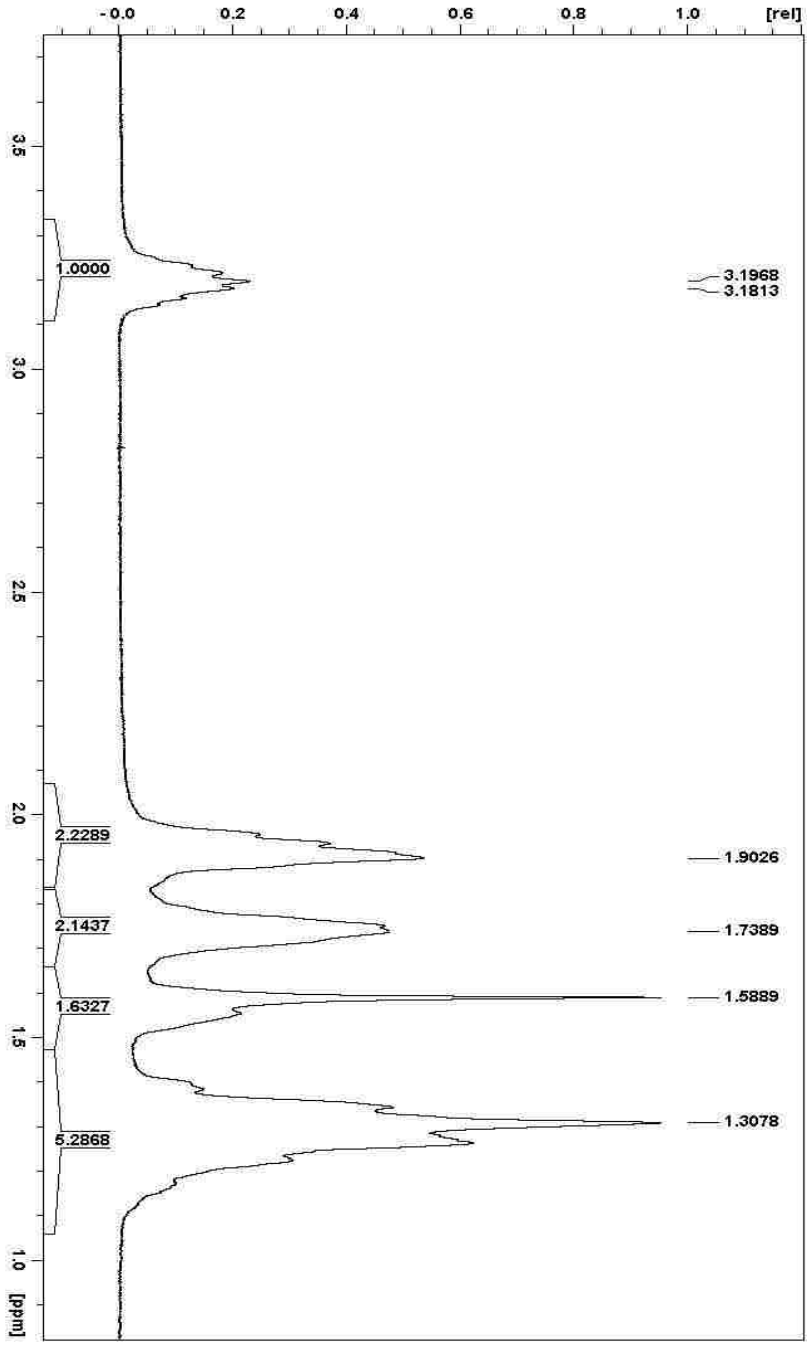

Figure 107. ^{1}H NMR of dicyclohexylcarbodiimide (DCC).

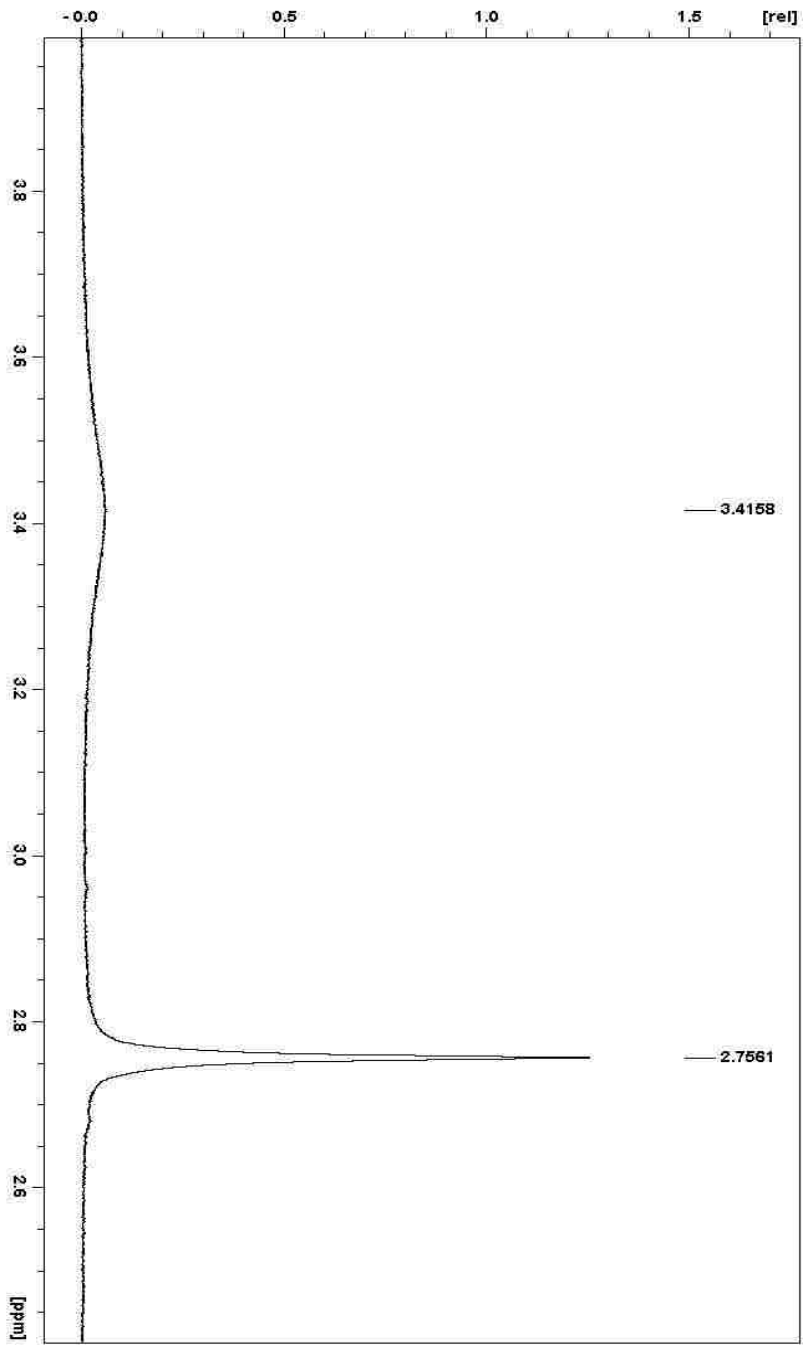

Figure 108. ^{1}H NMR of N-hydroxysuccinimde (NHS).

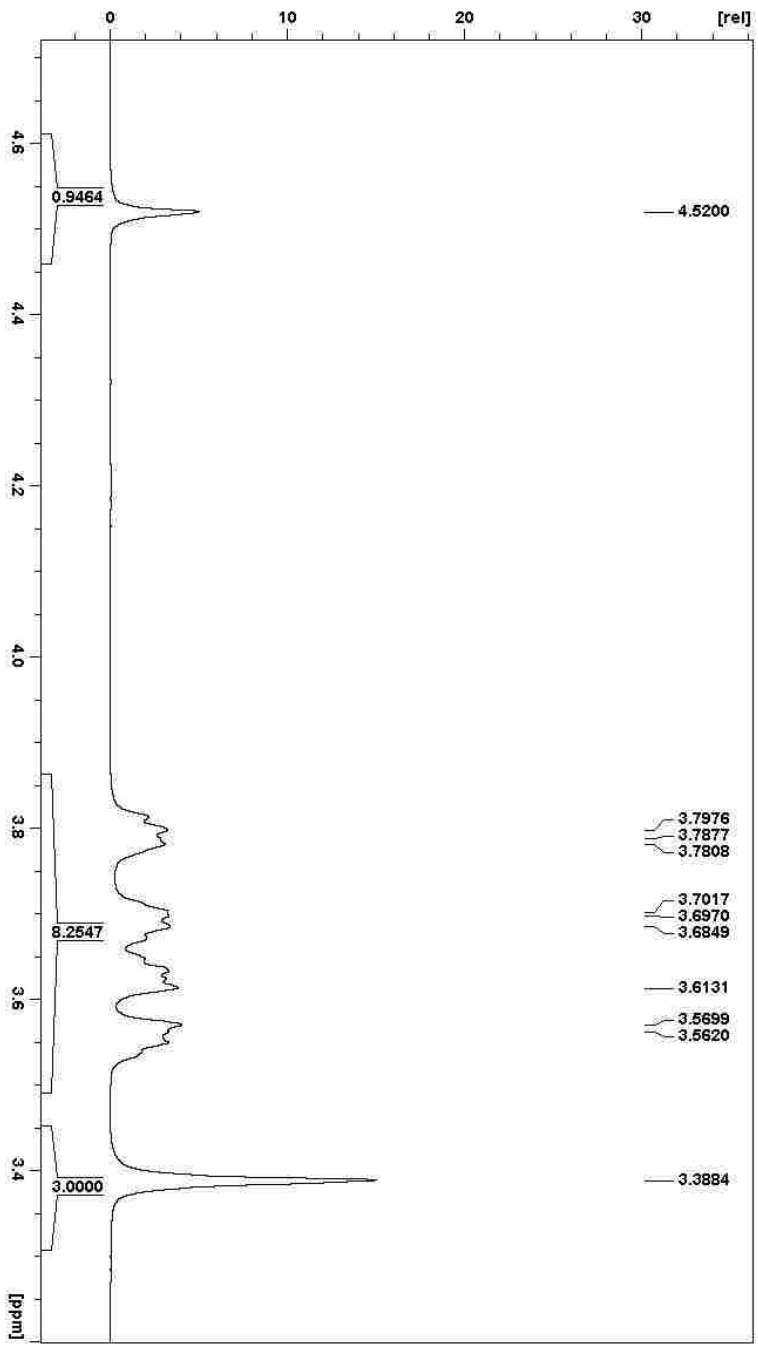

Figure 109. ^{1}H NMR of N-2-[2-(2-methoxyethoxy)ethoxy]acetic acid.

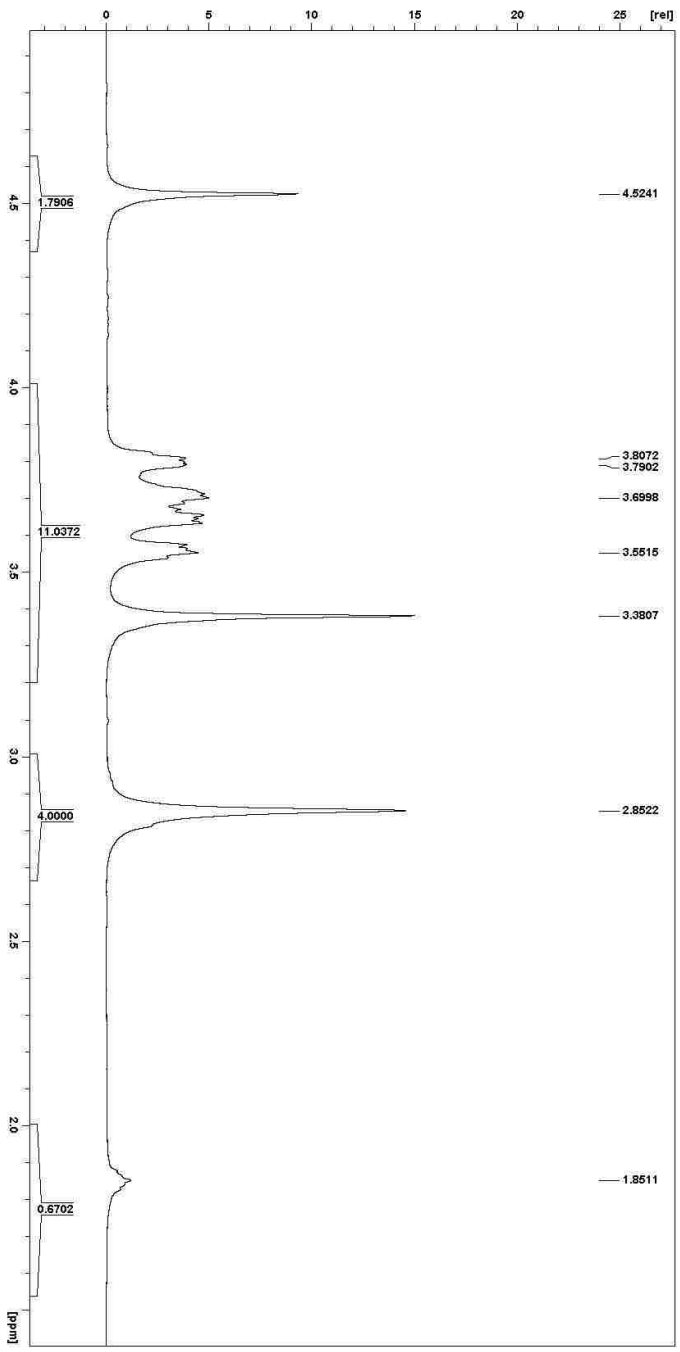

Figure 110. ^{1}H NMR of N-Hydroxysuccinimidyl 2-[2-(2-methoxyethoxy)ethoxy]acetate.

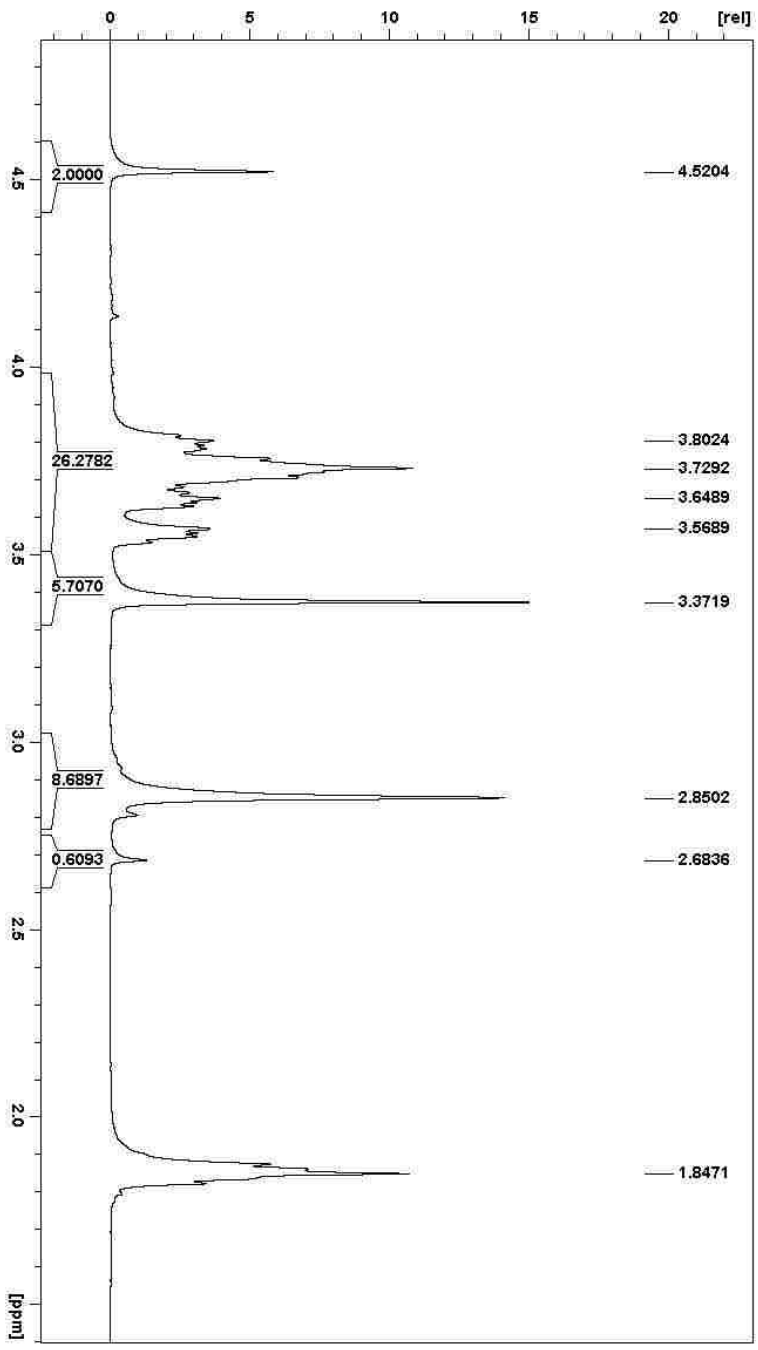

Figure 111. ^{1}H NMR of N-Hydroxysuccinimidyl 2-[2-(2-methoxyethoxy)ethoxy]acetate without complete reaction. The right shoulder on the peak centered at 2.8502 is due to unreacted N-hydroxysuccinimde.

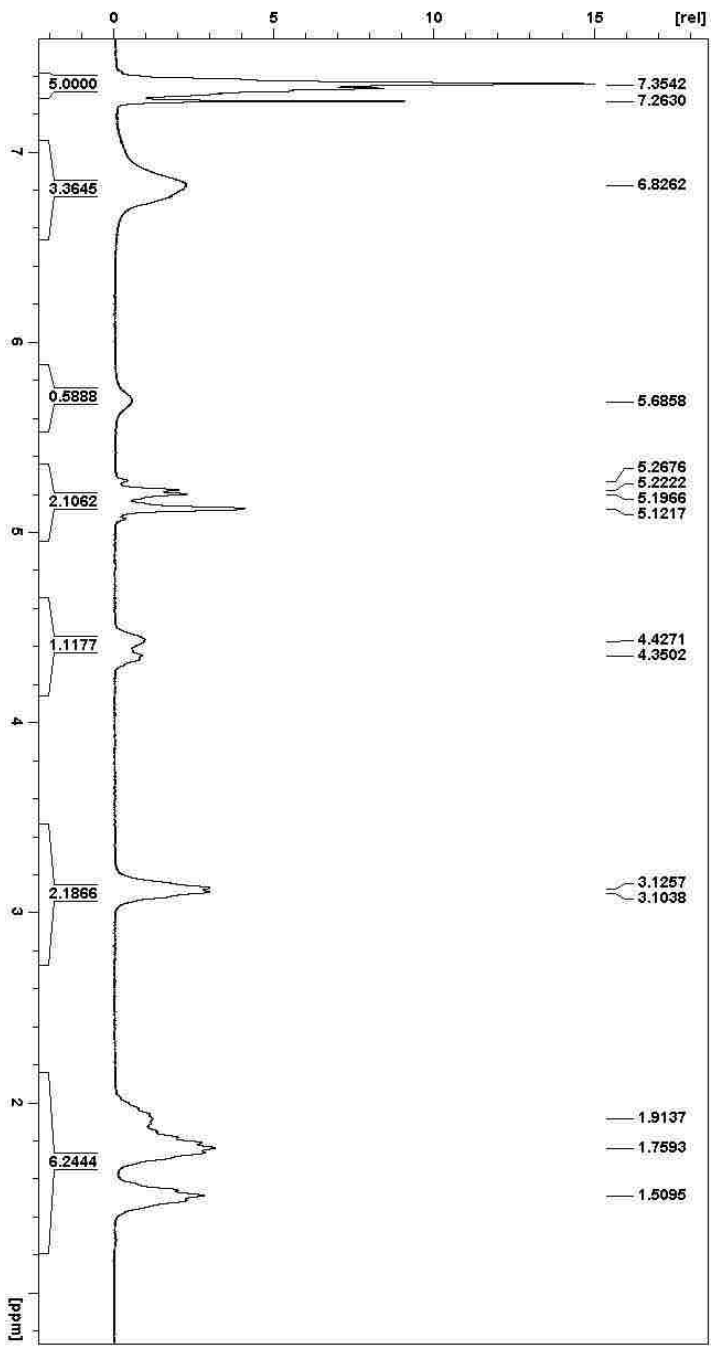

Figure 112. ^{1}H NMR of N_{α} -Z-L-Lysine.

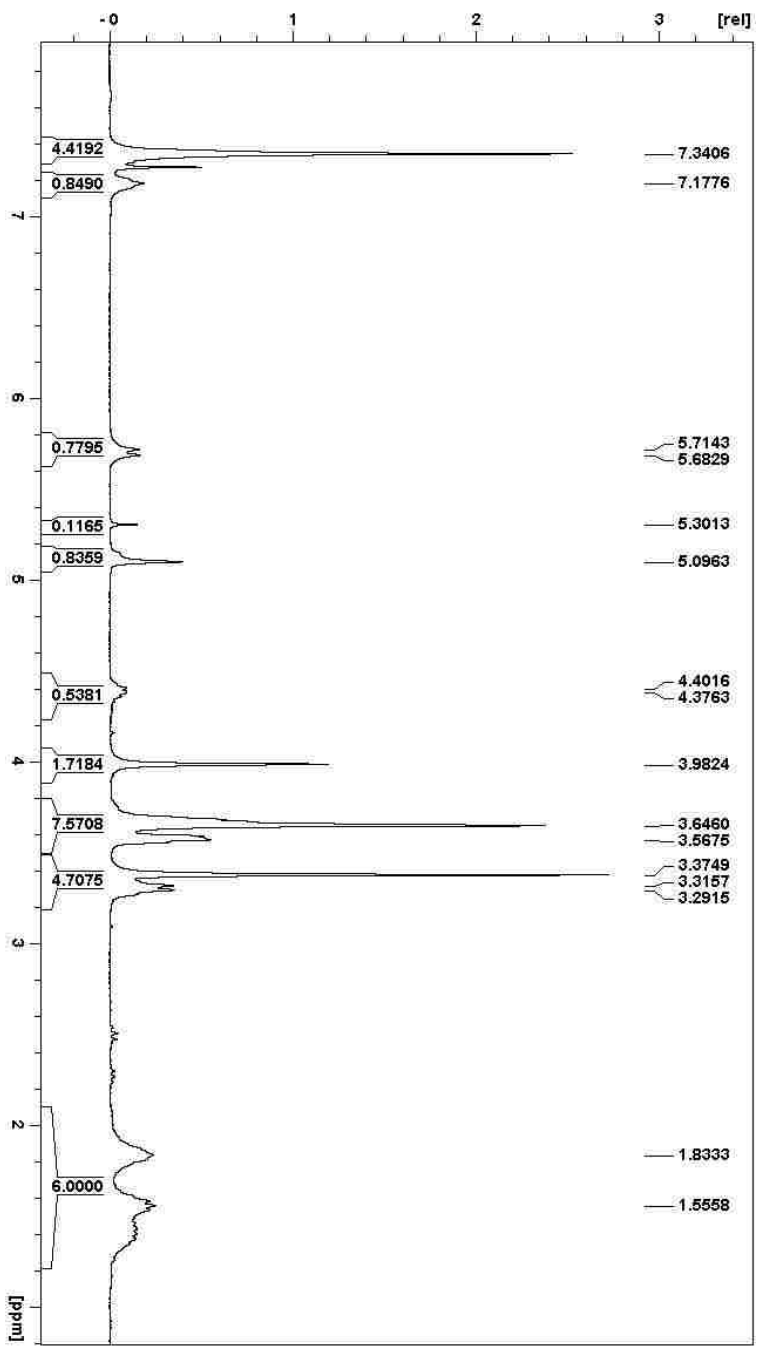

Figure 113. ^{1}H NMR of N_{ε}-2-[2-(2-methoxyethoxy)ethoxy]acetyl-N_{α}-Z-L-Lysine.

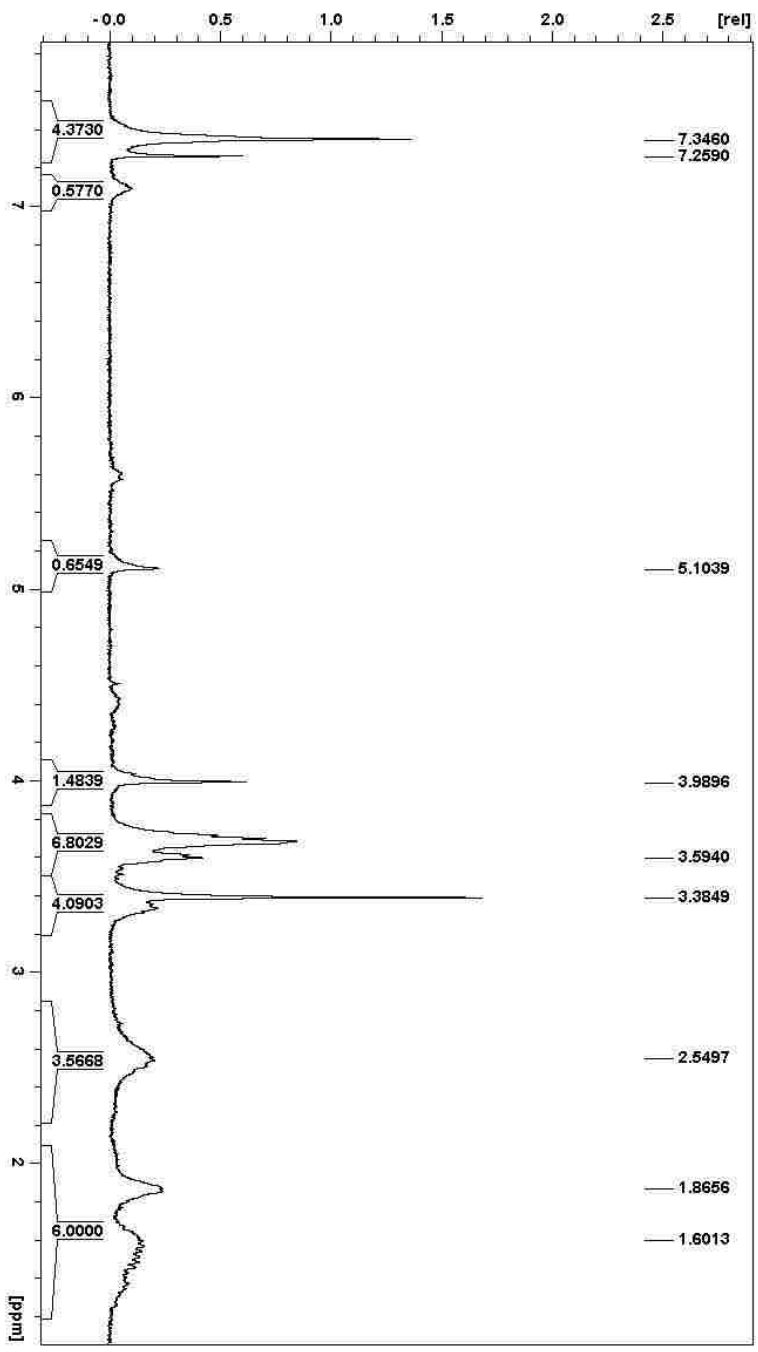

Figure 114. ^{1}H NMR of PEG-Lysine NCA.

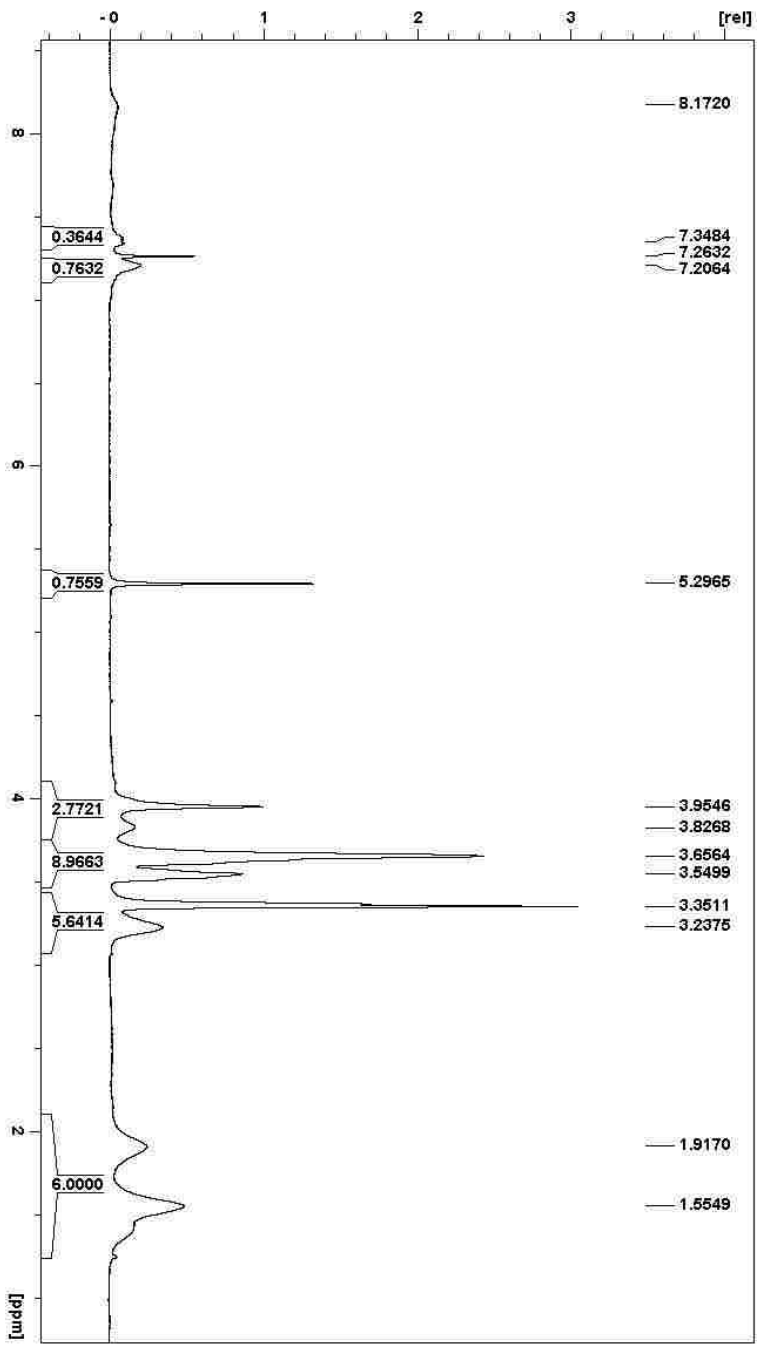

Figure 115. ^{1}H NMR of PEGL polymer.

Appendix 2 - Crystal Structure Data for EG-NCA

Huberty1

Wayne Huberty

(Huberty1)

Crystal data

$C_{10}H_{10}N_2O_5$	$F(000) = 712$
$M_r = 332.35$	$D_x = 1.524$ Mg m^{-3}
Orthorhombic, $P2_12_12_1$	Cu $K\alpha$ radiation, $\lambda = 1.54184$ Å
Hall symbol: P 2ac 2ab	Cell parameters from 3234 reflections
$a = 5.0453$ (6) Å	$\theta = 3.2–66.4°$
$b = 11.952$ (3) Å	$\mu = 0.90$ mm^{-1}
$c = 27.650$ (5) Å	$T = 90$ K
$V = 1667.3$ (6) Å^3	Needle, Colourless
$Z = 4$	0.31 × 0.05 × 0.02 mm

Data collection

Bruker Kappa APEX-II DUO diffractometer	2806 independent reflections
Radiation source: 1µS microfocus	2351 reflections with $I > 2\sigma(I)$
QUAZAR multilayer optics monochromator	$R_{int} = 0.046$
ϕ and ω scans	$\theta_{max} = 66.4°$, $\theta_{min} = 3.2°$
Absorption correction: Multi-scan *SADABS* (Sheldrick, 2004)	$h = -5 \rightarrow 4$
$T_{min} = 0.760$, $T_{max} = 0.982$	$k = -12 \rightarrow 14$
13261 measured reflections	$l = -31 \rightarrow 32$

Refinement

Refinement on F^2	Secondary atom site location: Difference Fourier map
Least-squares matrix: Full	Hydrogen site location: Inferred from neighbouring sites
$R[F^2 > 2\sigma(F^2)] = 0.031$	H atoms treated by a mixture of independent and constrained refinement
$wR(F^2) = 0.115$	$w = 1/[\sigma^2(F_o^2) + (0.0236P)^2 + 1.3076P]$ where $P = (F_o^2 + 2F_c^2)/3$
$S = 1.06$	$(\Delta/\sigma)_{max} = 0.001$
2806 reflections	$\Delta\rho_{max} = 0.20$ e Å^{-3}
242 parameters	$\Delta\rho_{min} = -0.27$ e Å^{-3}
17 restraints	Absolute structure: 1108 Friedel pairs (Flack, 1983)
Primary atom site location: Structure-invariant direct methods	Flack parameter: −0.1 (4)

Special details

Geometry. All esds (except the esd in the dihedral angle between two l.s. planes) are estimated using the full covariance matrix. The cell esds are taken into account individually in the estimation of esds in distances, angles and torsion angles; correlations between esds in cell parameters are only used when they are defined by crystal symmetry. An approximate (isotropic) treatment of cell esds is used for estimating esds involving l.s. planes.

Refinement. Refinement of F^2 against ALL reflections. The weighted R-factor wR and goodness of fit S are based on F^2, conventional R-factors R are based on F, with F set to zero for negative F^2. The threshold expression of $F^2 > 2\sigma(F^2)$ is used only for calculating R-factors(gt) etc. and is not relevant to the choice of reflections for refinement. R-factors based on F^2 are statistically about twice as large as

Notes based on F_o and R- factors based on ALL data will be even larger.

Fractional atomic coordinates and isotropic or equivalent isotropic displacement parameters (Å²)

	x	y	z	U_{iso}*/U_{eq}	Occ. (<1)
O1	0.0208 (5)	0.35171 (18)	0.39012 (10)	0.0640 (7)	
O2	0.2620 (6)	0.4429 (2)	0.3331 (3)	0.0703 (9)	
O3	−0.1335 (5)	0.2895 (2)	0.46082 (11)	0.0607 (10)	
O4	0.2944 (4)	0.3977 (2)	0.59203 (7)	0.0500 (7)	
N1	0.3871 (5)	0.4540 (2)	0.43379 (11)	0.0500 (8)	
H1N	0.502 (8)	0.508 (3)	0.4114 (13)	0.060*	
N2	0.4884 (6)	0.7469 (3)	0.62705 (10)	0.0691 (10)	
H2N	0.528 (8)	0.713 (3)	0.6535 (10)	0.083*	
C1	0.2523 (8)	0.4224 (3)	0.37509 (14)	0.0555 (9)	
C2	0.0324 (7)	0.3423 (3)	0.43937 (15)	0.0634 (11)	
C3	0.2662 (6)	0.4068 (3)	0.45089 (12)	0.0501 (11)	
H3	0.3992	0.3989	0.4714	0.071*	
C4	0.1883 (6)	0.4035 (3)	0.49607 (12)	0.0620 (11)	
H4A	0.1023	0.4478	0.5239	0.074*	
H4B	0.0564	0.3411	0.4834	0.074*	
C5	0.4214 (6)	0.3555 (4)	0.51694 (13)	0.0643 (12)	
H5A	0.5651	0.3834	0.5262	0.080*	
H5B	0.4903	0.3056	0.4914	0.080*	
C6	0.3426 (7)	0.6250 (4)	0.56069 (12)	0.0694 (13)	
H6A	0.1964	0.6758	0.5513	0.083*	
H6B	0.2744	0.5743	0.5961	0.083*	
C7	0.5653 (7)	0.6942 (4)	0.59171 (13)	0.0711 (13)	
H7A	0.7213	0.6433	0.5874	0.085*	
H7B	0.6174	0.7527	0.5762	0.085*	
C8	0.3909 (6)	0.8415 (4)	0.62881 (11)	0.0619 (11)	
C9A	0.2754 (18)	0.8075 (6)	0.6789 (3)	0.0383 (16)	0.497 (2)
H9A1	0.3852	0.8758	0.6814	0.046*	0.497 (2)
H9A2	0.0969	0.8305	0.6790	0.046*	0.497 (2)
O5A	0.3205 (11)	0.8361 (4)	0.73032 (18)	0.0333 (9)	0.497 (2)
C10A	0.5625 (14)	0.8617 (5)	0.7449 (3)	0.0361 (12)	0.497 (2)
H10A	0.5275	0.9104	0.7731	0.043*	0.497 (2)
H10B	0.6663	0.8810	0.7229	0.043*	0.497 (2)
C11A	0.678 (2)	0.7527 (3)	0.7609 (3)	0.0351 (16)	0.497 (2)
H11A	0.8383	0.7661	0.7807	0.042*	0.497 (2)
H11B	0.5478	0.7113	0.7868	0.042*	0.497 (2)
O6A	0.7454 (8)	0.6886 (3)	0.71902 (14)	0.0379 (7)	0.497 (2)
C12A	0.8681 (17)	0.5854 (6)	0.7310 (3)	0.0458 (14)	0.497 (2)
H12A	0.7463	0.5480	0.7519	0.055*	0.497 (2)
H12B	1.0315	0.5986	0.7506	0.055*	0.497 (2)
C13A	0.934 (2)	0.5238 (10)	0.6858 (5)	0.046 (2)	0.497 (2)
H13A	1.0356	0.5730	0.6658	0.055*	0.497 (2)
H13B	1.0439	0.4573	0.6932	0.055*	0.497 (2)
O7A	0.6900 (10)	0.4999 (4)	0.66324 (10)	0.0470 (9)	0.497 (2)
C14A	0.725 (3)	0.4070 (12)	0.6276 (6)	0.065 (3)	0.497 (2)
H14A	0.5574	0.3879	0.6129	0.098*	0.497 (2)
H14B	0.8051	0.3401	0.6426	0.098*	0.497 (2)
H14C	0.8406	0.4353	0.6027	0.098*	0.497 (2)
C9B	0.2593 (16)	0.8559 (6)	0.6761 (3)	0.0303 (16)	0.503 (2)
H9B1	0.2805	0.9227	0.6872	0.046*	0.503 (2)
H9B2	0.0442	0.8501	0.6733	0.046*	0.503 (2)

O5B	0.8237 (11)	0.7803 (4)	0.71221 (18)	0.0333 (9)	0.503 (2)
C16B	0.5758 (13)	0.8072 (5)	0.7336 (3)	0.0361 (12)	0.503 (2)
H16C	0.5576	0.8716	0.7559	0.043*	0.503 (2)
H16D	0.7032	0.8274	0.7081	0.043*	0.503 (2)
C11B	0.670 (2)	0.7059 (5)	0.7606 (3)	0.0331 (16)	0.503 (2)
H11C	0.8396	0.7235	0.7770	0.042*	0.503 (2)
H11D	0.5334	0.6899	0.7961	0.042*	0.503 (2)
O6B	0.7056 (9)	0.6118 (3)	0.73004 (13)	0.0379 (7)	0.503 (2)
C12B	0.9639 (14)	0.6052 (6)	0.7103 (3)	0.0439 (14)	0.503 (2)
H12C	1.0889	0.6152	0.7363	0.053*	0.503 (2)
H12D	0.9919	0.6651	0.6961	0.053*	0.503 (2)
C13B	1.000 (2)	0.4945 (10)	0.6874 (5)	0.046 (2)	0.503 (2)
H13C	1.1872	0.4843	0.6775	0.053*	0.503 (2)
H13D	0.9543	0.4347	0.7107	0.053*	0.503 (2)
O7B	0.8312 (11)	0.4874 (4)	0.64582 (16)	0.0478 (9)	0.503 (2)
C14B	0.631 (3)	0.5763 (11)	0.6286 (6)	0.065 (3)	0.503 (2)
H14D	0.7115	0.5753	0.5986	0.098*	0.503 (2)
H14E	0.7697	0.5255	0.6513	0.098*	0.503 (2)
H14F	1.0107	0.5392	0.6164	0.098*	0.503 (2)

Atomic displacement parameters (Å²)

	U^{11}	U^{22}	U^{33}	U^{12}	U^{13}	U^{23}
O1	0.0867 (17)	0.0979 (12)	0.0999 (19)	−0.0053 (13)	0.0006 (15)	0.0209 (13)
O2	0.110 (2)	0.0817 (14)	0.0495 (14)	−0.0191 (16)	0.0132 (15)	0.0077 (11)
O3	0.0367 (13)	0.0730 (17)	0.132 (3)	0.0113 (13)	0.0222 (18)	0.0687 (19)
O4	0.0294 (11)	0.1021 (19)	0.0364 (11)	0.0137 (12)	0.0020 (10)	0.0256 (12)
N1	0.0546 (14)	0.0636 (19)	0.0510 (16)	0.0034 (13)	0.0101 (13)	0.0338 (15)
N2	0.0244 (15)	0.134 (3)	0.0491 (17)	0.0056 (18)	0.0032 (13)	0.0512 (19)
C1	0.062 (2)	0.0550 (17)	0.069 (2)	−0.0018 (17)	0.013 (2)	0.0162 (17)
C2	0.0366 (19)	0.055 (2)	0.098 (3)	0.0171 (18)	0.016 (2)	0.030 (2)
C3	0.0250 (17)	0.082 (2)	0.067 (2)	0.0164 (17)	0.0195 (16)	0.054 (2)
C4	0.0248 (16)	0.105 (3)	0.037 (2)	0.0133 (18)	0.0096 (15)	0.050 (2)
C5	0.0253 (18)	0.116 (3)	0.055 (2)	0.015 (2)	0.0121 (15)	0.050 (2)
C6	0.0266 (17)	0.130 (4)	0.0511 (19)	0.013 (2)	0.0099 (16)	0.050 (2)
C7	0.0290 (17)	0.122 (4)	0.062 (2)	0.014 (2)	0.0110 (17)	0.052 (2)
C8	0.0257 (14)	0.127 (3)	0.0424 (18)	0.0033 (19)	0.0021 (14)	0.037 (2)
C9A	0.026 (3)	0.054 (5)	0.0347 (19)	−0.015 (3)	−0.0006 (17)	0.019 (3)
O5A	0.0296 (12)	0.042 (3)	0.0265 (17)	−0.003 (3)	−0.0014 (13)	0.006 (2)
C10A	0.035 (2)	0.036 (4)	0.039 (3)	0.000 (3)	−0.001 (2)	0.002 (3)
C11A	0.040 (2)	0.033 (5)	0.0318 (16)	0.008 (3)	−0.0046 (15)	0.002 (4)
O6A	0.0347 (16)	0.0343 (17)	0.0447 (16)	−0.0002 (16)	−0.0004 (14)	0.0025 (15)
C12A	0.043 (4)	0.042 (3)	0.038 (4)	−0.001 (3)	−0.010 (3)	0.004 (3)
C13A	0.043 (5)	0.040 (6)	0.054 (2)	0.010 (4)	−0.003 (3)	0.011 (3)
O7A	0.057 (3)	0.0389 (14)	0.045 (2)	0.002 (2)	−0.0014 (18)	−0.0042 (17)
C14A	0.098 (10)	0.051 (7)	0.047 (2)	0.000 (5)	0.002 (6)	0.003 (4)
C9B	0.026 (3)	0.054 (5)	0.0347 (19)	−0.015 (3)	−0.0006 (17)	0.019 (3)
O5B	0.0296 (12)	0.042 (3)	0.0265 (17)	−0.003 (3)	−0.0014 (13)	0.006 (2)
C10B	0.033 (2)	0.036 (4)	0.039 (3)	0.000 (3)	−0.001 (2)	0.002 (3)
C11B	0.040 (2)	0.033 (5)	0.0318 (16)	0.008 (3)	−0.0046 (15)	0.002 (4)
O6B	0.0347 (16)	0.0343 (17)	0.0447 (16)	−0.0002 (16)	−0.0004 (14)	0.0025 (15)
C12B	0.043 (4)	0.042 (3)	0.038 (4)	−0.001 (3)	−0.010 (3)	0.004 (3)
C13B	0.043 (5)	0.040 (6)	0.054 (2)	0.010 (4)	−0.003 (3)	0.011 (3)
O7B	0.057 (3)	0.0389 (14)	0.045 (2)	0.002 (2)	−0.0014 (18)	−0.0042 (17)
C14B	0.098 (10)	0.051 (7)	0.047 (2)	0.000 (5)	0.002 (6)	0.003 (4)

Geometric parameters (Å, º)

O1—C2	1.367 (5)	C11A—H11A	0.9900
O1—C1	1.422 (4)	C11A—H11B	0.9900
O2—C1	1.196 (4)	O6A—C12A	1.424 (8)
O3—C2	1.203 (4)	C12A—C13A	1.505 (11)
O4—C9	1.211 (4)	C12A—H12A	0.9900
N1—C1	1.323 (5)	C12A—H12B	0.9900
N1—C3	1.451 (4)	C13A—O7A	1.439 (11)
N1—H1N	0.88 (4)	C13A—H13A	0.9900
N2—C9	1.328 (5)	C13A—H13B	0.9900
N2—C7	1.436 (5)	O7A—C14A	1.410 (10)
N2—H2N	0.839 (19)	C14A—H14A	0.9900
C2—C3	1.489 (6)	C14A—H14B	0.9900
C3—C4	1.520 (5)	C14A—H14C	0.9900
C3—H3	1.0000	C9B—O5B	1.413 (8)
C4—C5	1.526 (5)	C9B—H9B1	0.9900
C4—H4A	0.9900	C9B—H9B2	0.9900
C4—H4B	0.9900	O5B—C10B	1.439 (8)
C5—C6	1.521 (5)	C10B—C12B	1.502 (9)
C5—H5A	0.9900	C10B—H10C	0.9900
C5—H5B	0.9900	C10B—H10D	0.9900
C6—C7	1.511 (6)	C11B—O6B	1.422 (8)
C6—H6A	0.9900	C11B—H11C	0.9900
C6—H6B	0.9900	C11B—H11D	0.9900
C7—H7A	0.9900	O6B—C12B	1.424 (8)
C7—H7B	0.9900	C12B—C13B	1.478 (10)
C8—C9B	1.433 (8)	C12B—H12C	0.9900
C8—C9A	1.639 (9)	C12B—H12D	0.9900
C9A—O5A	1.446 (8)	C13B—O7B	1.433 (10)
C9A—H9A1	0.9900	C13B—H13C	0.9900
C9A—H9A2	0.9900	C13B—H13D	0.9900
O5A—C10A	1.430 (8)	O7B—C14B	1.408 (11)
C10A—C11A	1.495 (9)	C14B—H14D	0.9900
C10A—H10A	0.9900	C14B—H14E	0.9900
C10A—H10B	0.9900	C14B—H14F	0.9900
C11A—O6A	1.428 (9)		

C2—O1—C1	107.9 (3)	C10A—C11A—H11A	109.9
C1—N1—C3	112.8 (3)	O6A—C11A—H11B	109.9
C1—N1—H1N	121 (2)	C10A—C11A—H11B	109.9
C3—N1—H1N	126 (2)	H11A—C11A—H11B	108.3
C9—N2—C7	122.7 (3)	C12A—O6A—C11A	111.6 (5)
C9—N2—H2N	119 (3)	O6A—C12A—C13A	108.1 (7)
C7—N2—H2N	118 (3)	O6A—C12A—H12A	110.1
O2—C1—N1	131.5 (3)	C13A—C12A—H12A	110.1
O2—C1—O1	120.0 (4)	O6A—C12A—H12B	110.1
N1—C1—O1	108.6 (3)	C13A—C12A—H12B	110.1
O3—C2—O1	120.2 (4)	H12A—C12A—H12B	108.4
O3—C2—C3	129.9 (4)	O7A—C13A—C12A	108.3 (8)
O1—C2—C3	109.8 (3)	O7A—C13A—H13A	110.0
N1—C3—C2	100.8 (3)	C12A—C13A—H13A	110.0
N1—C3—C4	114.9 (3)	O7A—C13A—H13B	110.0
C2—C3—C4	111.8 (3)	C12A—C13A—H13B	110.0
N1—C3—H3	109.7	H13A—C13A—H13B	108.4

C2—C3—H3	108.7	C14A—O7A—C13A	112.6 (3)
C4—C3—H3	108.7	O5A—C14A—H14A	109.5
C3—C4—C5	113.7 (3)	O5A—C14A—H14B	109.5
C3—C4—H4A	108.8	H14A—C14A—H14B	109.5
C5—C4—H4A	108.8	O5A—C14A—H14C	109.5
C3—C4—H4B	108.8	H14A—C14A—H14C	109.5
C5—C4—H4B	108.8	H14B—C14A—H14C	109.5
H4A—C4—H4B	107.7	O9B—C9B—C8	116.8 (6)
C6—C5—C4	111.9 (3)	O9B—C9B—H9B1	108.1
C6—C5—H5A	109.2	C8—C9B—H9B1	108.1
C4—C5—H5A	109.2	O9B—C9B—H9B2	108.1
C6—C5—H5B	109.2	C8—C9B—H9B2	108.1
C4—C5—H5B	109.2	H9B1—C9B—H9B2	107.3
H5A—C5—H5B	107.9	O9B—O9B—C10B	114.5 (5)
C7—C6—C5	114.2 (3)	O9B—C10B—C11B	107.6 (7)
C7—C6—H6A	108.7	O9B—C10B—H10C	110.2
C5—C6—H6A	108.7	C11B—C10B—H10C	110.2
C7—C6—H6B	108.7	O9B—C10B—H10D	110.2
C5—C6—H6B	108.7	C11B—C10B—H10D	110.2
H6A—C6—H6B	107.6	H10C—C10B—H10D	108.5
N2—C7—C6	111.7 (3)	O6B—C11B—C10B	112.3 (7)
N2—C7—H7A	109.3	O6B—C11B—H11C	109.1
C6—C7—H7A	109.3	C10B—C11B—H11C	109.1
N2—C7—H7B	109.3	O6B—C11B—H11D	109.1
C6—C7—H7B	109.3	C10B—C11B—H11D	109.1
H7A—C7—H7B	107.9	H11C—C11B—H11D	107.9
O4—C8—N2	123.1 (5)	C11B—O6B—C12B	113.0 (7)
O4—C8—C9B	126.0 (5)	O6B—C12B—C13B	108.3 (8)
N2—C8—C9B	108.9 (4)	O6B—C12B—H12C	109.9
O4—C8—C9A	112.1 (4)	C13B—C12B—H12C	109.9
N2—C8—C9A	124.2 (4)	O6B—C12B—H12D	109.9
O5A—C9A—C8	110.4 (5)	C13B—C12B—H12D	109.9
O5A—C9A—H9A1	109.6	H12C—C12B—H12D	108.3
C8—C9A—H9A1	109.6	O7B—C13B—C12B	109.2 (7)
O5A—C9A—H9A2	109.6	O7B—C13B—H13C	109.8
C8—C9A—H9A2	109.6	C12B—C13B—H13C	109.8
H9A1—C9A—H9A2	108.1	O7B—C13B—H13D	109.8
C10A—O5A—C9A	112.6 (5)	C12B—C13B—H13D	109.8
O5A—C10A—C11A	106.7 (7)	H13C—C13B—H13D	108.3
O5A—C10A—H10A	110.4	C14B—O7B—C13B	111.0 (8)
C11A—C10A—H10A	110.4	O7B—C14B—H14D	109.5
O5A—C10A—H10B	110.4	O7B—C14B—H14E	109.5
C11A—C10A—H10B	110.4	H14D—C14B—H14E	109.5
H10A—C10A—H10B	108.6	O7B—C14B—H14F	109.5
O6A—C11A—C10A	108.7 (6)	H14D—C14B—H14F	109.5
O6A—C11A—H11A	109.9	H14E—C14B—H14F	109.5

C8—N1—C1—O2	−177.6 (4)	C7—N2—C8—C9A	−176.2 (4)
C8—N1—C1—O1	2.1 (4)	O4—C8—C9A—O5A	174.7 (4)
C2—O1—C1—O2	180.0 (3)	N2—C8—C9A—O5A	−14.0 (7)
C2—O1—C1—N1	0.3 (4)	C8—C9A—O5A—C10A	101.5 (6)
C1—O1—C2—O3	177.3 (3)	C9A—O5A—C10A—C11A	−142.3 (7)
C1—O1—C2—C3	−2.4 (4)	O5A—C10A—C11A—O6A	64.7 (9)
C1—N1—C3—C2	−3.4 (4)	C10A—C11A—O6A—C12A	177.3 (7)

C1—N1—C3—C4	−123.7 (3)	C11A—O6A—C12A—C13A	−179.6 (9)
O3—C2—C3—N1	−176.3 (4)	O6A—C12A—C13A—O7A	−68.3 (11)
O1—C2—C3—N1	3.4 (3)	C12A—C13A—O7A—C14A	−163.9 (11)
O3—C2—C3—C4	−53.7 (5)	O4—C5—C9B—O5B	177.6 (4)
O1—C2—C3—C4	126.0 (3)	N2—C5—C9B—O5B	3.9 (7)
N1—C3—C4—C5	−65.3 (4)	C5—C9B—O5B—C10B	88.7 (7)
C2—C3—C4—C5	−179.4 (3)	C9B—O5B—C10B—C11B	−165.3 (6)
C3—C4—C5—C6	−171.4 (3)	O5B—C10B—C11B—O6B	61.2 (10)
C4—C5—C6—C7	−179.4 (3)	C10B—C11B—O6B—C12B	69.7 (9)
C5—N2—C7—C6	−92.8 (4)	C11B—O6B—C12B—C13B	168.7 (7)
C5—C6—C7—N2	−172.3 (3)	O6B—C12B—C13B—O7B	67.4 (12)
C7—N2—C5—O4	−5.9 (5)	C12B—C13B—O7B—C14B	−172.2 (11)
C7—N2—C5—C9B	163.3 (4)		

Hydrogen-bond geometry (Å, º)

D—H···*A*	*D*—H	H···*A*	*D*···*A*	*D*—H···*A*
N1—H1N···O4^{i}	0.88 (4)	1.92 (4)	2.790 (4)	178 (3)
N2—H2N···O5B	0.86 (2)	2.08 (4)	2.529 (6)	111 (3)
N2—H2N···O6A	0.86 (2)	2.14 (3)	2.938 (8)	155 (4)

Symmetry code: (i) $x+1/2$, $-y+3/2$, $-z+1$.

Appendix 3 - Permissions

9/16/13 RightsLink® by Copyright Clearance Center

Copyright Clearance Center RightsLink®

Home | Create Account | Help

ACS Publications

Title: The History of the Discovery of the Amino Acids.
Author: Hubert Bradford. Vickery and Carl L. A. Schmidt
Publication: Chemical Reviews
Publisher: American Chemical Society
Date: Oct 1, 1931
Copyright © 1931, American Chemical Society

User ID
Password
Enable Auto Login
Login
Forgot Password/User ID?
If you're a copyright.com user, you can login to RightsLink using your copyright.com credentials. Already a RightsLink user or want to learn more?

PERMISSION/LICENSE IS GRANTED FOR YOUR ORDER AT NO CHARGE

This type of permission/license, instead of the standard Terms & Conditions, is sent to you because no fee is being charged for your order. Please note the following:

- Permission is granted for your request in both print and electronic formats, and translations.
- If figures and/or tables were requested, they may be adapted or used in part.
- Please print this page for your records and send a copy of it to your publisher/graduate school.
- Appropriate credit for the requested material should be given as follows: "Reprinted (adapted) with permission from (COMPLETE REFERENCE CITATION). Copyright (YEAR) American Chemical Society." Insert appropriate information in place of the capitalized words.
- One-time permission is granted only for the use specified in your request. No additional uses are granted (such as derivative works or other editions). For any other uses, please submit a new request.

If credit is given to another source for the material you requested, permission must be obtained from that source.

BACK | CLOSE WINDOW

Copyright © 2013 Copyright Clearance Center, Inc. All Rights Reserved. Privacy statement.
Comments? We would like to hear from you. E-mail us at customercare@copyright.com

https://s100.copyright.com/App/Checkout/Serial 1/1

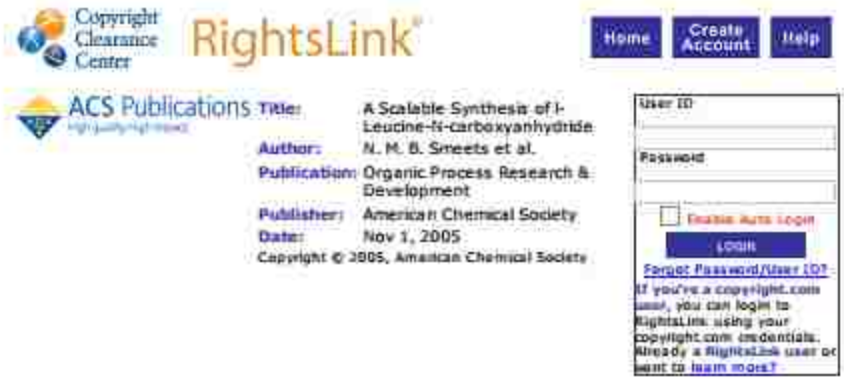

PERMISSION/LICENSE IS GRANTED FOR YOUR ORDER AT NO CHARGE

This type of permission/license, instead of the standard Terms & Conditions, is sent to you because no fee is being charged for your order. Please note the following:

- Permission is granted for your request in both print and electronic formats, and translations.
- If figures and/or tables were requested, they may be adapted or used in part.
- Please print this page for your records and send a copy of it to your publisher/graduate school.
- Appropriate credit for the requested material should be given as follows: "Reprinted (adapted) with permission from (COMPLETE REFERENCE CITATION). Copyright (YEAR) American Chemical Society." Insert appropriate information in place of the capitalized words.
- One-time permission is granted only for the use specified in your request. No additional uses are granted (such as derivative works or other editions). For any other uses, please submit a new request.

If credit is given to another source for the material you requested, permission must be obtained from that source.

BACK CLOSE WINDOW

PERMISSION/LICENSE IS GRANTED FOR YOUR ORDER AT NO CHARGE

This type of permission/license, instead of the standard Terms & Conditions, is sent to you because no fee is being charged for your order. Please note the following:

- Permission is granted for your request in both print and electronic formats, and translations.
- If figures and/or tables were requested, they may be adapted or used in part.
- Please print this page for your records and send a copy of it to your publisher/graduate school.
- Appropriate credit for the requested material should be given as follows: "Reprinted (adapted) with permission from (COMPLETE REFERENCE CITATION). Copyright (YEAR) American Chemical Society." Insert appropriate information in place of the capitalized words.
- One-time permission is granted only for the use specified in your request. No additional uses are granted (such as derivative works or other editions). For any other uses, please submit a new request.

If credit is given to another source for the material you requested, permission must be obtained from that source.

BACK | CLOSE WINDOW

Copyright Clearance Center RightsLink®

Home | Create Account | Help

ACS Publications

Title:	POLYPEPTIDES. Xa. ADDITIONAL COMMENTS OF THE AMINE-INITIATED POLYMERIZATION
Author:	Paul Doty and R. D. Lundberg
Publication:	Journal of the American Chemical Society
Publisher:	American Chemical Society
Date:	May 1, 1957

User ID

Password

Enable Auto Login

LOGIN

Forgot Password/User ID?

If you're a copyright.com user, you can login to RightsLink using your copyright.com credentials. Already a RightsLink user or want to learn more?

PERMISSION/LICENSE IS GRANTED FOR YOUR ORDER AT NO CHARGE

This type of permission/license, instead of the standard Terms & Conditions, is sent to you because no fee is being charged for your order. Please note the following:

- Permission is granted for your request in both print and electronic formats, and translations.
- If figures and/or tables were requested, they may be adapted or used in part.
- Please print this page for your records and send a copy of it to your publisher/graduate school.
- Appropriate credit for the requested material should be given as follows: "Reprinted (adapted) with permission from (COMPLETE REFERENCE CITATION). Copyright (YEAR) American Chemical Society." Insert appropriate information in place of the capitalized words.
- One-time permission is granted only for the use specified in your request. No additional uses are granted (such as derivative works or other editions). For any other uses, please submit a new request.

If credit is given to another source for the material you requested, permission must be obtained from that source.

BACK | CLOSE WINDOW

ELSEVIER LICENSE
TERMS AND CONDITIONS

Apr 02, 2014

This is a License Agreement between Wayne Huberty ("You") and Elsevier ("Elsevier") provided by Copyright Clearance Center ("CCC"). The license consists of your order details, the terms and conditions provided by Elsevier, and the payment terms and conditions.

All payments must be made in full to CCC. For payment instructions, please see information listed at the bottom of this form.

Supplier	Elsevier Limited The Boulevard,Langford Lane Kidlington,Oxford,OX5 1GB,UK
Registered Company Number	1982084
Customer name	Wayne Huberty
Customer address	236 Choppin Hall Baton Rouge, LA 70803
License number	3360790576455
License date	Apr 02, 2014
Licensed content publisher	Elsevier
Licensed content publication	Tetrahedron Letters
Licensed content title	The preparation of N-carboxyanhydrides of α-amino acids using bis(trichloromethyl)carbonate
Licensed content author	William H. Daly,Drew Poché
Licensed content date	1988
Licensed content volume number	29
Licensed content issue number	46
Number of pages	4
Start Page	5859
End Page	5862
Type of Use	reuse in a thesis/dissertation
Portion	figures/tables/illustrations
Number of figures/tables/illustrations	1
Format	both print and electronic
Are you the author of this Elsevier article?	No

RightsLink®

Home | Account Info | Help

Title: Living Polypeptides
Author: Thrasyvoulos Aliferis,Hermes Iatrou, and, and Nikos Hadjichristidis*
Publication: Biomacromolecules
Publisher: American Chemical Society
Date: Sep 1, 2004

Logged in as:
Wayne Huberty
Account #:
3000518662

Logout

PERMISSION/LICENSE IS GRANTED FOR YOUR ORDER AT NO CHARGE

This type of permission/license, instead of the standard Terms & Conditions, is sent to you because no fee is being charged for your order. Please note the following:

- Permission is granted for your request in both print and electronic formats, and translations.
- If figures and/or tables were requested, they may be adapted or used in part.
- Please print this page for your records and send a copy of it to your publisher/graduate school.
- Appropriate credit for the requested material should be given as follows: "Reprinted (adapted) with permission from (COMPLETE REFERENCE CITATION). Copyright (YEAR) American Chemical Society." Insert appropriate information in place of the capitalized words.
- One-time permission is granted only for the use specified in your request. No additional uses are granted (such as derivative works or other editions). For any other uses, please submit a new request.

If credit is given to another source for the material you requested, permission must be obtained from that source.

BACK | CLOSE WINDOW

JOHN WILEY AND SONS LICENSE TERMS AND CONDITIONS

Mar 27, 2014

This is a License Agreement between Wayne Huberty ("You") and John Wiley and Sons ("John Wiley and Sons") provided by Copyright Clearance Center ("CCC"). The license consists of your order details, the terms and conditions provided by John Wiley and Sons, and the payment terms and conditions.

All payments must be made in full to CCC. For payment instructions, please see information listed at the bottom of this form.

License Number	3357260973687
License date	Mar 27, 2014
Licensed content publisher	John Wiley and Sons
Licensed content publication	Biopolymers
Licensed content title	Brownian motion of highly charged poly(L-lysine). Effects of salt and polyion concentration
Licensed copyright line	Copyright © 1978 John Wiley & Sons, Inc.
Licensed content author	Sung-Chang Lin,Wylie I. Lee,J. Michael Schurr
Licensed content date	Feb 1, 2004
Start page	1041
End page	1064
Type of use	Dissertation/Thesis
Requestor type	University/Academic
Format	Print and electronic
Portion	Figure/table
Number of figures/tables	1
Original Wiley figure/table number(s)	Figure 1
Will you be translating?	No
Title of your thesis / dissertation	Synthesis and Characterization of a water-soluble, non-ionic, rod-like polymer
Expected completion date	Aug 2014
Expected size (number of pages)	150
Total	0.00 USD
Terms and Conditions	

Terms and Conditions are not available at this time.

If you would like to pay for this license now, please remit this license along with your

RightsLink®

Home | Account Info | Help

Title: POLYPEPTIDES. Xa. ADDITIONAL COMMENTS OF THE AMINE-INITIATED POLYMERIZATION

Author: Paul Doty and R. D. Lundberg

Publication: Journal of the American Chemical Society

Publisher: American Chemical Society

Date: May 1, 1957

Logged in as: Wayne Hubarty
Account #: 3000518662

LOGOUT

PERMISSION/LICENSE IS GRANTED FOR YOUR ORDER AT NO CHARGE

This type of permission/license, instead of the standard Terms & Conditions, is sent to you because no fee is being charged for your order. Please note the following:

- Permission is granted for your request in both print and electronic formats, and translations.
- If figures and/or tables were requested, they may be adapted or used in part.
- Please print this page for your records and send a copy of it to your publisher/graduate school.
- Appropriate credit for the requested material should be given as follows: "Reprinted (adapted) with permission from (COMPLETE REFERENCE CITATION). Copyright (YEAR) American Chemical Society." Insert appropriate information in place of the capitalized words.
- One-time permission is granted only for the use specified in your request. No additional uses are granted (such as derivative works or other editions). For any other uses, please submit a new request.

If credit is given to another source for the material you requested, permission must be obtained from that source.

BACK | CLOSE WINDOW

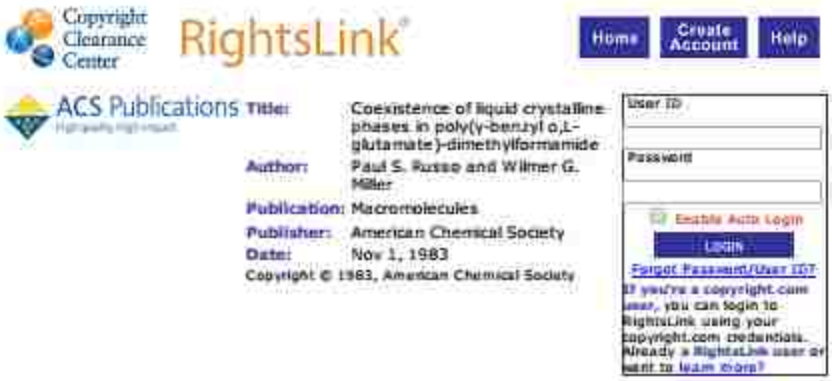

PERMISSION/LICENSE IS GRANTED FOR YOUR ORDER AT NO CHARGE

This type of permission/license, instead of the standard Terms & Conditions, is sent to you because no fee is being charged for your order. Please note the following:

- Permission is granted for your request in both print and electronic formats, and translations.
- If figures and/or tables were requested, they may be adapted or used in part.
- Please print this page for your records and send a copy of it to your publisher/graduate school.
- Appropriate credit for the requested material should be given as follows: "Reprinted (adapted) with permission from (COMPLETE REFERENCE CITATION). Copyright (YEAR) American Chemical Society." Insert appropriate information in place of the capitalized words.
- One-time permission is granted only for the use specified in your request. No additional uses are granted (such as derivative works or other editions). For any other uses, please submit a new request.

If credit is given to another source for the material you requested, permission must be obtained from that source.

BACK CLOSE WINDOW

JOHN WILEY AND SONS LICENSE TERMS AND CONDITIONS

Apr 02, 2014

This is a License Agreement between Wayne Huberty ("You") and John Wiley and Sons ("John Wiley and Sons") provided by Copyright Clearance Center ("CCC"). The license consists of your order details, the terms and conditions provided by John Wiley and Sons, and the payment terms and conditions.

All payments must be made in full to CCC. For payment instructions, please see information listed at the bottom of this form.

License Number	3360790934665
License date	Apr 02, 2014
Licensed content publisher	John Wiley and Sons
Licensed content publication	Wiley Books
Licensed content title	Light Scattering, Size Exclusion Chromatography and Asymmetric Flow Field Flow Fractionation: Powerful Tools for the Characterization of Polymers, Proteins and Nanoparticles
Book title	Light Scattering, Size Exclusion Chromatography and Asymmetric Flow Field Flow Fractionation: Powerful Tools for the Characterization of Polymers, Proteins and Nanoparticles
Licensed copyright line	Copyright © 2011, John Wiley and Sons
Licensed content author	Stepan Podzimek
Licensed content date	Mar 1, 2011
Type of use	Dissertation/Thesis
Requestor type	University/Academic
Format	Print and electronic
Portion	Figure/table
Number of figures/tables	1
Original Wiley figure/table number(s)	Figure 2.21
Will you be translating?	No
Title of your thesis / dissertation	Synthesis and Characterization of a water-soluble, non-ionic, rod-like polymer
Expected completion date	Aug 2014
Expected size (number of pages)	150
Total	0.00 USD
Terms and Conditions	

Terms and Conditions are not available at this time.

Appendix 4 - List of symbols and abbreviations

CHCA	α-cyano-4-hydroxycinnamic acid
2 EXP	2 exponential fit
N_a	Avogadro's number
k_B	Boltzmann's constant
°C	Celsius
cm	Centimeters
DNA	Deoxyribonucleic acid
DLS	Dynamic light scattering
GPC	Gel permeation chromatography
GPC/MALS	Gel permeation chromatography with multi-angle laser light scattering
R_{h}	Hydrodynamic radius
R_{g}	Radius of gyration
m/z	Mass to charge ratio
MALDI	Matrix assisted laser desorption ionization
kHz	Kilohertz
μL	Microliter
mL	Milliliter
min	Minutes
M	Molar
mM	millimolar
mol	Mole
M	Molecular weight

M_w	Weight-average molecular weight
M_n	Number-average molecular weight
N_2	Nitrogen
PDI	Polydispersity index
^{1}H NMR	Proton nuclear magnetic resonance spectroscopy
R_g	Radius of gyration
R_θ	Rayleigh factor
q	Scattering vector
s	Seconds
η_o	Solvent viscosity
SLS	Static light scattering
T	Temperature
T_{cp}	Cloud point temperature
NAM	Normal amine mechanism
AMM	Activated monomer mechanism
NCA	N-carboxyanhydride
HVT	High vacuum technique
PBLG	Poly-γ-L-glutamate
PEGL	Poly(diethylene glycol lysine)
PEG	Poly(ethylene glycol)
a_p	Persistence length
η_{sp}	Specific viscosity
η_{rel}	Relative Viscosity

$[\eta]$	Intrinsic viscosity
Γ	Decay rate
q	Scattering vector
CUMU	Cumulant fits
3CUMU	Third cumulant fit
2-EXP	Two exponential fits
D	Diffusion coefficient
LCST	Lower critical solution

Vita

Wayne Huberty was born in Colorado Springs in 1985. He grew up in Appleton Wisconsin and graduated high school in 2004. He attended a small state school, University of Wisconsin-Stevens Point and obtained the Bachelor of Science in Chemistry and Biology. He earned a M.S. degree in chemistry in May 2012 and will graduate with his PhD in chemistry in December 2014.